

On the influence of feedstock properties and composition on process development of expanded bed adsorption

Einfluss der Eigenschaften und Zusammensetzung biotechnologischer Rohlösungen auf die Prozessentwicklung im Rahmen der Fließbettadsorption

In a u g u r a l - D i s s e r t a t i o n

zur

Erlangung des Doktorgrades der
Mathematisch-Naturwissenschaftlichen Fakultät
Der Heinrich-Heine-Universität Düsseldorf

Vorgelegt von

Diplom Biologe Peter Jochen Brixius

aus

Köln

2003

Gedruckt mit der Genehmigung der Mathematisch-Naturwissenschaftlichen Fakultät der
Heinrich-Heine-Universität Düsseldorf

Referentin: Prof. Dr. Maria Regina Kula

Korreferent: Prof. Hanns Weiss

Tag(e) der mündlichen Prüfung: 03.06.2003

DANKSAGUNG

Diese Arbeit entstand am Institut für Enzymtechnologie der Heinrich Heine Universität Düsseldorf im Forschungszentrum Jülich unter der Leitung von Frau Prof. Dr. Maria Regina Kula.

Frau Prof. Dr. Kula gilt mein besonderer Dank für die freundliche Aufnahme in ihrem Institut, die Überlassung des Promotionsthemas sowie der stetigen Diskussionsbereitschaft und fachkundigen Unterstützung. Herr Prof. Dr. Weiss gilt mein Dank für die Übernahme des Korreferates.

Ein besonderer Dank geht auch an die Firma Novo Nordisk und hier insbesondere an Frau Inger Mollerup, Herr Ole E. Jensen, Herr Jesper S. Johansen, Herr Henrik Valore sowie an alle anderen Mitarbeitern des Protein Purifikation Department sowie des hgH Projects & Optimisation Departments für eine hervorragende Kooperation in den letzten drei Jahren sowie für die freundlich Aufnahme und Unterstützung während meiner Arbeiten in den Labors von Novo Nordisk Gentofte (Dänemark) und nicht zuletzt auch danke für die finanzielle und materielle Unterstützung die diese Arbeit erst ermöglicht hat.

Ganz herzlich danken möchte ich mich auch der Arbeitsgruppe „Aufarbeitung“ unter der Leitung von Herrn Priv.-Doz. Dr. Jörg Thömmes und seit Januar 2001 Herrn Dr. Jürgen J. Hubbuch für eine stets angenehme und fruchtbare Arbeitsatmosphäre. Besonders erwähnt seien hier Markus Halfar für seine praktische Unterstützung sowie Dipl. Ing. Esther Knieps-Grünhagen, Dipl. Ing. Holger Gieren, Dr. Ute Reichert und Dr. Dong-Qiang Lin. Desweiteren möchte ich mich bei Sina Paezold bedanken die als studentische Hilfskraft diese Arbeit tatkräftig unterstützt hat. Außerdem gilt mein Dank allen Mitarbeitern des Instituts für Enzymtechnologie die hier noch nicht erwähnt worden sind.

1 CONTENT

1	CONTENT	I
2	FIGURES AND TABLES	V
3	ABSTRACT (GERMAN)	1
4	SYMBOLS & ABBREVIATIONS	4
5	INTRODUCTION	9
5.1	Downstream Processing	9
5.1.1	Extractive Separation	12
5.1.2	Adsorptive Separations	12
5.1.3	Stable fluidization	13
5.1.4	Chromatographic interactions	17
5.1.5	Ion Exchange Chromatography in Expanded Bed Adsorption.....	20
5.2	Biomass-Adsorbent Interactions	23
5.2.1	Quantification of biomass/adsorbent interaction	23
5.2.2	Deep bed filtration theory – A mechanistic approach	26
5.3	Properties of biomass suspension	30
5.3.1	Particle size analysis	30
5.3.2	Zeta Potential	32
5.4	Microbial cell wall properties	35
5.4.1	<i>E. coli</i>	36
5.4.2	<i>Saccharomyces cerevisiae</i>	39
5.5	Cell disruption	40
5.5.1	Sonication	41

5.5.2	Bead mill.....	42
5.5.3	High pressur Homogenization	44
5.6	Protein properties used in process design studies	46
5.6.1	Insulin	46
5.6.2	Human Growth Hormone (hGH).....	48
5.6.3	Formate dehydrogenase	49
6	RESULTS AND DISCUSSION.....	52
6.1	Feedstock properties & Biomass-Adsorbent Interactions in Expanded Bed Adsorption.....	52
6.1.1	Zeta potential development of intact cells during high cell density cultivation of <i>Escherichia coli</i>	53
6.1.2	Impact of cell disruption on feedstock properties.....	57
6.1.3	Escherichia coli host strains.....	75
6.1.4	Scalability and feasibility study.....	77
6.1.5	Saccharomyces cerevisiae.....	83
6.1.6	Summary and Conclusions I.....	87
6.2	EBA & Downstream Process development	89
6.2.1	Insulin	89
6.2.2	Summary and Conclusions II (Insulin Precursor MI3).....	102
6.2.3	Human Growth Hormone (hGH).....	104
6.2.4	Anion Exchange Chromatography (EBA-mode).....	105
6.2.5	Cation Exchange Chromatography (EBA-mode).....	115
6.3	Aqueous two phase systems	124
6.3.2	Summary and Conclusions III (hGH).....	130
7	MATERIAL & METHODS	132
7.1	Protein Analysis	139
7.1.1	Total Protein Determination (Bradford Assay).....	139
7.1.2	SDS Page	140

7.1.3	RP-HPLC-Analysis for Insulin Precursor MI3.....	140
7.1.4	FPLC-Analysis for hGH.....	144
7.2	Protein Adsorption.....	149
7.2.1	Finite bath uptake experiments.....	149
7.2.2	Breakthrough Analysis.....	153
7.2.3	Modeling of Breakthrough Curves in Packed Beds.....	156
7.3	Biomass-Adsorbent Interactions.....	161
7.3.1	Pulse-Response Experiment.....	161
7.3.2	Residence Time Distribution (RTD) (Fernández-Lahore <i>et al.</i> , 2001).....	163
7.4	Protein adsorption in expanded bed mode.....	165
7.4.1	Human insulin precursor mi 3.....	165
7.5	Cell cultivation.....	166
7.5.1	Saccharomyces cerevisiae.....	166
7.5.2	E. coli.....	167
7.6	Cell disruption.....	171
7.6.1	Bead Mill.....	171
7.6.2	French Press.....	172
7.6.3	Ultrasound.....	173
7.7	Aqueous two phase system (ATPS).....	173
7.7.1	Preparation of ATPS.....	173
7.7.2	Ultrafiltration of ATPS top phases.....	173
7.8	Physical and chemical Properties of Biomass Suspension.....	174
7.8.1	Zeta Potential.....	174
7.8.2	Size analysis.....	175
7.8.3	Viscosity.....	175
7.9	DNA analysis.....	176
8	APENDIX.....	177

8.1	RTD analysis	177
8.1.1	Evaluation of RTD curve:.....	177
8.1.2	Tanks in series Model	179
8.1.3	Moments of RTD	180
8.2	Modeling of breakthrough curves.....	181
8.2.1	Transport mechanism & appropriated models.....	182
8.3	Electrostatic interactions	183
8.4	Particle Size Distribution Data.....	185
8.4.1	Homogenization technique	185
8.4.2	Homogenization conditions in the French Press.....	187
8.4.3	Pilot scal cell disruption.....	194
8.4.4	Saccharomyces cerevisiae Homogenization conditions in the French Press 202	
8.5	ATPS hGH.....	208
9	REFERENCES.....	209

2 FIGURES AND TABLES

a FIGURES

FIG. 5-1: IMPACT OF THE NUMBER OF UNIT OPERATIONS EMPLOYED DURING DOWNSTREAM PROCESSING ASSUMING A GIVEN YIELD PER STEP: 99% (□); 95% (■); 90% (○); 85% (●) (FISH AND LILLY, 1984).	10
FIG. 5-2: DOWNSTREAM PROCESSING SCHEME	11
FIG. 5-3: PERFECTLY CLASSIFIED EXPANDED BED.....	15
FIG. 5-4: CELL PULSE TRANSMISSION THROUGH AN EXPANDED BED OF STREAMLINE SP AT PH 7.0 (FEUSER <i>ET AL.</i> , 1999).....	21
FIG. 5-5: CELL PULSE TRANSMISSION THROUGH AN EXPANDED BED OF STREAMLINE DEAE (FEUSER <i>ET AL.</i> , 1999).....	22
FIG. 5-6: SET-UP OF A PULSE RESPONSE EXPERIMENT AND TYPICAL RESULTS OF A PULSE RESPONSE EXPERIMENT WITH (CTI = 0.22) AND WITHOUT (CTI =1.0) BIOMASS/ABSORBER INTERACTION.	24
FIG. 5-7: GRAPHICAL DESCRIPTION OF THE PDE MODEL. (N: MASS TRANSFER BETWEEN ZONES, PE: OVER ALL AXIAL DISPERSION, α : FRACTION OF LIQUID IN PLUG FLOW) .	26
FIG. 5-8: CORRESPONDING SPHERES, USING DIFFERENT TECHNIQUES FOR PARTICLE SIZE DETERMINATION (HTTP://WWW.MALVERN.DE).....	31
FIG. 5-9: DIFFERENT DISPERSION CONDITIONS OF A COLLOID SYSTEM (HTTP://WWW.MALVERN.DE).....	32
FIG. 5-10: CHARGE DISTRIBUTION IN THE STERN DOUBLE LAYER MODEL	33
FIG. 5-11: COMPARISON BETWEEN GRAM POS. (RIGHT) AND GRAM NEG. (LEFT) CELL WALL (PAUSTIAN, 2001).....	36
FIG. 5-12: LIPOPOLYSACCARIDE (NIKAIDO, 1996).	37
FIG. 5-13: MAJOR PHOSPHOLIPIDS IN THE CYTOPLASMIC MEMBRANE OF <i>ESCHERICHIA COLI</i> 70-80 % PHOSPHATIDYLETHANOLAMINE, 15-25 % PHOSPHATIDYLGLYCEROL, 5-10 % CARDIOLIPIN. R ₁ : SATURATED FATTY ACID, R ₂ : UNSATURATED FATTY ACID (KADNER, 1996).	38
FIG. 5-14: RELATIONSHIPS AMONG COMPONENTS OF <i>SACCHAROMYCES CEREVISIAE</i> CELL WALLS. (A) PROTOTYPICAL MODULE WITH COMPONENTS INDIVIDUALLY LABELED	

AND COLORED. THE MANNOPROTEIN POLYPEPTIDE IS BLUE, AND OLIGOSACCHARIDES ARE SHOWN IN YELLOW, LABELED AS N OR O LINKED. ONLY A FEW OF THE BRANCH POINTS OF THE GLUCANS ARE SHOWN. CHITIN CAN ALSO BE LINKED TO THE B1,6 GLUCAN. (B) ASSOCIATION OF MODULES TO FORM A WALL LATTICE. COLORS ARE AS IN PANEL A. THE B1,3 GLUCAN CHAINS ARE INTERTWINED TO DESIGNATE TRIPLE HELICES, AND CHITIN IS SHOWN AS A CRYSTALLINE MICRO-DOMAIN. CROSS-LINKING OF MANNOPROTEINS THROUGH DISULFIDE AND OTHER BONDS IS NOT DEPICTED (LIPKE AND OVALLE, 1998)..... 40

FIG. 5-15: CELL DISRUPTION METHODS 41

FIG. 5-16: BEAD MILL WITH HORIZONTAL GRINDING CHAMBER SYSTEM TriNEX® (NETZSCH-FEINMAHLTECHNIK, GERMANY) 42

FIG. 5-17: DETAILS OF VALVE SEAT OF APV-GAULIN HIGH-PRESSURE HOMOGENIZER... 44

FIG. 5-18: ENZYMATIC PROCESSING OF INSULIN (STRYER, 1994)..... 46

FIG. 5-19: COMPARISON OF PIG, BOVINE AND HUMAN INSULIN..... 47

FIG. 5-20: PRIMARY STRUCTURE OF HGH..... 48

FIG. 5-21: COFACTOR REGENERATION USING FDH..... 49



FIG. 5-22: *ESCHERICHIA COLI* HOMOGENATE TRANSMISSION, MEASURED BY THE PULSE-RESPONSE EXPERIMENT FOR DIFFERENT ADSORBENTS AT PH 7,5 AND 5 MS/CM CONDUCTIVITY (1M AMMONIUM SULPHATE ADDED FOR ADSORPTION TO STREAMLINE PHENYL) (REICHERT *ET AL.*, 2001) 51

FIG. 6-1: SURFACE CHARGE OF AN REC. L-PHE PRODUCTION *ESCHERICHIA COLI* STRAIN (CELLS RECEIVED FROM NICOLE RÜFFER IBT II OF THE RESEARCH CENTRE JÜLICH, GERMANY) DURING A FED BATCH CULTIVATION MEASURED IN 10 mM Na_2HPO_4 /CITRIC ACID BUFFER AT A CONSTANT CONDUCTIVITY $\kappa= 5 \text{ MS CM}^{-1}$ ADJUSTED WITH SOLID NaCl AND VARIOUS pH. AT (■) PH 2, (●) PH 3, (▲) PH 7 55

FIG. 6-2: SURFACE CHARGE OF *ESCHERICHIA COLI* JM 101 CELLS DURING A FED BATCH CULTIVATION MEASURED IN 10 mM Na_2HPO_4 /CITRIC ACID BUFFER AT A CONSTANT CONDUCTIVITY $\kappa= 5 \text{ MS CM}^{-1}$ ADJUSTED WITH SOLID NaCl AND VARIOUS pH. AT (■) PH 2, (●) PH 3, (▲) PH 7. ($C_{\text{MG}}^{2+} = 14 \text{ G L}^{-1}$ IN THE FEED MEDIA)..... 55

FIG. 6-3: SURFACE CHARGE OF *ESCHERICHIA COLI* JM 105 CELLS DURING A FED BATCH CULTIVATION MEASURED IN 10 mM Na_2HPO_4 /CITRIC ACID BUFFER AT A CONSTANT

CONDUCTIVITY $\kappa= 5 \text{ mS cm}^{-1}$ ADJUSTED WITH SOLID NaCl AND VARIOUS pH. (■) pH 2, (●) pH 3, (▲) pH 7. ($C_{\text{MG}}^{2+} = 10 \text{ g L}^{-1}$ IN THE FEED MEDIA).....	56
FIG. 6-4: SURFACE CHARGE OF <i>ESCHERICHIA COLI</i> JM 105 REC FDH CELLS DURING A FED BATCH CULTIVATION MEASURED IN 10 mM Na_2HPO_4 /CITRIC ACID BUFFER AT A CONSTANT CONDUCTIVITY $\kappa= 5 \text{ mS cm}^{-1}$ ADJUSTED WITH SOLID NaCl AND VARIOUS pH. AT (■) pH 2, (●) pH 3, (▲) pH 7. ($C_{\text{MG}}^{2+} = 10 \text{ g L}^{-1} \text{ MgSO}_4$ IN THE FEED MEDIA).....	56
FIG. 6-5: VISCOSITY OF 40 % <i>E. COLI</i> HOMOGENATE OBTAINED FROM DIFFERENT CELL DISRUPTION METHODS (USING A BIOMASS SUSPENSION OF $C_B = 40 \text{ \% WW}$)	58
FIG. 6-6: 0,8 % AGAROSE GEL ANALYSIS OF HOMOGENATES OBTAINED FROM VARIOUS CELL DISRUPTION METHODS.....	59
FIG. 6-7: VISCOSITY OF <i>ESCHERICHIA COLI</i> BIOMASS SUSPENSION ($C_B = 40\% \text{ WW}$) DURING MULTIPLE PASSAGE HOMOGENIZATION IN A FRENCH PRESS AT TWO DIFFERENT OPERATING PRESSURES (▼) 482 BAR AND (■) 965 BAR.	60
FIG. 6-8: 1,5 % AGAROSE GEL ANALYSIS ETHIDIUMBROMIDE STAINED FRENCH PRESS HOMOGENATE AT DIFFERENT HOMOGENIZATION CYCLES AND A OPERATION PRESSURE OF 965 BAR.....	60
FIG. 6-9: CTI USING BEAD MILL HOMOGENATE WITH & WITHOUT BENZONASE™ TREATMENT (<i>ESCHERICHIA COLI</i> JM105).	61
FIG. 6-10: AVERAGE SIZE DISTRIBUTION OBTAINED BY DIFFERENT CELL DISRUPTION METHODS USING 40 % WW <i>ESCHERICHIA COLI</i> JM 101, SUSPENSION.	63
FIG. 6-11: SURFACE CHARGE OF CELL DEBRIS OBTAINED BY DIFFERENT CELL DISRUPTION METHODS. USING 40 % WW <i>ESCHERICHIA COLI</i> JM 101. MEASUREMENT IN 100 mM TRIS/HCL pH 8.0 $\kappa= 10 \text{ mS cm}^{-1}$	63
FIG. 6-12: AVERAGE SIZE DISTRIBUTION OF <i>ESCHERICHIA COLI</i> HOMOGENATE TREATED WITH DIFFERENT PRESSURE AND CYCLES IN THE FRENCH PRESS (■) 965 BAR, (●) 482 BAR.....	65
FIG. 6-13: SURFACE CHARGE OF <i>ESCHERICHIA COLI</i> HOMOGENATE TREATED WITH DIFFERENT PRESSURE AND CYCLES IN THE FRENCH PRESS. (■) 965 BAR, (●) 482 BAR.	65
FIG. 6-14: IMPACT OF PARTICLE SIZE ON THE SURFACE CHARGE OF <i>ESCHERICHIA COLI</i> CELL DEBRIS.....	66

- FIG. 6-15: IMPACT OF VARIOUS FORCES ON THE ELECTROPHORETIC MOBILITY OF A PARTICLE IN AN ELECTRICAL FIELD. F_1 - ACCELERATING FORCE, F_2 - RETARDING FORCE, F_3 - ELECTROPHORETIC RETARDATION, F_4 - RELAXATION EFFECT (NITZSCHE, 2002). 67
- FIG. 6-16: CTI OF VARIOUS HOMOGENATES DEPENDING ON THE HOMOGENIZATION METHOD (pH 8,0; 68
- FIG. 6-17: THE ζ -POTENTIAL \sim CTI RELATION FOR INTACT YEAST CELLS AND STREAMLINE DEAE VARYING IONS (NaCl (\square), NH_4Cl (\bullet), Na_2SO_4 (Δ), $(\text{NH}_4)_2\text{SO}_4$ (\square), CaCl_2 (\blacksquare)) AND pH (+). (LIN ET AL., 2002)..... 69
- FIG. 6-18: THE $(-\zeta_A \zeta_B) \sim P$ RELATION FOR INTACT YEAST CELLS AND STREAMLINE DEAE USING VARYING IONS (NaCl (\square), NH_4Cl (\circ), Na_2SO_4 (Δ), $(\text{NH}_4)_2\text{SO}_4$ (\diamond), CaCl_2 (\blacktriangle)) AND pH (\bullet) (LIN ET AL., 2002)..... 70
- FIG. 6-19: CORRELATION OF MEAN SIZE DISTRIBUTION AND CTI (ESCHERICHIA COLI JM 105 FRENCH PRESS HOMOGENATE AT 300 BAR DIFFERENT CYCLES). 71
- FIG. 6-20: EVALUATION OF SIZE ζ -POTENTIAL AND TRANSMISSION USING THE CORRELATION AFTER LIN ET AL. () LINEAR FIT ($Y = A + B \cdot X$ WITH $A = 1,007$; $B = -0,05$; $R = 0,92$) 71
- FIG. 6-21: ELECTROSTATIC INTERACTION POTENTIAL (ϕ_{EL}). INFLUENCE BETWEEN THE OPPOSITELY CHARGED PARTICLES (CELL DEBRIS AND ADSORBENT) VERSUS THE DISTANCE BETWEEN THE PARTICLES. CALCULATED AT VARIOUS BIOMASS PARTICLE SIZES AND SURFACE CHARGE AT CONSTANT CONDITIONS FOR THE ADSORBENT PARTICLE. (---) $x = 1000$ NM AND $\zeta = -20$ MV, (...) $x = 1000$ NM AND $\zeta = -15$ MV, (...) $x = 1000$ NM AND $\zeta = -10$ MV, (---) $x = 300$ NM AND $\zeta = -20$ MV, (-...-) $x = 300$ NM AND $\zeta = -15$ MV, (-...-) $x = 300$ NM AND $\zeta = -10$ MV 73
- FIG. 6-22: THE IMPACT OF BIOMASS PARTICLE SIZE (x) ON THE DIMENSIONLESS NUMBER FOR INTERCEPTION (N_R) (IVES, 1975). 74
- FIG. 6-23: ZETA POTENTIAL OF VARIOUS *ESCHERICHIA COLI* STRAINS A COMPARISON IN 100MM TRI HCL pH 8,0 $\kappa = 10 \text{MS CM}^{-1}$.  WHOLE CELLS,  HOMOGENATE.... 75
- FIG. 6-24: BIOMASS TRANSMISSION OF DIFFERENT FRENCH PRESS HOMOGENATE OF *ESCHERICHIA COLI* STRAINS (pH 8,0 $\kappa = 10 \text{MS CM}^{-1}$). 76

- FIG. 6-25: VISCOSITY DURING HIGH PRESSURE HOMOGENIZATION IN AN APV GAULIN HOMOGENIZER. (■) *ESCHERICHIA COLI* JM 105; (●) *ESCHERICHIA COLI* JM 105 REC. FDH. 78
- FIG. 6-26: ZETA POTENTIAL OF *ESCHERICHIA COLI* JM 105 AND *ESCHERICHIA COLI* REC. FDH& JM 105 SUSPENSION (40 % WW) DISRUPTED IN A PILOT SCALE HOMOGENIZER (GAULIN) AND THE FRENCH PRESS. (■) *ESCHERICHIA COLI* JM 105 PILOT SCALE HOMOGENIZER, (●) *ESCHERICHIA COLI* JM 105 REC FDH PILOT SCALE HOMOGENIZER, (▲) *ESCHERICHIA COLI* JM 105 FRENCH PRESS. 79
- FIG. 6-27: COMPARISON OF THE MEAN SIZE DISTRIBUTION AFTER DIFFERENT PASSAGE IN A GAULIN HIGH PRESSURE HOMOGENIZER AND FRENCH PRESS OF HOST AND REC. *ESCHERICHIA COLI* STRAIN. (■) *ESCHERICHIA COLI* JM 105 PILOT SCALE HOMOGENIZER, (●) *ESCHERICHIA COLI* JM 105 REC FDH PILOT SCALE HOMOGENIZER, (▲) *ESCHERICHIA COLI* JM 105 FRENCH PRESS. 79
- FIG. 6-28: PROTEIN RELEASE AND FDH ACTIVITY DURING HIGH PRESSURE HOMOGENIZATION IN A PILOT SCALE HOMOGENIZER. (■) *ESCHERICHIA COLI* JM 105 PILOT SCALE HOMOGENIZER, (●) *ESCHERICHIA COLI* JM 105 REC FDH PILOT SCALE HOMOGENIZER, (▲) FDH ACTIVITY..... 80
- FIG. 6-29: RTD IN 10 % WW HIGH PRESSURE HOMOGENATE OF *ESCHERICHIA COLI* JM105 AND *ESCHERICHIA COLI* JM 105 REC .FDH (pH 8,0 AND $\kappa = 10 \text{ mS cm}^{-1}$). (–) *ESCHERICHIA COLI* JM 105, (...) *ESCHERICHIA COLI* JM 105 REC. FDH. 81
- FIG. 6-30: RTD IN 10 % WW HIGH PRESSURE HOMOGENATE OF *ESCHERICHIA COLI* JM105 AND *ESCHERICHIA COLI* JM 105 REC .FDH (pH 8.0 AND $\kappa = 5 \text{ mS cm}^{-1}$). (–) *ESCHERICHIA COLI* JM 105, (...) *ESCHERICHIA COLI* JM 105 REC. FDH. 81
- FIG. 6-31: STREAMLINE DEAE AFTER APPLICATION OF *ESCHERICHIA COLI* BEAD MILL HOMOGENATE 82
- FIG. 6-32: PARTICLE SIZE REDUCTION OF *SACCHAROMYCES CEREVISIAE* DURING MULTIPLE PASSAGE HOMOGENIZATION IN A FRENCH PRESS (40 % WW IN 50 mM TRIS/HCL pH 7,5) AT DIFFERENT OPERATION PRESSURE. (■) 300 BAR, (●) 482 BAR, (▲) 965 BAR AND (▼) 2068 BAR..... 84
- FIG. 6-33: SURFACE CHARGE OF *SACCHAROMYCES CEREVISIAE* HOMOGENATE OBTAINED BY MULTIPLE PASSAGES THROUGH A FRENCH PRESS (40 % WW IN 50 mM TRIS/HCL pH

7,5) AT DIFFERENT OPERATING PRESSURES. (■) 300 BAR, (●) 482 BAR, (▲) 965 BAR
 85

FIG. 6-34: THE IMPACT OF CELL DISRUPTION OF *SACCHAROMYCES CEREVISIAE* ON THE CTI
 IN EBA (TRANSMISSION DATA FROM CELLS AND BEAD MILL HOMOGENATE TAKEN
 FROM (LIN *ET AL.*, 2002)). X = APP. 7000 NM (WHOLE CELLS); X = APP. 2000 NM (2
 CYCLE 482 BAR), X = APP. 1000 NM (5 CYCLE 965 BAR); X = APP. 1400 NM (BEAD
 MILL). 86

FIG. 6-35: CORRELATION ZETA PARAMETER VERSUS BIOMASS TRANSMISSION IN EBA
 FOR *SACCHAROMYCES CEREVISIAE* AND *ESCHERICHIA COLI*. (■) *SACCHAROMYCES
 CEREVISIAE*, (▲) *ESCHERICHIA COLI*, (-) LINEAR REGRESSION (R= 0,96). 87



FIG. 6-36: ISOTHERMAL BINDING OF MI3 PRECURSOR ON STREAMLINE SP AT PH 3.
 UNDILUTED FEED: CONDUCTIVITY. $\kappa = 14.2 \text{ mS cm}^{-1}$, 1:2 DILUTED FEED.
 CONDUCTIVITY $\kappa = 6.2 \text{ mS cm}^{-1}$. EXPERIMENTAL RESULTS FROM 1:2 DILUTED FEED
 COULD BE FITTED AS A LANGMUIR ISOTHERM ($K_A = 0.031$; $Q_{MAX} = 57.75$; $R^2 =$
 0.998), UNDILUTED FEED RESULTED IN A LINEAR FIT ($A = -0.378$; $B = 0.162$; $R^2 =$
 0.992). (●) UNDILUTED FEEDSTOCK, (■) 1:2 DILUTED FEEDSTOCK. 92

FIG. 6-37: ADSORPTION KINETICS OF STREAMLINE SP AND ZIRCONIA S AT PH 3 USING
 1:2 DIL. CLARIFIED CULTURE BROTH ($\kappa = 7 \text{ mS cm}^{-1}$, PH 3.0) (■) STREAMLINE SP,
 (●) ZIRCONIA S. 93

FIG. 6-38: BREAKTHROUGH ANALYSIS OF MI3 ADSORPTION TO STREAMLINE SP AT PH
 3.0, LINEAR VELOCITY 5 CM/MIN, AT 5CM SEDIMENTED. BED HEIGHT. DATA OF 1:2
 DILUTED . FEEDSTOCK ARE FITTED USING THE MODEL AFTER HALL ET AL. (1966).
 Q_{MAX} WAS ESTIMATED BY A FIT OF THE LANGMUIR ISOTHERM (FIG. 6-36). (●)
 UNDILUTED; (■) 1:2 DILUTED. 94

FIG. 6-39: SIMULATING SORPTION EFFICIENCY OF THE INSULIN PRECURSOR ON
 STREAMLINE SP FOR BREAKTHROUGH AT 10 %. OBTAINED FROM BREAKTHROUGH
 CURVES SIMULATED AFTER HALL ET AL. (1966) AT VARIOUS FLUID VELOCITIES AND
 SEDIMENTED BED HEIGHTS. 1:2 DILUTED CULTURE LIQUID PH 3. 96

FIG. 6-40: BED EXPANSION OF ZIRCONIA S AND STREAMLINE SP IN A 15 % WW CULTURE
 BROTH (PH 3.0; $\kappa = 5 \text{ mS cm}^{-1}$). (■) STREAMLINE SP; (●) ZIRCONIA S. 96

- FIG. 6-41: CTI OF *SACCHAROMYCES CEREVISIAE* PULSES (35 ML) IN 40 mM Na_2HPO_4 /CITRIC ACID BUFFER WITH DIFFERENT PH AND CONDUCTIVITY'S THROUGH AN EXPANDED BED OF 10 CM STREAMLINE SP..... 97
- FIG. 6-42: RTD ANALYSIS AT $C_B = 30\%$ (WW) (1:2 DIL. AND $C_B = 15\%$ WW BIOMASS CONCENTRATION). (-) PH 4.0 12 MS CM^{-1} , $C_B = 15\%$ WW; (--) PH 4.0 6.3 MS CM^{-1} , $C_B = 15\%$ WW; (...) PH 3.0 6.3 MS CM^{-1} $C_B = 30\%$ WW. 98
- FIG. 6-43:  YIELD AND  MASS BALANCE OF VARIOUS EBA EXPERIMENTS IN LAB SCALE (STREAMLINE 25 2.5 CM I.D.) AND PILOT SCALE (STREAMLINE 200/ 20 CM I.D.) USING 1:2 DILUTED CULTURE BROTH (15-16 % WW, PH 3.0, 4-5 MS/CM) AND UNDILUTED BROTH (30 % WW; PH 3,0; 12 MS CM^{-1}) MARKED WITH UNDILUTED. FOR ALL EXPERIMENTS A SEDIMENTED BED HEIGHT OF 20 CM WAS USED. 100
- FIG. 6-44: SDS PAGE (COMASSIE BLUE STAINED) ANALYSIS OF VARIOUS FRACTIONS DURING EBA PROCESSING MI3 ON STREAMLINE SP IN PILOT SCALE AS DESCRIBED ABOVE..... 101
- FIG. 6-45: BATCH ISOTHERMS OF HGH ON STREAMLINE DEAE USING CLARIFIED *ESCHERICHIA COLI* HOMOGENATE AT VARIOUS CONDITIONS (■) PH 9 $\kappa = 10$ MS CM^{-1} ; $Q_{\text{MAX EFF.}} = 2.0$ MG ML^{-1} ; (●) PH 9 $\kappa = 5$ MS CM^{-1} $Q_{\text{MAX EFF.}} = 4.0$ MG ML^{-1} (▲) PH 7.5 $\kappa = 5$ MS CM^{-1} . $Q_{\text{MAX EFF.}} = 5.2$ MG ML^{-1} 106
- FIG. 6-46: BATCH ISOTHERMS HGH ON STREAMLINE QXL USING CLARIFIED *ESCHERICHIA COLI* HOMOGENATE AT VARIOUS CONDUCTIVITY'S. (■) PH 9 10 MS CM^{-1} $Q_{\text{MAX EFF.}} = 2.7$ MG ML^{-1} ; (●) PH 9 $\kappa = 5$ MS CM^{-1} $Q_{\text{MAX EFF.}} = 7.5$ MG ML^{-1} ; (▲) PH 9 $\kappa = 15$ MS CM^{-1} $Q_{\text{MAX EFF.}} = 3.8$ MG ML^{-1} 107
- FIG. 6-47: BREAK THROUGH ANALYSIS STREAMLINE DEAE PACKED BED 14.5 CM BED HEIGHT, VELOCITY 300 CM H^{-1} . DATA FITTED USING THE MODEL AFTER HALL ET AL. (1966) USING FOLLOWING CONDITIONS (■) PH 7.5, 5 MS CM^{-1} ; (●) PH 9, 10 MS CM^{-1} ; (▲) PH 9, 5 MS CM^{-1} 108
- FIG. 6-48: CHROMATOGRAM OF THE GRADIENT ELUTION USING 25 mM TRIS HCL PH 7,5 AS BUFFER A AND BUFFER B = BUFFER A + 1M NaCl. GRADIENT 30 CV 0- 50 % B. APPLICATION OF 1.4 MG ML^{-1} AT PH 9 $\kappa = 5$ MS CM^{-1} 109
- FIG. 6-49: SDS PAGE GRADIENT ELUTION COMPARE FIG. 6-48 110
- FIG. 6-50: BIOMASS TRANSMISSION USING BEAD MILL HOMOGENATE (*ESCHERICHIA COLI* MC1061) AND STREAMLINE DEAE AT VARIOUS CONDITIONS. 111

- FIG. 6-51: ζ -POTENTIAL OF *ESCHERICHIA COLI* MC1061 HOMOGENATE SUSPENDED IN TRIS/HCL BUFFER OF VARIOUS pH AND CONDUCTIVITIES. (■) pH 7.0; (●) pH 7.5; (▲) pH 9.0 111
- FIG. 6-52: CTI USING HIGH PRESSURE HOMOGENATE OF *ESCHERICHIA COLI* MC1061 (5 CYCLE AT 965 BAR IN A FRENCH PRESS) AND STREAMLINE DEAE AT pH 8.0 AND $\kappa=10 \text{ MS CM}^{-1}$ 112
- FIG. 6-53: CTI USING PRODUCTION HOMOGENATE AND STREAMLINE DEAE..... 113
- FIG. 6-54: RTD COMPARISON OF FLUIDIZATION PERFORMANCE EMPLOYING HIGH PRESSURE HOMOGENATE FROM THE DUMMY AND THE PRODUCTION STRAIN ($C_B=10\%$ WW) ON A STREAMLINE DEAE COLUMN ($U=300 \text{ CM H}^{-1}$). (-) HOMOGENATE FROM HGH PRODUCTION; (---) HOMOGENATE OBTAINED FROM DUMMY STRAIN; (...) BUFFER..... 114
- FIG. 6-55: ZETA POTENTIAL – pH RELATIONSHIP OF THE HOMOGENATE (5 MS CM^{-1}). CELL DEBRIS SUSPENDED IN NA_2HPO_4 /CITRIC OF VARIOUS pH VALUES AND A CONSTANT CONDUCTIVITY OF $\kappa=5 \text{ MS CM}^{-1}$ 116
- FIG. 6-56: MICROSCOPIC PICTURE OF *ESCHERICHIA COLI* CELL DEBRIS (FROM HGH PRODUCTION) FLOCCULATION AT ACIDIC CONDITIONS SUSPENDED IN 30 mM NA_2HPO_4 /CITRIC ACID BUFFER OF VARIOUS pH AND CONDUCTIVITY (ADJUSTED WITH SOLID NaCl). 117
- FIG. 6-57: CTI *ESCHERICHIA COLI* HOMOGENATE USING STREAMLINE SP XL AT VARIOUS pH AND CONDUCTIVITIES..... 118
- FIG. 6-58: pH DEPENDED SOLUBILITY OF HCP AND HGH AND PURIFICATION FACTOR STARTING WITH UNDILUTED FEEDSTOCK. (■) $C/C_{0 \text{ HGH}}$; (●) $C/C_{0 \text{ TP}}$; (▲) PURIFICATION FACTOR..... 120
- FIG. 6-59: pH DEPENDENT SOLUBILITY OF HCP AND HGH AND PURIFICATION FACTOR USING 1:4 DILUTED FEEDSTOCK. (■) $C/C_{0 \text{ HGH}}$; (●) $C/C_{0 \text{ TP}}$; (▲) PURIFICATION FACTOR 120
- FIG. 6-60: ADSORPTION ISOTHERM SP SEPHAROSE[®] BIG BEADS CLARIFIED HOMOGENATE, 1:4 DILUTED $\kappa=5 \text{ MS CM}^{-1}$. (■) pH 4.0; (●) pH 3.5..... 121
- FIG. 6-61: pH GRADIENT ELUTION OF HGH FROM SP SEPHAROSE BB. APPLICATION AT pH 3.5 $\kappa=5 \text{ MS CM}^{-1}$ 10 CM SED. BED HEIGHT, $U=76 \text{ CM H}^{-1}$. pH GRADIENT ELUTION TITRATED USING 100 mM NA_2HPO_4 TO LOWER THE pH IN 30 CV. 122

FIG. 6-62: SDS-PAGE ANALYSIS OF HGH pH GRADIENT ELUTION. SAMPLE ASSIGNMENT SEE FIG. 6-61.	123
FIG. 6-63: SDS PAGE ANALYSIS OF ATPS SYSTEMS. PEG HAS BEEN REMOVED FROM THE TOP PHASE USING PD10 COLUMNS (2.5 ML SAMPLE WAS ELUTED IN TWO 3.5 ML FRACTIONS).....	125
FIG. 6-64: CROSS FLOW FILTRATION SARATORIUS SARTOCON [®] II MINI MODULE 30 kDA CUT OFF POLYSULFON MEMBRANE THE VOLUME HAS KEPT CONSTANT AT 600 ML BY SUPPLEMENTING THE FILTRATED VOLUME BY 25 mM TRIS/HCL pH 7,5. THE INLET PRESSURE HAS BEEN ADJUSTED BY INCREASING THE CROSS FLOW. (■) TRANS MEMBRANE FLUX; (●) TRANS MEMBRANE PRESSURE; (▲) CROSS FLOW.	129
FIG. 6-65: VISCOSITY OF THE LIQUID PHASE DURING ATPS AND ULTRA FILTRATION. THE ATPS TOP PHASE WAS CROSS FLOW FILTRATED (FIG. 6-64) THE FILTRATED VOLUME WAS SUPPLEMENTED BY 25 mM TRIS/HCL pH 7,5 UNTIL 2 TIMES OF THE INITIAL TOP PHASE VOLUME WAS PASSED THROUGH THE MEMBRANE.	129
FIG. 7-1: ÄKTA [™] FLOWPATH FOR FAST DESALTING STEP.	145
FIG. 7-2: ÄKTA [™] FLOW PATH FOR FAST MONO Q ANION EXCHANGE STEP.....	146
FIG. 7-3: UNICORN METHOD BREAKTHROUGH ANALYSIS	154
FIG. 7-4: EXPERIMENTAL SETUP OF PULSE-RESPONSE EXPERIMENT	162
FIG. 7-5: EXPERIMENTAL SET-UP OF RTD MEASUREMENT.	165
FIG. 7-6: FEED & DISSOLVED OXYGEN CONTROL SEQUENCE (IRIS).....	170
FIG. 8-1: TANKS IN SERIES MODEL	179
 b TABLES	
TABLE 4-1: SYMBOLS	4
TABLE 4-2: GRECIAN LETTERS.....	6
TABLE 4-3: ABBREVIATIONS	8
TABLE 5-1: COMMONLY USED ION EXCHANGE LIGANDS (JANSON AND RYDEN, 1998)...	18
TABLE 5-2: TRANSPORT MECHANISM IN DEEP BED FILTRATION	28
TABLE 5-3: COMMON TECHNIQUES FOR PARTICLE SIZING	30
TABLE 5-4: MAJOR COMPONENTS OF <i>SACCHAROMYCES CEREVISIAE</i> CELL WALLS (LIPKE AND OVALLE, 1998).	39
TABLE 5-5: PROCESS VARIABLES OF AGITATOR BALL MILL (KULA AND SCHÜTTE, 1987)	43

TABLE 5-6: FDH PURIFICATION PROTOCOL AND IMPLEMENTATION OF EBA.....	50
TABLE 6-1: FEEDSTOCK CHARACTERISTIC DEPENDING ON THE CELL DISRUPTION METHOD	67
TABLE 6-2: PARAMETER OF PDE ANALYSIS USING PILOT SCALE HIGH PRESSURE HOMOGENATE	82
TABLE 6-3: FEEDSTOCK PROPERTIES OF PILOT SCALE BEAD MILL HOMOGENATE (0,5 MM GLASS BEADS, 2500 RPM, NETZSCH LAB STAR BEAD MILL)	82
TABLE 6-4: MINIMUM SIZE AFTER FRENCH PRESS HOMOGENIZATION AT VARIOUS OPERATION PRESSURES.	84
TABLE 6-5: FEEDSTOCK PROPERTIES OF MI3 CAPTURE (WHOLE BROTH CONTAINS 30-35 % WW CELLS BEFORE DILUTION).....	89
TABLE 6-6: CONVENTIONAL PURIFICATION PROTOCOL AND IMPLEMENTATION OF EBA (MOLLERUP <i>ET AL.</i> , 1999).....	90
TABLE 6-7: MODELING PARAMETER OBTAINED BY FITTING THE EXPERIMENTAL RESULTS TO THE PDE MODEL.....	99
TABLE 6-8: PROCESS CONDITIONS FOR THE RECOVERY OF INSULIN PRECURSOR M3 USING EBA.	99
TABLE 6-9: PRODUCT CONCENTRATION BEHAVIOUR OF THE SCALE UP EXPERIMENT.....	101
TABLE 6-10: CONVENTIONAL PROCESS AND THE IMPLEMENTATION OF EBA	104
TABLE 6-11: FEEDSTOCK PROPERTIES OF HGH PRODUCTION	105
TABLE 6-12: ADSORPTION DATA ON STREAMLINE DEAE OBTAINED DURING PACKED BED STUDIES.	108
TABLE 6-13: PDE EVALUATION OF FIG. 6-54.	114
TABLE 6-14: HGH AND TOTAL PROTEIN CONCENTRATIONS FOR VARIOUS PROCESS STEPS	123
TABLE 6-15: COMPOSITION OF ATPS 22 % PEG (MW SEE TABLE.) 13.63 % K_2HPO_4 , 2.37 % KH_2PO_4 , 50 % FEEDSTOCK (PH APP. 8.6).....	124
TABLE 6-16 ATPS WITH DECREASED PHOSPHATE CONCENTRATION AS A MIXTURE OF 85.2 % K_2HPO_4 AND 14.8 % KH_2PO_4 WAS USED. TO REACH A PH OF 8.6.	125
TABLE 6-17: ATPS WITH HIGHER MW PEG AND MIXTURES (PARTITIONING OF THE CELL DEBRIS AND HGH)	126
TABLE 6-18: PH AND CONDUCTIVITY OF DIFFERENT DILUTED ATPS TOP PHASES	127

TABLE 6-19:.....	130
TABLE 7-1: CHEMICALS.....	132
TABLE 7-2: CHROMATOGRAPHY RESINS	133
TABLE 7-3: CHEMICALS FOR CELL CULTIVATION.....	133
TABLE 7-4: CONSUMABLES	134
TABLE 7-5: EQUIPMENT.....	135
TABLE 7-6 CHROMATOGRAPHY SYSTEMS AND COLUMNS.....	137
TABLE 7-7 MICROORGANISM.....	138
TABLE 7-8: GRADIENT ELUTION-PROTOCOL:	142
TABLE 7-9: GRADIENT ELUTION- PROTOCOL:.....	146
TABLE 7-10.....	164
TABLE 8-1: PEAK ANALYSIS EVALUATED BY THE INTENSITY.....	185
TABLE 8-2: RAW DATA OF THE SIZE DISTRIBUTION (INTENSITY) WHOLE CELLS AND LAB BEAD MILL HOMOGENATE.	185
TABLE 8-3: : RAW DATA OF THE SIZE DISTRIBUTION (INTENSITY) FRENCH PRESS AND ULTRASOUND HOMOGENATE	186
TABLE 8-4: PEAK ANALYSIS EVALUATED BY THE INTENSITY.....	187
TABLE 8-5: RAW DATA OF THE SIZE DISTRIBUTION (INTENSITY).....	187
TABLE 8-6: RAW DATA OF THE SIZE DISTRIBUTION (INTENSITY).....	188
TABLE 8-7: PEAK ANALYSIS EVALUATED BY THE INTENSITY.....	189
TABLE 8-8: RAW DATA OF THE SIZE DISTRIBUTION OPERATION PRESSURE P = 482 BAR (INTENSITY)	189
TABLE 8-9: RAW DATA OF THE SIZE DISTRIBUTION (INTENSITY).....	190
TABLE 8-10: PEAK ANALYSIS EVALUATED BY THE INTENSITY 965 BAR.....	191
TABLE 8-11: RAW DATA OF THE SIZE DISTRIBUTION 965 BAR (INTENSITY).....	192
TABLE 8-12: RAW DATA OF THE SIZE DISTRIBUTION 965 BAR (INTENSITY).....	193
TABLE 8-13: PEAK ANALYSIS EVALUATED BY THE INTENSITY.....	194
TABLE 8-14: RAW DATA OF THE SIZE DISTRIBUTION (INTENSITY).....	194
TABLE 8-15: RAW DATA OF THE SIZE DISTRIBUTION (INTENSITY).....	195
TABLE 8-16: PEAK ANALYSIS EVALUATED BY THE INTENSITY.....	197
TABLE 8-17: RAW DATA OF THE SIZE DISTRIBUTION (INTENSITY).....	197
TABLE 8-18: PEAK ANALYSIS EVALUATED BY THE INTENSITY.....	198

TABLE 8-19: RAW DATA OF THE SIZE DISTRIBUTION (INTENSITY).....	199
TABLE 8-20: RAW DATA OF THE SIZE DISTRIBUTION (INTENSITY).....	200
TABLE 8-21: PEAK ANALYSIS EVALUATED BY THE INTENSITY.....	201
TABLE 8-22: RAW DATA OF THE SIZE DISTRIBUTION (INTENSITY).....	201
TABLE 8-23: PEAK ANALYSIS EVALUATED BY THE INTENSITY <i>SACCHAROMYCES CEREVISIAE</i> 300 BAR.....	202
TABLE 8-24: RAW DATA OF THE SIZE DISTRIBUTION (INTENSITY) <i>SACCHAROMYCES</i> <i>CEREVISIAE</i> 300 BAR.....	202
TABLE 8-25: RAW DATA OF THE SIZE DISTRIBUTION (INTENSITY).....	203
TABLE 8-26: PEAK ANALYSIS EVALUATED BY THE INTENSITY <i>SACCHAROMYCES CEREVISIAE</i> 482 BAR.....	204
TABLE 8-27: RAW DATA OF THE SIZE DISTRIBUTION (INTENSITY) <i>SACCHAROMYCES</i> <i>CEREVISIAE</i> 482 BAR.....	204
TABLE 8-28: RAW DATA OF THE SIZE DISTRIBUTION (INTENSITY) <i>SACCHAROMYCES</i> <i>CEREVISIAE</i> 482 BAR.....	205
TABLE 8-29: PEAK ANALYSIS EVALUATED BY THE INTENSITY <i>SACCHAROMYCES CEREVISIAE</i> 965 BAR.....	205
TABLE 8-30: RAW DATA OF THE SIZE DISTRIBUTION (INTENSITY) <i>SACCHAROMYCES</i> <i>CEREVISIAE</i> 965 BAR.....	206
TABLE 8-31: RAW DATA OF THE SIZE DISTRIBUTION (INTENSITY) <i>SACCHAROMYCES</i> <i>CEREVISIAE</i> 965 BAR.....	206
TABLE 8-32: PEAK ANALYSIS EVALUATED BY THE INTENSITY <i>SACCHAROMYCES CEREVISIAE</i> 2068 BAR.....	207
TABLE 8-33: RAW DATA OF THE SIZE DISTRIBUTION (INTENSITY) <i>SACCHAROMYCES</i> <i>CEREVISIAE</i> 2068 BAR.....	207
TABLE 8-34 ATPS WITH DECREASED SLAT CONCENTRATION AS SALT A MIXTURE OF 85,2 % K_2HPO_4 AND 14,8 % KH_2PO_4 WAS USED.	208
TABLE 8-35: ATPS WITH HIGHER MW PEG AND MIXTURES	208

3 ABSTRACT (GERMAN)

In den letzten Jahren hat sich die Fliessbettadsorption (EBA) zu einer etablierten Methode in der Aufarbeitung biologischer Produkte entwickelt. Unter Ausbildung eines perfekt klassierten Fließbettes (auch **Expanded Bed Adsorption** oder kurz EBA genannt) ist eine adsorptive Aufreinigung biotechnologischer Produkte direkt aus feststoffbelasteten Rohlösungen, wie z.B. Zellsuspensionen oder Zellhomogenaten, möglich (Thömmes, 1997). Mit der Einführung von Feststoffen in das System wird diese Art der Chromatographie deutlich komplexer im Vergleich zur Festbettchromatographie. Die eingebrachten Feststoffe (Zellen, Zelltrümmer,...) können während der Applikation mit dem Adsorber wechselwirken, wodurch es zur Ausbildung von Biomasse/Adsorber Aggregaten kommen kann. Dies wiederum führt zu nicht durchströmten Totzonen, Kanalbildung und kann im Extremfall zum vollständigen Zusammenbruch des Fließbettes führen (Feuser *et al.*, 1999, Fernández-Lahore *et al.*, 1999, Fernández-Lahore *et al.*, 2000). Derartige Probleme sind in der Literatur hauptsächlich für Anionenaustausch Chromatographie beschrieben (Draeger and Chase, 1991, Fernández-Lahore *et al.*, 1999, Fernández-Lahore *et al.*, 2000, Feuser *et al.*, 1999, Lin *et al.*, 2001) – welche häufig für die ersten Isolierungsschritte eingesetzt wird. Wie bereits von Lin *et al.* (2003) gezeigt kann hier insbesondere von elektrostatischen Wechselwirkungen zwischen Biomasse und Adsorber ausgegangen werden. Aufgrund der kommerziellen Bedeutung intrazellulär expremierter Proteine beschäftigt sich der erste Teil dieser Arbeit hauptsächlich mit der Biomasse/Adsorber Interaktion während der Anionenaustausch Chromatographie beim Einsatz verschiedener Zellhomogenate. Bei Vergleich von *Escherichia coli* Homogenaten resultierend aus verschiedenen Standard Aufschlusstechniken zeigten sich deutliche Unterschiede im Hinblick auf die Viskosität, die Partikelgrößenverteilung der Zelltrümmer und der netto Oberflächenladung. Alle drei Parameter nahmen in folgender Reihenfolge Kugelmühle > Ultraschall > French Press signifikant ab. Die Viskosität kann hierbei direkt mit der Molekulargewichtsverteilung der DNA korreliert werden. Proben höherer Viskosität enthalten mehr hochmolekulare DNA als Proben niedriger Viskosität.

In gleicher Reihenfolge konnte auch eine Zunahme der Zell Transmission (CTI, ein Maß für die Stärke der Biomasse/Adsorber Interaktion, hohe CTI Werte \Rightarrow niedrige Biomasse Interaktion) im Fließbett festgestellt werden.

Die Zunahme des CTI konnte bei weiterführenden Untersuchungen verschiedener French Press Homogenate direkt mit der Abnahme der mittleren Partikelgrößenverteilung korreliert werden. Die mittlere Partikelgrößenverteilung der Zelltrümmer ist wiederum eine direkte Funktion der Anzahl der Aufschluss Zyklen und des verwendeten Druckes, bis ein Minimum erreicht ist. Gleiches gilt für die Oberflächenladung. Mit kleiner werdenden Partikeln nimmt auch die netto Oberflächenladung der Zelltrümmer ab. Für Gram⁻ Bakterien wie *Escherichia coli* kann dies durch die asymmetrische Zellwandstruktur erklärt werden. Die negative Oberflächenladung ganzer Zellen resultiert hauptsächlich aus der stark negativ geladenen Lipopolysaccharidschicht der äußeren Zellmembran. Nach Zellaufschluss gewinnt die neutrale innere Zellmembran an Bedeutung für die Gesamtladung der Zelltrümmer, wodurch die Nettoladung abnimmt. Ferner konnte gezeigt werden, dass zur mechanistischen Erklärung der Biomasse Interaktion auf theoretische Grundlagen der Tiefenfiltration zurückgegriffen werden kann. Versteht man ein Fließbett als einen höchst ineffizienten Tiefenfilter mit vergrößertem Zwischenkornvolumen so kann die Biomasse/Adsorber Wechselwirkung auf zwei grundlegende Mechanismen zurückgeführt werden. Zum einen den Transport des Biomassepartikels zur Adsorber Oberfläche und zum zweiten die Adsorption am Adsorber. Der Sperreffekt kann für die Bedingungen wie sie im Fließbett vorliegen als grundlegender Transportmechanismus angesehen werden und für die Anionen Austausch Chromatographie kann man von elektrostatischen Wechselwirkungen als Adsorptionsmechanismus ausgehen. Für beide Mechanismen besteht eine direkte Abhängigkeit von der Partikelgröße wobei, die elektrostatische Wechselwirkung zusätzlich von der Oberflächenladung abhängt. Verringert man nun durch geeignete Aufschlussbedingungen sowohl die mittlere Partikelgrößenverteilung als auch die Nettoladung der Zelltrümmer kann damit die Biomasse Interaktion im Fließbett deutlich reduziert werden. Es konnte weiterhin eine lineare Korrelation zwischen einem Parameter ($-\zeta_b \zeta_{ax}$) bestehend aus dem negativen Produkt der ζ -Potentiale von Zelltrümmer und Adsorber und dem CTI gezeigt werden. Erste Ergebnisse weisen darauf hin, dass diese Korrelation unabhängig von der

verwendeten Biomasse (*Saccharomyces cerevisiae* oder *E. coli*) ist. Unter Verwendung dieses Parameters kann ausgehend von messbaren Parametern der Biomasse Suspension (Partikelgrößenverteilung und ζ -Potential) unter definierten Bedingungen (pH, Leitfähigkeit) auf die Biomasse/Adsorber Interaktion im Fließbett geschlossen werden. Mit einem optimierten Zellaufschluss können gegebenenfalls auch stark interagierende Systeme verarbeitet werden.

Im zweiten Teil der Arbeit wurden die Entwicklungen zweier Aufarbeitungsprozesse gezeigt, die sich besonders mit der Optimierung des ersten Isolierungsschrittes beschäftigen. Für einen rekombinanten Insulin Precursor (MI3), exprimiert in *Saccharomyces cerevisiae*, wurde ein effizienter Fließbettprozess entwickelt. Mittels Kationen Austauschchromatographie im Fließbett ist es nun möglich, den Insulin Precursor MI3 direkt aus dem Kulturüberstand zu isolieren. Somit gelang es insgesamt sechs Verfahrensschritte des bestehenden Aufarbeitungsprozesses (drei Zentrifugationsschritte, ein chromatographischer Schritt, eine Filtration und ein Kristallisationsschritt) in einen einzigen Fließbettschritt zu integrieren. Biomasse/Adsorber Interaktion war eines der Hauptprobleme beim Einsatz der Fließbettadsorption zur Aufarbeitung eines rekombinanten Precursor des menschlichen Wachstumshormons hGH aus *Escherichia coli* Homogenat, die vermutlich durch Optimierung der Aufschlussmethode hin zu kleineren Partikelgrößenverteilung und geringerer Nettoladung der Zelltrümmer minimiert werden kann. Als Alternative zur Fließbettadsorption wurden noch Verfahren wie Präzipitation mit anschließender Kationenaustausch Chromatographie und wässrigen Extraktion in Zweiphasen Systemen (ATPS) untersucht. Hierbei konnte mit der Kombination von ATPS und anschließender Ultrafiltration ein effizienter Prozess mit einer Gesamtausbeute über beide Schritte von 84 % entwickelt werden.

4 SYMBOLS & ABBREVIATIONS

Table 4-1: Symbols

Symbol	Description	Unit
A	area	(-)
c	concentration	mg*L ⁻¹
C ₀	initial concentration	g*L ⁻¹
C _b	biomass Concentration in wet weight	%
C _{eq}	equilibrium concentration	g*L ⁻¹
d	average size of the adsorbent	nm
E	sorption efficiency	(-)
e	elementary charge e= 1.6022*10 ⁻¹⁹	C
k _A	Langmuir constant	m ³ *kg ⁻¹
k _b	Boltzmann constant k= 1,3807*10 ⁻²³	J*K ⁻¹
L	bed length	m
m ₀	0 th moment of RTD	(-)
m ₁	1st moment of RTD	(-)
m ₂	2nd moment of RTD	(-)
m _k	kth moment of RTD	(-)
N _A	Avogardo constant N _A = 6,023*10 ²³	mol ⁻¹
N _R	dimensionless group for Interception mechanism	(-)
Q	capacity of the stationary phase	mg*ml ⁻¹
Q _{dyn.}	dynamic capacity at 10 % breakthrough	mg*ml ⁻¹
Q _{eq}	equilibrium capacity	mg*ml ⁻¹

Q_{\max}	maximal isothermal binding capacity	$\text{mg}\cdot\text{ml}^{-1}$
$Q_{\max \text{ eff}}$	maximum equilibrium capacity effective at certain product concentration	$\text{mg}\cdot\text{ml}^{-1}$
T	absolute temperature [K] $25^{\circ}\text{C} = 298 \text{ K}$	K
U	linear velocity	$\text{cm}\cdot\text{h}^{-1}$
V_L	volume of the liquid phase	L
V_s	dumping volume of the stationary phase	ml
x	biomass particles	nm
x	z-average (average size of a biomass particle)	nm
z	valenz of an ion	(-)
U_t	free settling velocity	$\text{m}\cdot\text{s}^{-1}$
g	gravity = 9,81	$\text{m}\cdot\text{s}^{-2}$
$A_{\text{input-pulse}}$	Area of the input pulse in the pulse response experiment	(-)
$A_{\text{pulse-response}}$	Area of the pulse response in the pulse response experiment	(-)
N	Mass transfer Parameter between well fluidized and stagnant zones in an expanded bed according the PDE model	(-)
N_p	Plate number	(-)
Re	Reynolds number $\text{Re} = \frac{U \cdot d \cdot \rho_l}{\eta}$	(-)
N_I	dimensionless ratio of inertia	(-)
N_G	dimensionless ratio of gravity	(-)
N_R	dimensionless ratio of interception	(-)
a, e_i	empiric constants	(-)

D_a	axial diffusion coefficient	m^2*s^{-1}
Pe	Peclet Number = $Bo = U*L/D_a$	(-)
Bo	see Pe	
d_{max}	maximal particle diameter	m
d_{min}	minimal particle diameter	m
v	velocity	$m*s^{-1}$
E_l	Electric field	
R_p	Fractional release of soluble protein	
k_l	Rate constant	$[MPa^{-1}]$
a	pressure exponent (depends on the microorganism and the growth conditions)	(-)
N_{pa}	Number of passes	(-)
P	operation pressure	(MPa)

Table 4-2: Grecian letters

Symbol	Description	Unit
ϵ_r	relative permittivity of the media $\epsilon_{water} = 78,2$	(-)
ϵ_0	permittivity of free space = 8.85×10^{-12}	$J^{-1}*C^2*M^{-1}$
η	Viscosity	mPa
κ	conductivity	$mS*cm^{-1}$
τ	mean residence time	(-)
ψ_d	electrostatic surface potential of the adsorbent	V
ζ	zeta potential	mV
ζ_a	zeta potential of adsorbent	mV

ζ_b	zeta potential of biomass (cells, cell debris)	mV
τ	mean residence time	(-)
σ	variance; dimensionless variance of RTD	(-)
μ_k	kth normalized moment of Residence time distribution	(-)
ρ_p	Density of the adsorbent particle	g*L
ρ_l	Liquid density	g*L
Θ	dimensionless time $\Theta = t/\tau$	(-)
τ	hydrodynamic residence time	s
γ	separation efficiency	(-)
γ_T	transport probability	(-)
γ_A	attachment probability	(-)
Ψ_x	electrostatic surface potential of the biomass particle	V
κ_d	reciprocal value of the Debye-Hückel-parameter	nm
ϵ	dielectric constant of the medium $\epsilon = \epsilon_r * \epsilon_0$, ϵ_0 : permittivity of free space ($8.85 \times 10^{-12} \text{ J}^{-1} \text{ C}^2 \text{ M}^{-1}$) & $\epsilon_r =$ relative permittivity of the media	
$f(\kappa a)$	correlation factor regarding the thickness of the double layer and particle diameter	
μ_E	electrophoretic mobility	

Table 4-3: Abbreviations

EBA	expanded bed adsorption
RTD	residence time distribution
IEC	ion exchange chromatography
HIC	hydrophobic interaction chromatography
AC	affinity chromatography
aa	amino acids
CTI	cell transmission index

5 INTRODUCTION

5.1 DOWNSTREAM PROCESSING

“The most cost intensive part in the biotechnological production of a bioproduct, about 50-80 % of the total production cost, account for the Downstream Processing. Increasing competition and the new challenges of recombinant DNA-based techniques or tissue culture techniques in the industry have triggered the development of novel separation technologies.” (Gupta and Mattiasson, 1994).

Biotechnological process fluids are generally of complex nature containing solids particles of various sizes, as well as solutes of various molecular masses and chemistry (Thömmes, 1997, Anspach *et al.*, 1999). The required purity of products in the biotechnological industry ranges from a crude but concentrated culture broth to a purity demand of greater than 99.999 % in case of a therapeutic protein used for frequent injection. A direct consequence of the latter is that purification processes comprise several low and high resolution steps, the number of steps and their complexity depending on the desired product purity (Wheelright, 1991). For high purity products step numbers between 7 and 14 can be found in literature (Wheelright, 1991, Fish and Lilly, 1984, Bonnerja *et al.*, 1986). With each additional step or unit operation product is lost and the overall yield decreases (Fig. 1-1). Thus, assuming an average step yield of 95%, approximately 40% of the product will be lost after 10 steps.

During the development of a pharmaceutical processes two phases can be distinguished. The early phase is dominated by a tight time schedule, the so called ‘time to market’ becoming the most important factor. The success the process in the second phase depends on the economy of the final production process (Ditz, 2002). The latter is directly related to the efficiency and thus productivity of the unit operations employed.

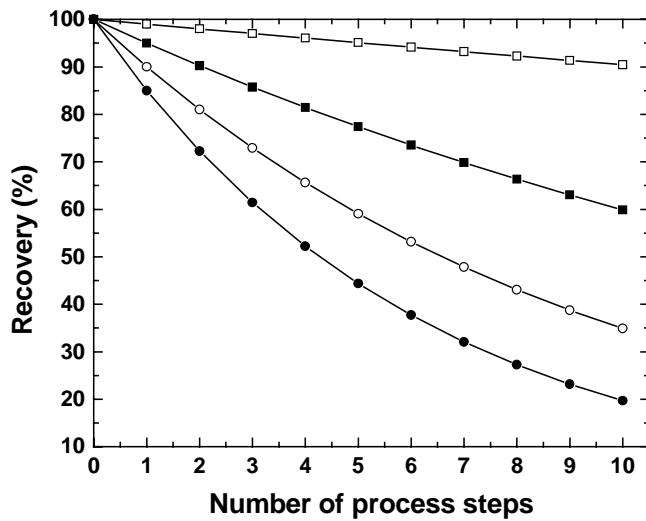


Fig. 5-1: Impact of the number of unit operations employed during downstream processing assuming a given yield per step: 99% (□); 95% (■); 90% (○); 85% (●) (Fish and Lilly, 1984).

Traditionally, downstream processing schemes (see Fig. 5-2) can be divided into three sections, each aiming at a distinct separation task within the overall process (Asenjo, 1990, Wheelwright, 1987). The objective of the capture steps is to isolate the desired product, to remove the major contaminant -which is water- and to stabilize the product against adverse conditions (proteases, glycosidases, oxidizing agents) in the culture liquor to avoid product degradation. The focus of primary capture lies on a fast process with a high recovery and high capacities at the expense of resolution. The most common technique is ion exchange chromatography using comparatively large adsorbent particles to allow high linear velocities for fast processing to avoid product degradation. Especially product degradation causes significant problems in the further downstream process. Due to the similarity of the degradation products with the desired protein the separation becomes more difficult and requires additional process steps resulting in a decreased product yield, so a fast and efficient primary capture step is crucial for the whole process performance. For the next steps the intermediate purification and for the polishing steps the resolution of the desired method becomes more and more important, while the importance of speed, capacity and recovery decreases. Especially for pharmaceutical products it is of an extraordinary importance to remove all impurities and end up with a highly purified product (Biosciences, 1999).

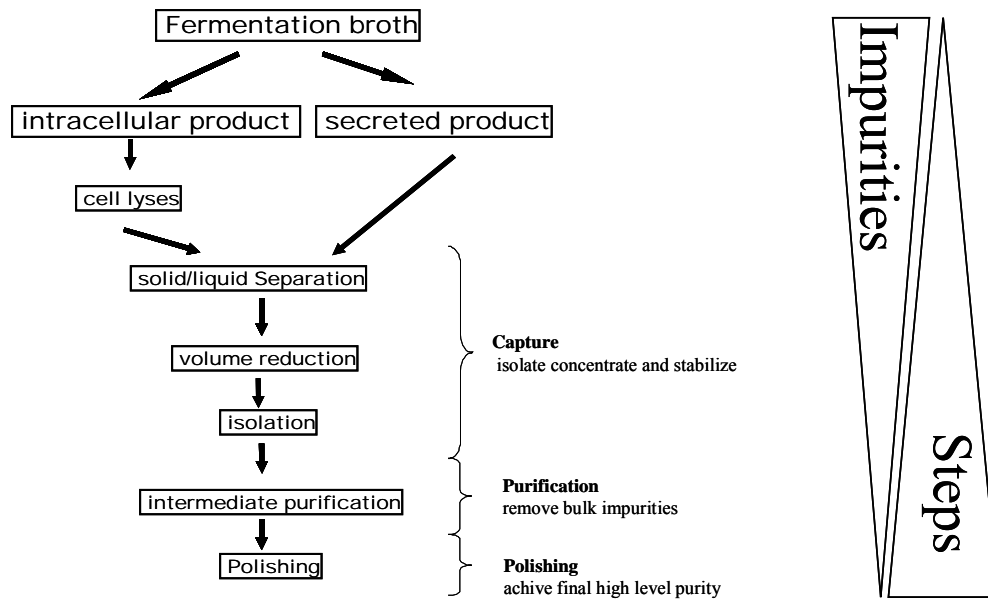


Fig. 5-2: Downstream processing scheme

From the above it becomes clear that the productivity and efficiency of unit operations employed for initial product capture play an important role regarding the success of a downstream process. The objective of capture steps is to isolate the desired product and generate a concentrated feedstock for successive high resolutions steps. A necessary prerequisite for the application of high resolution steps is, however, the complete removal of particulates in the process liquor.

Thus, unit operations aiming at a solid-liquid separation are normally applied right upfront. Standard protocols used at lab scale for clarification and removal of solids are usually comparatively quick and easy to follow. Common clarification methods are centrifugation and micro filtration. Datar and Rosen (1996) showed that centrifugation is a very efficient method for clarification up to very large scale for process liquors containing relatively large particulates such as yeast cells. The performance is rapidly reduced with decreasing particle size (bacterial cells or cell homogenates). Besides shear sensitive organisms like mammalian cells might be damaged in a centrifugal field as described by Kempken *et al.* (1995). Cross flow filtration as an alternative is well established up to production scale for eucaryotic and prokaryotic systems whole broth as well as for homogenates, but suffers from comparatively low steady state liquid flux rates due to fouling of the membrane by small particles, lipids or nucleic acids. High membrane costs limits the scale of operation. At high product concentration as achieved when using recombinant DNA technology irreversible adsorption of the protein of interest may also result in a reduced product yield (Thömmes, 1997).

In order to reduce the number of unit operations recent developments are focused on integrated purification processes, combining direct product capture and efficient solid-liquid separation. The most prominent unit operations are aqueous two phase extraction (ATPS) and expanded bed adsorption (EBA).

5.1.1 EXTRACTIVE SEPARATION

ATPS is based on the incompatibility of two different hydrophilic polymers (i.e. polyethylenglycol/dextran) in the common solvent water separating into two aqueous phases. One of the polymers can also be replaced by a multivalent lyotropic salt (phosphate, citrate, sulphate). Depending on the respective properties of the aqueous phases and the substances present in the process liquor a situation might be reached where cells, cell debris and contaminants present in solution distribute predominately in one phase while the actual product remains in the other phase. ATPS is usually put in the early phase of an isolation process, using cell homogenates or whole culture broth, since it allows the concomitant removal of solids, a product enrichment and concentration in a single step (Hustedt *et al.*, 1985, Hustedt *et al.*, 1988).

5.1.2 ADSORPTIVE SEPARATIONS

a SINGLE STAGE EQUILIBRIUM – REACTORS BASED ON IDEAL BACK MIXING

The direct capture of products from solid containing feedstocks employing adsorptive processes is long known (Thömmes *et al.*, 1997). The most simple process set-up is based on a batch adsorption of the product in stirred tanks containing the crude process liquor and a suitable adsorbent. Following product capture the adsorbent is separated from the broth, washed and eluted. This method has been described for the recovery of various proteins and antibiotics (Brummelhuis, 1980, Krützfeldt *et al.*, 1992, Roe, 1987). In order to ease the separation of solids from the product loaded adsorbents fluidized beds were used. Bartels *et al.* (1958) employed this technique for the adsorptive recovery of the secondary metabolite streptomycin. Another process integrating primary capture and solid liquid separation arises in the combination of modified non-porous magnetic adsorbents to capture the product in batch adsorption mode followed by their separation using high gradient magnetic separation (Hubbuch *et al.*, 2001b, Hubbuch, 2000). The potential advantage of this process lies in its robustness as product adsorption and the recovery of the product loaded adsorbents are uncoupled and thus the degree of freedom increased in the speed of processing, and the ease of

scalability. The use of non-porous adsorbents allows rapid adsorption, and the recovery of product loaded adsorbents allows processing rates 10 fold higher than found in fluidized beds. The technology is still under development. All approaches have in common that, due to an ideal mixing, only one adsorptive stage is realized leading often to an inefficient product capture.

b MULTIPLE PLATE ADSORPTION

Expanded Bed Adsorption (EBA) is based on a controlled and stable fluidization of specially designed chromatographic adsorbents. The incentive is to allow cells and cell debris to pass freely through the column, while at the same time perform a chromatographic capture step of the product from the crude process liquor. EBA is an integrated separation technology combining solid-liquid separation, product concentration and initial purification in a single unit operation. The development was triggered by Chase and co-workers in the beginning of 1990 trying to adapt chromatographic processes to crude process liquors. Since then EBA has been developed into an important technology for primary capture. The different aspects of this technology have been described in various reviews (Anspach *et al.*, 1999, Chase, 1994, Thömmes, 1997). Furthermore a detailed strategy for EBA process design has been developed in order to allow feasibility studies based on a few simple experiments enabling a rapid and rational process development (Lin *et al.*, 2001, Thömmes, 1999).

5.1.3 STABLE FLUIDIZATION

In an expanded bed a liquid stream directed upwards will fluidize the adsorbent particles. This stream increases the void fraction of the adsorbent bed allowing particulates present in the feed to pass freely through the interstitial volume of the bed (Thömmes, 1997, Chase, 1994). In contrast to a well mixed fluidized bed, however, the choice of special resins reduces the dispersion or back mixing of the adsorbents in the column creating a situation close to packed beds with multiple adsorption stages. The stabilization of the bed can be reached by several techniques such as multi stage operation (Agosto *et al.*, 1993), magnetic stabilization (Burns and Graves, 1985) or hydrodynamic stabilization (Chase, 1994, Draeger and Chase, 1990). The latter being the method of choice in present systems.

a ADSORBER DESIGN

The position of an adsorbent particle within a expanded bed – in a first approximation – is determined by the gravitational force and the buoyancy drag force of the fluid. The settling velocity can be calculated by the Stokes law (Eq. 5-1).

Stokes Law

$$U_t = \frac{d^2 (\rho_p - \rho_l) g}{18\eta} \quad (\text{Eq. 5-1})$$

U_t :	Settling velocity	(m*s ⁻¹)
d :	Particle size	(nm)
ρ_p :	Particle density	(g*L ⁻¹)
ρ_l :	liquid density	(g*L ⁻¹)
η :	viscosity	(Pa*s)

From (Eq. 5-1) it becomes evident that the position of a single adsorbent particle is mainly determined by its size (d) and density (ρ_p). The application of mono-disperse adsorbents would therefore lead to a high degree of back-mixing as all adsorbents would have approximately the same fluidization properties. But a reduction of the back-mixing within the bed can be reached by using adsorbents with a well defined gradient of size and or density. The successive classification of the adsorbent particles during fluidization will thus lead to a situation where the larger particles are located closer to the bottom of the bed, while the smaller and lighter ones will be distributed towards the top of the bed (see Fig. 5-3). In this context it was found by Al-Dibouni and Garside (1975) that an ideal classified fluidization arises for a diameter ratio of the adsorbents d_{\max}/d_{\min} greater 2.2. A stable classified bed is termed expanded bed as opposed to randomly fluidized beds.

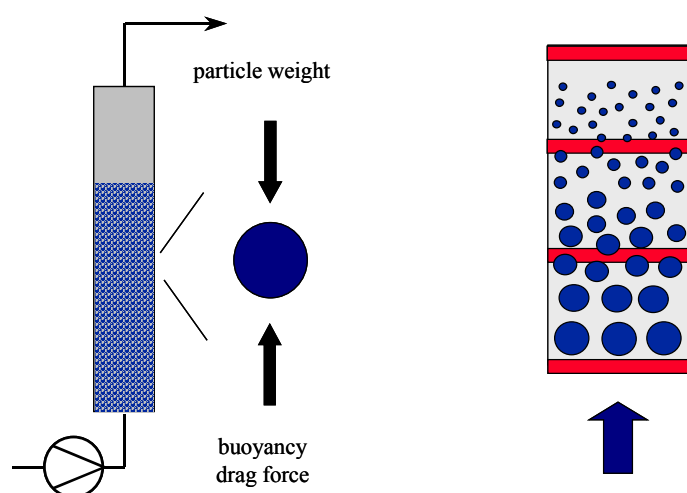


Fig. 5-3: Perfectly classified expanded bed

Conventional chromatographic adsorbents, even though exhibiting a considerable size distribution, are designed for an application in packed beds and thus not optimized for the use in EBA. Due to their low density of approximately 1131 kg m^{-3} measured for agarose adsorbents (Draeger and Chase, 1991) only limited linear fluid velocities are applicable, i.e. 222 cm h^{-1} for buffer systems without biomass (Chase and Draeger, 1992, Thömmes, 1997). For crude process liquors with higher viscosities and large amounts of cells or cell debris, usable flow rates were even lower. As a consequence special EBA adsorbents have been developed exhibiting a distinct size ratio and a significant increase in density. The latter was realized by either using different resin backbones like zirconium dioxide (Voute *et al.*, 1999) (BioSeptra, Ciphergene, USA) or by incorporation of density enhancers like glass, quartz, stainless steel or tungsten carbide in agarose based matrices (Streamline™ Amersham Biosciences, Uppsala, Sweden, FastLine® Upfront, Copenhagen, Denmark). Today special designed EBA adsorbents are commercially available for various kinds of chromatographic processes.

b DISPERSION IN EXPANDED BEDS

As pointed out above the incentive during the development of expanded bed adsorption has been the reduction of back mixing or the dispersion during fluidization. Dispersion can be contributed to various parameters (Thömmes, 1999). The diffusion of the solutes might contribute to the overall dispersion but can be regarded as negligible for proteins due to the low diffusivity with a diffusion coefficient of $D < 10^{-11}$. System properties such as tubing, detector, pump etc are fixed for a given system and can be minimized by a proper set-up. The most prominent factor in dispersion is thus non-ideal flow of the mobile phase due to fluidisation

properties in the expanded bed. The quantification of dispersion in a fluidized bed can be carried out analogous to the analysis of reactor systems in the process industries, by analyzing the residence time distribution (RTD) of a step or pulse signal applied at the inlet of the system (Levenspiel, 1972).

By plotting the E (Θ)-function of the output signal versus the dimensionless time (Θ) the normalized moment of RTD can be calculated (see Appendix). Characterizing the RTD according to the dispersion model Eq. 5-2 yields a dimensionless number, which describes the dispersion within the bed. Traditionally this technique has been applied to evaluate dispersion in systems used in the processing industry and thus the dimensionless number has been termed differently for different systems. The exact term describing the dispersion in mass transfer investigations would be the Bodenstein number, while the equivalent in heat transfer studies is termed the Peclet number. Even though these terms do not strictly apply for fluidized systems, both terms are found in EBA literature to describe the dispersion in the fluidized beds and are also used in this work. It is however recognized that the mechanistically correct term would be ‘the inverse of the vessel dispersion number’ as pointed out by Levenspiel (1972).

The influence of various system parameters such as fluid velocity (Bascoul *et al.*, 1988a, Bascoul *et al.*, 1988b, Dasari *et al.*, 1993, Karau *et al.*, 1997), viscosity (Chang and Chase, 1996a), adsorbent size distribution (Karau *et al.*, 1997) or bed height (Thömmes, 1997) has been intensively studied during the course of EBA development. Even though the complex relationship of the various parameters is still unclear, a rule of thumb is given by various authors claiming that the impact of axial dispersion on adsorption performance is negligible at $Bo > 40$ (Anspach *et al.*, 1999, Chang and Chase, 1996a, Levenspiel, 1972).

Eq. 5-2 :Dispersion Model (Baerns *et al.*, 1999)

$$E(\Theta) = \sqrt{\frac{Pe}{4 \cdot \pi \cdot \Theta}} \cdot \exp\left(-\frac{Pe \cdot (1-\Theta)^2}{4 \cdot \Theta}\right)$$

$$Pe = Bo = \frac{U \cdot L}{D_A}$$

Pe: Peclet number

U: liquid velocity (m/s)

Θ : Dimensionless time t/τ

L: Bed length (m)

D_A : axial diffusion coefficient

The qualitative equivalent in chromatographic systems is termed the plate number. This has been derived from the assumption that a chromatographic column can be modeled as a ‘tanks in series’, i.e. the model assumes a column as a series of well mixed batch adsorption systems where the number of tanks N_p (or theoretical plates) characterizes the extent of dispersion. The N_p -value is obtained by describing the obtained residence time distribution data with the tanks in series model – in systems with low dispersion this procedure leads to the relationship $N_p = 2 Bo$. As a rule of thumb in EBA, a reasonably good value for N_p can be defined within the range 25-30 at a sedimented bed height of 15 cm and a linear velocity of 300 cmh^{-1} (Biosciences)

5.1.4 CHROMATOGRAPHIC INTERACTIONS

Chromatographic separation methods are based on differences in the retention time of solute molecules in the mobile phase when passing through a bed of chromatographic adsorbents (stationary phase). The most common materials used for the stationary phases are natural polymers like agarose, cellulose and dextran, organic polymers or silica. Modern stationary phases in common is their chemical inertness, stability against pressure, acids, bases, and organic solvents. The degree of retention and thus the separation of two or more components can be attributed to variations in the molecular weight (gel filtration) or adsorptive interactions with the employed matrix. The most common adsorptive methods are described below.

For adsorption/desorption chromatography three basic principles are commonly used: Ion exchange chromatography (IEC), hydrophobic interaction chromatography (HIC) and affinity chromatography (AC) and a special case of AC immobilized affinity chromatography (IMAC). Depending on the employed interaction mechanism a suitable ligand is immobilized at a stationary phase described above. The desired product binds to the ligand while contaminants pass through the column and after a washing step the product can be selectively desorbed from the matrix by an appropriate elution buffer resulting in a purified product solution.

a ION EXCHANGE CHROMATOGRAPHY

Ion exchange chromatography is based on electrostatic interactions between charged groups at the protein surface and the oppositely charged ligands attached to the surface of the ion exchange resin. Commonly used ligands are summarized in Table 5-1 and can be classified in strong and weak ion exchangers referring to the pK_a value of their charged groups. The second important parameter is given by the surface properties of the protein of interest, which is basically related to its amino acid sequence and three dimensional structure. As all proteins contain both positively and negatively charged groups, a varying degree of amino acid protonation depends on the sequence and the surrounding pH in solution, which determines the effective surface charge for various process conditions. A third important parameter for IEC is the ion concentration in the feedstock, as ions in solution compete for the oppositely charged groups on the ion exchanger.

Table 5-1: Commonly used ion exchange ligands (Janson and Ryden, 1998).

Ligand	Aberration	Chemical formula	pK_a
Anion exchange			
Diethylaminoethyl	DEAE	$-\text{OC}_2\text{H}_5\text{N}^+\text{H}(\text{C}_2\text{H}_5)_2$	9.0 – 9.5
Trimethylaminoethyl	TMAE	$-\text{OCH}_2\text{CH}_2\text{N}^+(\text{CH}_3)_3$	-
Dimethylaminoethyl	DMAE -	$-\text{OCH}_2\text{CH}_2\text{N}^+\text{H}(\text{CH}_3)_2$	app. 10
Quaternary amine	Q	$-\text{OCH}_2\text{N}^+(\text{CH}_3)_3$	
Cation exchange			
Carboxymethyl	CM	$-\text{OCH}_2\text{COOH}$	3.5 – 4
Sulfonate	S	$-\text{OCH}_2\text{SO}_3\text{H}$	2
Sulfopropyl	SP	$-\text{OCH}_2\text{CH}_2\text{CH}_2\text{SO}_3\text{H}$	2 – 2.5

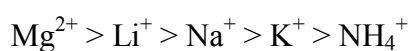
The pK_a values given mostly refer to an ionic strength of 0.1

b HYDROPHOBIC INTERACTION CHROMATOGRAPHY

Besides the hydrophilic charged character of protein surfaces, globular proteins can also exhibit extensive hydrophobic patches. The presence of these hydrophobic regions and their interaction with hydrophobic ligands is exploited during HIC (Janson and Ryden, 1998). Hydrophobic interactions can additionally be influenced by ions. The influence of different anions follows the Hofmeister (lyotropic) series. Ions on the left side promote hydrophobic interaction:



Also cations influence the strength of interaction:



Elution and thus separation of different proteins is generally achieved by a decreasing salt concentration in the eluent. In some cases a decrease of the solvent polarity is used in addition to a salt gradient. Depending on the hydrophobic character of the desired product a broad range of different hydrophobic ligands is available, mainly differing in their hydrophobicity and ligand density.

c AFFINITY CHROMATOGRAPHY

Affinity chromatography separates proteins on the basis of specific interactions between the protein and a specific ligand, as exhibited for example by enzyme-substrate or antibody-antigen interactions. The advantage of this method is a very high selectivity resulting in a highly purified product. Affinity ligands, especially peptide ligands, are usually quite sensitive against harsh CIP conditions, which make multiple use and CIP evaluation difficult. A further disadvantage is the comparatively high cost of affinity matrices. More robust and cheaper ligands are based on dyes or the metal affinity of certain amino acids (Janson and Ryden, 1998).

d IMMOBILIZED METAL ION AFFINITY CHROMATOGRAPHY (IMAC)

A special kind of affinity chromatography is IMAC, which is based on the property of a broad range of proteins to form multidentate complexes (chelates) with metal ions. IMAC resins contain a metal chelating group coupled via a spacer to the matrix. The complex is formed, when metal ions such as Cu, Zn, or Ni are added and should allow the binding of solvent or solute molecules via coordination sites on the surface (Janson and Ryden, 1998). Kagedal, (1998) summarized some special features of IMAC as follows:

Exposure of certain amino acid residues (histidine, cysteine, tryptophan) on the “surface” of proteins is required for the adsorption of proteins. The steric arrangement of the protein chain plays an important role, which means that molecules with closely similar properties, with respect to charge, molecular size, and amino acid composition, but with difference in their secondary and tertiary structure, can be separated. Simple ionic adsorption and other complicating factors can be suppressed or modified by buffers of high ionic strength. Binding is influenced by pH. Low pH causes elution of adsorbed substances. Exceptions to this are known. Several elution techniques are available (pH gradient, competitive ligands, organic solvents, chelating agents). IMAC is a general technique for purifying proteins. Metalloproteins do not bind specifically at their metal coordination sites, but rather through amino acid residues exposed at the protein surface.

5.1.5 ION EXCHANGE CHROMATOGRAPHY IN EXPANDED BED ADSORPTION

Ion exchange chromatography can be considered as the “working horse” of chromatographic processes and is usually applied as the first chromatographic step. It has found a widespread application for the initial purification of proteins, polypeptides, polynucleotides and other charged molecules. Ion exchange resins have usually a high resolving power, high capacity and are comparatively cheap and thus represent a primary candidate for use in EBA processes. In the scientific literature several successful EBA processes based on cation-exchange are described using *Escherichia coli* as an expression system for intracellular products. Prior to EBA processing, different techniques for cell disruption such as bead mill homogenization (Zanette *et al.*, 1998) high pressure homogenization (Garke *et al.*, 2000) or a microfluidizer (Pyo *et al.*, 2001) for protein release were used to obtain appropriate homogenates. In all cases EBA showed acceptable process performance despite the application of these crude process liquors. There is furthermore an extensive list of EBA processes for the recovery of extracellular products from a variety of expression systems; the direct recovery of recombinant human chymotrypsinogen (Curvers *et al.*, 2001) or mouse Endostatin (Trinh *et al.*, 2000) from *Pichia pastoris*, the recovery of a rec. human insulin precursor from a *Saccharomyces cerevisiae* culture broth (Brixius *et al.*, 2003) or the pilot scale production of a rec. human epidermal growth factor secreted by *Bacillus brevis* (Miyachi *et al.*, 1998).

While EBA processes based on cation-exchange soon became a success story, applications employing anion exchange chromatography showed a comparatively poor performance. Many reports describe problems arising from the interaction of cells and adsorbents affecting the

binding capacities and fluidization quality (Anspach *et al.*, Hjorth *et al.*, 1995, 1999, Reichert *et al.*, 2001) . Draeger and Chase (1991) mentioned for example that the available capacity is significantly reduced in the presence of cells using anion exchange systems, concluding that cation exchange might be more beneficial for direct adsorption techniques (Chase and Draeger, 1992). A more detailed investigation of this phenomenon has been carried out by Thömmes and coworkers (Fernández-Lahore *et al.*, 1999, Fernández-Lahore *et al.*, 2000, Lin *et al.*, 2001). The cell retention in an EBA column as a parameter of adsorbent properties and the characteristics of biomass present in the feedstock has been investigated by Feuser *et al.*, (1999) employing a pulse response technique described in detail below. It was found that employing cation exchange systems (Streamline SP) a quantitative recovery of the employed bio-pulse 100 % cell transmission or a cell transmission index (CTI) of 1 could be reached (Fig. 5-4).

The picture significantly changes using an anion exchange adsorbents (Streamline DEAE). For all feedstock's under investigation (whole cells and cell homogenates) a severe retention was found, while for hybridoma cells a complete collapse of the bed occurred (see Fig. 5-5).

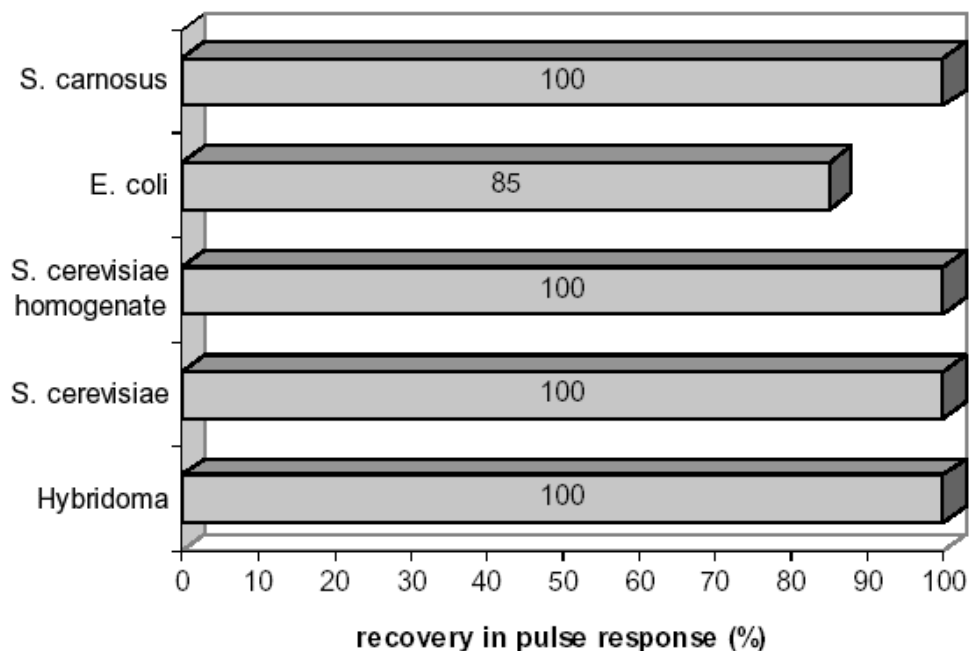


Fig. 5-4: Cell pulse transmission through an expanded bed of STREAMLINE SP at pH 7.0 (Feuser *et al.*, 1999).

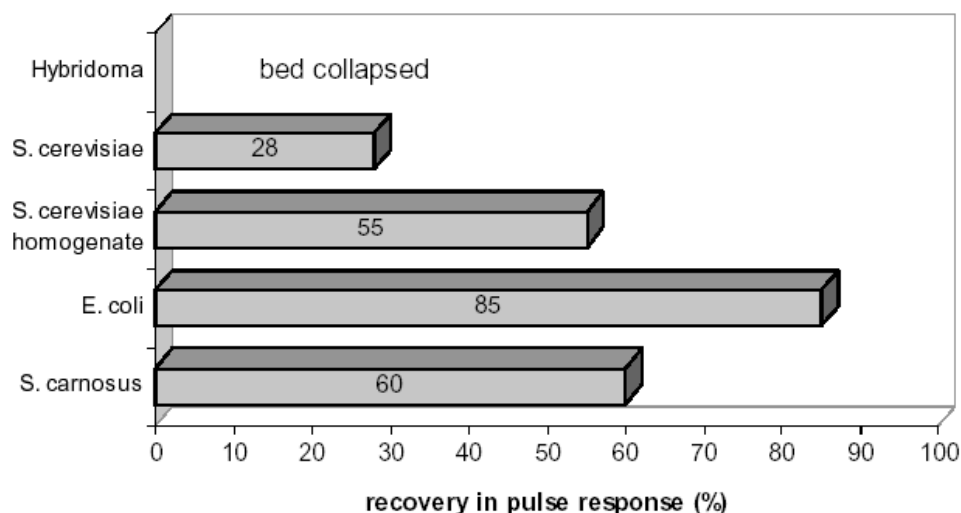


Fig. 5-5: Cell pulse transmission through an expanded bed of STREAMLINE DEAE (Feuser *et al.*, 1999).

Despite the above mentioned findings few 'successful' EBA processes based on anion exchange have been reported in literature. In all of these processes, however, precautions were taken to avoid extensive biomass retention. This was achieved by avoiding high cell concentrations or feedstock viscosities (Barnfield-Frej *et al.*, 1994, Johansson *et al.*, 1996), employing relatively low solid concentrations in the feedstock or low application volumes so that the column was only faced with a small amount of cells (Chang *et al.*, 1998, Shiloach and Kaufman, 1999). Only few authors described AIX EBA processes without stating any problems when processing unclarified *Escherichia coli* homogenate as a feedstock (Asplund *et al.*, Chang *et al.*, 1998, 2000, Zhou *et al.*, 1998). The common parameter of these applications lies in the homogenization methods used by the authors (high pressure or French press homogenates) and will be dealt with in detail during this study. The choice of an ion exchange process depends on the pI of the protein of interest and the stability of the protein with regard to pH. Anion exchange processes are of high interest in protein purification, since many proteins have pI values < 5 and limited stability in the acidic range.

5.2 BIOMASS-ADSORBENT INTERACTIONS

From observations made during anion exchange adsorption processes described above, it becomes evident that EBA process performance – even though the adsorptive interaction between stationary phase and the product might be assured – is directly linked to the success of the second task of a primary capture steps, namely efficient solid/liquid separation. Insufficient solid/liquid separation might not only lead to a lower mass transfer and thus reduced capacity, but also to contamination of the eluate with remaining solids (Ameskamp *et al.*, 1999) or reduced cycle times due to cleaning and regeneration cycles (Hjorth *et al.*, 1998, Feuser *et al.*, 1999) but in most cases to unacceptable process performance due to low fluidization quality of the bed. Typical consequences of an enhanced biomass-adsorbent interaction are an increase of back-mixing reducing the plate number, channeling of the bed leading to an early breakthrough or the collapse of the bed due to large aggregates formed by cells, DNA and adsorbents. A necessary prerequisite for successful EBA process design is therefore the understanding and control of the parameters responsible for biomass-adsorbent interactions.

5.2.1 QUANTIFICATION OF BIOMASS/ADSORBENT INTERACTION

EBA is an adsorptive primary capture step, the adsorptive interactions used for product capture have also to be considered for the interactions between the adsorbent and particulates present in the feedstock. Cells or cell debris have therefore to be treated as simply another main contaminant in the chromatographic process, with the single exception that the binding of this contaminant – even to a minor extent – has to be avoided in view of the overall process performance. The mechanism of the biomass/adsorbent interactions are analogous to protein - resins interactions described for chromatographic separations. Among the various adsorptive interaction modes contributing to biomass-adsorbent binding, ionic and hydrophobic interactions are probably the most dominant ones. It is therefore not surprising that electrostatic interactions were identified as the major adsorption mechanism (Fernández-Lahore *et al.*, 2000, Feuser *et al.*, 1999, Lin *et al.*, 2001) during previous research work on ion exchange EBA.

EBA process design should thus include the evaluation of possible biomass-adsorbent interactions. To do so analytical techniques were developed enabling the identification and quantification of parameters having an impact on the fluidization properties due to biomass binding to the adsorbent particles (Fernández-Lahore, 2001, Fernández-Lahore *et al.*, 2000, Fernández-Lahore *et al.*, 1999, Lin *et al.*, 2001).

a BIOMASS PULSE-RESPONSE METHOD (Feuser *et al.*, 1999)

The pulse-response method is a relatively fast and simple method for the identification and quantification of biomass/adsorbent interaction during early process design. This method was developed to screen for biomass adsorbent interactions neglecting the influence of particulate load, viscosity or DNA content. By doing so a rapid screening with a relatively small amount of crude feedstock can be carried out. The adsorbent under investigation is fluidized using buffer systems relevant for the protein of interest until a stable fluidized bed is reached. Following this, a small pulse of diluted biomass is applied at the column inlet. The biomass pulse is measured by optical density analysis at 600 nm at the inlet and outlet of the column. Comparing the area of the biomass peaks before ($A_{\text{input-pulse}}$) and after column passage ($A_{\text{pulse-response}}$) results into the fraction of biomass lost due to adsorption in the column. The fraction can be expressed in a cell transmission index CTI (Eq. 5-3) quantifying the extent of biomass/adsorbent interaction. The experimental set up and some typical results are shown in Fig. 5-6.

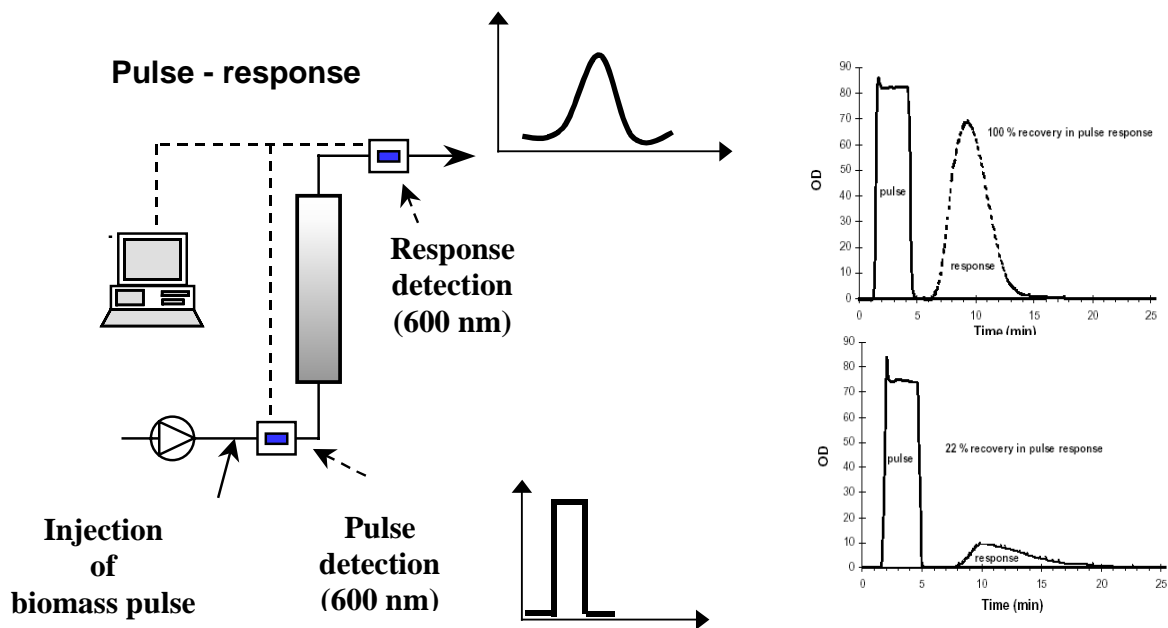


Fig. 5-6: Set-up of a pulse response experiment and typical results of a pulse response experiment with (CTI = 0.22) and without (CTI = 1.0) biomass/absorber interaction.

Eq. 5-3

$$CTI = \frac{A_{pulsresponse}}{A_{input-pulse}}$$

CTI: Cell transmission index

$A_{input\ puls}$: Area of the input pulse

$A_{pulsresponse}$: Area of the pulse response

From a wide variety of experiments a threshold value of CTI ~ 0.9 has been determined as a prerequisite for the formation of stable expanded beds during fluidization in biomass containing feedstock (Lin *et al.*, 2002).

RTD analysis in the presence of cells

Analogue to the determination of dispersion (Bo) or plate numbers (N) in an EBA systems (see chapter 1.2.2) it is also possible to use RTD analysis for the quantification of biomass-adsorbent interaction under realistic process conditions (Fernández-Lahore *et al.*, 1999). Due to the high background noise of the crude process liquor traditional tracer substances such as acetone can not be used however. As a suitable tracer bromide (Br^-) for cation exchange chromatography and Lithium (Li^+) for anion exchange chromatography in combination with an ion selective electrode were found (Lin *et al.*, 2001, Fernández-Lahore *et al.*, 2001). The differences between the RTD obtained with clear buffer systems and during application of crude process liquor can be seen as direct indication of the changes occurring in the bed due to the feedstock properties (particulate load, viscosity, DNA content). A quantification of the impact of the crude feedstock can be carried out employing the so-called PDE model – plug flow with axial dispersion and mass exchange – (see Chapter 7.3.2) (Villiermaux and van Swaaij, 1969). The model divides the expanded bed in two different regions, a perfectly fluidized region (α) with plug flow conditions (characterized by the Peclet number) and a region ($1-\alpha$) with aggregative fluidization and stagnant zones and a mass exchange parameter (N) between these regions. A graphical description of the PDE model is shown in Fig. 5-7. Detailed information on the mathematical model treatment and its application is given by Fernández-Lahore *et al.* (1999) and in the Appendix. From a wide variety of experiments a threshold value of $\alpha > 0.8$ has been determined for successful EBA process design.

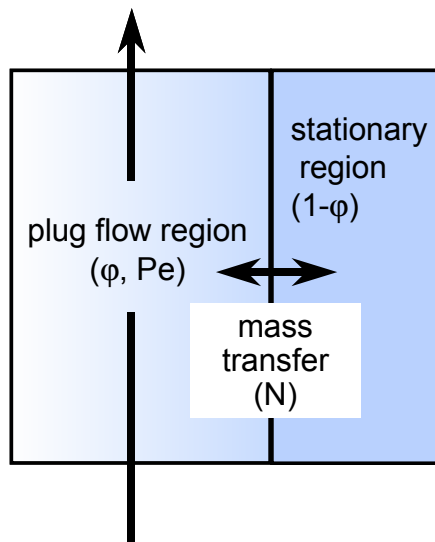


Fig. 5-7: Graphical description of the PDE model. (N: mass transfer between zones, Pe: over all axial dispersion, α : fraction of liquid in plug flow)

5.2.2 DEEP BED FILTRATION THEORY – A MECHANISTIC APPROACH

In order to gain a better understanding and to discriminate the processes responsible for biomass adsorbent interaction during EBA a theoretical approach from deep bed filtration (DBF) can be applied. In this context EBA can be visualized as a deep bed filter with a comparatively large voidage between the filter particles – opposite to traditional DBF processes – and the objective is a free passage of the particles through the filter. In DBF theory the capture of fine particles is divided in two principal steps (Ives, 1975):

- a) Transport of the turbid particle to the stationary phase
- b) Attachment of the turbid particle onto the stationary phase

The resulting filtration efficiency is therefore given by the product of the transport probability and the retention probability of the investigated system (Eq. 5-4).

$$\gamma = \gamma_T \cdot \gamma_A \quad \text{Eq. 5-4}$$

γ : separation efficiency

γ_T : transport probability

γ_A : attachment probability

Transport mechanism

In deep bed filtration theory it is normally differentiated between five transport mechanism. The relevance of the different mechanism for EBA is discussed in the following and shown in Table 1-2 (Ives, 1975).

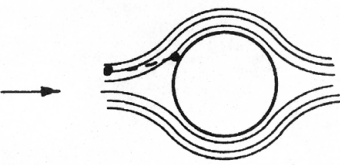
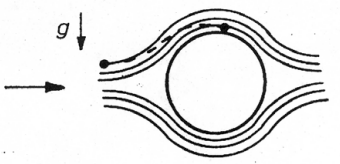
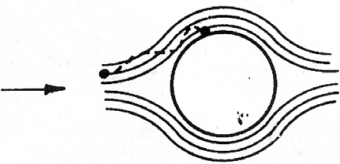
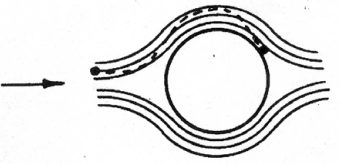
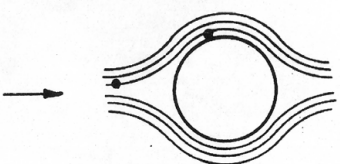
The mechanisms are termed inertia, gravity, diffusion, hydrodynamic transport and interception. Inertia (N_I) depends on particle features such as density (ρ_p) and diameter (x), the velocity, fluid viscosity (η) and the diameter of the filter particle. N_I is independent of the fluid density. Inertia is most relevant for air filtration. Due to the relatively low linear velocities, and high viscosity of the fluid (compared to air filtration) N_I is low in liquid filtration and might be neglected.

Transport by gravity is important for large density differences between particulate and fluid and large particulates ($d > 1 \mu\text{m}$). Due to the small particle size experienced during EBA applications and the low differences in density transport by gravity should also play a minor role during EBA processes.

Transport by diffusion is more important for smaller particles ($d < 1 \mu\text{m}$) in contrast to the above discussed effects arising from gravity. The influence of Brownian motion and diffusion increases with decreasing particle size. The actual impact of these mechanisms during EBA applications remains to be evaluated but is considered as minor. Hydrodynamic transport is characterized by the Reynolds Number (Re), which depends on the filtration velocity (U), diameter of filter particle (d) and the conditions of the liquid phase (viscosity (η) & density (ρ_l)). Due to the very low Reynolds number for the conditions present in EBA this transport mode can be assumed to contribute little to solid separation.

Interception appears to be the most significant mechanism for EBA processes. Implying a laminar flow, particles distributed in the liquid have to move along the streamlines, surrounding the adsorbents. If the Streamlines around the adsorbent particle is smaller than the actual particulate diameter a collision of the two entities result. This transport mechanism is called interception and can be described by the dimensionless ratio of Interception N_R , which depends on the size of the adsorbent and the turbid particle.

Table 5-2:Transport mechanism in deep bed filtration

Mechanism		Equation
Inertia		$N_I = \frac{\rho_p \cdot x^2 \cdot U}{18 \cdot \eta \cdot d}$
Gravity		$N_G = \frac{(\rho_p - \rho_l) \cdot g \cdot x^2}{18\eta U}$
Diffusion		$Pe = \frac{U \cdot d}{D_a}$
Hydrodynamic transport		$Re = \frac{U \cdot d \cdot \rho_l}{\eta}$
Interception		$N_R = \frac{x}{d}$

Based on these transport mechanisms Ives proposed a phenomenological equation for the transport efficiency.

Eq. 5-5

$$V_{0,T} = a \cdot Pe^{e_1} \cdot N_R^{e_2} \cdot N_G^{e_3} \cdot N_I^{e_4}$$

a, e_i= empiric constants

With regard to the biomass adsorbent interactions during expanded bed adsorption sedimentation (N_G) is negligible, because of the small biomass particle diameter and the upward directed flow. In terms of the comparatively (to gas) high viscosity of the fluid and the low linear velocity inertia can be neglected as well. Therefore interception remains as the main transport mechanism.

Attachment mechanism

The attachment mechanisms in deep bed filtration are very similar to the binding of proteins to an adsorbent surface as discussed in chapter 5.1.4. Depending on the surface properties of the filter particle and the turbid particle different interaction mechanism are possible. These are intermolecular van der Waals forces, chemical bonds, hydrophobic interaction and electrostatic interaction. The following chapter will focus on electrostatic interactions because of their importance in ion exchange chromatography.

The mechanism of electrostatic interaction is based on short distance electrostatic attraction forces between two oppositely charged surfaces. Fuerstenau (Sonntag, 1977) derived an equation to calculate the electrostatic interaction energy between oppositely charged globular particles. The respective equation is given in Eq. 5-6; for more detailed information see Appendix. The electrostatic attachment energy between particles depends on the diameter of both particles, the surface potential, and the distance between the particles.

Eq. 5-6

$$\varphi_{el} = \frac{\epsilon_0 \epsilon_r x d (\psi_d^2 + \psi_x^2)}{4(d+x)} \left\{ \frac{2\psi_d \psi_x}{\psi_d^2 + \psi_x^2} \ln \frac{[1 + \exp(-\kappa_d d)]}{[1 - \exp(-\kappa_d d)]} + \ln[1 - \exp(-2\kappa_d d)] \right\}$$

ψ_d	electrostatic surface potential of the adsorbent (V)
ψ_x	electrostatic surface potential of the biomass particle (V)
d	diameter of the adsorbent particle (m)
x	diameter of the biomass particle (m)
κ_d	reciprocal value of the Debye-Hückel-parameter (nm)

5.3 PROPERTIES OF BIOMASS SUSPENSION

From the discussion in the last chapter two critical parameters for biomass interactions can be identified. For practical purposes the complex retention behavior of cells or cell debris may be reduced to a description depending on size distribution and surface charge of the particulates present in the feedstock. The transport term of the particulates to the adsorber surface is mainly a function of the relative size, while retention on the surface can be described by size and surface charge characteristics of the particulate and the adsorbent. A quantitative measure for the effective surface charge is given by the zeta potential.

5.3.1 PARTICLE SIZE ANALYSIS

Particle sizing is a widely used analytical tool for the characterization of particulate suspensions handled in the processing industries such as agrochemical, ceramics, cosmetic, food and drink, paint, pharmaceutical and biotechnology industry. The complex morphology of particles makes it difficult to describe the respective particles by a simple number. Furthermore, different particle sizing methods, rely on the determination of different particle dimensions (max. length, min. length, volume, surface area, etc...) and will yield various size distribution, differing even though identical samples are employed (see Fig. 5-8). It is therefore very important to compare only size data obtained by the same analytical method. An overview of different particle sizing techniques is given in Table 5-3.

Table 5-3: Common Techniques for particle sizing

Technique	measuring range	Comments
Sieves	> 38 μ m	Cheap and readily usable for large particles
Sedimentation	2-50 μ m	Depends on the terminal settling velocity. Based on the Stokes law the so called Stokes diameter is calculated, which is simply a comparison of the particle settling rate to a sphere settling at the same rate.
Electro zone sensing	> 1-2 μ m	Developed for sizing of blood cells. The principle of operation is very simple. A dilute suspension is made to flow through an orifice and a voltage is applied across it. As particles flow through the

		orifice the capacitance alters and this is indicated by a voltage pulse or spike. The peak height or area can be correlated to a standard latex.
Microscopy		Excellent and cheap method to analyze individual particles. Analyzing large numbers of particles is very costly or even impossible.
Laser diffraction (Photon Correlation Spectroscopy (PCS))	0.1-6000 nm	Relies on the fact that the diffraction angle of a laser on a particle is inversely proportional to the particle size

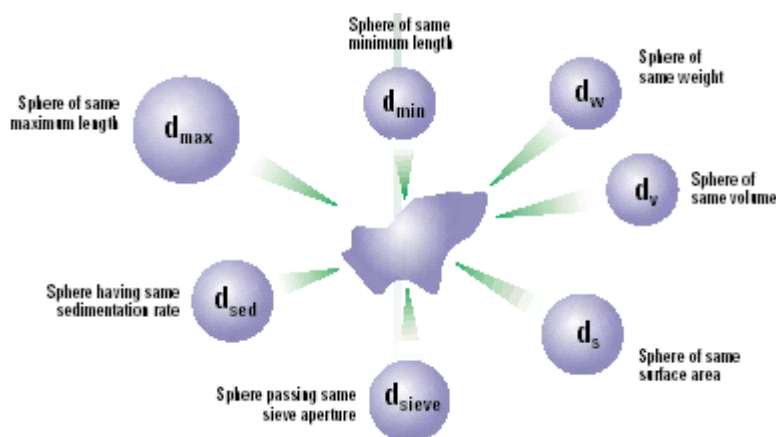


Fig. 5-8: Corresponding spheres, using different techniques for particle size determination (<http://www.malvern.de>)

During this study the method based on photon correlation spectroscopy has been used. It relies on the fact that the diffraction angle of a laser on a particle is inversely proportional to the particle size. The size of the particle directed to the laser is measured but in a well mixed sample this should represent the average size distribution. The advantages of this technology are the broad measuring range covering the whole range needed in this investigation, reproducible results, easy operation and the possibility to measure very small particles.

5.3.2 ZETA POTENTIAL

Surfaces of biological material (microbial cells, cells from cell culture production or raw material from herbal, animal sources) carry a certain charge depending on the molecules or chemical groups found on the surface. It is thus not surprising that electrostatic interactions are found as the main parameter for bacterial adhesion at charged surfaces (Boonaert and Rouxhet, 2000, Krekeler *et al.*, 1989, Mozes *et al.*, 1986, van Loosdrecht *et al.*, 1987a). Biomass-adsorbent interaction during ion exchange chromatography can thus be treated in an analogy to the interactions of charged proteins with the respective ion exchange resins.

A common parameter to measure and describe the effective surface charge of a suspended particle is the zeta potential. The measurement of zeta potential finds its traditional application in the Mineral-, Pharmaceutical-, and Paint industries where colloid interaction are a main parameter for product quality. Examples for various dispersion conditions are shown in Fig. 5-9

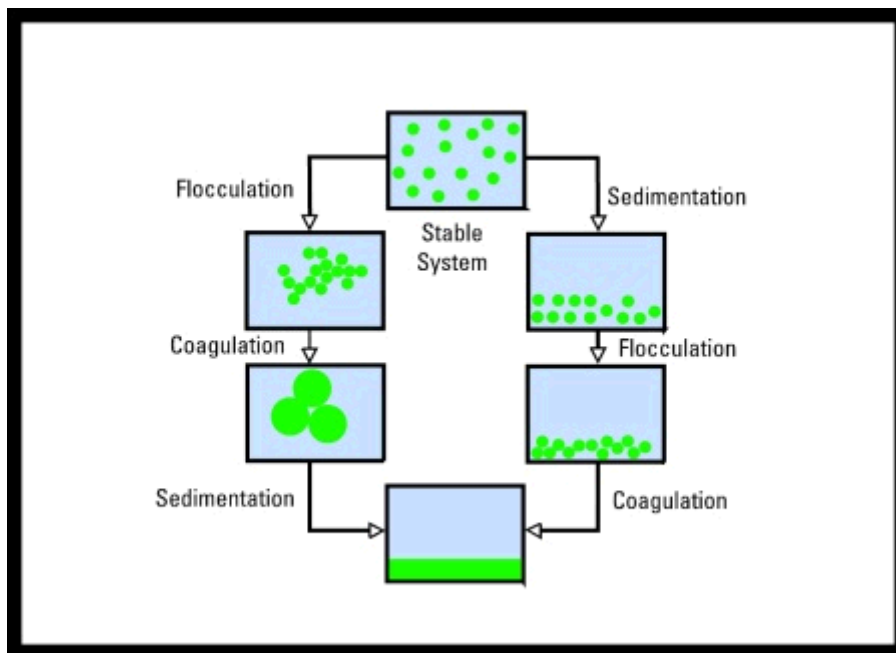


Fig. 5-9: Different dispersion conditions of a colloid system (<http://www.malvern.de>)

a THE STERN DOUBLE LAYER MODEL:

The charge of a colloid particle, suspended in an aqueous solution, is compensated in the liquid phase by opposite charged counter ions achieving electrical neutrality in the system as a whole. The charge distribution surrounding a charged colloid is described by the STERN double layer model. Initially, attraction from a negatively charged colloid causes some of the positive ions

(so called counter-ions) to form a firmly attached layer around the surface of the colloid. This layer of counter-ions is known as the STERN layer. Additional positive ions are still attracted by the negatively charged colloid but now they are also repelled by the positive STERN layer and by other nearby positive ions that are also trying to approach the colloid. A dynamic equilibrium establishes, forming a diffuse layer of counter-ions, which has a high concentration near the colloid, gradually decreasing with distance until it reaches equilibrium with the bulk solution. The negative ions (so called co-ions) act in a similar but opposite fashion. Their concentration will gradually increase as the repulsive forces of the colloid are screened out by the positive ions. The diffuse layer can be visualized as a charged atmosphere surrounding the colloid. Charge density is greatest near the colloid and rapidly diminishes towards zero as the concentration of positive and negative ions merge together. The attached counter-ions in the STERN layer and the charged atmosphere in the diffuse layer are what we refer to as the *double layer* (see Fig. 5-10)

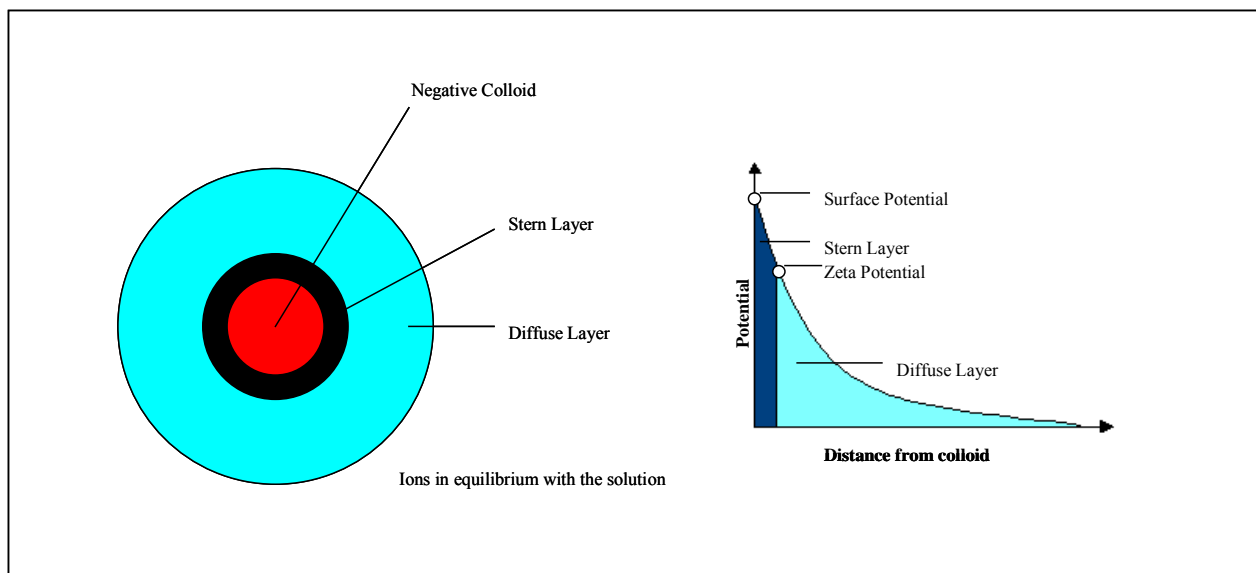


Fig. 5-10: Charge distribution in the STERN Double Layer Model

An electric potential is built up between the surface of the particle and any point in the surrounding liquid. This voltage difference is in the order of mV and depends on the magnitude of surface potential and the thickness of the double layer.

Particle movement, due to potential measurements with a fixed velocity in an applied electric field depends on the dielectric constant, viscosity of the surrounding media and the electrical potential at the boundary between the moving particle and the liquid. This boundary is called the slip plane and is usually defined as the plane between the Stern layer and the diffuse layer.

The potential at this junction is related to the mobility of the particle and is called the “Zeta Potential”.

b MEASUREMENT OF ZETA POTENTIAL

The usual method to measure Zeta Potential is to analyze the migration rate of dispersed particles in an electric field. Traditionally the migration was observed using a microscope and a stopwatch. The modern technique based on laser doppler velocimetry (LDV), which is more accurate and able to measure smaller particles, has almost replaced the conventional methods. The electrophoretic mobility (important for zeta potential calculation) can be calculated using Eq. 5-7.

Eq. 5-7

$$v / E_l = \mu_E$$

v : velocity

E_l : electric field

μ_E : electrophoretic mobility

The Zeta Potential can be calculated from the electric mobility using the so called Henry equation (Eq. 5-8).

Eq. 5-8

$$\mu_E = 2\varepsilon_d \zeta f(\kappa a) / 3\eta$$

ε_d : dielectric constant of the medium $\varepsilon_d = \varepsilon_r * \varepsilon_0$, ε_0 : permittivity of free space ($8.85 \times 10^{-12} \text{ J}^{-1} \text{ C}^2 \text{ M}^{-1}$) & ε_r = relative permittivity of the media

η : viscosity of the medium

$f(\kappa a)$: correlation factor regarding the thickness of the double layer and particle diameter

ζ : zeta potential

κ : describes the thickness of the double layer

In practice an approximation for the correlation factor $f(\kappa a)$ is made as follows: $f(\kappa a) = 1.0$ for non polar media and $f(\kappa a) = 1.5$ for polar media. For aqueous solution $f(\kappa a) = 1.5$ and particle > 100 nm the so called Smoluchowski approximation can be used (Hunter, 1981):

Eq. 5-9

$$\mu_E = \varepsilon_d \zeta / \eta$$

for aqueous media at 25°C it can be assumed

$$\eta : 8,95 \cdot 10^{-3} \text{ Pa} \cdot \text{s} [= \text{N m}^{-2} \text{ s}] \text{ at } 25^\circ \text{C}$$

$$\varepsilon_d : \varepsilon_d = \varepsilon_r \cdot \varepsilon_0 = 8.85 \times 10^{-12} \text{ J}^{-1} \text{ C}^2 \text{ m}^{-1} \cdot 78,2$$

finally Eq. 5-9 can be simplified to: $\zeta = 12,85 \mu_E \text{ mV}$

5.4 MICROBIAL CELL WALL PROPERTIES

During cell adhesion studies at various kinds of surfaces it became apparent that physical and chemical properties of bacterial surfaces are very important for the actual adsorption processes. X-ray photoelectron spectroscopy was used to investigate the chemical composition of the surface of yeast and bacteria (Mozes *et al.*, 1989). The surface charge properties were characterized by the electrophoretic mobility or the zeta potential and the hydrophobicity has been measured by contact angle measurement (Mozes *et al.*, 1986, van Loosdrecht *et al.*, 1987a, van Loosdrecht *et al.*, 1987b, van Loosdrecht *et al.*, 1989). The correlation of these physical and chemical properties has been summarized by Buchholz and Kasche (Buchholz and Kasche, 1997):

- Phosphate groups play a decisive role for the surface charge, while the surface charge conditions are related to the nitrogen/ phosphate (N/P) ratio at the cell surface.
- Bacteria show a higher N/P ratio than yeast. For the individual strain the elementary composition depends on the cultivation and growth conditions.
- The hydrophobicity is related to the proteins on the cell surface. The hydrophobicity is proportional to the N/P ratio for yeast and inversely proportional to the oxygen

concentration for bacteria. For bacteria the hydrophobicity is directly proportional to the amount of carbohydrates on the cell surface.

- The major interaction mechanism between cells and surfaces are van der Waals forces, dipole-dipole- and electrostatic interactions.

5.4.1 *E. COLI*

The cell wall of *Escherichia coli* as a Gram negative (G-) bacteria consists of three layers, namely the outer membrane (OM), a thin peptidoglycan layer and the cytoplasmic membrane. In contrast, the cell wall of a Gram positive (G+) bacteria is composed of a thick peptidoglycan layer and the cytoplasmic membrane as illustrated in Fig. 5-11.

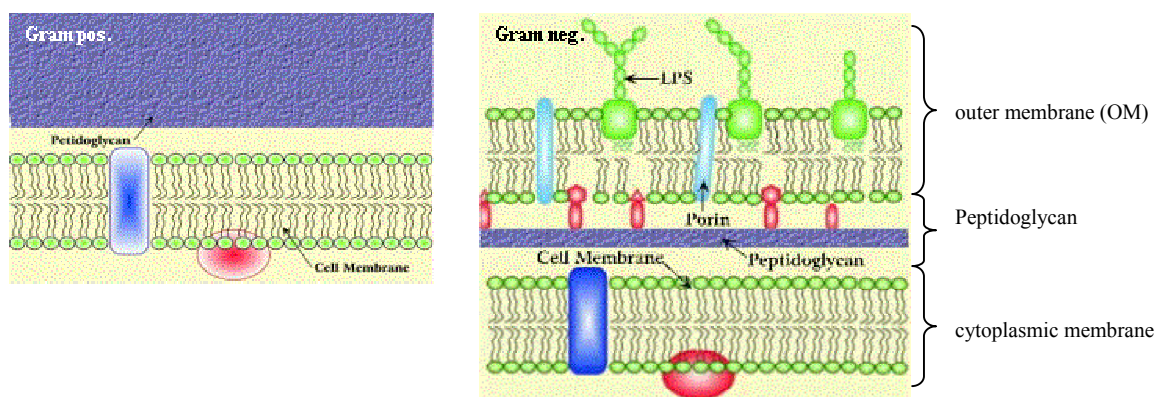


Fig. 5-11: Comparison between Gram pos. (right) and Gram neg. (left) cell wall (Paustian, 2001).

a OUTER MEMBRANE

The outer membrane of a G- cell wall is a lipid bilayer similar to the cytoplasmic membrane containing phospholipids and proteins. In addition a main component of the OM are lipopolysaccharides (LPS), which are negatively charged and play an important role for the surface charge of the organisms (see Fig. 5-12) (Paustian, 2001). In lipopolysaccharides three parts are differentiated a lipid part which anchors the LPS in the OM, a conserved core oligosaccharide and the O-antigen, which varies between the species. The O-antigens are exposed to the media and play an important role in virulence and immune reactions. Typical laboratory strains such as *Escherichia coli* K12 produce incomplete LPS without the O-antigens (Nikaido, 1996, Paustian, 2001).

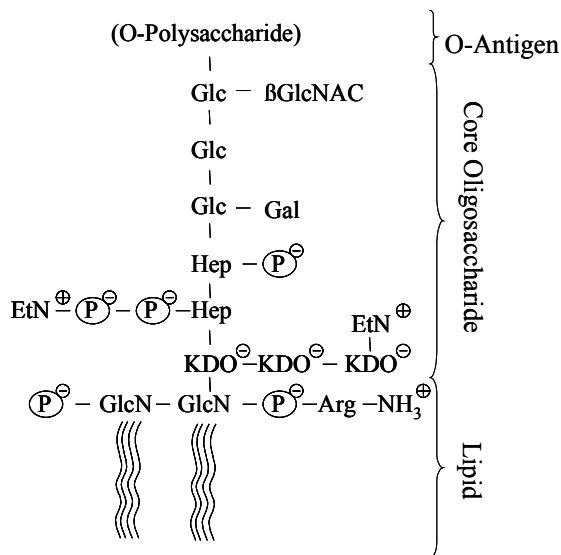
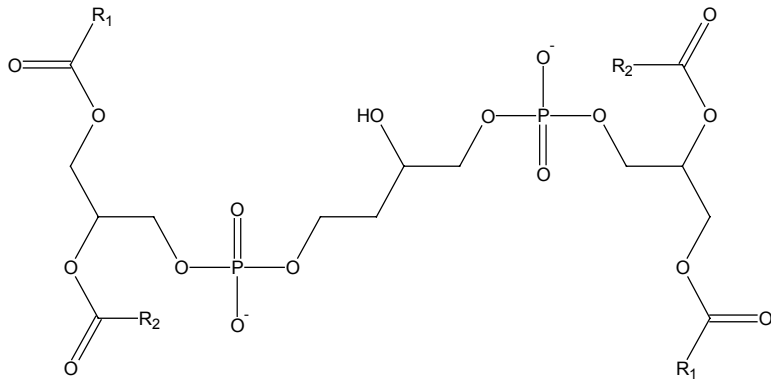


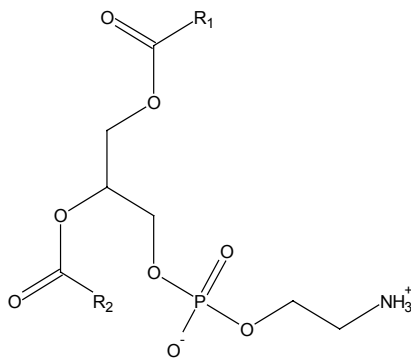
Fig. 5-12: Lipopolysaccharide (Nikaido, 1996).

b CYTOPLASMIC MEMBRANE

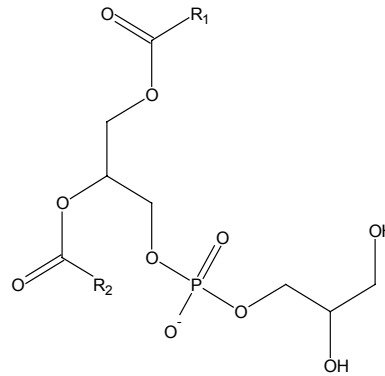
The cytoplasmic membrane is built up by a lipid bilayer containing integral membrane proteins. Roughly 50 % of the cytoplasmic membrane consists of mainly three kinds of phospholipids in the following order: Phosphatidylethanolamine > Phosphatidylglycerol > Cardiolipin (see Fig. 5-13) (Kadner, 1996). Compared to the LPS at the outer membrane the major components (Phosphatidylethanolamine) carries less net charges.



Cardiolipin or di-Phosphatidylglycerol



Phosphatidylethanolamine



Phosphatidylglycerol

Fig. 5-13: Major phospholipids in the cytoplasmic membrane of *Escherichia coli* 70-80 % Phosphatidylethanolamine, 15-25 % Phosphatidylglycerol, 5-10 % Cardiolipin. R₁: saturated fatty acid, R₂: unsaturated fatty acid (Kadner, 1996).

c PEPTIDOGLUCAN

Peptidoglycan is a rigid layer of different thickness found in G⁺ and G⁻ cells. It is composed of an overlapping lattice of 2 sugars (N-acetyl glucosamine (NAG) and N-acetyl muramic acid (NAM)) that are cross linked by peptide bridges. The exact molecular structure of these layers is specific for different organisms (Paustian, 2001).

5.4.2 *SACCHAROMYCES CEREVISIAE*

The yeast cell wall represents 15-32 % dry weight of the cell and 25-50 % of the cell volume depending on the growth conditions. The major components (80-90 %) are carbohydrate and mannoproteins. The composition of the fractions varies with the species: Mannoprotein 25-34 %, alkali-insoluble glucan 15-48 %, alkali-soluble glucan 10-48 % (Nguyen *et al.*, 1998). A schematic composition the *Saccharomyces cerevisiae* cell wall is shown in Table 5-4 and Fig. 5-14. The surface charge of yeast cells is mainly related to the phosphorylation of mannosyl side chains (Orlean, 1997).

Table 5-4: Major components of *Saccharomyces cerevisiae* cell walls (Lipke and Ovalle, 1998).

Component (degree of polymerisation)	Mean molecular mass (kDa)	% of cell wall mass	Relative molar ratio to β -1,3 glucan
β 1,3 glucan (1,500)	240	50	1,0
β 1,6 glucan (150)	24	10	2
Mannoprotein	100-200	40	1,2-1,4
Chitin (120)	25	1-3	0,1-0,3

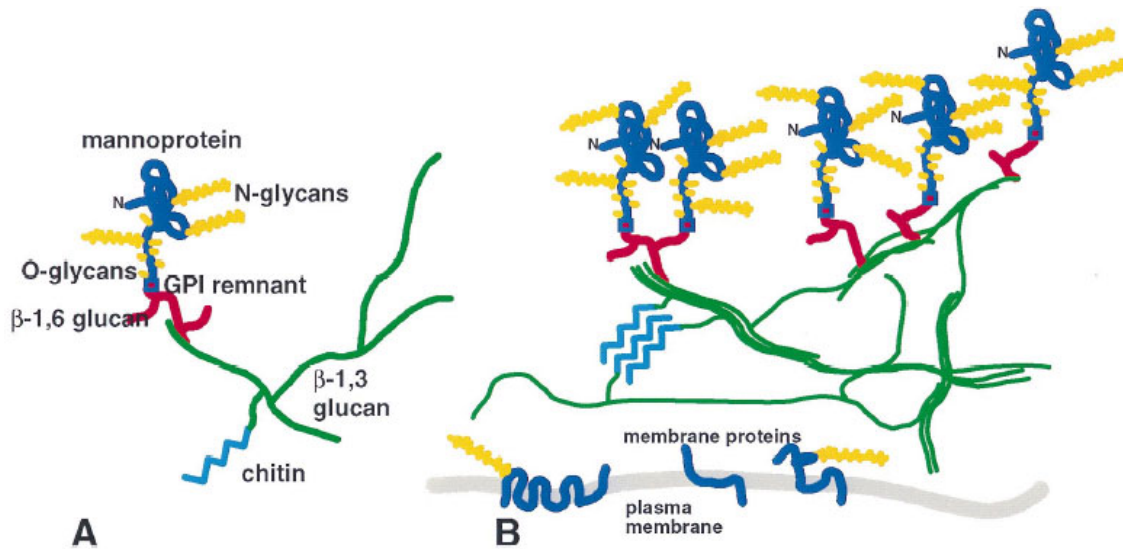


Fig. 5-14: Relationships among components of *Saccharomyces cerevisiae* cell walls. (A) Prototypical module with components individually labeled and colored. The mannoprotein polypeptide is blue, and oligosaccharides are shown in yellow, labeled as N or O linked. Only a few of the branch points of the glucans are shown. Chitin can also be linked to the β 1,6 glucan. (B) Association of modules to form a wall lattice. Colors are as in panel A. The β 1,3 glucan chains are intertwined to designate triple helices, and chitin is shown as a crystalline micro-domain. Cross-linking of mannoproteins through disulfide and other bonds is not depicted (Lipke and Ovalle, 1998).

5.5 CELL DISRUPTION

Feedstock properties (size distribution, zeta potential, viscosity, ...) of a biomass suspension change dramatically by cell disintegration, which is, however, a necessary prerequisite for any process aiming at the recovery of intracellular proteins. It is therefore of utmost importance for successful EBA process design to gain a closer understanding of the changes of feedstock properties resulting from different homogenization methods. In order to achieve cell disruption and release of intra cellular proteins, a broad range of different cell disruption methods are available (see Fig. 5-15) and described in literature (Kula and Schütte, 1987, Middelberg, 1995). Industrial relevant are mechanical disintegrators, high-pressure homogenizers or bead mills.

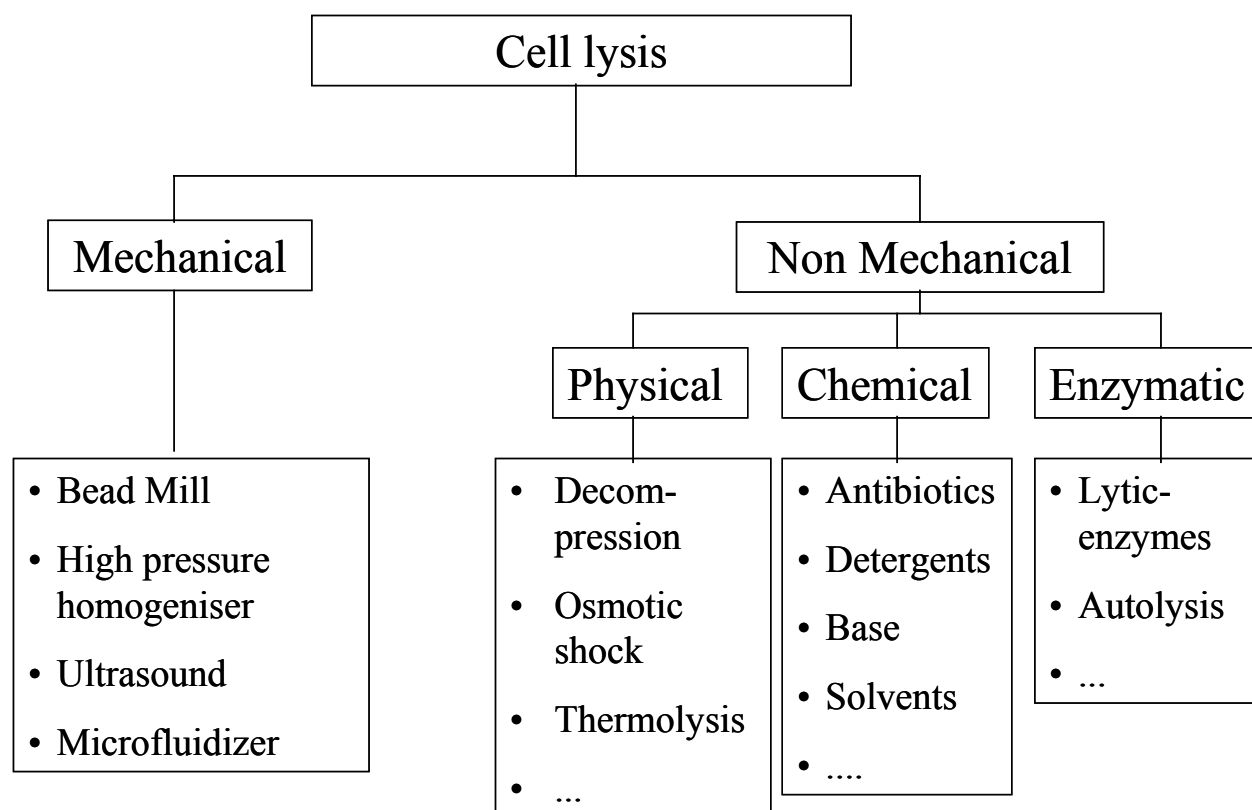


Fig. 5-15: Cell disruption methods

5.5.1 SONICATION

Ultrasound treatment (>18 kHz) of microorganism results in inactivation and disruption of the cells. Ultrasound is characterized by high frequency moderate displacement ($50\ \mu\text{m}$), steep transverse velocity gradients (up to $4000\ \text{s}^{-1}$) and very high acceleration ($80000\ \text{g}$). The major disruption mechanism is cavitation, where the collapse of bubbles converts sonic energy in mechanical energy in the form of shock waves equivalent to several thousand atmospheres ($300\ \text{MPa}$). An additional mechanism is micro-streaming, which occurs near radially vibrating bubbles of gas caused by the ultrasound. Most of the energy applied is adsorbed by the suspension and thus sufficient cooling is essential to avoid degradation of temperature sensitive proteins. Even though equipment for large scale and continuous operation has been described, ultrasound treatment has not yet found its application in current large scale biotechnological production processes. This might be due to the sensibility of some proteins against sonication and the high energy demand of the process.

5.5.2 BEAD MILL

Wet milling is developed for comminuting pigments in the paint and lacquer industry. The basic setup of a wet mill is a jacketed grinding chamber with a rotating shaft through its center. The shaft is fitted with agitators of varied design that impact kinetic energy to small beads in the chamber, forcing them to collide with each other. The beads are retained in the grinding chamber by a sieve or an axial slot smaller than the bead size (Middelberg, 1995) see Fig. 5-16.

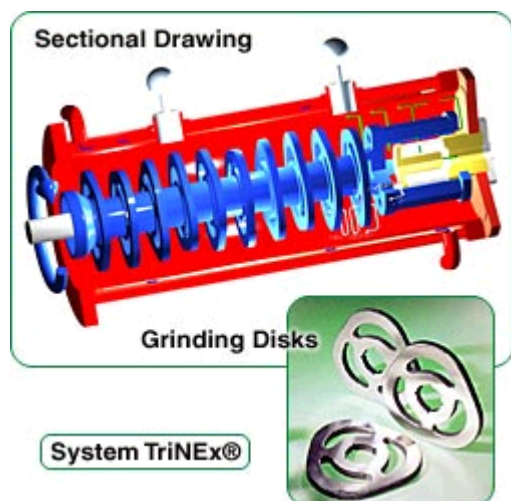


Fig. 5-16: Bead mill with horizontal grinding chamber System TriNEx® (NETZSCH-Feinmahltechnik, Germany)

Microbial suspensions exhibit, in comparison to pigment suspension, a rather low viscosity, which makes the use of smaller glass beads necessary (Kula and Schütte, 1987). The efficiency of bead milling depends on a series of parameters. 44 parameters were identified by Mölls and Hörnle (Mölls and Hörnle, 1972). The most important are summarized in Table 5-5. The impacts of each parameter are outlined in the literature (Middelberg, 1995, Kula *et al.*, 1990, Kula and Schütte, 1987). Wet milling is a sufficient and scalable method for cell disintegration of microorganisms and is employed in industrial protein production.

Table 5-5: Process Variables of Agitator Ball Mill (Kula and Schütte, 1987)

Processing parameters	Grinding beads	Hardware
Feed rate	Size of beads	Geometry of the grinding chamber
Agitator speed	Specific weight of beads	Design of stirrer
Cell density	Packing density of beads	
Temperature		

5.5.3 HIGH PRESSUR HOMOGENIZATION

Similar to bead milling, high-pressure homogenization has been adapted for cell disruption from other industries (food and pharmaceutical). The basic design consists of a high-pressure displacement pump that forces the suspension through a specially designed adjustable discharge valve (see Fig. 5-17). Pressures up to 150 MPa can be achieved, resulting in radial velocities up to 300 m s^{-1} during passage through the discharge valve. The direction of flow is changed twice during the passage and the suspension finally impinges at the impact ring, as shown in Fig. 5-17. A feeding pump is used to transport the cell suspension to the high-pressure pump. For large-scale application, homogenizer with multiple pistons providing an almost constant pressure in excess of 100 MPa are available (Kula *et al.*, 1990, Middelberg, 1995).

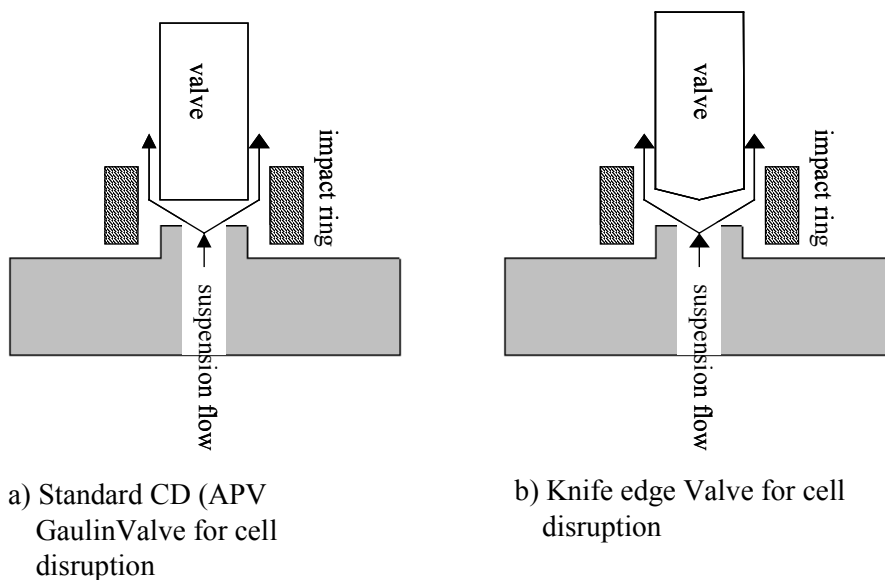


Fig. 5-17: Details of Valve seat of APV-Gaulin high-pressure homogenizer

By passing through the discharge valve the cells are subjected to turbulence, cavitations, liquid- and solid shear. The exact impact of each parameter is still under discussion. The main disruptive factors considered are the pressure drop at the valve (Kleinig and Middelberg, 1996, Kula and Schütte, 1987) and the impingement stress that is proportional to the operating pressure. The main process parameter of a high pressure homogenizer are the operating pressure, valve design, cell density and temperature. Multiple passes through the homogenizer translates into higher protein release, but also into decreased throughput efficiency and smaller

particles. Hetherington et al. (1971) modeled the cell disintegration as a first order process, which can be described by Eq. 5-10.

Eq. 5-10

$$\log\left(\frac{1}{1-R_p}\right) = k_1 N_{pa} P^a$$

R_p : Fractional release of soluble protein

k_1 : Rate constant [MPa^{-a}]

a : pressure exponent (depends on the microorganism and the growth conditions)

N_{pa} : Number of passes

P : operation pressure (MPa)

5.6 PROTEIN PROPERTIES USED IN PROCESS DESIGN STUDIES

5.6.1 INSULIN

Insulin, a 5.6 kD peptide hormone, plays an important role in the human glucose metabolism in cooperation with glucagon. Insulin consists of two polypeptide chains chain A (21 aa) and B (30 aa) connected by two disulfide bridges, a third disulfide bridge is formed within the B chain. Insulin is produced in the beta cells in the pancreas as a precursor, the so called präproinsulin, consisting of a A and B chain connected by a 30 aa C-peptide. The A chain contains a N-terminal signal sequence, which directs the protein to the endoplasmatic reticulum (ER). By entering the ER the signal sequence is cleaved resulting in proinsulin. Proinsulin is transported to the secretory granula passing the golgi complex. In the granula the final enzymatic processing to insulin takes place. A fusion of the ripe granula with the plasma membrane leads to a secretion of the processed mature insulin.

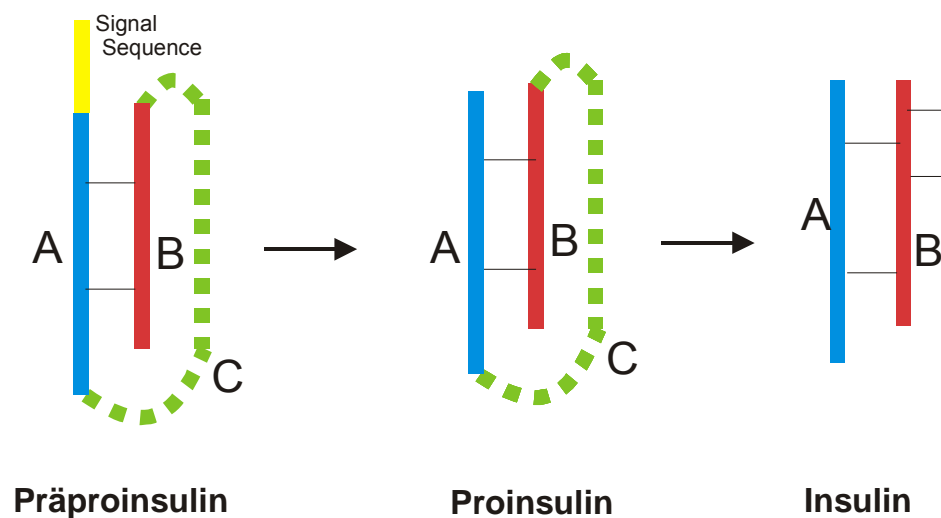


Fig. 5-18: Enzymatic processing of Insulin (Stryer, 1994)

Until 1982 the insulin used for treatment of type 1 diabetes, was solely obtained from extraction of pig or bovine pancreas. The difference between pig and human insulin is just one amino acid. The C-terminal aa B30 of the B chain in human insulin is threonine, whereas in pig insulin alanin is present. Bovine insulin in addition has two amino acids changes (see Fig. 5-19) in the A chain. In 1982 Novo Nordisk launched a semi-synthetic human insulin produced by trypsin catalyzed conversion of pig insulin into human insulin. Around the same time insulin produced by recombinant DNA technology became available using different methods. Eli Lilly and others developed different routes to obtain human insulin using *Escherichia coli*. First the

intracellular expression of Insulin A & B chain was carried out in two separate *Escherichia coli* expression systems followed by a purification and chemical combination of the two chains to yield the active hormone. Later the expression of an insulin precursor in one *Escherichia coli* strain was performed followed by folding, formation of correct disulphide bonds and finally removal of the C peptide (Mollerup *et al.*, 1999) (Frank and Chance, 1983).

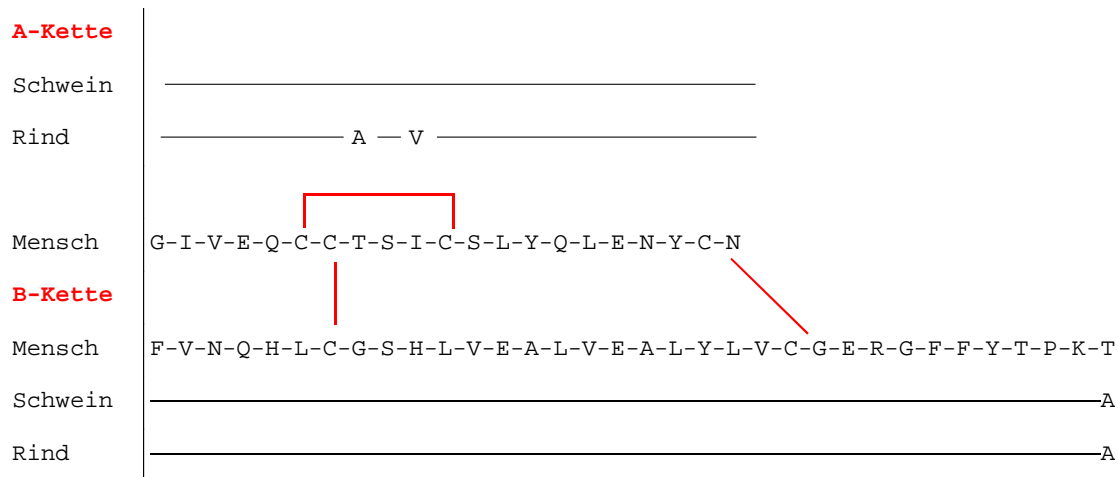


Fig. 5-19: Comparison of pig, bovine and human insulin

Since 1988 recombinant insulin is produced by Novo Nordisk using recombinant *Saccharomyces cerevisiae* strains. In the respective process insulin is produced as a precursor (Insulin precursor MI3) in *Saccharomyces cerevisiae* as an extra cellular product. The secretion into the culture broth has beneficial effects for the downstream process; lower amount of contaminants, the product representing the main protein component in solution and no requirement for cell lyses. The MI3 precursor (5.96 kD; IEP = 5.3) contains one A and B-chain each connected by a mini artificial C-chain (-Ala-Ala-Lys-) and the α -leader sequence from *Saccharomyces cerevisiae* to direct the gene product to the secretory pathway. One of the aims of the present study has been the development of an EBA process for the direct isolation of the insulin precursor MI3 from whole broth in order to evaluate the technology.

5.6.2 HUMAN GROWTH HORMONE (hGH)

Human growth hormone is a 191 aa (22 kD) single chain peptide hormone (IEP 4,9) ordinarily produced in the pituitary gland of the brain. The primary structure of correctly folded hGH consists of two disulfide bridges, one between Cys 53 and Cys 165 and a second one between Cys 182 and Cys 189 (Jespersen *et al.*, 1994). The physiological function of hGH was found to be important for growth regulation during the growth phase of children as well as the metabolism of adults (fat-, protein-, carbohydrate metabolism, muscle and bone build-up). hGH deficiency results in different diseases such as growth retardation, Ullrich Turner Syndrom and Chronic Renal Disease in children. In adults hGH deficiency causes a disturbance in carbohydrate, fat, protein metabolism, increased blood pressure, weakened heart muscle contraction and heart rate and abnormal body composition.

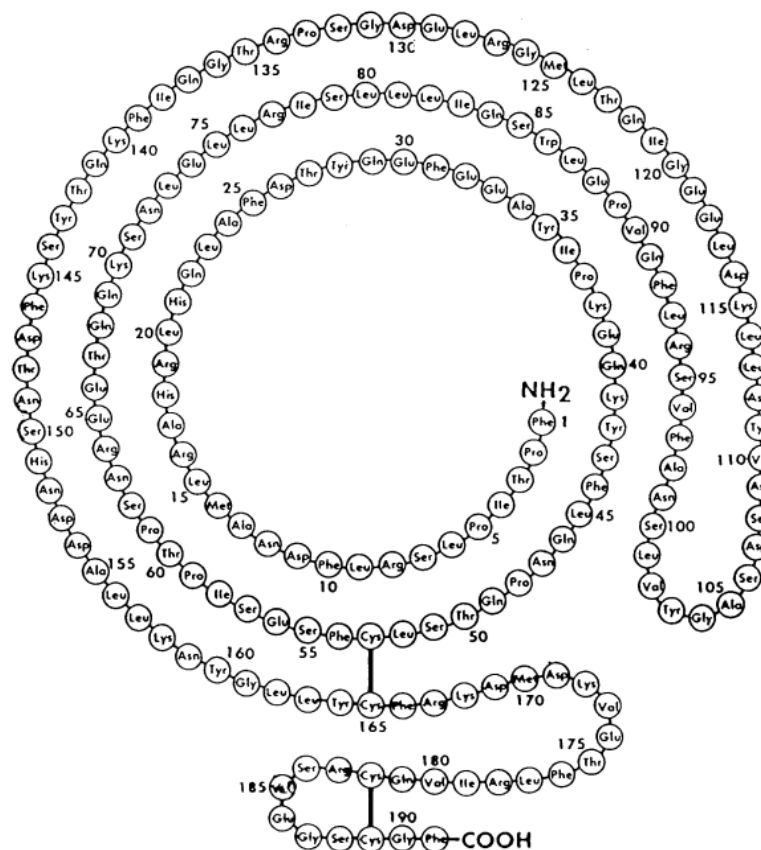


Fig. 5-20: Primary structure of hGH

In the early times hGH was isolated from the pituitary gland of cadavers, which accounted for the high world market price. Since 1988 hGH is produced in recombinant *Escherichia coli* as a precursor including a N-terminal amino acid extension (MAE) with an isoelectric point of 4,3. Eucaryotic proteins expressed in *Escherichia coli* always contain an N-terminal Met encoded by the translation initiation codon AUG (Goeddel *et al.*, 1979). To obtain the authentic eucaryotic sequence hGH is expressed as a precursor followed by a specific enzymatic cleavage. In this process the exopeptidase dipeptidylaminopeptidase I (DAP I) is used. This enzyme catalyses a stepwise removal of dipeptides from the N-terminus of proteins. DAP I cannot cleave peptide bonds involving a proline residue, since proline is the second amino acid in hGH, DAP I treatment of the hGH precursor results in the precise removal of the pre-sequence (Dalboege *et al.*, 1987).

5.6.3 FORMATE DEHYDROGENASE

NAD-dependent formate dehydrogenases (MW 80 kDa and isoelectric point of 5,5) are found in many methylotrophic bacteria and yeasts (Popov and Lamzin, 1994). FDH catalyzes the oxidation of formate to carbon dioxide concomitant with the reduction of NAD to NADH. Because of the favourable thermodynamic equilibrium of the reaction, the enzyme is used for in situ regeneration of NADH during asymmetric synthesis of chiral compounds (Wichmann *et al.*, 1981). A schematic scheme of cofactor regeneration is shown in Fig. 5-21.

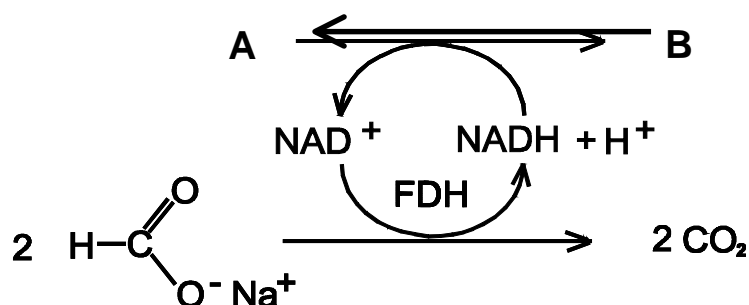


Fig. 5-21: Cofactor regeneration using FDH

FDH was produced originally as an intracellular homodimer by the yeast *Candida boidinii*, using continuous cultivation (Weuster-Botz *et al.*, 1994). In order to perform enzymatic reductions on a large scale, a production and downstream process has been established (Weuster-Botz *et al.*, 1994). However, the enzyme shows a considerable inactivation under biotransformation conditions (Kragl *et al.*, 1996) resulting in higher costs for the biocatalyst. Therefore, the FDH gene from *Candia boidinii* was cloned and over-expressed in *Escherichia coli* (Slusarczyk *et al.*, 2000) and mutants obtained with improved properties (Felber, 2001).

In this study, the rec. wild type FDH expressed in *Escherichia coli* was chosen as a model system to investigate biomass interaction in EBA. Table 1-8 shows the traditional downstream process and provides an indication for a possible EBA integration into the downstream process scheme.

Table 5-6: FDH purification protocol and implementation of EBA

Unit operation	Purification step	Implementation of EBA
cell disruption	capture	
heat precipitation	capture	E B A
ATPS I	capture	
ATPS II (back extraction into the salt phase)	capture	
ultra filtration	salt exchange & concentration	
Anion exchange chromatography	intermediate purification	

The use of EBA for FDH purification has already been investigated (Reichert *et al.*, 2001). During those studies biomass adsorbent interactions were found to be the major drawback using ion exchange or hydrophobic interaction chromatography media (see Fig. 5-22).

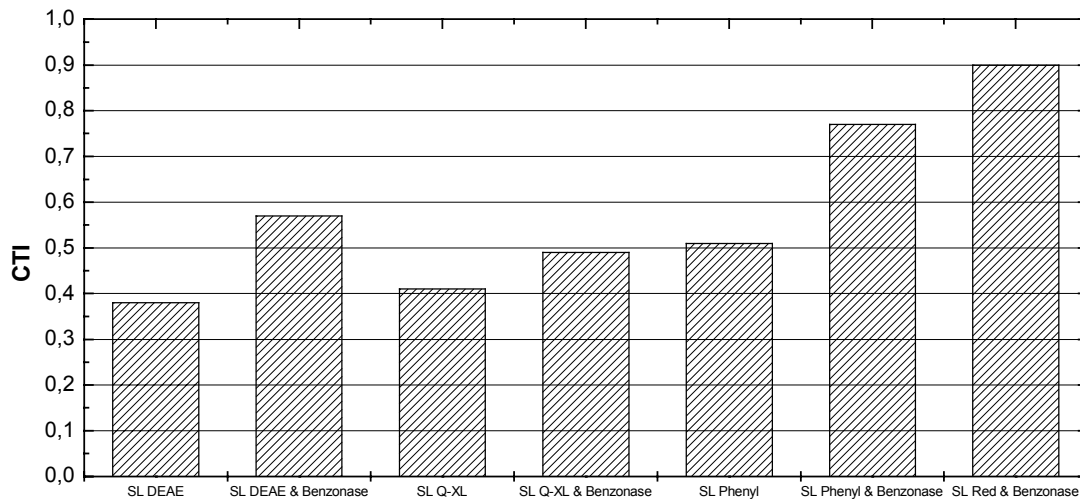


Fig. 5-22: *Escherichia coli* homogenate transmission, measured by the pulse-response experiment for different adsorbents at pH 7,5 and 5 mS/cm conductivity (1M ammonium sulphate added for adsorption to Streamline Phenyl) (Reichert *et al.*, 2001)

As seen in Fig. 1-32, only the application of a pseudo affinity ligand – based on the interaction of the immobilized dye with the NAD binding site of the enzyme – led to an acceptable cell transmission index. Any other adsorbent tested showed a severe cell retention in the EBA column. Detailed information can be found in Reichert *et al* (2001).

6 RESULTS AND DISCUSSION

6.1 FEEDSTOCK PROPERTIES & BIOMASS-ADSORBENT INTERACTIONS IN EXPANDED BED ADSORPTION

The successful application of EBA processes is closely linked to a good understanding of biomass adsorbent interactions occurring during feedstock application. In this context anion exchange chromatography has been identified as the most critical mode due to the fact that cells or cell debris carries a negative charge under common process conditions. The implication of this, namely significant biomass/adsorbent interactions, have already been extensively reported (Fernández-Lahore *et al.*, 1999, Karau *et al.*, 1997, Lin *et al.*, 2001, Thömmes, 1997). Thus, in the present study a closer investigation of the biomass adsorbent interaction during anion exchange EBA has been performed. *Escherichia coli* was chosen as the most common expression system in recombinant DNA technology. Additionally some initial experiments have been carried out using the yeast system *Saccharomyces cerevisiae*. As a stationary phase for EBA Streamline DEAE was used as a common anion exchange resin.

In order to find parameters affecting biomass/adsorbent interaction the following feedstock characteristics have been investigated using various *Escherichia coli* strains:

- 1) The influence of growth phase and growth conditions during *Escherichia coli* cultivation onto surface charge conditions of the cells.
- 2) The impact of different cell disruption methods and operational parameters on feedstock properties and their relation to biomass interactions in EBA. The main parameter under investigation were: DNA, cell surface charge, particle size distribution.

6.1.1 ZETA POTENTIAL DEVELOPMENT OF INTACT CELLS DURING HIGH CELL DENSITY CULTIVATION OF *ESCHERICHIA COLI*

During ion exchange chromatography, Biomass adsorbent interactions in expanded beds are mainly due to electrostatic interactions. Therefore, the impact of cultivation conditions on the surface charge of *Escherichia coli* cells has been investigated. It is well known that the hydrophobicity of bacteria increases with increasing growth rate (1987b, Boonaert and Rouxhet, 2000, van Loosdrecht *et al.*) and that the surface charge is related to the N/P ratio at the cell surface (Krekeler *et al.*, 1989, Büchs *et al.*, 1988). The N/P ratio can further be correlated with the phosphate concentration in the cultivation media.

During this study fed-batch cultivations of various *Escherichia coli* strains and cultivation conditions have been examined, analyzing the effective surface charge during cultivation. In order to account for the various ionization states of chemical groups on the cell surface, zeta potential measurements were carried out under a range of pH values, keeping the conductivity constant. The following strains were used for this investigation: *Escherichia coli* JM 101, JM 105, a rec. *Escherichia coli* rec. L-phe (L-phe production) strain and JM 105 rec. FDH producing *Candida bondinii* FDH.

In two fed batch cultivation (*Escherichia coli* JM 101 and *Escherichia coli* JM 105 rec. FDH) the zeta potential, when measured at pH 2 and 3, increases from 5 to 10 mV during the cultivation time, while at pH 7 the zeta potential keeps constant, depending on the cultivation, in a strongly negative range between -38 and -26 mV. Fig. 6-2 to Fig. 6-4 show the zeta potential development for the investigated cultivation conditions. The differences obtained between different pH-values arise from the pH dependent degree of ionization of charge relevant amino- and carboxyl groups at the cell surface.

Comparing the cultivations shown in Fig. 6-2 and Fig. 6-3, it is apparent that the surface charge of *Escherichia coli* JM 101 (Fig. 6-2) increases faster (18,5 mV in 37 h) than the surface charge of *Escherichia coli* JM 105 (Fig. 6-3) (8 mV in 38 h). These cultivations however not only differ in the strain used but in the Mg^{2+} concentration in the feed media (Fig. 6-2: $C(Mg^{2+}) = 14 \text{ g L}^{-1}$, Fig. 6-3: $C(Mg^{2+}) = 10 \text{ g L}^{-1}$). Hence the variation observed is not only related to the strain itself but more likely linked to the specific cultivation conditions. This leads to the assumption that higher Mg^{2+} concentration in the feed reduces the negative Zeta potential of cells during the cultivation. It is known

from previous investigations that divalent cations have a significant impact on the surface charge of microbial cells (Lin *et al.*, 2002). As the zeta potential measurements are carried out at a 500 fold dilution of the cell suspension an impact of the cultivation media on the actual measurement can be ruled out. Hence the Mg^{2+} concentration plays an important role for the surface charge of the cells. This might be a result of the incorporation of Mg^{2+} into the outer cell membrane or a strong chelating attachment of the Mg^{2+} ions at the cell surface. The influence of the Mg^{2+} concentration in the feed can further be seen during the cultivation of *Escherichia coli* JM 105 rec. FDH shown in Fig. 6-4. Approximately 3 h after a feed pulse – containing a 10 times higher Mg^{2+} concentration than the cultivation media – a significant increase of the zeta potential measured at pH 7 could be found. Measurements at pH 2 and 3 showed a decrease of the surface charge to approximately 0 mV. After another 2 hours this change in the zeta potential disappeared leading to a zeta potential to a level observed prior to the pulse. The long response time on the feed pulse seems to indicate that the impact of magnesium is not only related to an adsorption of the cation on the cell surface, which should be a much faster process, but rather to the implementation of the magnesium into the outer membrane. From literature it is known that divalent cations such as Mg^{2+} and Ca^{2+} are integral components of the *Escherichia coli* outer membrane (Nikaido, 1996).

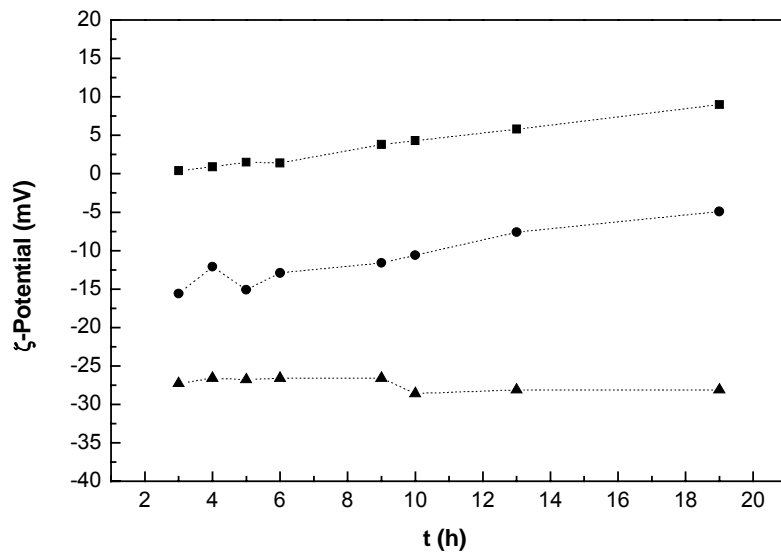


Fig. 6-1: Surface charge of an rec. L-phe production *Escherichia coli* strain (cells received from Nicole Rüffer IBT II of the research centre Jülich, Germany) during a fed batch cultivation measured in 10 mM Na_2HPO_4 /citric acid buffer at a constant conductivity $\kappa=5\text{ mS cm}^{-1}$ adjusted with solid NaCl and various pH. At (■) pH 2, (●) pH 3, (▲) pH 7

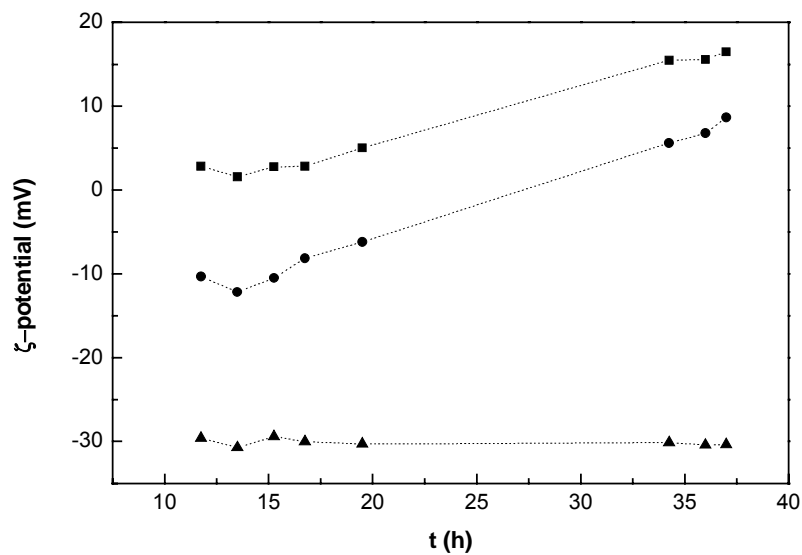


Fig. 6-2: Surface charge of *Escherichia coli* JM 101 cells during a fed batch cultivation measured in 10 mM Na_2HPO_4 /citric acid buffer at a constant conductivity $\kappa=5\text{ mS cm}^{-1}$ adjusted with solid NaCl and various pH. At (■) pH 2, (●) pH 3, (▲) pH 7. ($C_{\text{Mg}^{2+}} = 14\text{ g L}^{-1}$ in the feed media)

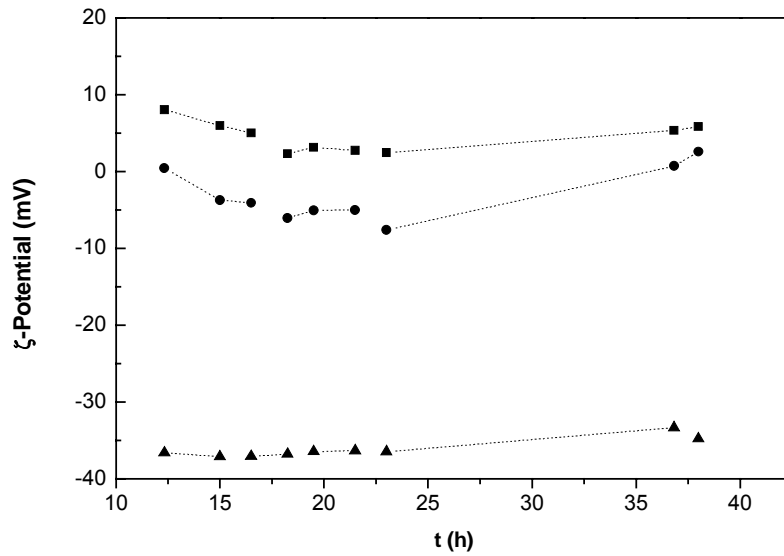


Fig. 6-3: Surface charge of *Escherichia coli* JM 105 cells during a fed batch cultivation measured in 10 mM Na_2HPO_4 /citric acid buffer at a constant conductivity $\kappa = 5 \text{ mS cm}^{-1}$ adjusted with solid NaCl and various pH. (■) pH 2, (●) pH 3, (▲) pH 7. ($C_{\text{Mg}^{2+}} = 10 \text{ g L}^{-1}$ in the feed media)

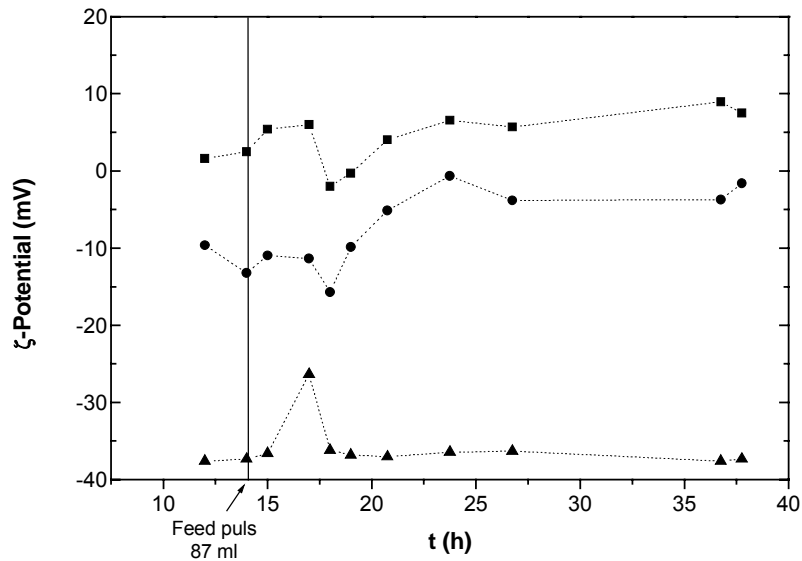


Fig. 6-4: Surface charge of *Escherichia coli* JM 105 rec FDH cells during a fed batch cultivation measured in 10 mM Na_2HPO_4 /citric acid buffer at a constant conductivity $\kappa = 5 \text{ mS cm}^{-1}$ adjusted with solid NaCl and various pH. At (■) pH 2, (●) pH 3, (▲) pH 7. ($C_{\text{Mg}^{2+}} = 10 \text{ g L}^{-1}$ MgSO_4 in the feed media)

6.1.2 IMPACT OF CELL DISRUPTION ON FEEDSTOCK PROPERTIES

Different cell disruption methods or different operational conditions during the actual disruption process have an influence on the physical properties of the homogenates. To evaluate this impact of different homogenates properties on EBA process performance a detailed investigation on the respective feedstock properties arising from differences during cell disruption has been carried out.

a DNA CONTENT AND MOLECULAR WEIGHT DISTRIBUTION

One of the major components in homogenate is DNA released during cell disruption. Chromosomal DNA is a large molecule, which is strongly negatively charged. In the case of EBA applications this might cause a bridging effect between the adsorbent particles resulting in larger aggregates and finally in channeling and dead water zones (Feuser *et al.*, 1999). It has been shown in several publications that feedstock viscosity had significant impact on the bed stability in EBA (Barnfield-Frej *et al.*, 1994, Chase, 1994, Feuser *et al.*, 1999, Johansson *et al.*, 1996, Pyo *et al.*, 2001) and that the viscosity of cell homogenates mainly depended on the release of DNA during cell disruption (Anspach *et al.*, 1999). A detailed investigation on the influence of cell disruption methods and conditions on DNA release, MW distribution and viscosity, and thus their impact on bed stability is, however, still missing. As a consequence the influence of different cell disruption methods and conditions on the DNA content and molecular weight distribution in the cell homogenate has been studied and their impact on the biomass adsorbent interactions in an expanded bed was analysed. Feedstock viscosity has been chosen as a first indicator for differences in DNA composition.

Cell disruption Method

Three common laboratory cell disruption techniques – ultra sound, bead mill and French press – were investigated regarding the DNA composition obtained in the respective *Escherichia coli* homogenate. Comparing the different cell disruption methods a significant variation of the DNA composition could be found. Cell disruption employing a lab scale bead mill resulted in a homogenate of rather high viscosity containing large DNA molecules. Feedstock's obtained by homogenization based on ultra sound or high pressure (French Press) showed a 50 % lower viscosity (Fig. 6-5). The results obtained from viscosity measurements can be confirmed by agarose gel electrophoretic analysis. DNA analysis after cell disruption in a small bead mill shows the presence of high molecular weight DNA (> 12,2 kb). Homogenates obtained using either ultra sound or French press homogenization exhibited an increased concentration of low molecular weight DNA, while high molecular weight DNA could not be detected anymore (Fig. 6-6).

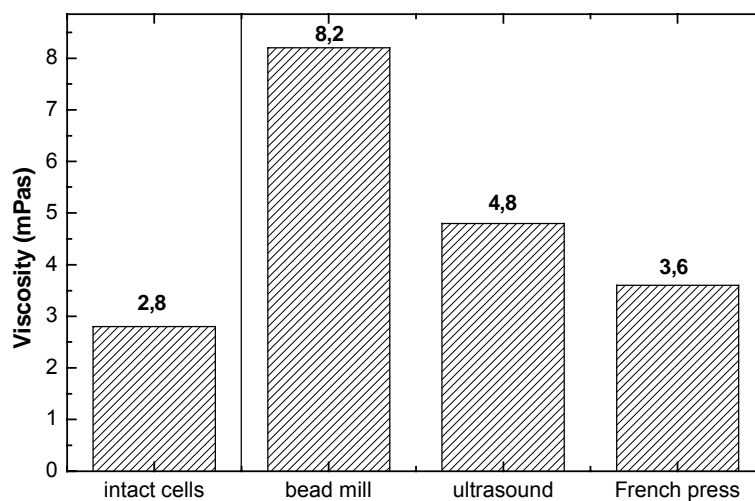


Fig. 6-5: Viscosity of 40 % *E. coli* homogenate obtained from different cell disruption methods (using a biomass suspension of $C_b = 40$ % ww)

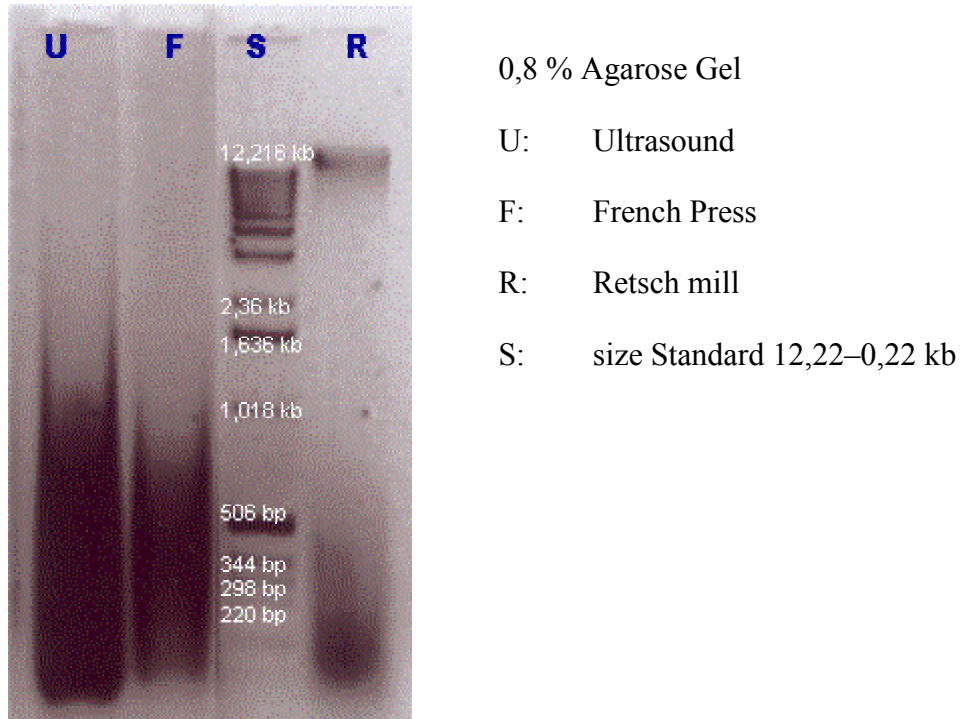


Fig. 6-6: 0,8 % Agarose gel analysis of homogenates obtained from various cell disruption methods

Cell disruption conditions during French Press homogenization

Important variables during high pressure homogenization are operation pressure and the cycle number. Increasing the applied pressure from 482 bar to 965 bar resulted in a more than three fold lower viscosity after a single passage when using 40% w/w *Escherichia coli* cell suspension (Fig. 6-7). During additional homogenization cycles this significant difference in the effectiveness of the homogenization procedure diminishes, while a viscosity difference of 1-2 mPa s remains (Fig. 6-7). The most significant effect during homogenization was found during the first two cycles while additional cycles led to a negligible reduction of the viscosity. This is in good agreement with findings by Barnefield-Fey et al. (1994) and was further confirmed by Agarose-Gel analysis (Fig. 6-8).

DNA detection using agarose gel electrophoresis depends on the intercalating of ethidium bromide into the DNA strands. A reduction in the polynucleotide chain length leads to a reduced efficiency in the staining procedure and thus lower signal on the

agarose gel. The reduced band intensity seen in Fig. 6-8 is therefore an indication for the size reduction of released DNA during the Homogenization procedure.

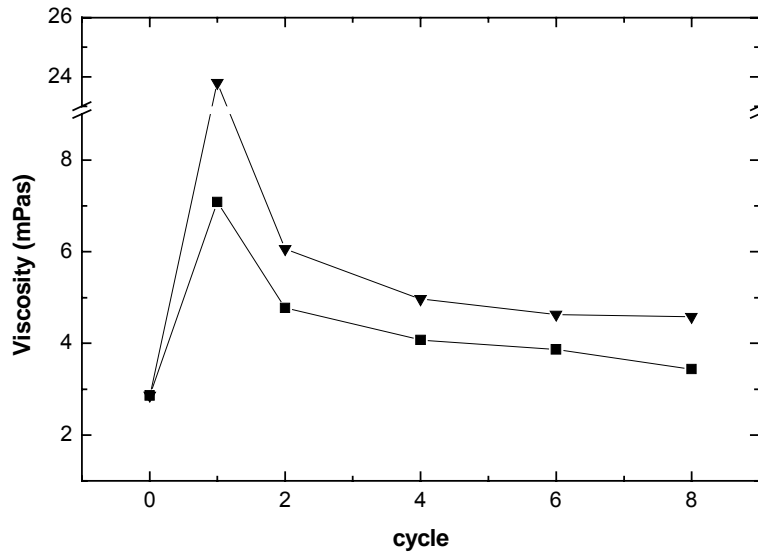


Fig. 6-7: Viscosity of *Escherichia coli* biomass suspension ($C_b = 40\%$ ww) during multiple passage homogenization in a French Press at two different operating pressures (\blacktriangledown) 482 bar and (\blacksquare) 965 bar.

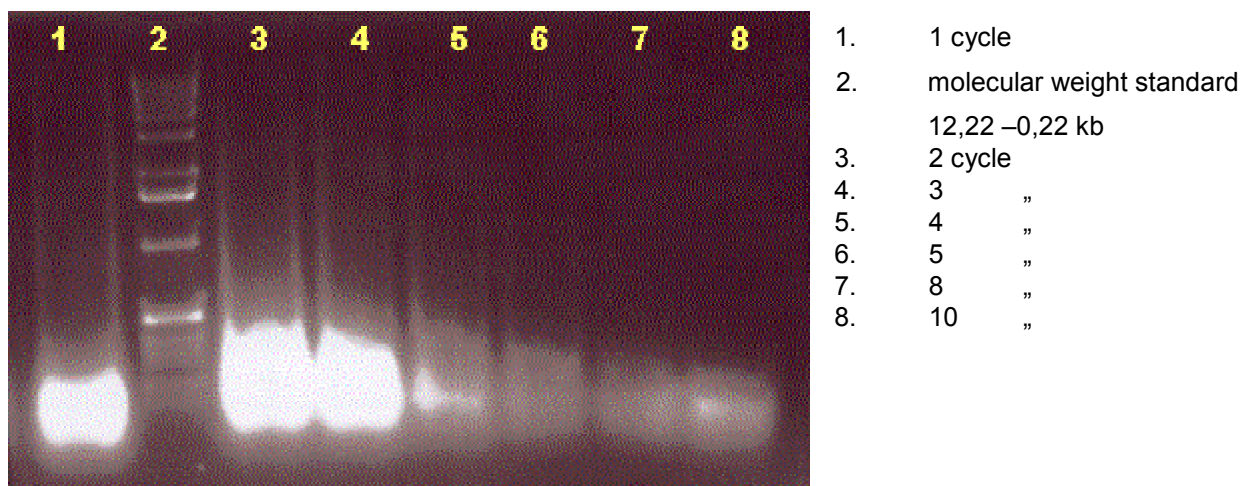


Fig. 6-8: 1,5 % agarose gel analysis ethidiumbromide stained French Press homogenate at different homogenization cycles and a operation pressure of 965 bar

In order to distinguish between the effect of DNA size presented and other effects occurring during homogenization on the biomass adsorbent interaction, pulse response

experiments were performed using bead mill homogenates with and without Benzonase™ (Merck, Darmstadt) treatment prior to its application. Benzonase™ is an unspecific endonuclease which cleaves DNA into smaller oligo nucleotides and is often used to decrease the viscosity of feedstocks and therefore to improve fluidisation quality in EBA (Barnfield-Frej *et al.*, 1994, Clemmitt and Chase, 2002, Johansson *et al.*, 1996, Pyo *et al.*, 2001). Even though it could have been expected that the untreated bead mill homogenate shows a significant biomass adsorbent interaction (Fig. 6-9) an only slight decrease in the CTI value was found when compared to the initial feedstock containing whole cells, while Benzonase™ treatment showed no effect on the CTI value and the measured zeta potential. In contrast to these findings Reichert *et al.* (2001) showed a strong positive impact of Benzonase™ treatment on the measured CTI value. These results were, however, obtained with feedstock based on different *Escherichia coli* strains and lower conductivities ($\kappa=5 \text{ mS cm}^{-1}$ instead of $\kappa=10 \text{ mS cm}^{-1}$). The most significant effect was found for the application of a pseudo affinity adsorber (Streamline Red), where an increase in the CTI of 0.1 could be measured. The CTI values does, however, only describe the cell retention in the column or possible bridging effects between adsorbent and biomass, the fluidisation behavior obtained when applying the real process liquor has to be evaluated using appropriate RTD measurements (see chapter 5.1.3).

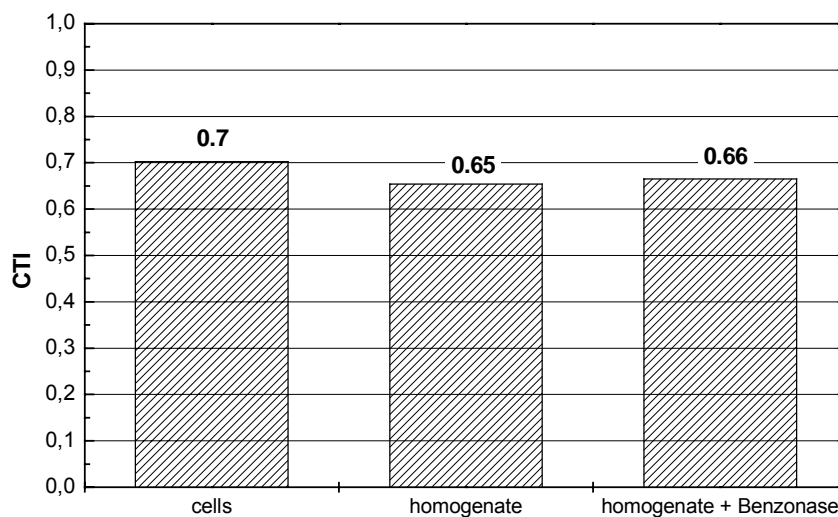


Fig. 6-9: CTI using bead mill homogenate with & without Benzonase™ treatment (*Escherichia coli* JM105).

b IMPACT OF SURFACE CHARGE & PARTICLE SIZE

Particle size analysis in this study yielded a size distribution. To simplify the evaluation of the particulate size data the average size (z-average) has been used, as calculated by the Malvern Zetasizer 4 analysis software. For a more detailed information complete size distribution data are given in the Appendix.

Cell disruption method

The impact of different homogenization techniques on size and effective surface charge of debris in the homogenate is shown in Fig. 6-10 and Fig. 6-11. Both parameters show clear trends when comparing the different disruption techniques, indicating that a decrease in size is linked to a decrease in the measured zeta potential. Cell disruption by sonication and high pressure (French Press) resulted in a 4-5.5 times more effective size reduction (1300 nm to 230 nm) of the cell debris when compared to measurements obtained with laboratory bead mill homogenate (1300 nm to 1200 nm). The latter findings indicate that the bead mill homogenate consisted of cells ripped open but not completely disrupted and therefore only minor size reduction were observed. With regard to surface charge, the same trend could be observed, the largest particles – whole cells – showed the highest net surface charge (-23 mV), whereas for the smaller cell debris obtained from French press a lower surface charge was measured (-16 mV). A possible explanation for the link found between the size and zeta potential will be discussed below.

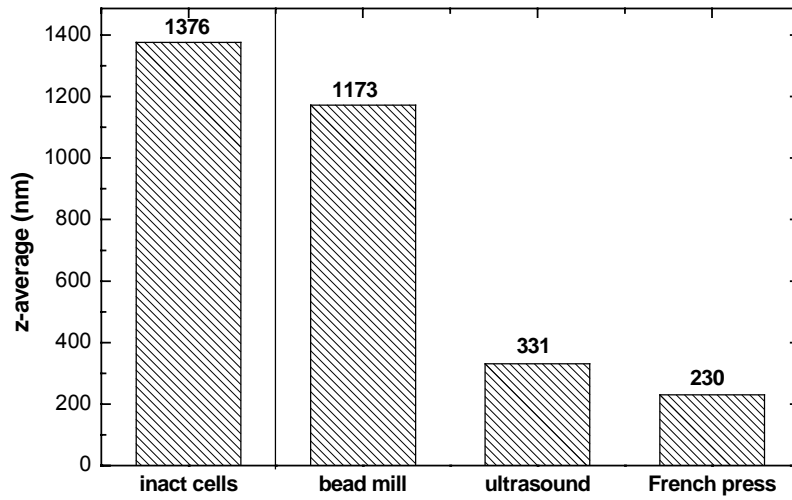


Fig. 6-10: Average size distribution obtained by different cell disruption methods using 40 % ww *Escherichia coli* JM 101, suspension.

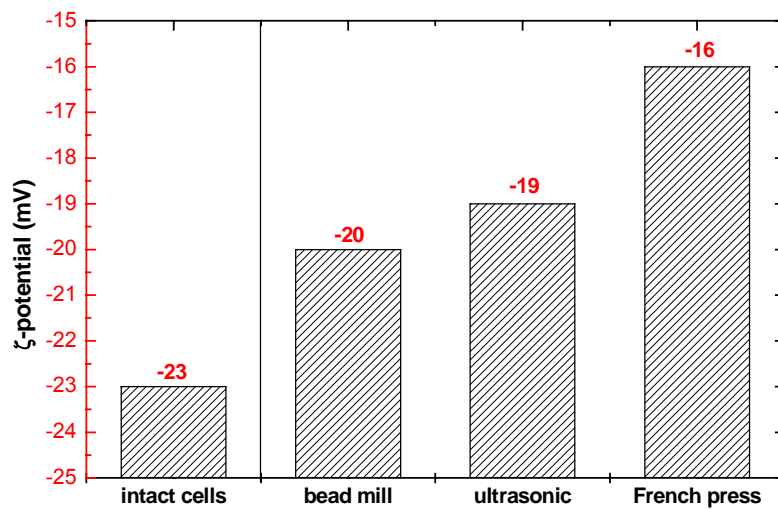


Fig. 6-11: Surface charge of cell debris obtained by different cell disruption methods. Using 40 % ww *Escherichia coli* JM 101. Measurement in 100 mM Tris/HCl pH 8.0 $\kappa = 10 \text{ mS cm}^{-1}$.

Homogenate properties at various Homogenization conditions in the French Press

In order to gain a deeper understanding of the relationship between the size and zeta potential measured for the different homogenates, a more detailed investigation was performed by altering homogenization conditions in the French press. The experiments resulted in a large number of homogenates exhibiting various combinations in size and zeta potential. It could be shown that a direct correlation exists between the particle size and number of cycles through the French press. In accordance to results described above (chapter 6.1.2 page 57), it was found that the degree of size reduction was directly linked to the applied pressure. This corresponds with results presented by Middelberg and co-workers where the cell disruption efficiency, measured by the release of intracellular protein, is directly related on the operating pressure (Middelberg *et al.*, 1990, Middelberg *et al.*, 1992) and on the number of cycles applied (Wong *et al.*, 1997) (Kula and Schütte, 1987, Kula *et al.*, 1990). With the two operating pressures in this study a limiting size of approximately 200 nm was reached. The number of cycles necessary for this reduction was, however, depending on the applied pressure (Fig. 6-12) at a higher pressure the minimum value was reached with fewer homogenization cycles (2 cycles at 965 bar versus 6 cycles at 482 bar).

Corresponding to the results obtained for different homogenization techniques, a direct link between size reduction and measured zeta potential could be found (Fig. 6-13). Multiple passages of homogenization leads to a reduction in the net surface charge of the cell debris until a minimum value of -16 mV was reached. The minimal value reached did not depend on the operating pressure, though a higher pressure let to a steeper slope of the ζ -potential/cycle dependency.

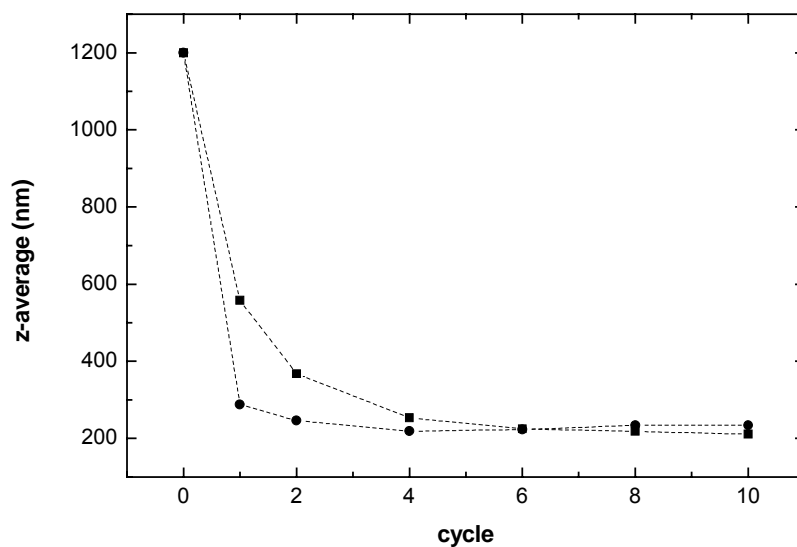


Fig. 6-12: Average size distribution of *Escherichia coli* homogenate treated with different pressure and cycles in the French Press (■) 965 bar, (●) 482 bar.

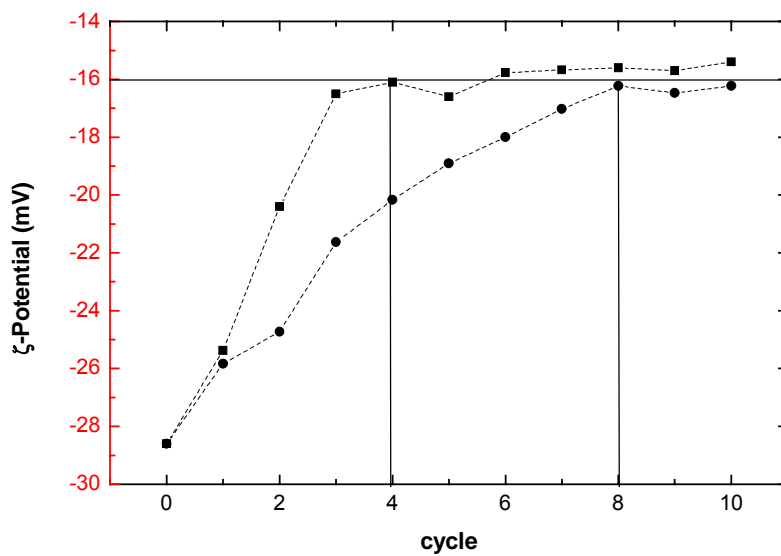


Fig. 6-13: Surface charge of *Escherichia coli* homogenate treated with different pressure and cycles in the French Press. (■) 965 bar, (●) 482 bar.

During the course of this study the decrease of the surface charge during high pressure homogenization was an unexpected result. Assuming a homogenous structure of the *Escherichia coli* cell wall, the decrease of the size during cell disruption should not affect the surface charge of the cell debris. A difference of the electrostatic mobility between isolated cell walls and whole cells has been already reported by Neihof et al (1973). Regarding the structure of a Gram⁻ cell wall as described in chapter 5.4.1 it is apparent, that the wall structure composed of the outer membrane (OM), the peptidoglycan layer, and the cytoplasmic membrane is of an asymmetric nature. The surface of the OM is characterized by strongly negatively charged lipopolysaccharides, which are the major components accounting for the surface charge of the intact bacterial cell.

During cell disruption the impact of the cytoplasmic membrane on the net surface charge becomes more important as schematically shown in Fig. 6-14 resulting in a decrease of the over all net surface charge of the cell debris. The impact of various charges on the electrophoretic mobility and therefore on the ζ -potential is illustrated in Fig. 6-15.

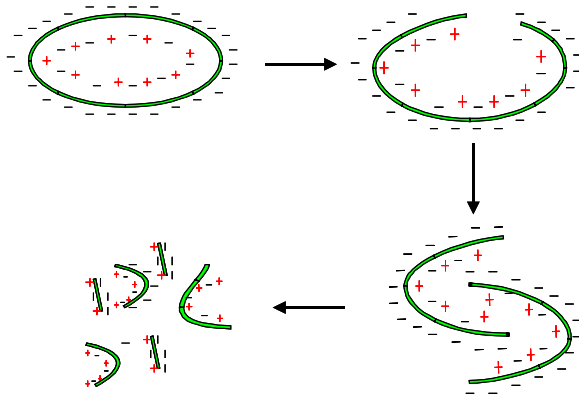


Fig. 6-14: Impact of particle size on the surface charge of *Escherichia coli* cell debris.

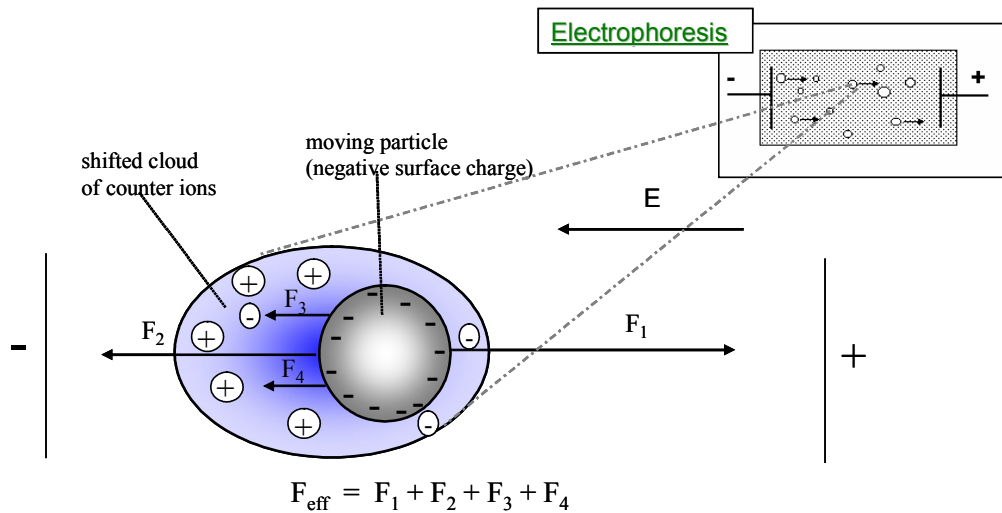


Fig. 6-15: Impact of various forces on the electrophoretic mobility of a particle in an electrical field. F_1 - accelerating force, F_2 - retarding force, F_3 - electrophoretic retardation, F_4 - relaxation effect (Nitzsche, 2002).

Correlation between disruption conditions and biomass adsorbent interactions

The results presented in the previous chapter show a significant difference between feedstock characteristics arising from the different cell disruption methods. The variation mainly relate to differences in DNA molecular weight distribution, particle size and surface charge of cell debris (see Table 6-1).

Table 6-1: Feedstock characteristic depending on the cell disruption method

	Viscosity mPa s	average size (nm)	ζ - potential (mV)
Intact cells	2,8	1376	-23,2
laboratory Bead mill	8,2	1173	-19,9
Ultrasound	4,8	331	-18,8
French press at 1378 bar	3,6	230	-16,1

When analyzing the different homogenates for biomass interactions a clear pattern for the CTI could be observed (Fig. 6-16). The lowest cell retention (or highest cell transmission) of CTI = 0.99 has been found using a French press homogenate, which is characterized by the smallest particle size, the lowest net charge and the lowest viscosity. The larger the particle the lower the CTI is in the series French Press (CTI = 0.99) > Ultrasound (CTI = 0.9) > bead mill (CTI = 0.71).

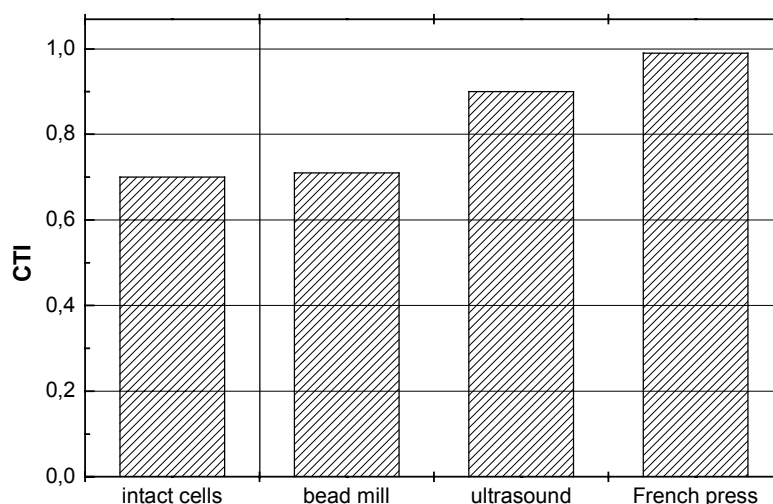


Fig. 6-16: CTI of various homogenates depending on the homogenization method (pH 8,0; $\kappa=10 \text{ mS cm}^{-1}$)

c THE IMPACT OF ELECTROSTATIC INTERACTION IN EBA

Extensive studies about the electrostatic interaction between cells, cell debris, and the adsorbent have been carried out by Lin et al (2002). These studies focused on the influence of conditions in the surrounding liquid (concentration and valancy of ions, conductivity, pH, surfactants) on the surface charge of the biomass. For monovalent cations a linear relation was found, correlating the ζ -potential (obtained for different ions and concentration) and the biomass interactions. At lower ζ -potential a higher cell transmission was observed (e.g. a ζ -potential $< |2 \text{ mV}|$ yields a CTI > 0.9) and for divalent cations a non linear relation was found. Ca^{2+} had a weaker impact on the biomass interaction at low concentration corresponding to a lower CTI below -4 mV compared to monovalent ions (Fig. 6-17). The biomass/adsorbent electrostatic interactions are taking place with particulates carrying opposite charges. It is obvious

that the liquid conditions not only influence the surface characteristics of the biomass but also the surface charge of the adsorbent. To take this into account a new parameter ($-\zeta_a\zeta_b$) has been defined including the zeta potential of the adsorbent (ζ_a) and the biomass (ζ_b). As shown in Fig. 6-18 a linear correlation between ($-\zeta_a\zeta_b$) and the cell transmission index was found including also various divalent cation. The threshold value of CTI = 0.9 cell transmission was reached at 20 mV^2 . Comparing different kinds of biomass (*Escherichia coli*, *Saccharomyces cerevisiae*, cells and homogenates) a difference in the slope of the linear correlation was observed, indicating that there is at least one additional parameter having an impact on the biomass adsorbent interaction in anion exchange EBA.

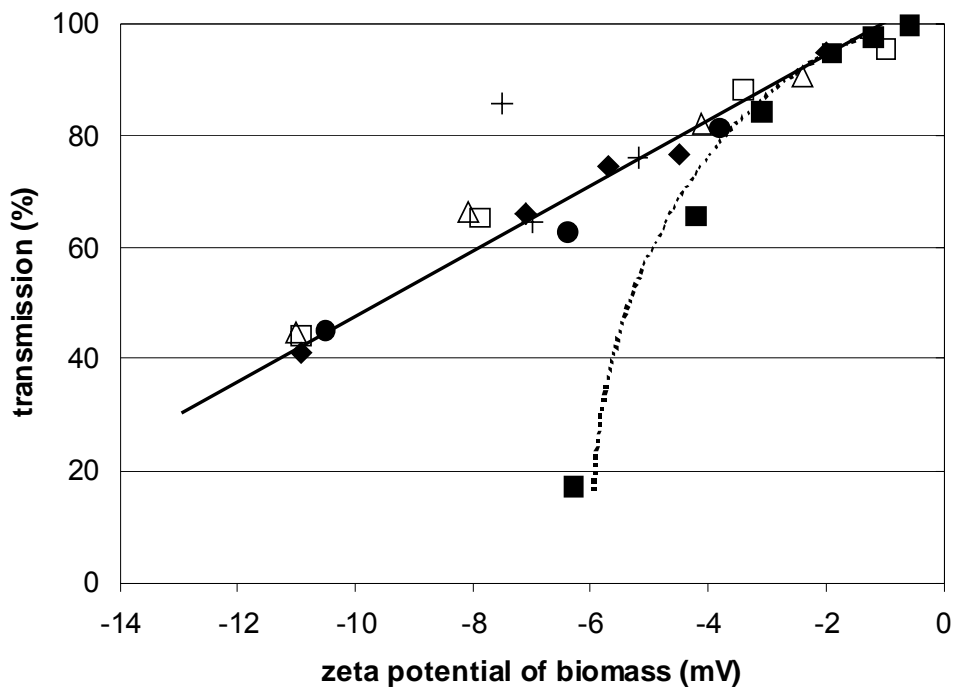


Fig. 6-17: The ζ -potential \sim CTI relation for intact yeast cells and Streamline DEAE varying ions (NaCl (□), NH₄Cl (●), Na₂SO₄ (Δ), (NH₄)₂SO₄ (□), CaCl₂ (■) and pH (+)).(Lin *et al.*, 2002)

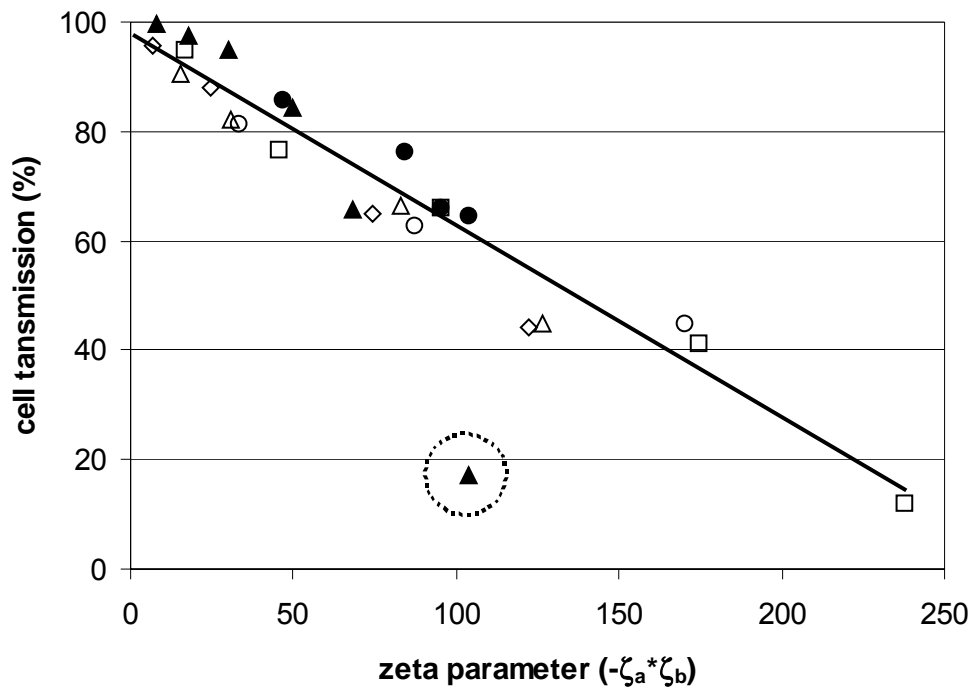


Fig. 6-18: The $(-\zeta_a \zeta_b) \sim P$ relation for intact yeast cells and Streamline DEAE using varying ions (NaCl (□), NH_4Cl (○), Na_2SO_4 (△), $(\text{NH}_4)_2\text{SO}_4$ (◇), CaCl_2 (▲)) and pH (●) (Lin *et al.*, 2002)

To account for the differences between various kind of feedstock, cells and homogenates from different organism a new parameter was introduced ($-\zeta_a \zeta_b d$) for the correlation shown in Fig. 6-18. This parameter includes the particle size x (obtained from literature) to account for the differences between the feedstock's. A variation of the cell disruption has not been investigated by Lin et al (2003)

Correlating the ζ -potential data with the corresponding CTI for various cell disruption methods and conditions no clear correlation could be found (data not shown). In contrast to the results from Lin et al. these homogenates differ in the particle size distribution in the sample. Besides the variation in the surface charge a broad range in size (250-1250 nm) existed.

A correlation of particle size and CTI is shown in Fig. 6-19. In a range from 270 nm up to approximately 500 nm a linear relation was found. Below a mean size of 270 nm full transmission was observed and above 500 nm the transmission reached a minimum of $\text{CTI} = 0.7$ at the conditions investigated.

Using the parameter and the results obtained from different cell disruption conditions a linear relationship with the cell transmission data in a range from 70-400 mV^2cm was found (Fig. 6-20).

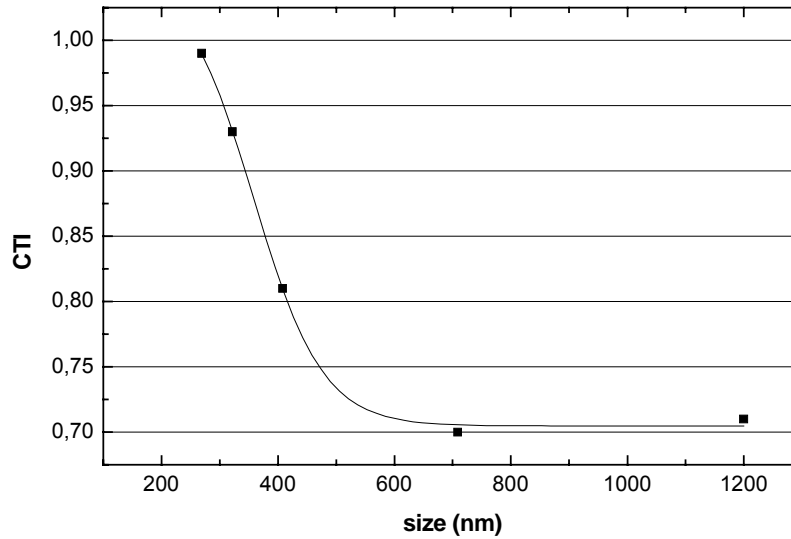


Fig. 6-19: Correlation of mean size distribution and CTI (Escherichia coli JM 105 French Press homogenate at 300 bar different cycles).

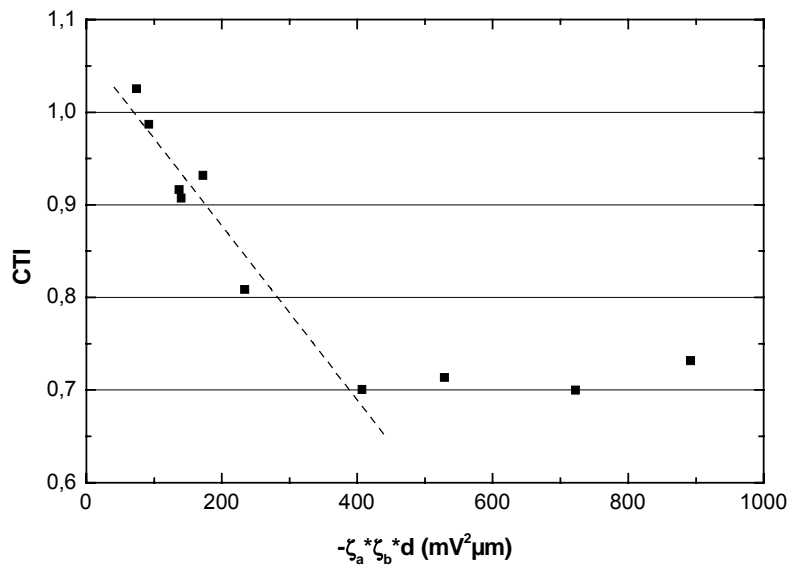


Fig. 6-20: Evaluation of size ζ -potential and transmission using the correlation after Lin et al. () linear fit ($y = a + b \cdot x$ with $a = 1,007$; $b = -0,05$; $R = 0,92$)

d EXPANDED BED ADSORPTION AS DEEP BED FILTRATION

In order to get a mechanistic understanding of biomass retention in EBA theoretical considerations from deep bed filtration (DBF) have been used. In this context EBA can be visualized as an inefficient deep bed filtration with a comparatively large voidage between the filter particles and the objective for EBA – contrary to traditional DBF processes – is a free passage of the particulates through the bed. In DBF theory the capture of fine particles is divided into two principal parameters (Ives, 1975):

- a. The attachment probability
- b. The transport or collision probability

As discussed in chapter 5.2 page 23 electrostatic interactions can be taken as the major attachment mechanism in ion exchange chromatography. The electrostatic interactions between biomass and adsorbent can be described using a correlation known from colloid theory. Fuerstenau (Lagaly *et al.*, 1997, Sonntag, 1977) derived a equation to calculate the electrostatic potential (φ_{ei}) between two oppositely charged colloid particles depending on the surface charge of both particles, the particle sizes and the distance (a) between the particles. The impact of surface charge and particle size on the electrostatic interaction potential φ_{ei} is shown in Fig. 6-21. In this calculation the surface charge and the particle size of the adsorbent was set constant. Plotting φ_{ei} versus the distance (a) between the particles, φ_{ei} increases rapidly if the particles come into close contact. With an increased distance between the particles the potential approaches zero. A decrease in the effective surface charge (ζ -potential in absolute value) of the biomass particle results in a shift of the curve towards the x axis, which means a lower charge leads to a φ_{ei} value shift. If particle size decreases in combination with the net surface charge a further shift could be observed. It can be concluded that a reduction in particle size as well as a decrease of the effective surface charge reduces the strength and the range of the electrostatic interaction potential between two oppositely charged particles. For successful attachment the distance between the particles has thus to be much smaller for small and less charged particles.

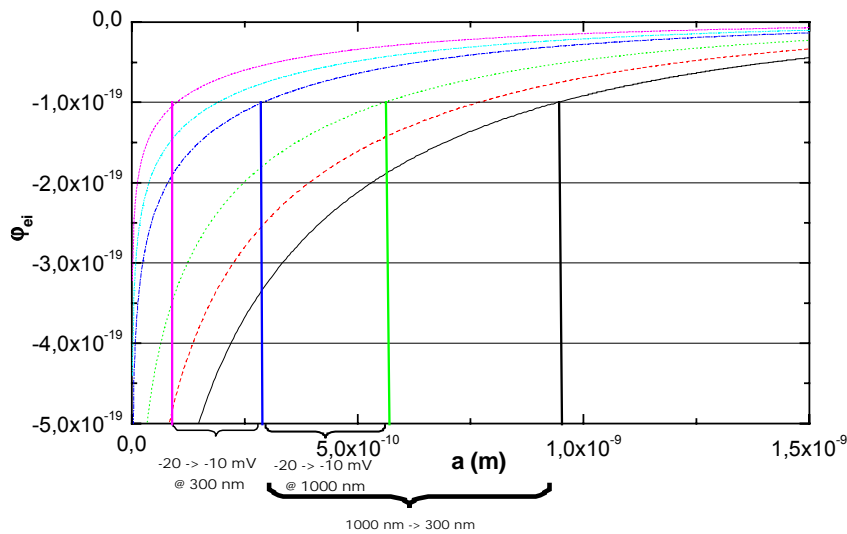


Fig. 6-21: Electrostatic interaction potential (ϕ_{ei}). Influence between the oppositely charged particles (cell debris and adsorbent) versus the distance between the particles. Calculated at various biomass particle sizes and surface charge at constant conditions for the adsorbent particle. (—) $x = 1000$ nm and $\zeta = -20$ mV, (···) $x = 1000$ nm and $\zeta = -15$ mV, (···) $x = 1000$ nm and $\zeta = -10$ mV, (---) $x = 300$ nm and $\zeta = -20$ mV, (-·-·) $x = 300$ nm and $\zeta = -15$ mV, (-·-·) $x = 300$ nm and $\zeta = -10$ mV.

Among the various transport mechanisms normally encountered during DBF, interception can be assumed to be the major transport mechanism at the conditions prevalent in an EBA column. This transport mechanism strongly depends on the particle size of both, the adsorbent and the biomass particle (Eq. 6-1). A size reduction in the biomass particulate will lead to a reduction in the collision probability (Fig. 6-22). From theoretical and experimental work an inverse relationship for the adsorbent particle has been found (Stevenson, 1997, Tiehm *et al.*, 1999)

Eq. 6-1: Dimensionless number of Interception

$$N_R = \frac{x}{d}$$

x = average particle diameter of cell debris
 d = diameter of the adsorbent particle

The parameter N_R describes the impact of interception on the particle transport to the adsorbent particle. In Fig. 6-22 the linear relation of N_R and the biomass size illustrates that the transport by interception of whole cells is more than 2.5 times more efficient than for bead mill homogenate and more than 5 times more efficient than for a French press homogenate. From the results presented above it can be concluded, that the biomass size has a dominating impact on the transport mechanism as well as on the attachment mechanism.

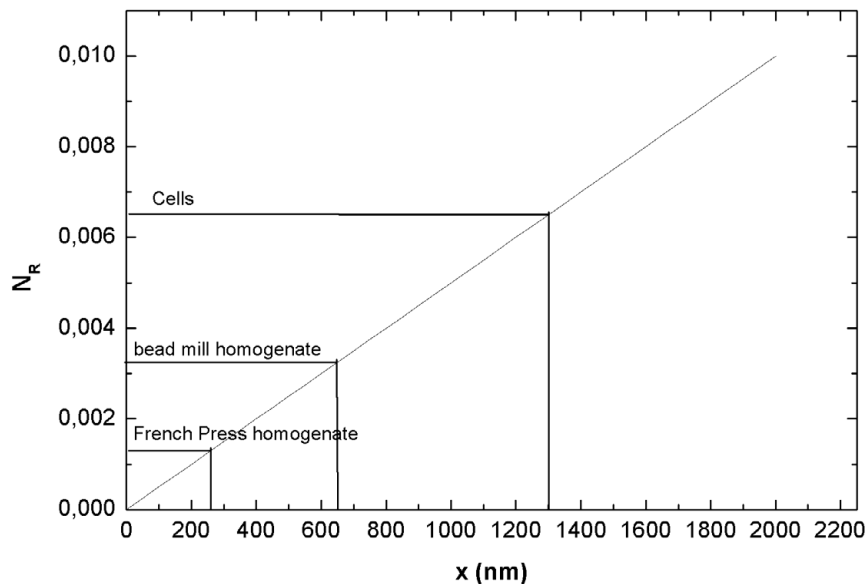


Fig. 6-22: The impact of biomass particle size (x) on the dimensionless number for Interception (N_R) (Ives, 1975).

In recent years operational parameters such as pH, salt concentration (conductivity) and biomass load were used to minimize biomass adsorbent interactions (Fernández-Lahore *et al.*, 2000, Lin *et al.*, 2001). Considering the results shown above the particle size resulting from different cell disruption methods and conditions is an important parameter for EBA process optimization. In addition the fact that the net surface charge of *Escherichia coli* decreases with decreasing particle size, demonstrates that cell disruption is an important unit operation for process design, as it precedes EBA for the recovery of intracellular proteins.

6.1.3 ESCHERICHIA COLI HOST STRAINS

Cell wall properties are known to be dependent on various factors such as media composition, cultivation conditions and the actual strain. It was for example shown by Li and MC Landsborough, (1999) that the surface charge for various pathogenic *Escherichia coli* varies among different isolates, serotypes and strains in a range of $\zeta = -4,9$ to $\zeta = -33,9$ mV. Fig. 6-23 shows the measured zeta potential for cells and homogenates using different *Escherichia coli* strains commonly employed for expression of foreign proteins. All *Escherichia coli* strains investigated are strongly negatively charged. Comparing the intact cells there are some differences in the surface charge between the strains (between $\zeta = -20$ and $\zeta = -30$ mV). The surface charge properties (zeta potential) of different organisms depends on the deprotonated phosphate groups which are partly neutralized by protonated amino groups (Krekeler *et al.*, 1991). This relation depends mainly on the N/P ratio at the bacterial cell surface (Krekeler *et al.*, 1989, Mozes *et al.*, 1989) and thus on the cultivation conditions.

After cell disruption with the French press (1378 bar 5 cycles) only minor differences of ± 2 mV were detectable between the strains, which may attributed to experimental errors.

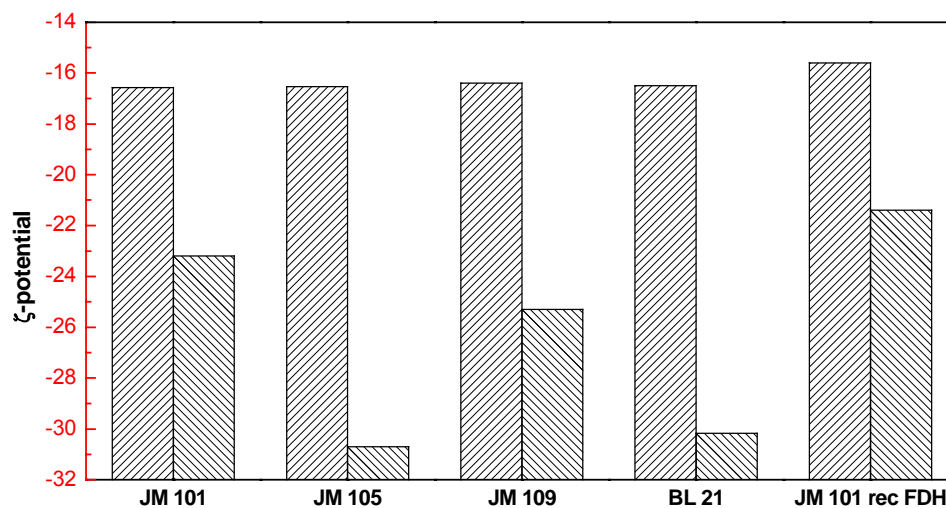


Fig. 6-23: Zeta Potential of various *Escherichia coli* strains a comparison in 100mM Tris HCl pH 8,0 $\kappa = 10\text{mS cm}^{-1}$. ▨ whole cells, ▩ homogenate

In order to compare the CTI of homogenates obtained from different *Escherichia coli* strains Streamline DEAE was chosen as standard stationary phase for anion exchange chromatography in EBA. The following strains and operational conditions have been investigated in the pulse response experiments:

Strains: JM 101, JM 105, JM 109, MC 1061, BL 21, JM 105 rec. FDH, JM 109 rec. FDH

Equilibration Buffer: 100 mM Tris/HCl pH 8,0 conductivity $\kappa=10 \text{ mS cm}^{-1}$ (adjusted with NaCl).

The pulse response experiments showed a good cell transmission (CTI > 0.9) for all *Escherichia coli* strains investigated (Fig. 6-24). Recalling the results from ζ -potential measurement (Fig. 6-23) this could be expected due to the small differences in the surface charge after cell disruption. It can be assumed that for the conditions investigated the combined effects of collision probability and attachment probability – reduced by a small particle size and a low net surface charge – were low enough to avoid strong biomass adsorbent interactions.

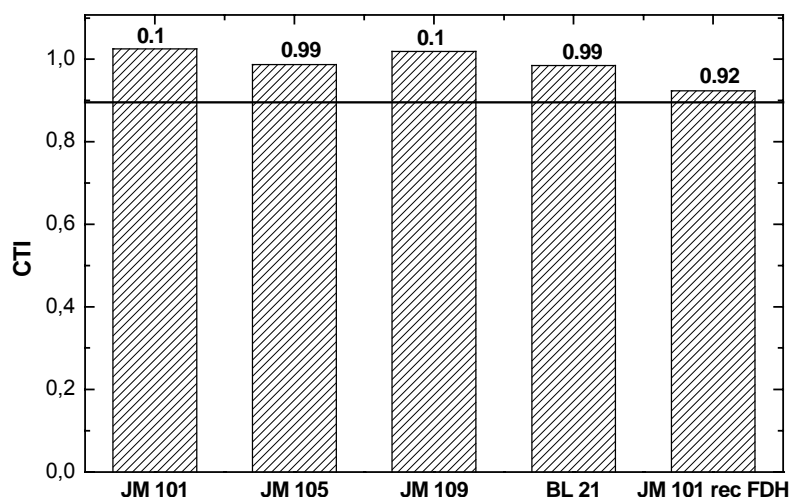


Fig. 6-24: Biomass transmission of different French Press homogenate of *Escherichia coli* strains (pH 8,0 $\kappa=10 \text{ mS cm}^{-1}$).

6.1.4 SCALABILITY AND FEASIBILITY STUDY

In previous chapters the impact of Homogenization methods on the CTI values were investigated. For a successful process design the impact on the fluidisation quality at process conditions need to be evaluated and the applicability of the obtained knowledge to a scalable industrial high pressure homogenizer has to be proven. Finally differences in cell wall strength of a host strain and a producing strain under real culture conditions had to be compared due to the fact that the relative strength of the cell wall depends strongly on growth conditions and history of the biomass (Kula and Schütte, 1987, Kula *et al.*, 1990,) (Engler and Robinson, 1981).

For these experiments the recovery of formate dehydrogenase produced in a rec. *Escherichia coli* was chosen as a model system and the feedstock properties after high pressure homogenization in pilot scale of the expression strain as well as the corresponding host strain were investigated.

a PROPERTIES OF HIGH PRSSURE HOMOGENATE FROM HOST STRAIN & REC. STRAIN

In the following homogenate properties obtained using a pilot scale APV Gaulin high pressure homogenizer are compared with data from French press homogenates under identical process conditions. Additionally the behavior of the host strain (HS) is compared with the production strain (PS) containing the plasmid coding for FDH expression. For all parameters investigated (viscosity, surface charge, and particle size) similar properties have been found. Fig. 6-25 shows that the homogenate viscosity of HS as well as for the PS decreases during multiple passage homogenization from $\eta = 3.2 \text{ mPa s}$ to $\eta = 2.3 \text{ mPa s}$. Surface charge and particle size (Fig. 6-26 & Fig. 6-27) decreased for all samples investigated. An overall decrease of effective surface charge from $\zeta = -26$ to $\zeta = -16 \text{ mV}$ was found in combination with a reduction in particle size from $x = 1400 \text{ nm}$ to $x = 300 \text{ nm}$.

Total protein release of the JM 105 rec. FDH (PS) is slightly higher as for the HS, which might be a result of the over expression of rec. FDH and follows the same trend (see Fig. 6-28) as shown for the HS. For both strains total protein release is already achieved after 3-4 homogenization cycles, further processing does not improve protein release. Product release – measured by the FDH activity – is already completed after

three cycles. Further homogenization cycles did not affect enzyme activity as no inactivation was found. It is clear that product release alone – as routinely measured for disruptions – is not enough information to judge the suitability of a homogenate for processing.

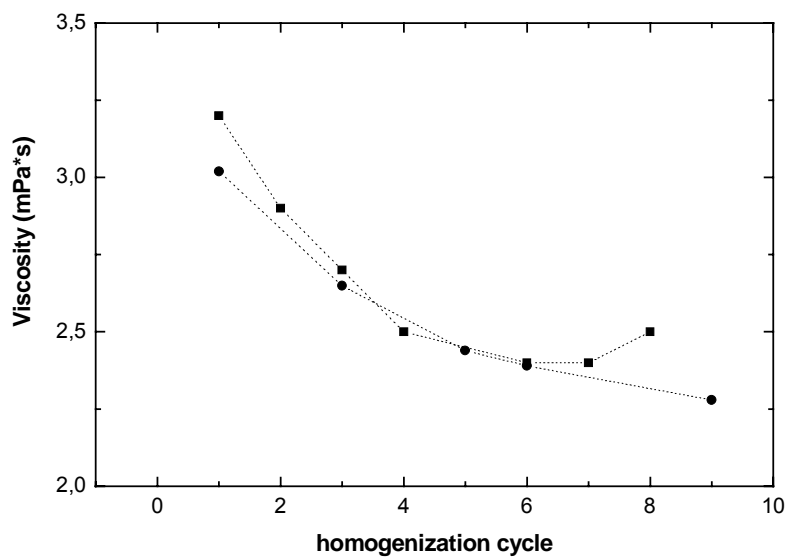


Fig. 6-25: Viscosity during high pressure homogenization in an APV Gaulin homogenizer. (■) *Escherichia coli* JM 105; (●) *Escherichia coli* JM 105 rec. FDH.

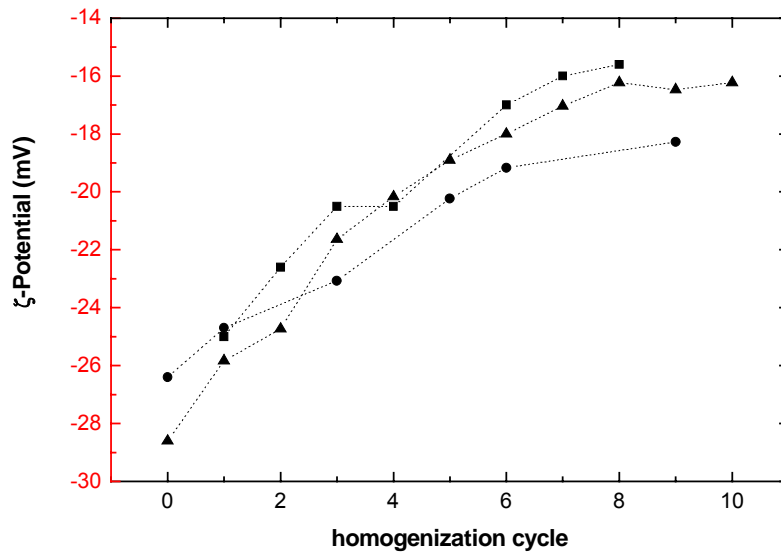


Fig. 6-26: Zeta Potential of *Escherichia coli* JM 105 and *Escherichia coli* rec. FDH& JM 105 suspension (40 % ww) disrupted in a pilot scale homogenizer (Gaulin) and the French Press. (■) *Escherichia coli* JM 105 pilot scale homogenizer, (●) *Escherichia coli* JM 105 rec FDH pilot scale homogenizer, (▲) *Escherichia coli* JM 105 French Press.

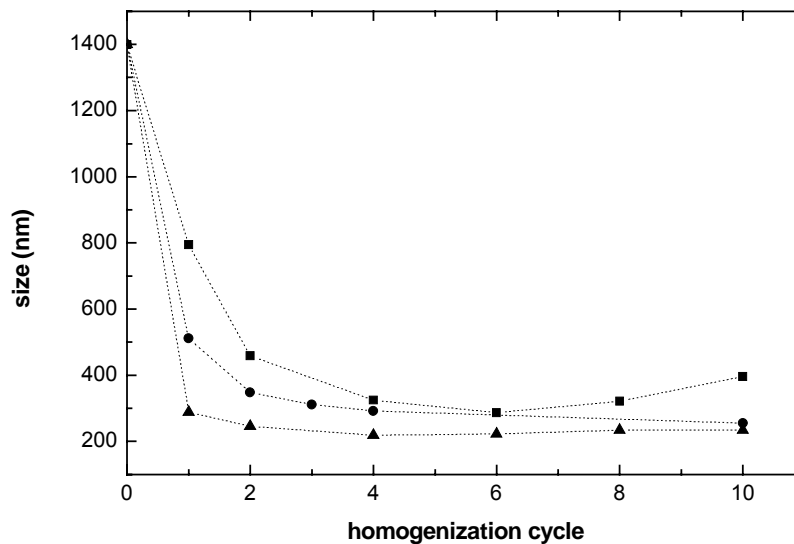


Fig. 6-27: Comparison of the mean size distribution after different passage in a Gaulin high pressure Homogenizer and French Press of host and rec. *Escherichia coli* strain. (■) *Escherichia coli* JM 105 pilot scale homogenizer, (●) *Escherichia coli* JM 105 rec FDH pilot scale homogenizer, (▲) *Escherichia coli* JM 105 French Press.

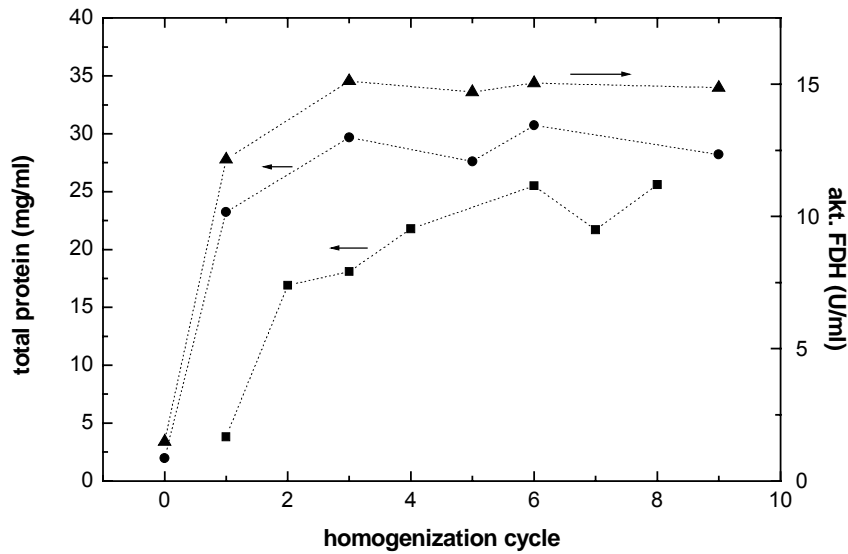


Fig. 6-28: Protein release and FDH activity during high pressure homogenization in a pilot scale homogenizer. (■) *Escherichia coli* JM 105 pilot scale homogenizer, (●) *Escherichia coli* JM 105 rec FDH pilot scale homogenizer, (▲) FDH activity.

b IMPACT OF THE CELL DISRUPTION ON THE QUALITY OF FLUIDISATION

The fluidisation quality has been investigated at two conductivities ($\kappa=5$ & $\kappa=10$ mS cm^{-1}) and compared for HS and PS using a pilot scale bead mill (Netzsch Lab Star) and a pilot scale APV high pressure homogenizer.

Using optimized conditions for high pressure homogenization in all experiments a symmetric RTD curve was observed. The evaluation of the RTD curves using the PDE model (Villiermaux and van Swaaij, 1969) shows an acceptable fluidisation ($\alpha > 0.8$) for all conditions investigated. The fluidisation quality in a bed of Streamline DEAE, at a conductivity of $\kappa=10$ mS cm^{-1} of the HS homogenate ($\alpha = 0.94$) was found slightly higher as of the PS ($\alpha = 0.88$). This is reflected in the Peclet number being $Pe = 137$ for the HS and $Pe = 99$ for the PS (Table 6-2). At lower conductivities α is reduced slightly indicating once more the electrostatic nature of the biomass/adsorbent interactions (Fig. 6-29).

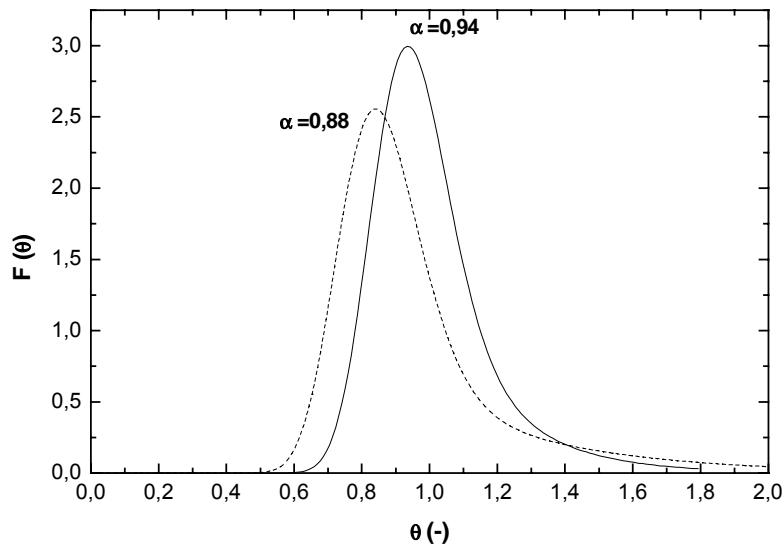


Fig. 6-29: RTD in 10 % ww high pressure homogenate of *Escherichia coli* JM105 and *Escherichia coli* JM 105 rec. FDH (pH 8,0 and $\kappa = 10 \text{ mS cm}^{-1}$). (–) *Escherichia coli* JM 105, (---) *Escherichia coli* JM 105 rec. FDH.

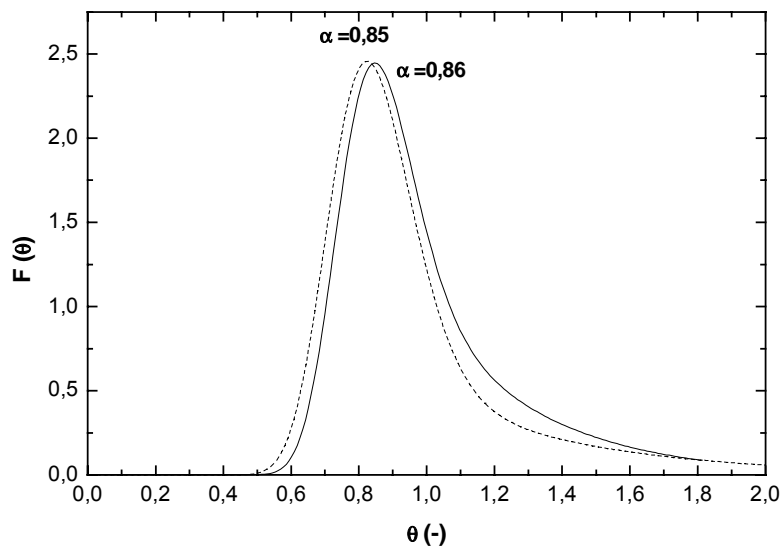


Fig. 6-30: RTD in 10 % ww high pressure homogenate of *Escherichia coli* JM105 and *Escherichia coli* JM 105 rec. FDH (pH 8.0 and $\kappa = 5 \text{ mS cm}^{-1}$). (–) *Escherichia coli* JM 105, (---) *Escherichia coli* JM 105 rec. FDH.

Table 6-2: Parameter of PDE analysis using pilot scale high pressure homogenate

Model Parameter	rec. FDH 10 mS cm ⁻¹	JM 105 10 mS cm ⁻¹	JM 105 5 mS cm ⁻¹	rec. FDH 5 mS cm ⁻¹
N	0.32	0.37	0.63	0.35
P	99	137	106	91
α	0.88	0.94	0.85	0.86

For both homogenates obtained by wet milling a total collapse of the fluidized bed was observed as illustrated in Fig. 6-31. These results illustrate again the impact of feedstock properties on the fluidisation quality, where high pressure homogenate resulted in a good fluidisation while for the unfavorable (in particle size and surface charge) bead mill homogenate (Table 6-3) a total collapse of the bed occurred.

Table 6-3: Feedstock properties of pilot scale bead mill homogenate (0,5 mm glass beads, 2500 rpm, Netzsch Lab Star bead mill)

Strain	z-average (nm)	Viscosity (mPas s)	ζ -Potential
JM 105	654.7	8.0	-18.9
JM 105 rec. FDH	595.05	6.75	-29.00

Fig. 6-31: Streamline DEAE after application of *Escherichia coli* bead mill homogenate

6.1.5 SACCHAROMYCES CEREVISIAE

Initial investigations with an eucaryotic expression system have been carried out using *Saccharomyces cerevisiae*. A significant disturbance of the fluidized bed using intact yeast cells and anion exchange adsorbents have been reported by several authors (Feuser *et al.*, 1999, Fernández-Lahore *et al.*, 1999, Lin *et al.*, 2001) and only one successful process is reported using yeast homogenate with Streamline DEAE as weak anion exchanger (Chang and Chase, 1996b). In the light of the results presented above some initial experiments have been performed to characterize the properties of *Saccharomyces cerevisiae* homogenate and whole cell suspension in terms of surface charge and particle size in order to correlate it with the cell retention in an EBA column.

Fig. 6-32 shows the size reduction during multiple passages through a French press at different operating pressures resulting in a size reduction from app $x = 8 \mu\text{m}$ to a final minimum value of $x = 1-2 \mu\text{m}$. The final minimum size hereby depended on the homogenization pressure applied as shown in Fig. 6-32. The latter finding is in contrast to the results of *Escherichia coli* cell disruption data, where the minimum value did not depend on the operating pressure used (see Fig. 6-12). The maximum size reduction obtained with yeast cells are summarized in Table 6-4, the value at 2068 bar homogenization is probably not the minimum value, because only two homogenization cycles have been carried out. The size determination of the intact yeast cells shows a rather broad variance (Fig. 6-32) as the maximal accurate detection limit in the size determination ($6 \mu\text{m}$) had been exceeded during this measurement.

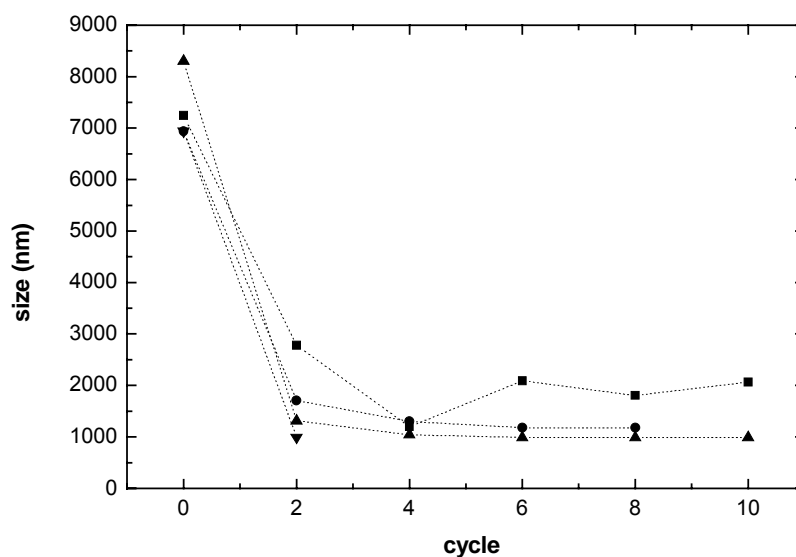


Fig. 6-32: Particle size reduction of *Saccharomyces cerevisiae* during multiple passage homogenization in a French press (40 % ww in 50 mM Tris/HCl pH 7,5) at different operation pressure. (■) 300 bar, (●) 482 bar, (▲) 965 bar and (▼) 2068 bar

Table 6-4: Minimum size after French press homogenization at various operation pressures.

Pressure	300 bar	482 bar	965 bar	2068 bar
min. size (nm)	1202	1179	989	998

Similar to the results obtained with *Escherichia coli*, size reduction of *Saccharomyces cerevisiae* is accompanied by a decrease of the net surface charge (Fig. 6-33). The charge of intact yeast cells (app. $\zeta = -7$ mV at relatively low ionic strength ($\kappa = 3.7$ mS cm^{-1}), is much lower than that of *Escherichia coli* cells (app. $\zeta = -25$ mV at $\kappa = 10$ mS cm^{-1}) thus the absolute decrease of the charge during cell disruption is lower than for *Escherichia coli*. This can be related to the different cell wall compositions of the two organisms. The surface charge of an *Escherichia coli* cell mainly arises from the strongly negatively charged lipopolysaccharide layer at the outer surface (see chapter 5.4.1 page 36). The surface charge of *Saccharomyces cerevisiae* on the other hand is due to the phosphorylation of mannosyl side chains (Orlean, 1997), which are less

negatively charged. Charge reduction during cell disruption follows the same principle discussed above (Fig. 6-14). Finally it should be mentioned that with a decrease of the cell debris size an increase of the importance of the charge of the inner cell membrane for the over-all net surface charge is experienced.

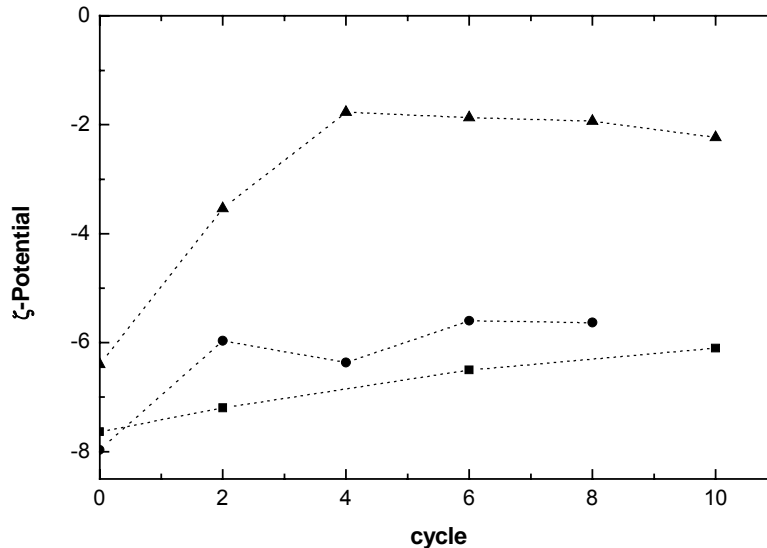


Fig. 6-33: Surface charge of *Saccharomyces cerevisiae* homogenate obtained by multiple passages through a French press (40 % ww in 50 mM Tris/HCl pH 7,5) at different operating pressures. (■) 300 bar, (●) 482 bar, (▲) 965 bar

Correlating the size of debris of different homogenates with the biomass transmission the results follow the same principal trend found for *Escherichia coli* (Fig. 6-19.). A cell transmission of CTI = 0.1 for the whole cells of app. $x = 8 \mu\text{m}$ and CTI = 0.89 for the smallest French press homogenate of app $x = 1 \mu\text{m}$ size has been observed as it is shown in Fig. 6-34. In agreement with the theoretical considerations presented in chapter 6.1.2d a reduction in the particle size leads to an increase of the CTI value. Because of the overall lower net surface charge of *Saccharomyces cerevisiae*, EBA systems can tolerate larger cell debris particulates of the yeast homogenates than in the case of *Escherichia coli* homogenates.

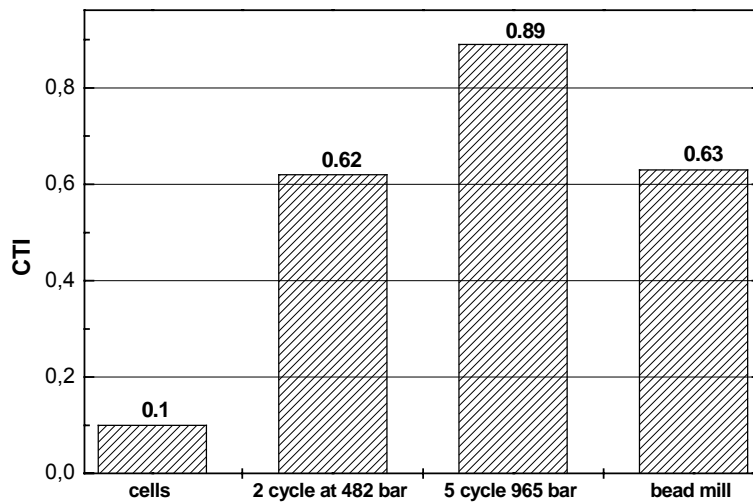


Fig. 6-34: The impact of cell disruption of *Saccharomyces cerevisiae* on the CTI in EBA (transmission data from cells and bead mill homogenate taken from (Lin *et al.*, 2002)). $x = \text{app. } 7000 \text{ nm}$ (whole cells); $x = \text{app. } 2000 \text{ nm}$ (2 cycle 482 bar), $x = \text{app. } 1000 \text{ nm}$ (5 cycle 965 bar); $x = \text{app. } 1400 \text{ nm}$ (bead mill).

Applying the ζ parameter introduced in chapter 6.1.2 to the results obtained from *Saccharomyces cerevisiae* again a linear correlation could be found, which incorporates nicely the data obtained from *Escherichia coli* (Fig. 6-35). This indicates that the parameter presented could be used as a correlation factor for feedstock properties and CTI in EBA systems using anion exchange chromatography independent from the kind of biomass used.

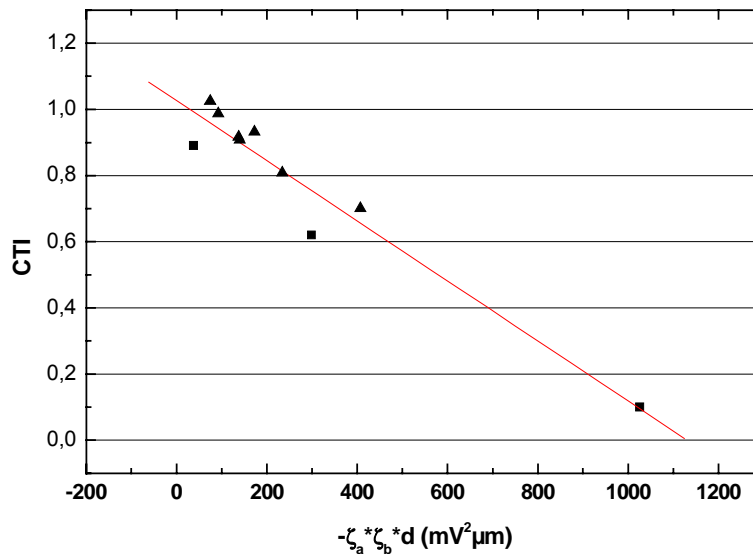


Fig. 6-35: Correlation Zeta Parameter versus biomass transmission in EBA for *Saccharomyces cerevisiae* and *Escherichia coli*. (■) *Saccharomyces cerevisiae*, (▲) *Escherichia coli*, (—) Linear regression (R= 0,96).

6.1.6 SUMMARY AND CONCLUSIONS I

A long list of publications on EBA described deteriorating effects of cell/cell debris containing feedstock during anion exchange processes (see chapter 5.2). Analogous to the theoretical considerations for deep bed filtration, biomass/adsorbent interaction in anion exchange chromatography can be divided into a term describing the transport probability of the particulate in the feedstock to the absorber followed by a term describing the binding on the adsorbent surface. Describing an EBA column as a deep bed filter, the filter efficiency can be defined as the product of collision probability and probability of binding, where for an optimized EBA process the filter efficiency has to be very low. There are five important transport mechanisms known for the transport of the turbid particle to the filter surface, of which to a minor extend diffusion, but mostly interception can be identified as important for the hydrodynamic conditions present in an EBA column. The probability of collision is directly correlated to the size of the particulate. Smaller particles lead to a lower degree of interaction between the cell/cell debris and the adsorbent. For ion exchange chromatography electrostatic interactions are the main parameter determining the binding of the cells/cell debris at the adsorbent

surface. Anion exchange resins by design have positively charged surfaces whereas the surface of the cells/cell debris is negatively charged at conditions usual for anion exchange processes. Employing the theory on electrostatic interactions between two oppositely charged colloid particles (Lagaly *et al.*, 1997, Sonntag, 1977) we further see that the important parameters determining the binding are the size of the cell debris, its surface charge and the surface charge of the adsorbent. The present study showed that using optimized high pressure homogenization for cell disruption a significant decrease of the particle size can be achieved. Furthermore it could be shown that, due to of the asymmetric structure of a Gram⁻ cell wall, a size reduction of the cell debris is linked to a decrease of the effective surface charge. Comparable results have been observed also for *Saccharomyces cerevisiae*. The differences in the surface charge between the two organisms can be explained by the difference in chemistry and abundance of the charge carrier at the cell surface. The negative surface charge (under physiological conditions) is derived from strongly negatively charged lipopolysaccharides at the *Escherichia coli* surface and the charge of *Saccharomyces cerevisiae* is mainly related to the phosphorylation of mannosyl side chains (Orlean, 1997), which are less abundant. For both cell types it was found that an efficient cell disruption generates a feedstock with decreased collision probability due to the small particle size and reduced probability of sorption due to the small size and reduced net surface charge.

The theoretical considerations presented by Lin *et al.* (2003) can be used a general correlation between feedstock properties (particle size and surface charge conditions) and biomass interaction in expanded beds during anion exchange chromatography using Streamline DEAE. This applies both for *Escherichia coli* and *Saccharomyces cerevisiae*.

Finally it can be concluded that the optimization of the cell disruption method towards small particulates and low effective surface charge improves EBA bed stability and leads to a successful application of anion exchange EBA processes. It should be noted that sufficient size reduction requires more passages than maximal product release, which is the only parameter routinely measured so far to judge cell disruption.

6.2 EBA & DOWNSTREAM PROCESS DEVELOPMENT

The second part of this thesis deals with the development of alternative primary capture steps for two industrial relevant production processes. The first case study is concerned with the recovery of a recombinant human insulin precursor (MI 3), which is produced by *Saccharomyces cerevisiae*. The precursor is secreted into the culture broth and thus represents an extra-cellular system. The second case study deals with the recovery of recombinant human growth hormone from an *Escherichia coli* homogenate.

6.2.1 INSULIN

Using secreting expression systems, in the absence of cell lysis no additional intracellular protein is released into the culture broth during cultivation, facilitating downstream processing. The process liquor is thus characterized by a rather low overall protein content with the actual product representing the major fraction. The boundary conditions given by the process liquor of the insulin precursor MI3 are shown in Table 6-5.

Table 6-5: Feedstock properties of MI3 capture (whole broth contains 30-35 % ww cells before dilution)

	Conductivity [mS cm^{-1}]	6 - 14 (undiluted) ^a 4 - 6 (1:2 diluted) ^a
	pH	5
MI 3 properties	Isoelectric Point	5,3
	Molecular weight [Da]	5960

^a after pH adjustment to pH 3 using 32 % HCl

The scale of the MI 3 production process lies in the range of several hundred cubic meter culture liquor a day, representing a critical factor during process design in terms of storage tank size, buffer consumption or waste water treatment. In this respect, feedstock dilution or other changes in the fluid phase like pH or temperature adjustment have a strong impact on process economics and should therefore be kept to a minimum. Finally, process design should aim at a scaleable and fast process to handle large volumes in a short time.

The purification protocol currently used for the production of insulin consists of three initial centrifugation steps followed by a cation exchange chromatography and several filtration, crystallization, and precipitation steps (Table 6-6). Every step within a purification protocol leads, however, to a decrease of the final product yield while simultaneously increasing the overall costs. The goal of the current process development has thus been to replace as many unit operations of the original process scheme by a single EBA step (Table 6-6).

Table 6-6: Conventional purification protocol and implementation of EBA (Mollerup *et al.*, 1999)

Unit operation	Purification step	Implementation of EBA
centrifugation 1	solid/liquid separation	E B A
centrifugation 2	solid/liquid separation	
centrifugation 3	solid/liquid separation	
cat ion exchange chromatography	capture	
filtration	solid/liquid separation	
crystallization 1	intermediate purification	
filtration	intermediate purification	
ethanol precipitation	polishing	
filtration	polishing	
crystallization 2	polishing	

In order to use existing knowledge and to link the initial capture to the following unit operations cation exchange was chosen as prime candidate for EBA process development and conditions for adsorption and elution were taken from the existing process. Feedstock application was thus performed at pH 3. Elution was carried out by a step elution using Tris/HCl buffer in ethanol solution. The latter is used because the MI3 precursor shows a good solubility in ethanol and the resulting eluate is obtained in the conditions required for successive processing steps such as ethanol precipitation and crystallization.

In addition to the above mentioned factors, cation exchange is favored for EBA process development due to its low tendency towards biomass/adsorbent interactions due to the electrostatic repulsion between the negatively charged biomass and the cation exchange resin.

a CHROMATOGRAPHIC PERFORMANCE

Optimal starting conditions for the cation exchange step can be seen as a trade off between processing volume and sorbent utilization or process economics. The original undiluted feedstock leads – due to its high conductivity – to an unfavorable product capture and thus low degree of sorbent utilization. Feedstock dilution, however, leads to larger volumetric feed streams but also to a reduction of the conductivity and thus significantly increased capacity and faster binding kinetics. Fig. 6-36 shows a comparison of the adsorption behavior using undiluted (14.2 mS cm^{-1}) and a 1:2 diluted feedstock (6.2 mS cm^{-1}) on Streamline SP. The final equilibrium concentrations of the MI3 Precursor during batch adsorption studies were limited by the product concentration in the feedstock. In the concentration range investigated linear isothermal binding has been observed for the undiluted feedstock resulting in a maximal sorbent capacity of 20 mg ml^{-1} under the conditions applied. Using the 1:2 diluted feedstock an isothermal binding behavior corresponding to a Langmuir Isotherm was found indicating a total capacity of $Q_{\text{max}} = 56.47$ and a associating constant $k_A = 0.03$. The maximum binding capacity reached under process condition was $Q_{\text{max eff.}} = 38 \text{ mg ml}^{-1}$.

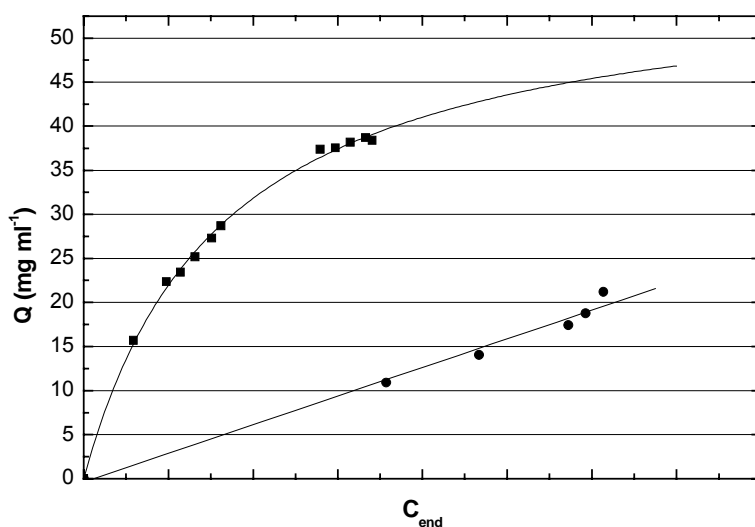


Fig. 6-36: Isothermal binding of MI3 precursor on Streamline SP at pH 3. Undiluted feed: conductivity $\kappa = 14.2 \text{ mS cm}^{-1}$, 1:2 diluted feed: conductivity $\kappa = 6.2 \text{ mS cm}^{-1}$. Experimental results from 1:2 diluted feed could be fitted as a Langmuir Isotherm ($k_A = 0.031$; $Q_{\max} = 57.75$; $R^2 = 0.998$), undiluted feed resulted in a linear fit ($a = -0.378$; $b = 0.162$; $R^2 = 0.992$). (●) undiluted feedstock, (■) 1:2 diluted feedstock.

A comparison of binding capacities using a 1:2 feedstock dilution on Zirconia S and Streamline SP resulted in a significantly higher capacity for Zirconia S (60 mg ml^{-1}) compared to Streamline Sp (38 mg ml^{-1}). This is in agreement with data published by the resin manufacturers for Lysozyme, where the binding capacity for Streamline SP is given with 60 mg ml^{-1} , whereas Zirconia S is reported to achieve a dynamic capacity of 89 mg ml^{-1} . A determination of Q_{\max} values for Zirconia S could not be carried out due to the low product titer available.

A comparison of adsorption kinetics for the two cation exchange resins is shown in Fig. 6-37. For both resins a halftime of $t_{1/2} = 23 - 24 \text{ min}$ for near complete saturation was found. Taking the differences in adsorbent size – $d_p = 70 \text{ }\mu\text{m}$ for Zirconia S and $d_p = 200 \text{ }\mu\text{m}$ for Streamline SP – into account, intra-particle transport seems to be not a limiting factor for this process. The latter might be explained by the rather low molecular weight of the MI3 precursor ($MW = 5.9 \text{ KD}$) leading to a diffusion coefficient of $D_{fs} = 1.6 \cdot 10^{-10} \text{ (m}^2 \text{ s}^{-1}\text{)}$ in free solution calculated after Young et al., (1980) while serum albumin in comparison exhibits a diffusion coefficient of $D_{fs} = 0.594 \cdot 10^{-10} \text{ (m}^2 \text{ s}^{-1}\text{)}$ (Tanford, 1961). The absence of pore diffusion limitations promises

a favorable combination of low residence times and high capacities for the EBA process.

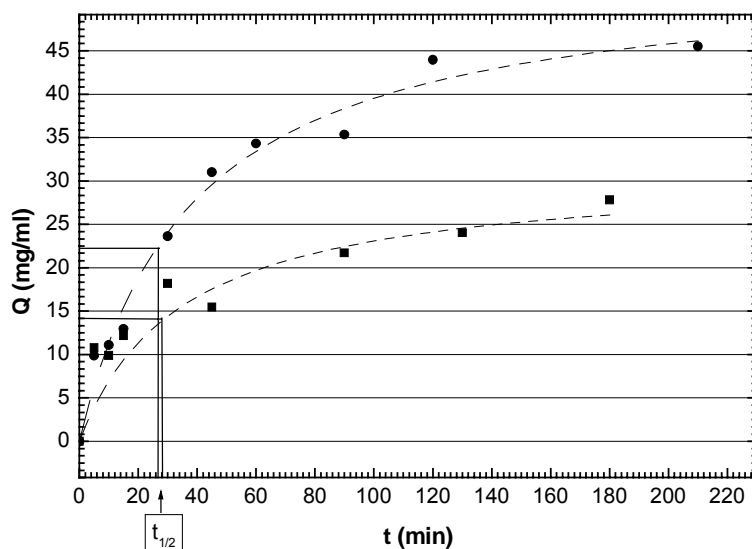


Fig. 6-37: Adsorption kinetics of Streamline SP and Zirconia S at pH 3 using 1:2 dil. clarified culture broth ($\kappa = 7 \text{ mS cm}^{-1}$, pH 3.0) (■) Streamline SP, (●) Zirconia S.

Despite the fact that Zirconia S showed comparable binding kinetics and a nearly two fold higher capacity – app. 45 mg ml^{-1} compared to 25 mg ml^{-1} for Streamline SP – further studies were carried out using Streamline SP. This decision was mainly motivated by the incompatibility of Zirconia resins and the available EBA column hardware. Due to the small adsorbent diameter Zirconia particles could pass through the bottom net of the Streamline column leading to a blockage of the feed pipe. Additionally, fine particles leaving the column led again to blocking effects and interfered with UV detection. Most of these problems could be avoided by a new column design using a rotating distributor at the inlet of the column (Asplund et al., 2002, Hubbuch et al., 2002), which was not available at the time.

b PROCESS DESIGN

In subsequent experiments the dynamic sorption performance for Streamline SP was characterized in breakthrough experiments in small packed beds. Fig. 6-38 compares the breakthrough performance of the clarified feedstock and the 1:2 diluted feedstock in a

packed bed of 5 cm bed height and a linear velocity of 5 cm/min. The undiluted feedstock exhibits an instantaneous breakthrough of approximately 30 %. This corresponds to the low binding affinity found under this conditions during the initial batch adsorption studies (see also Vermeulen et al., 1973). The breakthrough analysis of the 1:2 diluted supernatant resulted in an S-shaped breakthrough curve, where in the first part of the curve very little breakthrough is found followed by a sharp increase of the concentration in the eluate to nearly full breakthrough (Fig. 6-38).

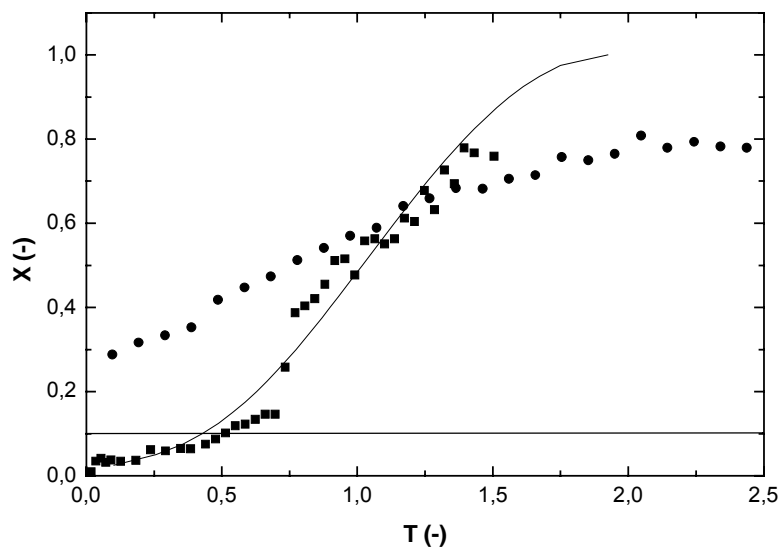


Fig. 6-38: Breakthrough analysis of MI3 adsorption to Streamline SP at pH 3.0, linear velocity 5 cm/min, at 5cm sedimented. bed height. Data of 1:2 diluted . feedstock are fitted using the model after Hall et al. (1966). Q_{\max} was estimated by a fit of the Langmuir isotherm (Fig. 6-36.) (●) undiluted; (■) 1:2 diluted.

In order to ease parameter estimation while at the same time reducing experimental work the obtained breakthrough data were fitted using various models developed for chromatographic process description (Hall *et al.*, 1966, Yoshida *et al.*, 1984, Yoshida *et al.*, 1994). The mathematical framework of the different models is given in the Appendix. The best fit of the experimental data has been obtained using the model from Hall et al. (1966) assuming combined film and pore transport.

Applying this model breakthrough behavior can be simulated for various process conditions such as linear velocity or sedimented bed height. A necessary prerequisite for the latter is that chromatographic performance of packed and expanded beds do not differ significantly and that the validity of the model is not hampered by the evaluated parameter combinations. Fig. 6-39 shows model calculations – $Q_{10\%} / Q_{eq}$ vs. U_{feed} – for the current process for various sedimented bed heights.

Another important parameter in EBA process design is the expansion behavior – H/H_0 vs. U_{feed} – of the bed under relevant process conditions. This is important when defining the minimum fluidisation velocity required to obtain a totally fluidized bed. The maximal velocity is given by the column length, optimal expansion rate and sedimented bed height used. Using a diluted culture broth from Insulin production with a biomass load of 15 % (w/w), expansion of Streamline SP and Zirconia S sorbents showed a linear behavior up to a linear velocity of app. 190 cm h^{-1} (see. Fig. 6-40). Using higher velocities Streamline SP exhibited an increased bed expansion when compared to Zirconia S (5.4 instead of 4.2 at 360 cm h^{-1}). The lower expansion rate of the Zirconia matrix was expected due to the smaller diameter and the higher density. The difference in expansion increased with increasing fluid velocity. An expansion factors above 3 should be avoided because large increases of the interstitial volume will lower sorption performance. Thus, maximal fluid velocities of 256 cm h^{-1} and 238 cm h^{-1} were found for Zirconia S and Streamline SP, respectively.

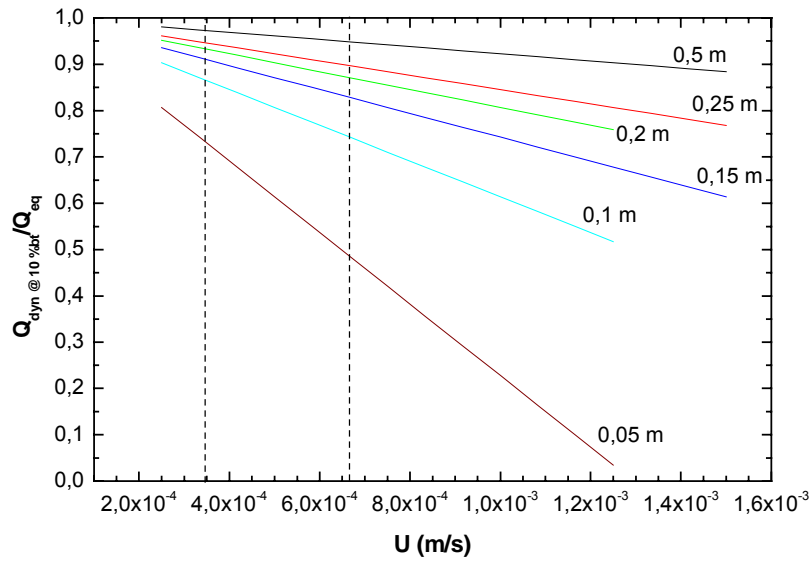


Fig. 6-39: Simulating sorption efficiency of the Insulin Precursor on Streamline SP for breakthrough at 10 %. Obtained from breakthrough curves simulated after Hall et al. (1966) at various fluid velocities and sedimented bed heights. 1:2 diluted culture liquid pH 3.

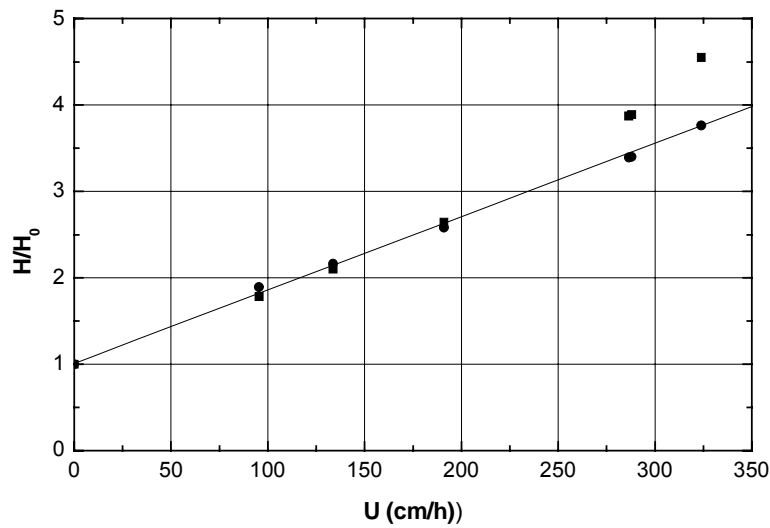


Fig. 6-40: Bed expansion of Zirconia S and Streamline SP in a 15 % ww culture broth (pH 3.0; $\kappa = 5 \text{ mS cm}^{-1}$). (■) Streamline SP; (●) Zirconia S.

Combining data from isotherm and breakthrough analysis, the results of the modeling approach and finally the expansion behaviour a window of stable operation can be defined (see dashed lines in Fig. 6-39), assuming a perfectly fluidized bed under relevant feedstock conditions. From this an initial evaluation of process conditions favoring a fast processing of the feedstock (high U and low sedimented bed height) or efficient usage of the employed matrix (low U and high sedimented bed height) can now be carried out simply by selecting the sedimented bed height and the linear velocity within the boundary conditions indicated by the dashed lines in Fig. 6-39.

c BIOMASS/ADSORBENT INTERACTION AND FLUIDISATION PERFORMANCE

The above conclusions can, however, only be drawn for negligible biomass / adsorbent interactions. The extend of such interactions has therefore been investigated for a range of process conditions (pH 3.0 – 4.5 and conductivities of $\kappa = 5 \text{ mS cm}^{-1}$ - $\kappa = 12.5 \text{ mS cm}^{-1}$) as shown in Fig. 6-41.

For all pH values and conductivities investigated, only weak biomass adsorbent interactions were observed (CTI= 0.88 - 1.0) when using whole *Saccharomyces cerevisiae* cells and Streamline SP (Fig. 6-41). Comparable results were obtained using Zirconia S (data not shown).

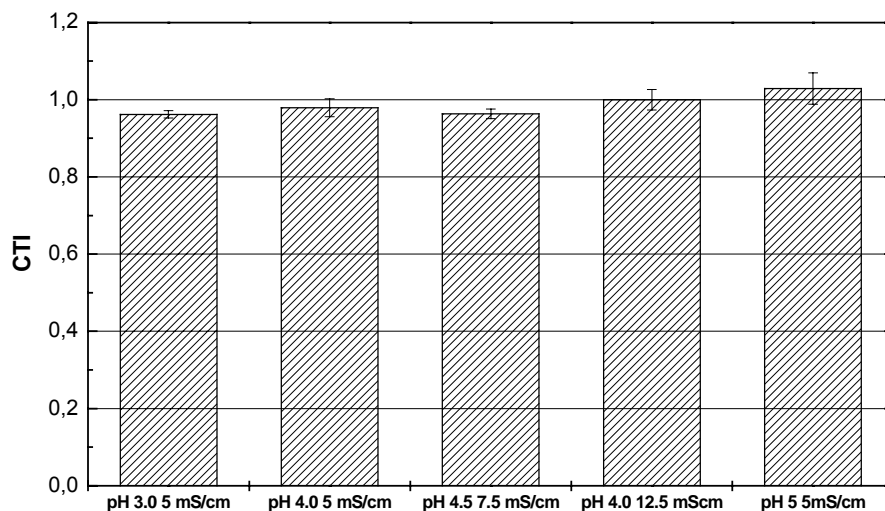


Fig. 6-41: CTI of *Saccharomyces cerevisiae* pulses (35 ml) in 40 mM Na_2HPO_4 /citric acid buffer with different pH and conductivity's through an expanded bed of 10 cm Streamline SP.

The influence of the biomass load in the process liquor on the fluidisation behaviour of the bed has been studied using real culture broth containing a biomass concentration of 15-30 % w/w.

The results from RTD analysis are presented in Fig. 6-42 and show for all conditions investigated (pH: 3, 4; $\kappa = 6.3 \text{ mS cm}^{-1}$, 12 & 6.3 mS cm^{-1}) a perfect fluidisation characterized by a nearly symmetric RTD curve. The evaluation of the data using the PDE model (chapter 5.2.1) is presented in Table 6-7. All α values are significantly above the critical value of 0.8 (Lin *et al.*, 2002). These results show clearly that the process liquor composition and interactions with the sorbents are not the critical parameters for EBA process performance when processing the current feedstock.

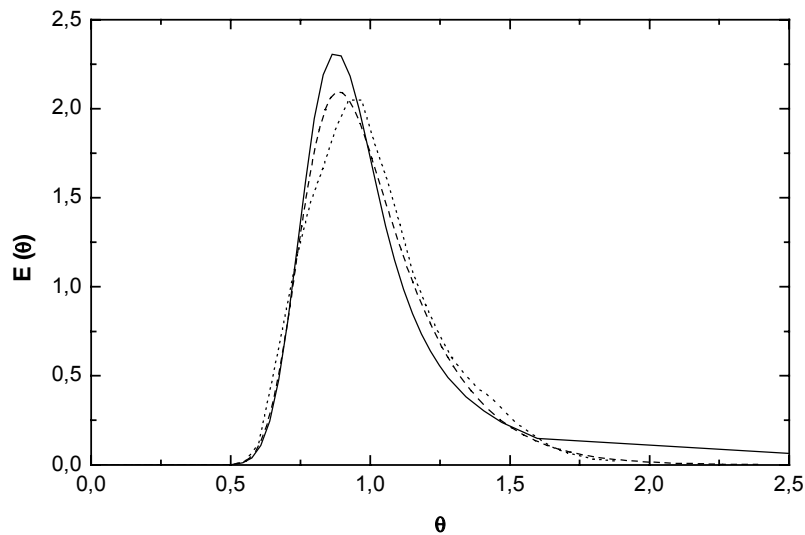


Fig. 6-42: RTD analysis at $C_b = 30 \%$ (ww) (1:2 dil. and $C_b = 15 \%$ ww biomass concentration). (-) pH 4.0 12 mS cm^{-1} , $C_b = 15 \%$ ww; (--) pH 4.0 6.3 mS cm^{-1} , $C_b = 15 \%$ ww; (...) pH 3.0 6.3 mS cm^{-1} , $C_b = 30 \%$ ww.

Table 6-7: Modeling Parameter obtained by fitting the experimental results to the PDE model

pH	κ mS/cm	C_b (% ww)	N	Pe	α
4,0	6,3	30	0,28	97,9	0,97
4,0	12	15	0,66	97,9	0,87
3,0	6,3	30	0,39	65,3	0,94

d PROCESS PARAMETERS AND SCALE UP

As a result of data and considerations presented in this chapter the following process conditions were chosen for the final EBA experiments:

Table 6-8: Process conditions for the recovery of Insulin precursor M3 using EBA.

	Buffer conditions	CV ^{a)}	U_{lin} (cm h ⁻¹)
Equilibration	30 mM Na ₂ HPO ₄ /citric acid – pH 3.0	10	200
Application	1:1 dilution of culture broth – pH 3	250-260 ^{b)}	216
Wash 1	30 mM Na ₂ HPO ₄ /citric acid – pH 3.0 – 3% glycerol ^{c)}	10	200
Wash 2	30 mM Na ₂ HPO ₄ /citric acid – pH 3.0	11	200
Elution	pH step elution using Tris /HCl Ethanol sol.	13	200
CIP	1 M NaOH in 1M NaCl	20	200
System: Streamline SP at a sedimented bed height of 20 cm. All steps are performed in expanded bed mode.			

^{a)} column volume equivalent to sedimented bed volume; ^{b)} equivalent to 24 h application; ^{c)} glycerol was added to the washing buffer as a density enhancer in order to achieve a washing solution denser as the application liquid to avoid back mixing, which normally results by washing with liquids of lower density. (Draeger and Chase, 1991)

Experiments using this protocol were performed in lab scale in a Streamline 25 (2.5 cm i.d.) column containing 100 ml Streamline SP applying 26 L whole broth as well as in pilot scale using a Streamline 200 column (20 cm i.d) containing app. 6.2 L Streamline SP and an application volume of 1600 L broth. The results of the EBA experiments indicate stable process performance while scale up did not impose any difficulties. After only one step a product purity could be obtained, which is comparable to the purity normally obtained after the second crystallization step in the current process (Fig. 6-44). The final product was 10 times concentrated (Table 6-9) when compared to the undiluted culture broth with an overall yield of 87-88 %. The lower yield is due to an unexpected instantaneous breakthrough of 10-12 % during the processing run.

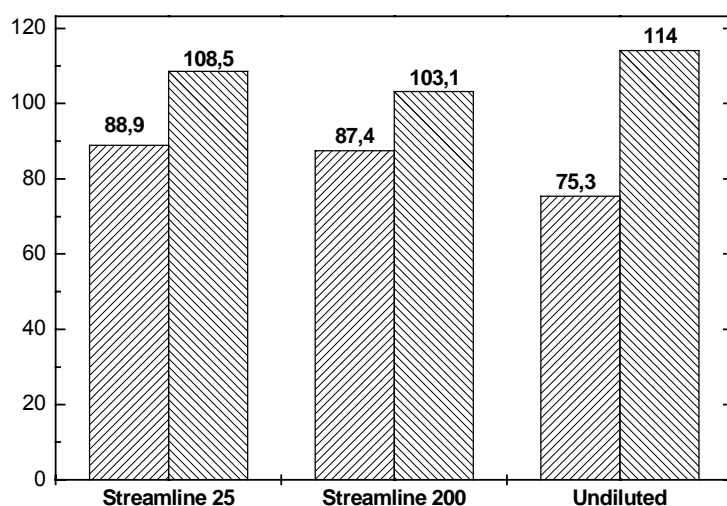
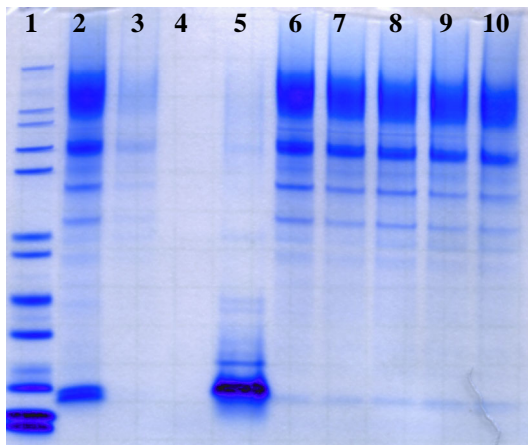


Fig. 6-43: Yield and mass balance of various EBA experiments in lab scale (Streamline 25 2.5 cm i.d.) and pilot scale (Streamline 200/ 20 cm i.d.) using 1:2 diluted culture broth (15-16 % ww, pH 3.0, 4-5 mS/cm) and undiluted broth (30 % ww; pH 3,0; 12 mS cm⁻¹) marked with undiluted. For all experiments a sedimented bed height of 20 cm was used.

Table 6-9: Product concentration behaviour of the scale up experiment

Sample	Volume (L)	Volume (sed CV)	C/Co ^(a)
application	1620	245.7	1
wash 1	95	14.4	0,04
wash 2	140.6	21.3	0
Elution 1	66	10.0	22,1
Total flow through	1620	245.7	n.d.
		Mass Balance	103 %
		Yield	87.4 %
		C_{elution} / C_{culture liquid}	11.05

a) C = actual concentration, Co = concentration of the application.



1. Marc 12 (MW Standard Novex)
2. Application
3. Wash 1
4. Wash 2
5. Elution Peak
6. Elution 2
- 7-10. Flow through fractions

Fig. 6-44: SDS Page (comassie blue stained) analysis of various fractions during EBA processing MI3 on Streamline SP in pilot scale as described above

6.2.2 SUMMARY AND CONCLUSIONS II (INSULIN PRECURSOR MI3)

Capture of MI3 from unclarified culture broth using expanded bed adsorption with cation exchangers has been developed as an efficient operation for primary capture. There are no significant biomass/adsorbent interactions when using Streamline SP, Streamline SP XL or Zirconia S.

The optimized conditions for binding are low pH (pH 3) and a 1:2 diluted culture broth. By diluting the culture broth a much better adsorption performance, a higher equilibrium capacity, in the concentration range used, and faster uptake kinetics could be obtained. These factors result in constant pattern breakthrough behaviour. In terms of the fluidisation quality, a perfectly classified bed has been observed using the optimized conditions, which means that biomass adsorbent interactions can be neglected in this system. Additionally a diluted feedstock has beneficial effect on the fluidisation performance in EBA mode due to the lower biomass concentration as it is explained in chapter 5.1.3.

Using these conditions a yield of app. 88 % and an acceptable adsorption performance could be achieved. Using just one purification step a product with high purity, 10 times concentrated compared to the undiluted culture broth and nearly cell free was obtained. The obtained purity is comparable to the purity after the second crystallization step in the current process. Using EBA nine unit operation (centrifugation 1-3, ion exchange chromatography, crystallization 1 - 2, ethanol precipitation) could be omitted.

This process was successfully scaled up from a lab scale (application of 26 L) to a pilot scale (application of 1600 L) with no significant difference between the scales.

The main problem encountered in scaling up this process was the column used. In the bottom of the column just on top of the distributor plate a very fine net is installed to retain the adsorbent in the column. This net was partially blocked by yeast cells during the application, which resulted in an extended washing and CIP procedure because the cells have to be removed during these steps. A solution of this problem can be a totally different column design without a net in the distribution system as it is already under

development (Hubbuch *et al.*, 2002, Asplund *et al.*, 2002). Using such a column, should lower washing and CIP volumes and process time.

Using the scale up data a process time of 32 h is required to handle a volume of 800 L undiluted culture broth corresponding to 1600 L diluted feedstock for the EBA process in a 0.2 m column. Herby the water consumption for dilution and buffers are $1.36 \text{ m}^3 \text{ m}^{-3}$ culture broth.

6.2.3 HUMAN GROWTH HORMONE (hGH)

The current purification protocol for primary capture in hGH production consists of 6-7 unit operations (Table 6-10). This process is characterized by a significant product loss during the primary capture steps. The most critical step in this respect is ultra filtration where a formation of a miss folded hGH derivative – containing a trisulphide (containing three sulfur groups instead of two) bridge between Cys 182-189 – occurs (Jespersen *et al.*, 1994). The miss folded hGH molecules not only reduce the yield of correctly folded hGH but are also difficult to remove and leading to a product loss of approximately 10 - 20 %. Therefore the aim of this investigation was to identify alternatives for the current primary capture scheme in order to provide a more efficient downstream process avoiding trisulfide hGH formation. Additionally to EBA other primary capture strategies such as precipitation followed by CIX or aqueous two phase systems have been explored.

Table 6-10: Conventional process and the implementation of EBA

Unit operation	Purification step	Implementation of EBA
Cell Harvest (Centrifugation)		
Cell Lyses (high Pressure)		
Centrifugation	capture	E B A sterile filtration
Cross flow Filtration	capture	
Ultra filtration	capture	
Sterile filtration	capture	
Ion exchange Chromatography (IEC)1	intermediate purification	
Hydrophobic Interaction Chromatography (HIC)	intermediate purification	
IEC 2	intermediate purification	
Desalting (Gelfiltration)	intermediate purification	
Enzymatic cleavage	postbiosynthesis modification (cleavage of amino acid extension)	
Isoelectric Prezipitation	removing of cleaved aa extension	
Desalting	intermediate purification	
IEC 3	removing of cleaved aa extension	
Desalting	polishing	
Formulation		

Conditions of the feedstock

The hGH precursors is expressed as an intracellular product in *Escherichia coli* during high cell density cultivation. In the current production process the cell disruption of a 40 % w/w suspension is carried out using a high pressure homogenizer as described in chapter 7.6.2. The resulting feedstock properties are described in Table 6-11 .

Table 6-11: Feedstock properties of hGH production

Feedstock properties	Biomass suspension	40 % w/w <i>Escherichia coli</i>
	Conductivity [mS cm^{-1}]	18.35 ± 2.6
	pH	6.7 ± 0.2
hGH	Isoelectric Point	4.3
	Molecular weight [kDa]	22

6.2.4 ANION EXCHANGE CHROMATOGRAPHY (EBA-MODE)

a CHROMATOGRAPHIC PERFORMANCE

The primary aim for an initial step is a near quantitative capture of hGH by simultaneously avoiding product loss resulting from miss folded hGH, while a possible improvement in product purity played a minor role. As hGH is characterized by a rather low pI of 4.3, anion exchange capture was initially tested using two EBA resins Streamline DEAE and Streamline QXL. In order to keep as close as possible to the real process conditions clarified homogenate from hGH production was used as a feedstock.

Batch adsorption on Streamline DEAE

Isothermal binding conditions have been investigated at a pH of 7.5 and 9.0. The respective product capacities were found as 5.3 mg ml^{-1} at pH 7.5 and $\kappa = 5 \text{ mS cm}^{-1}$ and 4 mg ml^{-1} at pH 9.0 and $\kappa = 5 \text{ mS cm}^{-1}$. The higher binding capacity at the lower pH obtained during these studies could not be explained and has also not been verified during packed bed studies. The rather low and similar capacities obtained for both pH values indicate that the employed variation in pH plays only a minor role for the adsorption of hGH on the weak anion exchanger Streamline DEAE (see Fig. 6-45). In

contrast to this, a change in feedstock conductivity showed a considerable impact on the binding capacity as a decrease of the conductivity from $\kappa = 10 \text{ mS cm}^{-1}$ to $\kappa = 5 \text{ mS cm}^{-1}$ resulted – within the employed concentration – in a twofold increase in maximal binding capacity.

Batch adsorption on Streamline Q XL

Using Streamline Q XL resulted in higher capacities at the given conditions. In comparison to the data obtained for Streamline DEAE a nearly twofold increase to $Q = 7.5 \text{ mg ml}^{-1}$ at pH 9 and $\kappa = 5 \text{ mS cm}^{-1}$ could be obtained. An increase of the conductivity to $\kappa = 10 \text{ mS cm}^{-1}$ resulted again in a decrease of the capacity to $Q = 2.8 \text{ mg ml}^{-1}$, while a further increase to 15 mS cm^{-1} did not lead to changes in the achieved product capacity. When analyzing the data shown below (Fig. 6-46) it has to be taken into account that only few data points at higher final concentration could be generated due to a limitation of the product concentration in the feedstock. Because only limited data points at higher final concentrations were available, a further analysis of the data using appropriate models such as the Langmuir model could not be carried out.

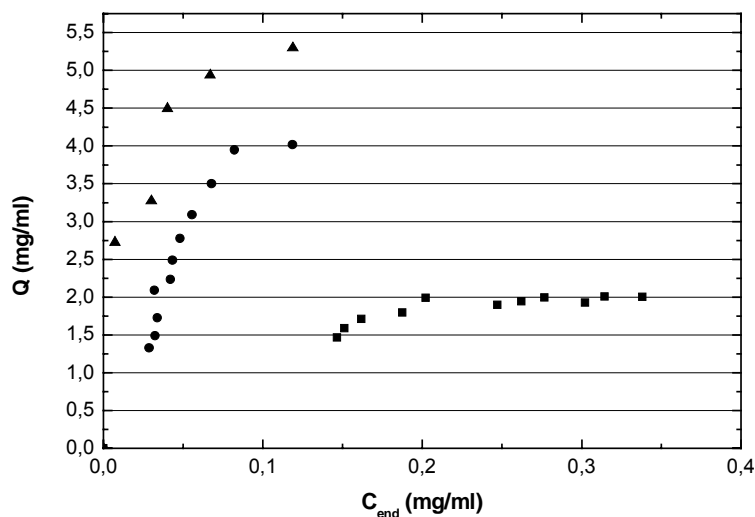


Fig. 6-45: Batch Isotherms of hGH on Streamline DEAE using clarified *Escherichia coli* homogenate at various conditions (■) pH 9 $\kappa = 10 \text{ mS cm}^{-1}$; $Q_{\text{max eff.}} = 2.0 \text{ mg ml}^{-1}$; (●) pH 9 $\kappa = 5 \text{ mS cm}^{-1}$ $Q_{\text{max eff.}} = 4.0 \text{ mg ml}^{-1}$ (▲) pH 7.5 $\kappa = 5 \text{ mS cm}^{-1}$. $Q_{\text{max eff.}} = 5.2 \text{ mg ml}^{-1}$

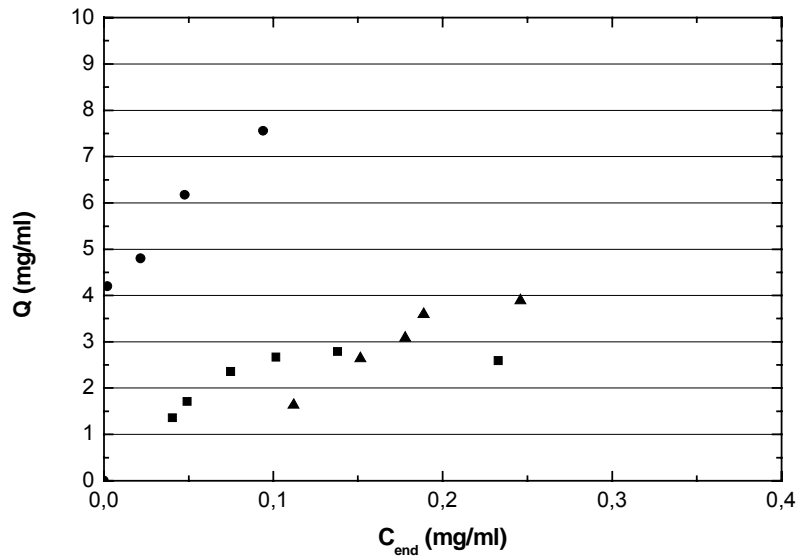


Fig. 6-46: Batch isotherms hGH on Streamline QXL using clarified *Escherichia coli* homogenate at various conductivity's. (\blacksquare) pH 9 10 mS cm^{-1} $Q_{\text{max eff.}} = 2.7 \text{ mg ml}^{-1}$; (\bullet) pH 9 $\kappa = 5 \text{ mS cm}^{-1}$ $Q_{\text{max eff.}} = 7.5 \text{ mg ml}^{-1}$; (\blacktriangle) pH 9 $\kappa = 15 \text{ mS cm}^{-1}$ $Q_{\text{max eff.}} = 3.8 \text{ mg ml}^{-1}$

Packed bed adsorption on Streamline DEAE

To evaluate adsorption behaviour of the hGH precursor during packed bed processing several breakthrough studies at different pH and conductivity have been performed (Fig. 6-47). Data obtained during batch adsorption studies and packed bed processing are summarized in Table 6-12.

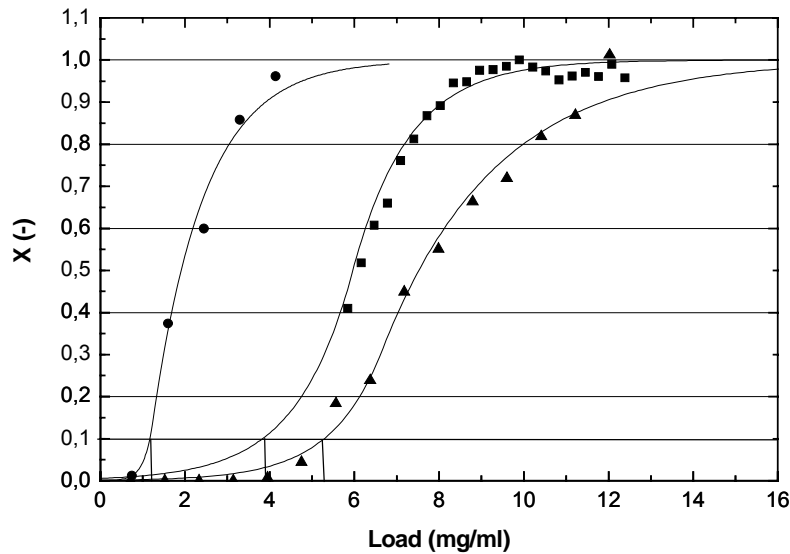


Fig. 6-47: Break through analysis Streamline DEAE packed bed 14.5 cm bed height, velocity 300 cm h⁻¹. Data fitted using the model after Hall et al. (1966) using following conditions (■) pH 7.5, 5 mS cm⁻¹; (●) pH 9, 10 mS cm⁻¹; (▲) pH 9, 5 mS cm⁻¹.

Table 6-12: Adsorption data on Streamline DEAE obtained during packed bed studies.

Batch adsorption	pH	Conductivity	
		5 mS cm ⁻¹	10 mS cm ⁻¹
	7.5	5.3	
	9.0	4.0	
Packed bed adsorption			
Q _{10%}	7.5	4.0	
Q _{EQ}		5.6	
Q _{10%}	9.0	5.0	1.0
Q _{EQ}		8.0	2.3

The dynamic capacities obtained during packed bed studies of $Q_{10\%} = 4.0 \text{ mg ml}^{-1}$ at pH 7.5 and $Q_{10\%} = 5.0 \text{ mg ml}^{-1}$ at pH 9.0 were generally in the order of the maximal capacities obtained during batch adsorption studies. The maximal equilibrium capacities were found $Q_{EQ} = 5.6 \text{ mg ml}^{-1}$ and $Q_{EQ} = 8.0 \text{ mg ml}^{-1}$ at pH 7.5 and pH 9.0 respectively. An increase in the conductivity lead again to a drastic decrease of the capacity to $Q_{10\%} = 1.1 \text{ mg ml}^{-1}$ and $Q_{EQ} = 2.3 \text{ mg ml}^{-1}$ at pH 9.0.

Gradient Elution Streamline DEAE

In order to evaluate possible improvements in product qualities a selective elution by a shallow (30 CV) salt gradient (0 – 500 mM NaCl) has been tested with a packed bed of Streamline DEAE at pH 7.5. The bed was loaded to a capacity of 1.4 mg ml^{-1} . The elution profile is shown in Fig. 6-48. During gradient elution two peaks were found, peak 1 having a distinct peak shoulder. A third peak was eluted with the wash in 100% 25 mM Tris/HCl pH 7.5 and 1 M NaCl (buffer B).

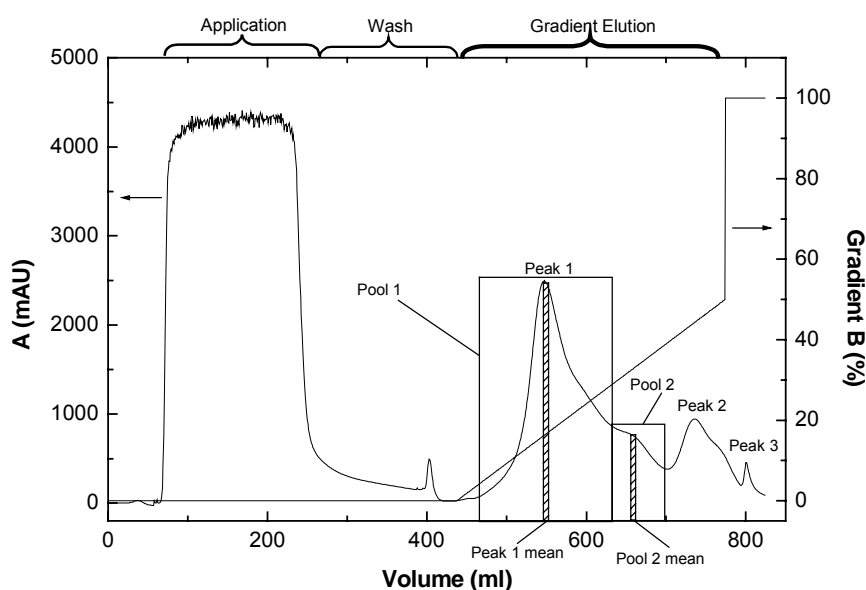
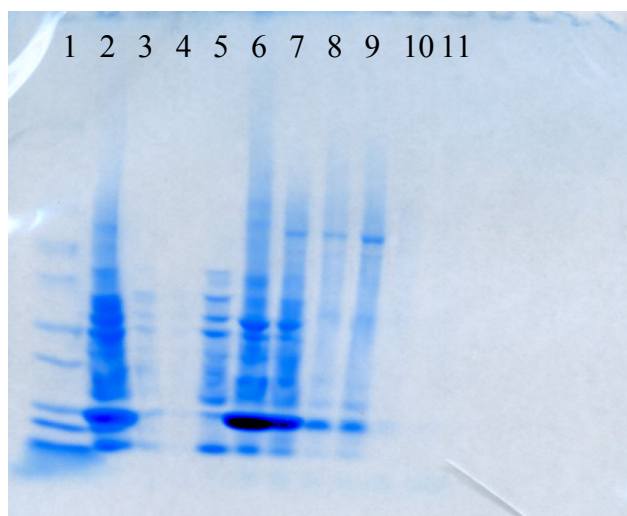


Fig. 6-48: Chromatogram of the gradient Elution using 25 mM Tris HCl pH 7,5 as Buffer A and buffer B = Buffer A + 1M NaCl. Gradient 30 CV 0- 50 % B. Application of 1.4 mg ml^{-1} at pH 9 $k = 5 \text{ mS cm}^{-1}$

Fig. 6-49 shows the protein composition of several fractions and pools obtained during load, wash and breakthrough. From this analysis it can be concluded that the main contaminants are co-eluting from the column at approximately 200 mM NaCl in the elution buffer (Peak 1 in Fig. 6-48). The purification factor of the anion exchange step is rather poor and a concentration factor of lower than 2 was observed, the yield was > 90 %. Peak 2 and 3 did not contain significant amounts of comassie blue stainable proteins (SDS-Page Fig. 6-49) but an increased concentration of DNA. While the DNA concentration in the flow through was measured to 0.8 ng ml^{-1} an increased concentration 1.7 ng ml^{-1} could be found in peak 2 and 3.



1. Size standard Marc 12 (Invitrogene)
2. Application
3. Wash 1
4. Wash 2
5. Total flow through
6. Pool 1 mean Fraction
7. Pool 1
8. Pool 2 mean Fraction
9. Pool 2
10. Peak 2
11. Peak 3

Fig. 6-49: SDS Page Gradient Elution compare Fig. 6-48

b BIOMASS ADSORBENT INTERACTIONS

Initial investigations were performed using *Escherichia coli* MC 1061 (host strain without the production plasmid).

Influence of homogenization technique and feedstock parameter

Initial homogenization was carried out using a laboratory bead mill at various feedstock conditions. For all homogenates CTI values between $CTI = 0.69$ and $CTI = 0.79$ were found and thus the homogenates could not be used for further EBA processing (Fig. 6-50). Generally an increase of the conductivity leads to an increase of the CTI value. The ζ -potential reaches a maximum of $\zeta = -15$ mV at conductivities above 20 mS cm^{-1} . When calculating the $(-\zeta_b \zeta_a)$ parameter with the present data a maximum of 310 mV² is reached at 20 mS cm^{-1} . A correlation found by Lin et al. (2002) indicates that this value equals to a CTI value of approximately $CTI = 0.8$. Earlier studies, however, revealed that a CTI value of greater than $CTI = 0.9$ is needed for successful EBA process design (Lin et al., 2001, Feuser et al., 1999, Fernández-Lahore et al., 1999, Fernández-Lahore et al., 2000). From adsorption studies shown above it is evident, that an increase in conductivity can not be used to decrease biomass adsorption interactions as it also significantly decreases the available product capacity.

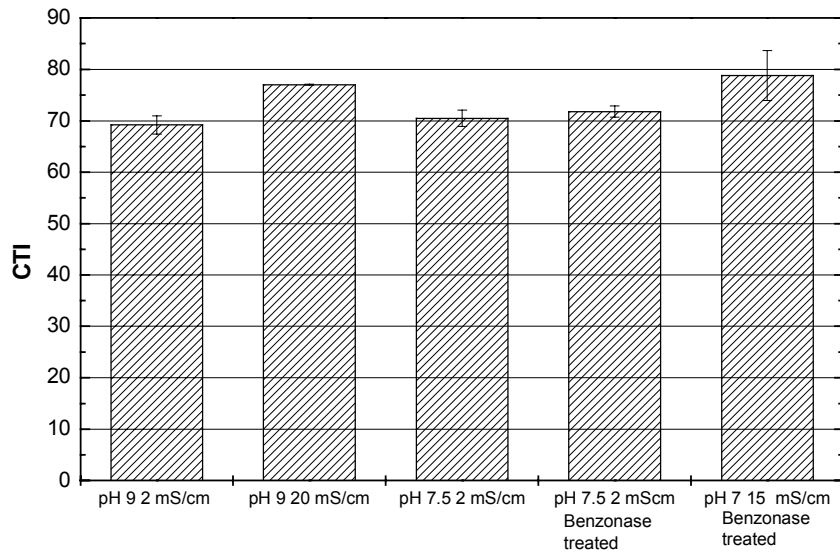


Fig. 6-50: Biomass Transmission using bead mill homogenate (*Escherichia coli* MC1061) and Streamline DEAE at various conditions.

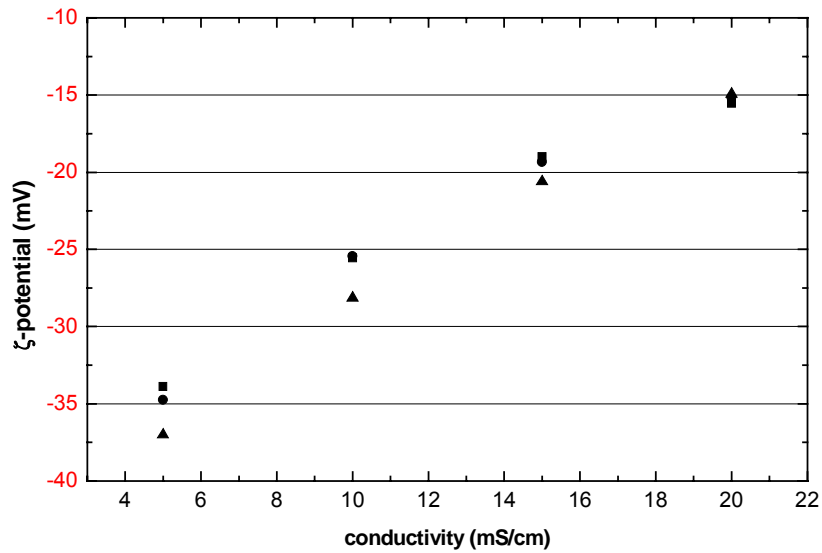


Fig. 6-51: ζ -potential of *Escherichia coli* MC1061 homogenate suspended in Tris/HCl buffer of various pH and conductivities. (■) pH 7.0; (●) pH 7.5; (▲) pH 9.0

A change in the actual homogenizing technique from a bead mill to a high pressure homogenizer let to a general increase of the CTI values ranging from CTI = 0.9 to CTI = 0.96. (minimal CTI = 0.9) i.e. in a lower biomass adsorbent interaction (Fig. 6-52). This corresponds to results presented in chapter 6.1. It further becomes evident that the main parameter governing the CTI value is the size and charge of the cell debris, while feedstock properties such as pH and ionic strength play a minor role.

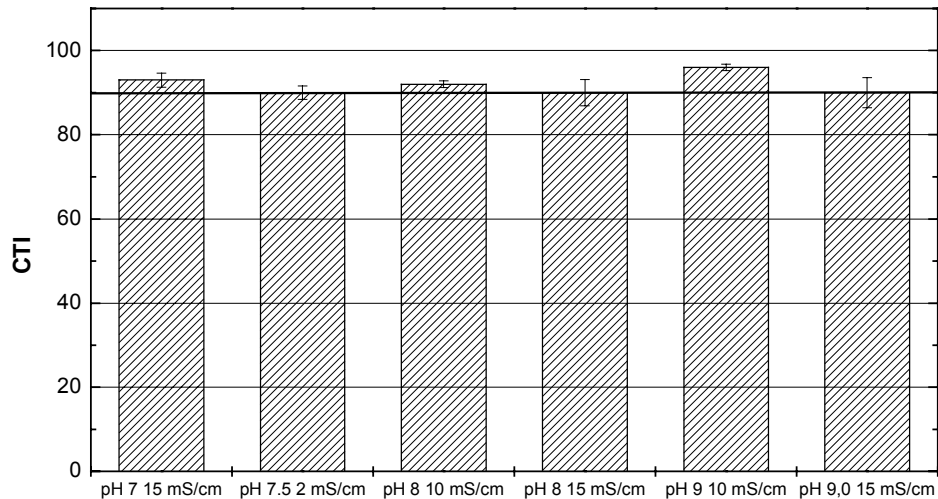


Fig. 6-52: CTI using high pressure homogenate of *Escherichia coli* MC1061 (5 cycle at 965 bar in a French Press) and Streamline DEAE at pH 8.0 and $\kappa = 10 \text{ mS cm}^{-1}$

Process performance: host strain vs. hGH production strain

Testing homogenates from hGH production significant differences were found. During production high pressure homogenization is employed using both a lower operating pressure and a lower number of cycles compared to studies summarized in Fig. 6-52. Approximately 1/3 of a 40 % ww *Escherichia coli* suspension is homogenized at 50 bar, followed by a homogenization of the second third at 700 bar. The obtained two homogenates are then mixed with the untreated 1/3 of the initial feedstock and finally homogenized at 700 bar. This procedure, however, is likely to result in a sub-optimal size reduction (chapter 6.1 page 52) and a larger particle size distribution as shown by Middelberg and co workers (Middelberg *et al.*, 1990, Middelberg *et al.*, 1992). Thus using homogenate from the current production resulted in similar cell transmission

results as observed with bead mill homogenate, and a maximal cell transmission of app. CTI = 0.7 (Fig. 6-53).

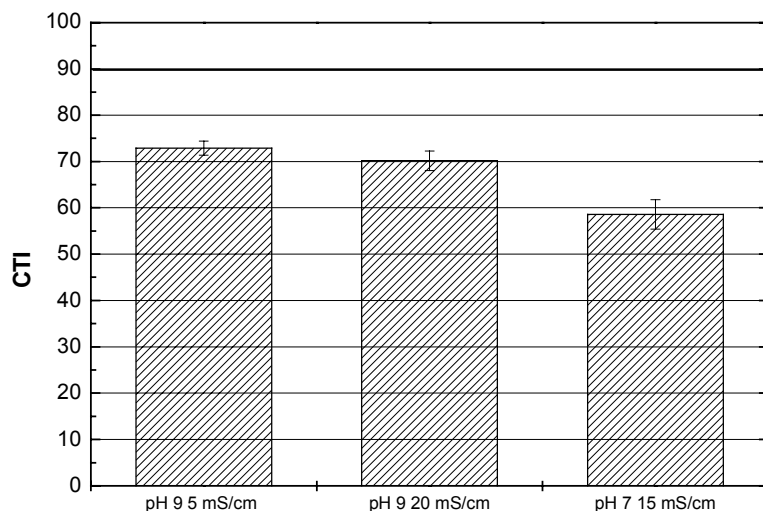


Fig. 6-53: CTI using production homogenate and Streamline DEAE.

The difference in performance between the optimal disrupted host strain and production homogenates becomes further evident when characterizing fluidization conditions by RTD analysis. The RTD analysis (Fig. 6-54) of high pressure homogenate obtained from the host strain confirms the results of the pulse response experiments. Under the conditions investigated, a perfectly fluidized bed was found. Evaluation by the PDE Model results in a high α value of > 0.95 and high Peclet (Pe) numbers (Table 6-13). Applying a high pressure homogenate obtained from hGH production strain under current production conditions (Novo Nordisk A/S, Gentofte, Denmark) a high degree of channeling and aggregation in the column was observed. This visual observation was confirmed by RTD analysis (Fig. 6-54). The RTD curve of the production homogenate showed a maximum at Θ (time/mean residence time) < 0.5 and an α value of 0.45 which indicates severe channeling and inhomogeneous fluidization. The evaluation by the PDE model resulted in a very low Peclet number. Unfortunately it was neither possible to evaluate particle size distribution and ζ -potential because suitable instrumentation was not available in the laboratory in Gentofte (DK) nor could the homogenization procedure be changed.

Another possibility for different behavior between the host strain and production strain could lie in variations of cell surface composition between the host strain and production strain, due to the genetic modification and the resulting growth behavior. In a recombinant organism a high degree of the metabolic capacity is used for the production of the recombinant protein, which results in a stress situation for the organism. It has been shown that cells react to growth limitation by a reduced growth and a strengthening of the cell wall (Kula *et al.*, 1990, Kula and Schütte, 1987). In order to disrupt these tougher cell walls harsher homogenization conditions would be needed.

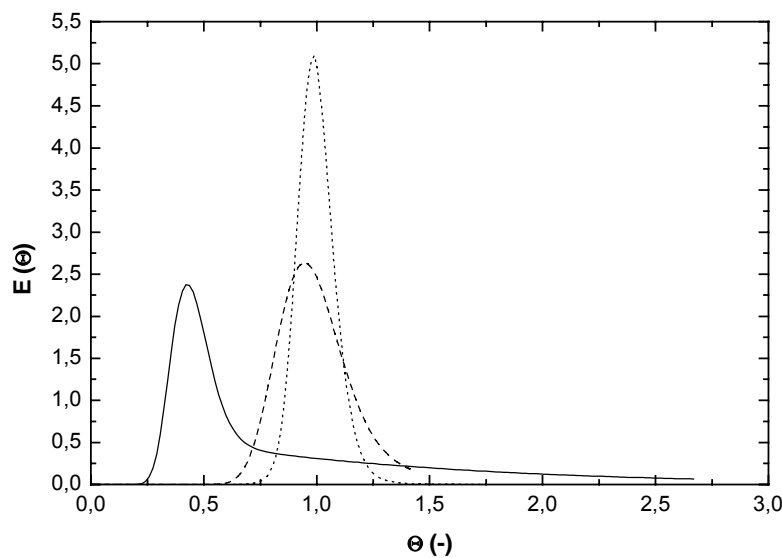


Fig. 6-54: RTD comparison of fluidization performance employing high pressure homogenate from the dummy and the production strain ($C_b = 10\%$ ww) on a Streamline DEAE column ($U = 300\text{ cm h}^{-1}$). (-) homogenate from hGH production; (---) homogenate obtained from dummy strain; (...) Buffer.

Table 6-13: PDE Evaluation of Fig. 6-54.

	Production strain	host strain
N	0,77	0,29
P	50,87	99,24
α	0,45	0,95

6.2.5 CATION EXCHANGE CHROMATOGRAPHY (EBA-MODE)

During process evaluation using anion exchange it was possible to choose pH values which were considerably above the pI of hGH. When considering cation exchange pI imposes initial boundary conditions. Even though binding of molecules on cation exchange resins above the pI is reported, a pH value of 1 unit below the pI is recommended for acceptable process capacity. Beside the pI of the target molecule, also the net-pI of the cell debris has to be taken into account when designing EBA processes. Thus the second boundary condition is given by the pI of the cell debris itself.

a BIOMASS ADSORBENT INTERACTION

Figure 1-22 shows the ζ -potential – pH relationship over a pH range between pH 3 and pH 9. The pI or zero net charge of the cell debris was found at pH 4.1. Over the whole pH range an S-shaped curve progression could be observed starting at + 16 mV at pH 3, approaching a net charge of approximately - 27 mV at pH 5.0 and reaching -37 mV at pH 9.0. From flocculation studies in biomass containing feedstock it is well known that biomass flocculation occurs at pH values close to the pI of the cells. This was also observed during the present study. The pH area where flocculation was visually observed is marked with a striped box in Fig. 6-51. This phenomena can be explained by the DLVO theory (Wiese and Healy, 1970).

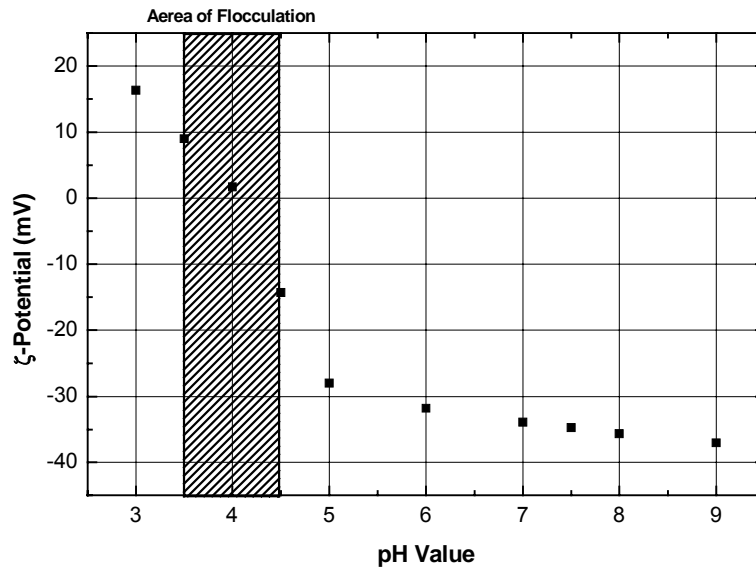


Fig. 6-55: Zeta Potential – pH relationship of the homogenate (5 mS cm^{-1}). Cell debris suspended in $\text{Na}_2\text{HPO}_4/\text{citric}$ of various pH values and a constant conductivity of $\kappa = 5 \text{ mS cm}^{-1}$

The visual impression could be confirmed by a microscopic analysis, which shows the aggregation (Fig. 6-56). It is clearly seen that large aggregates are formed at pH values between 4.5 to 3.5. At pH 5.0 no aggregates were found. By increasing the conductivity aggregation could be avoided (Fig. 6-57 pH 4.5 and $\kappa=10 \text{ mS cm}^{-1}$) which is in agreement with common theory, but contraindicated as it lowers product capacity.

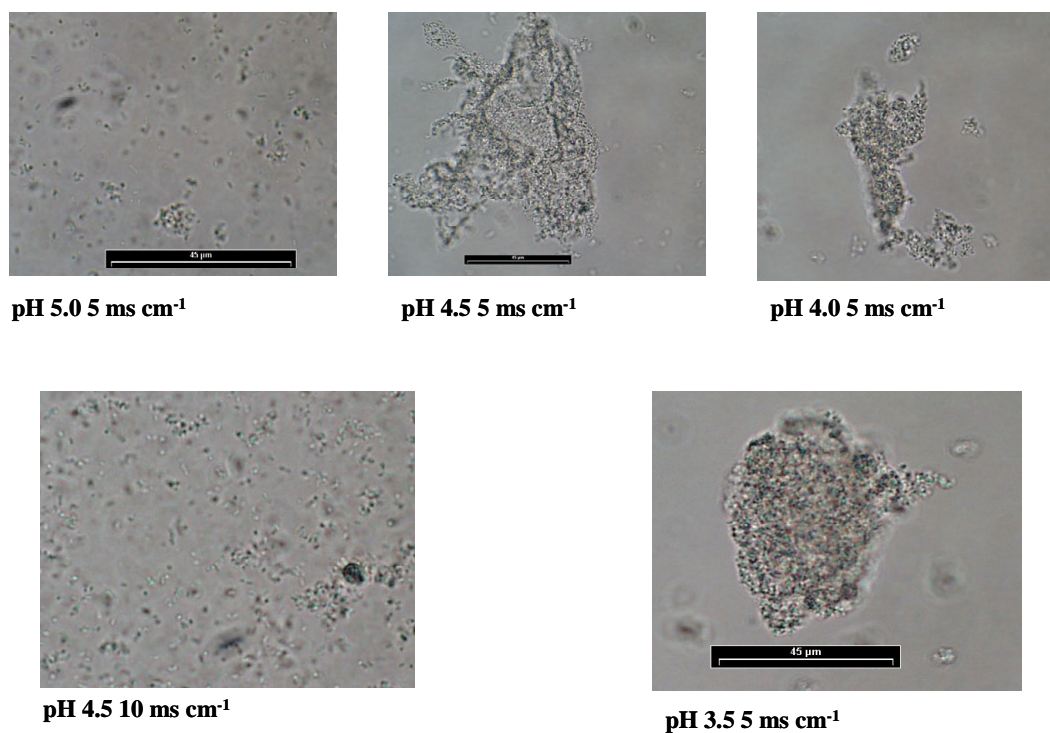


Fig. 6-56: Microscopic picture of *Escherichia coli* cell debris (from hGH production) Flocculation at acidic conditions suspended in 30 mM Na₂HPO₄/citric acid buffer of various pH and conductivity (adjusted with solid NaCl).

Pulse response experiments, employing Streamline SP XL, showed a good cell transmission for pH > pH 4.5 and conductivities $\kappa \geq 10 \text{ mS cm}^{-1}$. Decreasing the conductivity to $\kappa = 5 \text{ mS cm}^{-1}$, however, led to a decrease of the CTI value from CTI > 0.9 at $\kappa = 15 \text{ mS cm}^{-1}$ to CTI = 0.63 at $\kappa = 5 \text{ mS cm}^{-1}$.

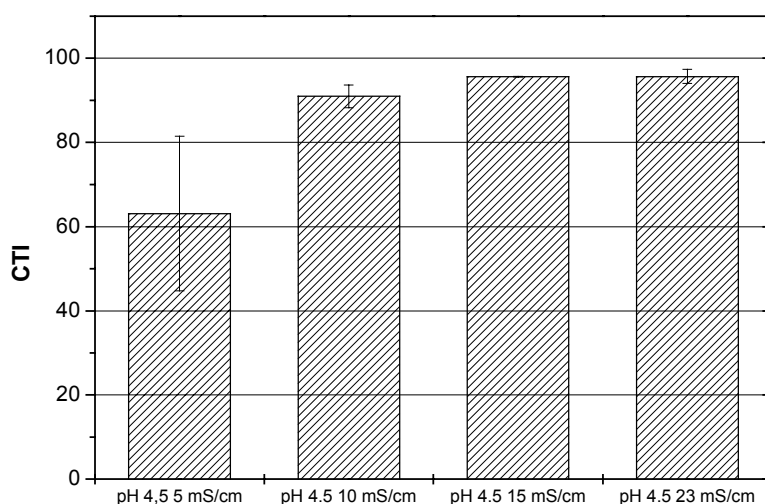


Fig. 6-57: CTI *Escherichia coli* homogenate using Streamline SP XL at various pH and conductivities.

To summarize the above, the following boundary conditions are given under the present process conditions. Due to the pI of 4.3 of the hGH molecule a pH below this value preferably < 3.8 should be used. Because of the flocculation of cells and low CTI values the pH range between 3.5 and 4.5 should be avoided, however, even at pH 3 a weak flocculation was still present, which means that the electrostatic repulsion of the – now positively charged cell debris – is not strong enough to avoid flocculation totally. The positively charged cells may also cause biomass adsorbent interactions when using cation exchange chromatography. Finally, a net-pI value of 4.1 of the cell debris indicates that – similar to anion exchange processes – biomass adsorption interactions have to be expected below pH 4.1.

b PACKED BED ADSORPTION

As an integral process of solid-liquid separation in combination with product adsorption seems to be hampered by significant biomass adsorbent interactions, cation exchange might still be the operation of choice, especially using resins with the ability to cope with minor particulate contamination. This could eventually replace the three unit operations – cross flow filtration, ultrafiltration and ion exchange (IEX1) – currently used during hGH production. In order to find optimal conditions regarding pH and ionic strength, precipitation of proteins in the pH range of interest had to be investigated. The intention of this investigation was thus to use different precipitation properties of hGH

and *Escherichia coli* host cell proteins (hcp) at acidic conditions followed by cation exchange chromatography. Therefore it is necessary to characterize the solubility of hcp and hGH at different pH and dilution of the feedstock to identify conditions with maximized solubility of the product and maximum precipitation of contaminant proteins.

Protein precipitation

In Figure 1-24 the solubility of hGH and contaminant proteins has been characterized in a pH range from pH 3 – pH 7.5. As expected, hGH shows a more defined precipitation pattern when compared to the total protein being a mixture of proteins. HGH precipitation starts approximately at pH 5.0 reaching its minimal solubility of ~10% initial concentration at approximately pH 4.0 (pI 4.3), while at pH 3.5 a solubility of ~85% is again reached. The data for total protein reveal a precipitation start at around pH 6.0 and a minimum value of 40% solubility at pH 4.0. At pH 3.5 a solubility of ~50% is reached. The latter leads to a purification factor of ~2 at pH 3.5 and a product loss of 15%.

In order to reduce the loss of 15% hGH during feedstock titration, a 1:4 dilution was used prior to a second investigation. Analyzing the precipitation behavior of 1:4 diluted feedstock (see Fig. 6-59) showed that the solubility of the target molecule hGH and the contaminant proteins are quite similar over the whole pH range. Total solubility of the hGH molecule was observed at an $\text{pH} \geq 5.0$ and $\text{pH} \leq 3.5$. The minimum solubility of 80% was detected at pH 4.5. The similar behavior of total protein and hGH resulted in a rather low purification factor of 1.3 at pH 5.0 but also in a relatively low product loss (max. 15 % at pH 4.5 and 1 % at pH 3.5).

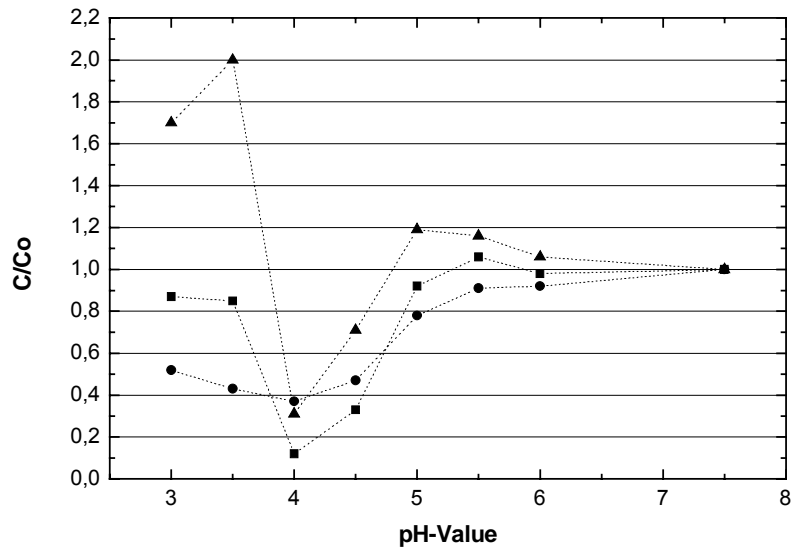


Fig. 6-58: pH depended solubility of hcp and hGH and purification factor starting with undiluted feedstock. (■) $C/C_{0\text{ hGH}}$; (●) $C/C_{0\text{ TP}}$; (▲) Purification factor.

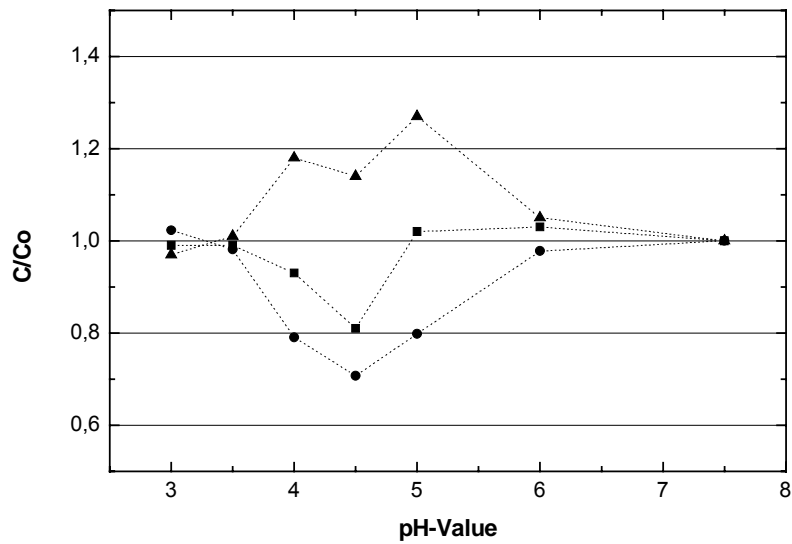


Fig. 6-59: pH dependent solubility of hcp and hGH and purification factor using 1:4 diluted feedstock. (■) $C/C_{0\text{ hGH}}$; (●) $C/C_{0\text{ TP}}$; (▲) Purification factor

Chromatographic performance

Due to the lower product loss and the lower feedstock conductivity, the 1:4 diluted homogenate was used for further processing by cation exchange chromatography.

Fig. 6-60 shows isothermal binding behavior of hGH at pH 3.5 and pH 4.0 and a conductivity of $\kappa = 5 \text{ mS cm}^{-1}$. Under the given conditions a maximal equilibrium capacity of $\sim 50 \text{ mg ml}^{-1}$ and $\sim 40 \text{ mg ml}^{-1}$ at pH 4.0 and pH 3.5 respectively was found. The higher capacity at pH 4.0 is probably related to a 20 % lower content of total protein at this pH value.

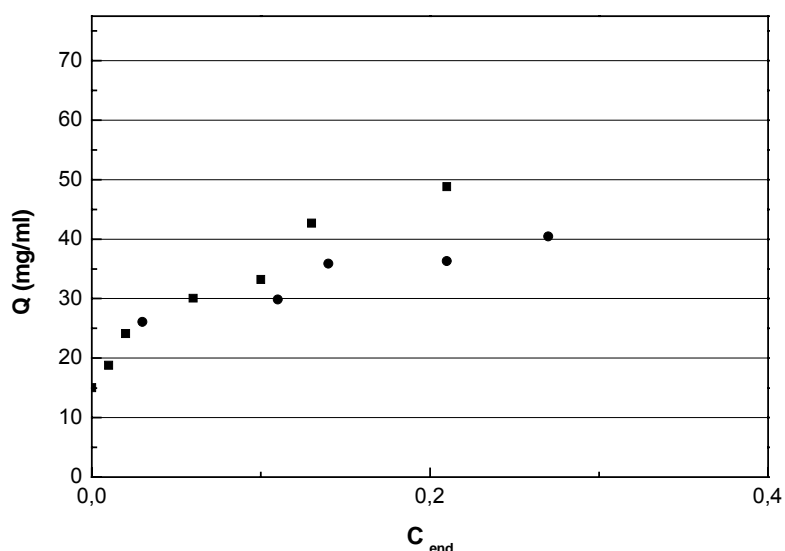


Fig. 6-60: Adsorption isotherm SP Sepharose[®] Big Beads clarified homogenate, 1:4 diluted $\kappa = 5 \text{ mS cm}^{-1}$. (■) pH 4.0; (●) pH 3.5.

In addition to batch adsorption packed bed breakthrough studies were performed at pH 3.5 and $\kappa = 5 \text{ mS cm}^{-1}$ using SP Sepharose BB. During these studies it was found that hGH adsorption was strongly dependent on the flowrate employed. At a flowrate of 300 cm h^{-1} a $Q_{10\%}$ value of 7 mg ml^{-1} was found, while a reduction of the linear velocity to 80 cm h^{-1} led to a twofold increase $Q_{10\%} = 15 \text{ mg ml}^{-1}$. This behavior clearly indicates a pore diffusion limitation which generally leads to residence time controlled sorption processes.

In order to evaluate possible improvements of the product quality by a selective elution a shallow (30 CV) pH gradient (pH 3.5 – pH 7.5) has been applied to a packed bed of Streamline DEAE. To do so, the EQ buffer (35 mM Na_2HPO_4 – pH 3.5) was titrated with 100 mM Na_2HPO_4 to a final pH of 7.5. The packed bed was loaded at pH 3.5 to a bed capacity of 4.8 mg ml^{-1} . The elution profile, described in Fig. 6-61 shows that the elution starts close to the isoelectric point of hGH at app. pH 4.5. The majority of hGH is eluted after app 10 CV and pH 5.1 the following peak shoulder (pool 3) still contains hGH (see Fig. 6-61, Fig. 6-62) and even in pool 4 & 5 up to 50 CV hGH is eluted from the column.

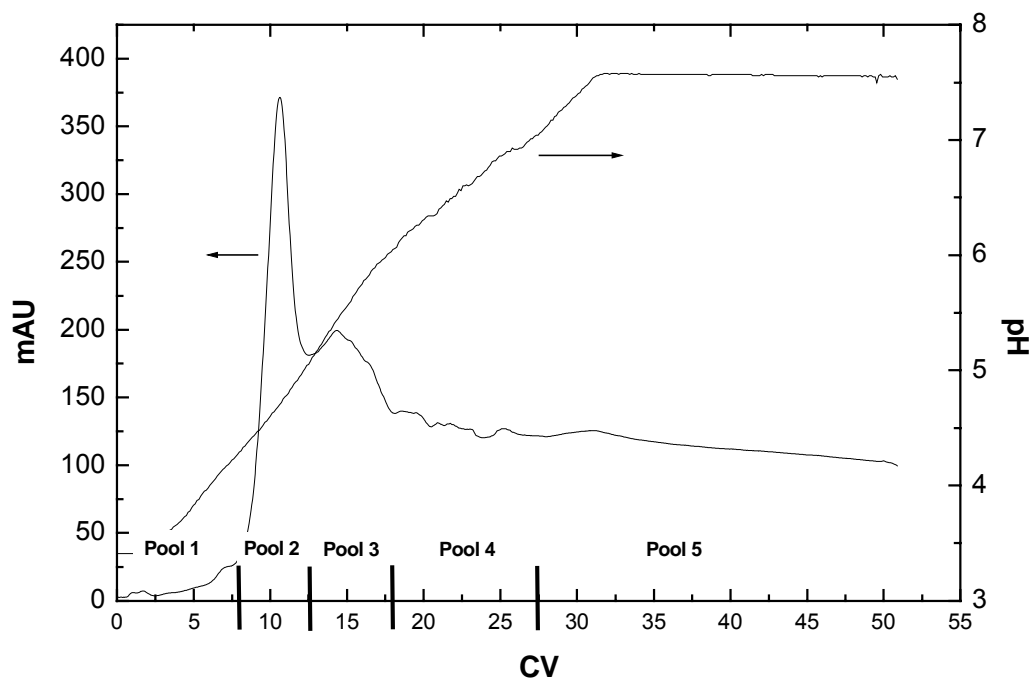


Fig. 6-61: pH Gradient elution of hGH from SP Sepharose BB. Application at pH 3.5 $\kappa=5 \text{ mS cm}^{-1}$ 10 cm sed. bed height, $U = 76 \text{ cm h}^{-1}$. pH gradient Elution titrated using 100 mM Na_2HPO_4 to lower the pH in 30 CV.

The SDS PAGE analysis of the various pools in Fig. 6-62 shows that hGH is present in all fractions even in low concentrations in the large fraction 5. The overall process performance is given in Table 6-14 demonstrates that the overall yield of 67% is linked to a rather low purification factor of 2.7 and a concentration factor of 0.2. Further investigations using a step elution at pH 7.5 resulted in a 50 % loss of hGH. Since the

material balance suggested that 50% hGH remained on the column it can be postulated that the step change led to a precipitation of hGH on the column.

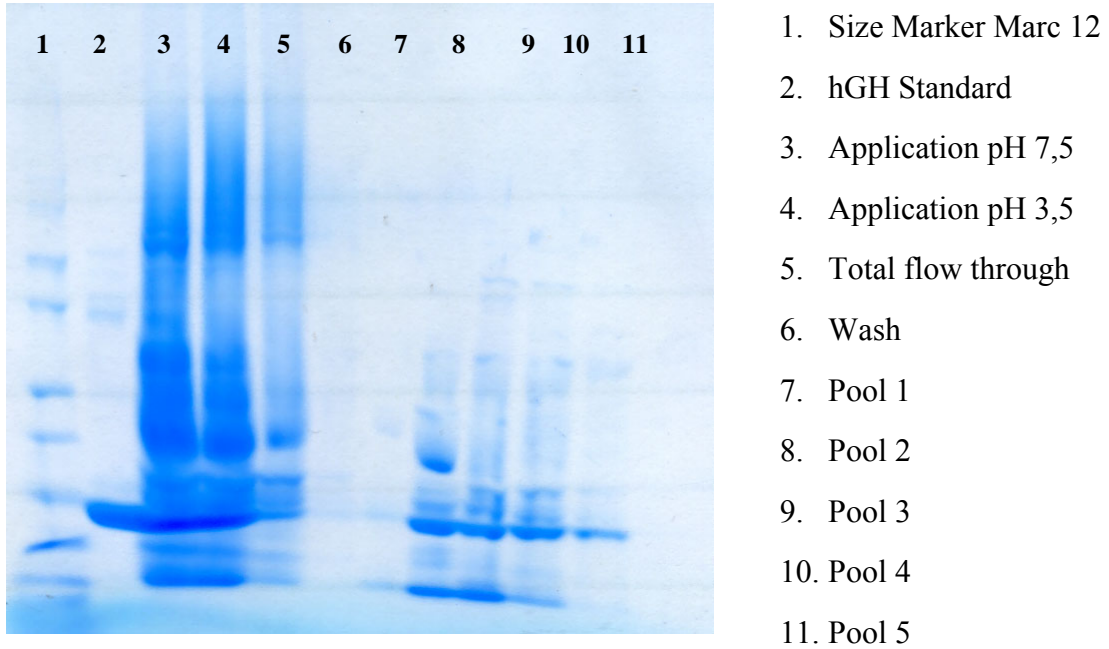


Fig. 6-62: SDS-PAGE analysis of hGH pH gradient elution. Sample assignment see Fig. 6-61.

Table 6-14: hGH and total protein concentrations for various process steps

	Total Protein C/Co	hGH C/Co	"Volumen (ml)"
Co pH 7.5	1	1	100
Co pH 3.5	0.68	0.83	100
total Flowthrough	0.14	0.08	100
wash	0.01	0.07	78,5
Elution Pool 1	0.01	0.10	80
Elution Pool 2	0.14	0.27	30
Elution Pool 3	0.12	0.26	40
Elution Pool 4	0.09	0.19	80
Elution Pool 5	0.02	0.15	170
Purification Factor	2.7		
$C_{hGH}(\text{app})/C_{hGH}(\text{Elution})$	4.9		
Mass balance	97 %		
Yield	67 %		

6.3 AQUEOUS TWO PHASE SYSTEMS

During this study a broad range of phase systems were investigated. The initial experiments were focused on phase systems containing relatively low molecular weight PEG to obtain top phases characterized by low viscosities. This is especially important for further processing of the top phase by direct application on a chromatography column (Thömmes *et al.*, 1999) or by ultra filtration.

a ATPS SCREENING

An initial screening was carried out using different low molecular weight PEG fractions and clarified hGH homogenate as summarized in Table 6-15. The composition of the initial phase systems was taken from Zaslavsky (1995).

Table 6-15: Composition of ATPS 22 % PEG (MW see table.) 13.63 % K₂HPO₄, 2.37 % KH₂PO₄, 50 % Feedstock (pH app. 8.6)

	PEG [MW]	PEG [%]	Salt [K ₂ HPO ₄ / KH ₂ PO ₄]	Feedstock [%]
System 1	200	22	13.63 / 2.37	50
System 2	300	22	13.63 / 2.37	50
System 3	400	22	13.63 / 2.37	50

System 1 showed no phase separation under the conditions employed presumably the composition was close to the binodale. System 2 and system 3 showed a distinct phase separation with the total protein pool present in the top phase as shown in the SDS-page analysis Fig. 6-63.

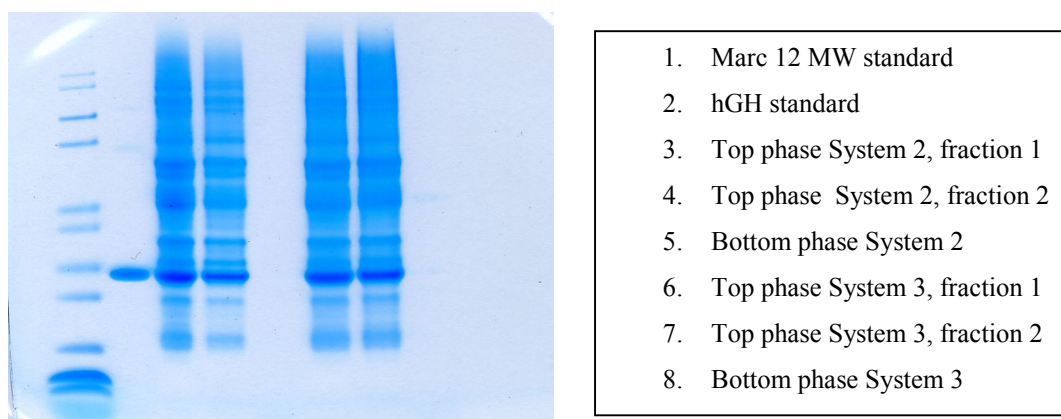


Fig. 6-63: SDS Page analysis of ATPS Systems. PEG has been removed from the top phase using PD10 columns (2.5 ml sample was eluted in two 3.5 ml fractions)

When using cell debris containing feedstock as a real system the biomass was accumulated in the top phase. Unlike soluble components, which partition between the two bulk phases, particulates can be partitioned between the top, bottom and the interphase. The tendency to accumulate at the interphase increases with the particle size and increased liquid-liquid interfacial tension. The affinity of a substance to the different phases depends on several parameters such as MW of the polymer, concentration of the components and the ionic composition (Albertsson, 1960).

In order to partition the cell debris into the inter- or bottom phase several systems with decreased phosphate concentration were investigated (see Table 6-16). It could be observed that the salt concentration had little impact on the partition of the cell debris. The cell debris remained in the top phase in all cases investigated.

Table 6-16 ATPS with decreased phosphate concentration as a mixture of 85.2 % K_2HPO_4 and 14.8 % KH_2PO_4 was used. to reach a pH of 8.6.

	System 1	System 2	System 3	System 4
Salt	16	14	12	10
PEG 400	19.40	19.40	19.40	19.40
comment	cell debris accumulates at the bottom of the Top phase	cell debris accumulates at the bottom of the Top phase	cell debris accumulates at the bottom of the Top phase	no phase system

As pointed out above the MW of the polymer is another highly important factor influencing the partitioning of particulates and proteins in ATPS systems. It was found by Albertson in various studies that higher MW PEG leads to a partitioning of cell debris into the bottom phase (Albertsson, 1960). Therefore several higher MW PEG and mixtures of different PEG molecular weights have been investigated.

As expected from theoretical considerations the cell debris was directed in the bottom phase increasing the MW of PEG. For phase systems using PEG 600 or 1000 turbid top phases were observed while for higher molecular weight PEG comparatively stable three phase systems have been formed with the cell debris in the inter phase as it is shown in Table 6-17. The best results in terms of cell debris partition and partition of the hGH were obtained with a system containing a mixture of PEG 1550 and PEG 400 (System nr. 6 in Table 6-17).

Table 6-17: ATPS with higher MW PEG and mixtures (partitioning of the cell debris and hGH)

ATPS System	PEG [MW] / [%]	Salt [%]	Volume of the Top phase [ml]	Yield in the Top phase [%]	comments
1	PEG 600 15	Na ₂ SO ₄ 16	3.2	57	3 phase system
2	PEG 600 14.5	Na ₂ SO ₄ 10.5	6.4	99	diffuse phase separation
3	PEG 1000 15	Na ₂ SO ₄ 10			diffuse phase separation 3 phases
4	PEG 1550 15	Na ₂ SO ₄ 10	4.2	2	3 phase system
5	PEG 1550 14	13	3.8	2	3 phase system
6	PEG 400 / 1550 18 / 7	K ₂ HPO ₄ 6	7.6	100	stable two phase system

b TOP PHASE PROCESSING

The top phase of ATPS systems contains comparatively high concentration of PEG and exhibits a increased viscosity of app. 5 mPas, which might disturb further purification steps. Therefore two different strategies to remove PEG from the process liquid have been investigated. The first strategy was a direct capture of hGH in a packed bed using high viscosity tolerating large adsorbent particles as already presented by Thömmes *et al.* (1999) for the isolation of chymotrypsinogen. As a second option ultra filtration was investigated carrying out a buffer exchange to desalt the phase and remove PEG simultaneously.

An absorber screening (anion exchanger DEAE and QXL challenged with various dilution (1:1 - 1:10 $\Rightarrow \kappa = 19.6 \text{ mS cm}^{-1}$ - $\kappa = 7.5 \text{ mS cm}^{-1}$, pH 8.0-8.5); HIC (Phenyl) undiluted and HIC (Phenyl) undiluted + $15 \text{ g L}^{-1} (\text{NH}_4)_2\text{PO}_4$), revealed only low binding capacities for all resins and conditions investigated. This could be expected when considering the rather high conductivity of the top phase. An acceptable conductivity of 6.5 mS cm^{-1} could be reached only at a 10 fold dilution. This, however, led to a diluted feedstock and thus unfavorable isothermal binding conditions. Therefore it has to be concluded that direct adsorption from the top phase can not be used for further purification of hGH.

Table 6-18: pH and conductivity of different diluted ATPS Top phases

	undiluted	1:3 dil.	1:10 dil.
pH	8.65	8.6	8.1
conductivity	19.5 mS cm^{-1}	17.3 mS cm^{-1}	6.5 mS cm^{-1}

In the initial ultrafiltration experiments UF membranes with different mean pore sizes or cut off have been employed in a stirred Amicon UF cell in order to evaluate the maximum pore size suitable in terms of hGH retention and membrane fouling. A large pore size is generally favorable due to a better removal of PEG and higher trans membrane flux. Considering the molecular weight of hGH = 22 kDa membranes with an average cut off of 10 and 30 kDa have been investigated. For both membranes no

product loss due to leaking or fouling could be observed, not even in a dead end operated Amicon cell.

To characterize ultra filtration under real process conditions the filtration performance in a cross flow filtration module has been investigated using a 30 kD cut off membrane. Fig. 6-64 shows a reasonable low trans membrane flux when compared to specifications from Sartorius for pure water (35 L h^{-1} for a 0.1 m^2 module and feed pressure of 1.5 bar). The trans membrane flux first decreases to a certain level followed by an increase corresponding to an increased cross flow. The latter was adjusted to compensate the decreasing trans membrane pressure during filtration. The low flux can be explained by the viscosity of the feedstock due to the high PEG concentration. During filtration PEG passes through the membrane and is continuously removed from the feedstock resulting in a decreased pressure and viscosity and thus a better filtration performance. These investigations clearly confirm the ability to remove PEG by a direct ultra filtration of the ATPS top phase. While the filtration efficiency needs still to be optimized, a clear decrease in the feedstock viscosity could be reached (Fig. 6-65).

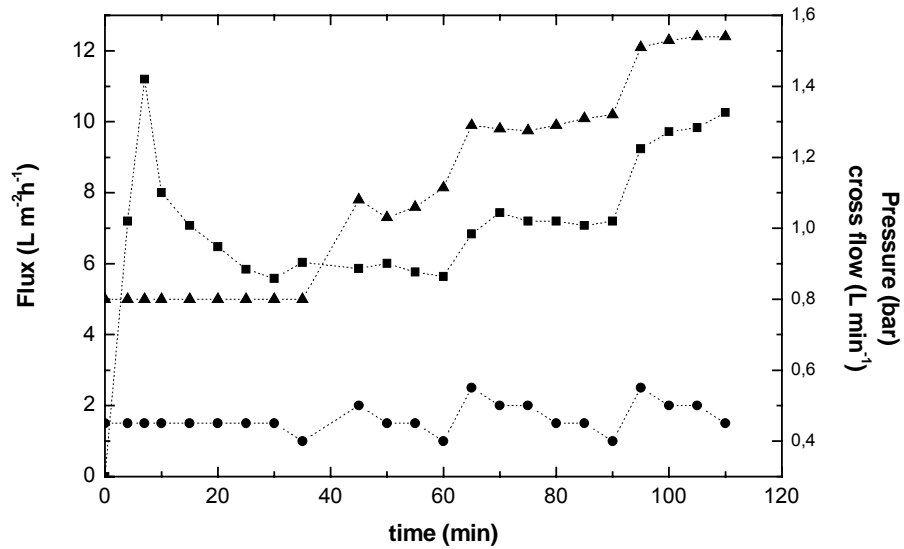


Fig. 6-64: Cross Flow filtration Sartorius Sartocoon[®] II mini module 30 kDa cut off polysulfon membrane. The volume has kept constant at 600 ml by supplementing the filtrated volume by 25 mM Tris/HCl pH 7,5. The inlet pressure has been adjusted by increasing the cross flow. (■) trans membrane flux; (●) trans membrane pressure; (▲) cross flow.

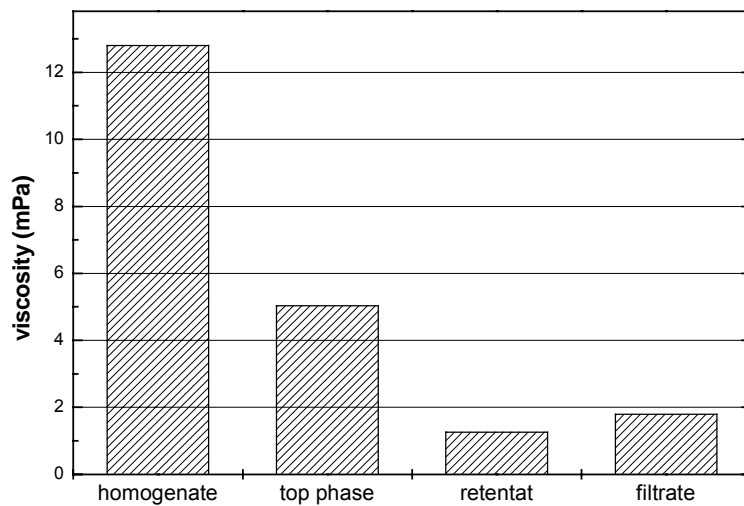


Fig. 6-65: Viscosity of the liquid phase during ATPS and ultra filtration. The ATPS top phase was cross flow filtrated (Fig. 6-64) the filtrated volume was supplemented by 25 mM Tris/HCl pH 7,5 until 2 times of the initial top phase volume was passed through the membrane.

Parameters characterizing the process performance are given in Table 6-19. Starting with ATPS in a 1 L scale resulted in an 86% recovery, while the ultra filtration step showed a yield of 97 % resulting in an over all yield of 84 %. The process liquor was further characterized as it is shown Table 6-19.

Table 6-19:

	Volume (ml)	hGH (mg/ml)	pH	LF (mS/cm)	Yield (%)
Homogenate	500	0.79	7.5	5	100
Top phase	660	0.68	8.6	20	86
Retentat	660	0.66	7.5	8.7	97
Filtrat	1320	nn	8.3	21	
				Over all yield	84

6.3.2 SUMMARY AND CONCLUSIONS III (hGH)

Employing anion exchanger such as Streamline DEAE or QXL a reasonable binding of hGH was found. However, this was accompanied by strong biomass adsorbent interactions resulting in dead water zones, a distinctive channeling and in extreme cases a final bed collapse. As a conclusion anion exchange – in combination with the feedstock investigated – can NOT be recommended for an EBA process.

Further optimization of the cell disruption conditions is recommended in this context especially regarding the weak biomass interaction found with a high pressure homogenate of the host strain and the mechanistic findings discussed in chapter 6.1. Since a lower number of cycles and lower operating pressure were performed at the product site (just one cycle at 700 bar) a larger particle size distribution has to be expected. Further it might be possible that the production strain exhibits differences at the cell surface due to its genetic modification, but particle size appears to dominate the results presented.

When investigating cation exchange processes as an alternative another limitation in terms of applicable processing pH was found. At a certain pH (pH 4.5) the cell debris

starts to flocculate, which results in bad fluidization of the expanded bed, while at a pH above pH 4.5 no product adsorption onto the matrix occurred. Although good binding from particulate free solution was found at lower pH values than 4.5, no window of operation exists for a suitable cation exchange EBA process.

Cation exchange seems to be possible in packed bed mode with a reasonable capacity. The elution using a pH gradient, however, led to a diluted elution pool and a inefficient process. A step elution using increased salt concentration might solve this problem and remains to be evaluated.

Using ATPS in combination with ultra filtration, a comparatively efficient capture process could be demonstrated resulting in a cell free top phase, from which PEG and salts can be removed by ultra filtration, delivering a solution with low conductivity and high product concentration, ready for final purification steps.

7 MATERIAL & METHODS

Table 7-1: Chemicals

Chemical	Supplier
Acetonitril HPLC gradient grade	Roth, Karlsruhe, Germany
Agarose	Merck, Darmstadt, Germany
Bovine Serum Albumin	Sigma-Aldrich, Munich, Germany
Citric acid p.a.	Merck Darmstadt, Germany
Comassie Brilliant Blue G250	Fluka, Buchs, Switzerland
CTBA (Hexadecyltrimethylammoniumbromide)	Merck, Darmstadt, Germany
Ethanol (100 %) p.a.	Fluka, Buchs, Switzerland
Ethanolamine p.a.	Merck, Darmstadt, Germany
H ₃ PO ₄ 85% p.a.	Merck, Darmstadt, Germany
Histidine p.a.	Merck, Darmstadt, Germany
Human Insulin reference solution P45	Novo Nordisk, Denmark
Hydrochloric acid 32 % p.a.	Merck Darmstadt, Germany
Lithium chloride p.a.	Merck Darmstadt, Germany
Na ₂ SO ₄ (anhydrous) p.a.	Merck, Darmstadt, Germany
PEG polyethylenglycole	Fluka, Buchs, Switzerland
Sodium Bromide	Merck Darmstadt, Germany
Sodium Chloride p.a.	Merck Darmstadt, Germany
Sodium dihydrogen phosphate monohydrate p.a.	Merck Darmstadt, Germany
Sodium hydroxide p.a.	Merck Darmstadt, Germany
Somatropin working standard	Novo Nordisk, Gentofte, Denmark
Tris-(hydroxymethyl)-aminomethan p.a.	Carl Roth GmbH & Co. KG Karsruhe, Germany
Urea p.a.	Merck, Darmstadt, Germany

Table 7-2: Chromatography resins

Streamline™ SP	Amersham Biosciences, Freiburg, Germany
Streamline™ DEAE	Amersham Biosciences, Freiburg, Germany
Streamline™ Q XL	Amersham Biosciences, Freiburg, Germany
Streamline™ Phenyl	Amersham Biosciences, Freiburg, Germany
Streamline™ Heparin	Amersham Biosciences, Freiburg, Germany
SP Sepharose Big Beads	Amersham Biosciences, Freiburg, Germany
Q Sepharose Big Beads	Amersham Biosciences, Freiburg, Germany
Zirconia S	Biosepra Process Devision of Ciphergene, Paris, France
Zirconia CM	Biosepra Process Devision of Ciphergene, Paris, France

Table 7-3: Chemicals for cell cultivation

Yeast extract	Sigma Alldrich, Munich, Germany
(NH ₄) ₂ SO ₄	Merck, Darmstadt, Germany
AlCl ₃ -6H ₂ O	Merck, Darmstadt, Germany
Amicase casein acid hydrolysate bovine milk	Sigma Alldrich, Munich, Germany
Ampicillin	Merck, Darmstadt, Germany
Biotin	Fluka, Buchs, Switzerland
CaCl ₂ 2H ₂ O	Merck, Darmstadt, Germany
Ca-Phanthotenat	Fluka, Buchs, Switzerland
cCyanocobalamin (B12)	Fluka, Buchs, Switzerland
CoCl ₂ -6H ₂ O	Merck, Darmstadt, Germany
CuCl ₂ -2H ₂ O	Merck, Darmstadt, Germany

FeSO ₄ -7H ₂ O	Merck, Darmstadt, Germany
Folsäure	Fluka, Buchs, Switzerland
Glucose	Sigma Alldrich, Munich, Germany
H ₃ BO ₃	Merck, Darmstadt, Germany
IPTG	Merck, Darmstadt, Germany
KH ₂ PO ₄	Merck, Darmstadt, Germany
MgSO ₄ -7 H ₂ O	Merck, Darmstadt, Germany
MnSO ₄ -H ₂ O	Merck, Darmstadt, Germany
Na ₂ -EDTA-2H ₂ O (Titriplex III)	Merck, Darmstadt, Germany
Na ₂ MoO ₄ -2H ₂ O	Merck, Darmstadt, Germany
NaH ₂ PO ₄ H ₂ O	Merck, Darmstadt, Germany
NH ₄ Cl	Merck, Darmstadt, Germany
Nicotinsäure	Fluka, Buchs, Switzerland
Peptone from casein	Sigma Alldrich, Munich, Germany
Pyridoxin-HCl	Fluka, Buchs, Switzerland
Riboflavin /(Vit B2)	Fluka, Buchs, Switzerland
Thiamin HCl	Merck, Darmstadt, Germany
Thiamin-HCl (B1)	Fluka, Buchs, Switzerland
ZnSO ₄ -7H ₂ O	Merck, Darmstadt, Germany

Table 7-4: Consumables

NuPAGE® Tris-glycine-Gel 10 %	NuPAGE®, Invitrogene GmbH, Karlsruhe, Germany
Cellulose Acetate membrane 0,45 µm pore size 47 mm	Sartorius AG, Goettingen, Germany
Mark12™ Unstained Standard	Invitrogene GmbH, Karlsruhe, Germany
MES-Running Buffer	NuPAGE®, Invitrogene GmbH, Karlsruhe, Germany
NuPAGE® Bis-Tris Gradient Gel 4-12%	NuPAGE®, Invitrogene GmbH, Karlsruhe, Germany
SimplyBlue™ SafeStain Comassie blue G250 Stain	Invitrogene GmbH, Karlsruhe, Germany

Tris-Glycine SDS-Running-Buffer	NuPAGE [®] , Invitrogene GmbH, Karlsruhe, Germany
YM 10 & 30 ultrafiltration membrane	Amicon, Beverly, USA
Sartorius Sartocan [®] II mini module (0,1 m ² , 30 kD)	Sartorius AG, Goettingen, Germany

Table 7-5: Equipment

Peristaltic Pump Verder Peristaltic	2400Verder, Düsseldorf, Germany
Hanging Bar Spinner Flask	Bellco Glass, Vineland, USA
Magnetic Stirrer MR 3000	Heidolph, Nürnberg, Germany
Overhad Stirrer RW 18	IKA-Werke GmbH & Co. KG, Staufen, Germany
Vacuum Pump Type 400171	ILMAVAC GmbH, Ilmenau, Germany
Duran glass filter funnel porosity 3	Robu Glas, Hattert, Germany
Peristaltic Pump Minipulse TM 3	Gilson, Viller Le Bel, France
Variable wavelength monitor	Knauer, Berlin, Germany
Combination Lithium-Selective Epoxy Body Electrode (ISE)	Cole-Parmer TM , Vernon Hills, Illinois
Combination Bromide-Selective Epoxy Body Electrode (ISE)	Cole-Parmer TM , Vernon Hills, Illinois
Besta motor valve	Besta-Technik, Wilhelmsfeld, Germany
WTW pH340A Monitor	WTW, Weilheim, Germany
Data recording Software Multi/Achat II	WTW, Weilheim, Germany
French [®] Press equipped with a 40K high pressure cell	Thermo Spectronic, Cambridge, UK
Plate heat exchanger Cryostat Model K140S	Colora Messtechnik GmbH, Lorch, Germany
Lab Star laboratory bead mill, equipped with TriNEX TM agitator system	Netzsch, Selb, Germany
Sonopuls HD 60 ultrasound homogenizer,	BANDELIN electronic GmbH & Co. KG,

equipped with Microtipe probe	Berlin, Germany
Zetasizer 2000	Malvern Instruments, Herrenberg, Germany
Zetasizer 4	Malvern Instruments, Herrenberg, Germany
Viscometer Rotovisco CV 100, equipped with ME 30 measuring device	Thermo Haake, Hamburg, Germany
Electrophoresis cell Xcell SureLock™	Novex, San Diego, USA
Power supply EASE™ 500	Novex, San Diego, USA
Incubator shaker	Infors HT, Bottmingen, CH
Bioreactor Techfors	Infors HT, Bottmingen, CH
Orbital shaker Certomat® MO	Bbraun, Melsungen, Germany
UV-Visible Recording Spectrophotometer UV 160	Shimadzu, Duisburg, Germany
Overhad shaker REAX 2	Heidolph, Nürnberg, Germany
Agarose gel electrophoresis chamber MiniSub cell GT	Bio Rad; München, Germany
Power supply for agarose electrophoresis Pharmacia LKB GPS 200/400	Amersham Biosciences, Freiburg, Germany
Autoclave, Varioclav steam sterilisator	H+P Labortechnik, Oberschließheim, Germany
Centrifuge, Sorvall® RC-5B Refrigerated Superspeed centrifuge	Kendro Laboratory Products GmbH, Hanau, Germany
Amicon Micro Centrifuge MC 13	Millipore, Schwalbach, Germany

Table 7-6 Chromatography Systems and columns

ÄKTAexplorer™ 100	Amersham Biosciences, Freiburg, Germany
ÄKTAbasic™ 10XT upgraded to an explorer system	Amersham Biosciences, Freiburg, Germany
C 10/20	Amersham Biosciences, Freiburg, Germany
Column oven T1	Techlab GmbH, Erkerode, Germany
Degasing Unit X-Act	Chromatographie Handel Müller GmbH, Fridolfingen, Germany
Filter Sartobran P cartridge (0.45 + 0.2 µm pore size)	Sartorius AG, Göttingen, Germany
High pressure homogenizer Type 40MC4-15RBF1	Invensys APV, Unna, Germany
HR 10/10 Fast Desalting column	Amersham Biosciences, Freiburg, Germany
In house designed EBA column, 0.02 m i.d., fluid distribution by a conic inlet and glass beads (Nagel, 2000)	Institute of Enzyme Technology, Heinrich-Heine University Düsseldorf, Germany
Mono Q HR 5/5 prepacked anion exchange column	Amersham Biosciences, Freiburg, Germany
RP-HPLC-Column C18 YMC OdDMeSi, (B-564), 120 Å, 5 µm, 125 x 4 mm ID	Novo Nordisk Protein Purification Dpt., Gentofte, Denmark
Streamline 200	Amersham Biosciences, Freiburg, Germany
Streamline 25	Amersham Biosciences, Freiburg, Germany

Table 7-7 Microorganism

<i>Saccharomyces cerevisiae</i> MT888	Host strain of the MI3 production strain. Obtained from Novo Nordisk (Gentofte, Denmark)
<i>Escherichia coli</i> MC 1061	Host strain of hGH production (Jensen and Carlsen, 1989) obtained from Novo Nordisk (Gentofte, Denmark)
<i>Escherichia coli</i> JM101	DSMZ No. 3948 (Yannisch-Perron <i>et al.</i> , 1985)
<i>Escherichia coli</i> JM105	DSMZ No. 3949 (Yannisch-Perron <i>et al.</i> , 1985)
<i>Escherichia coli</i> JM109	DSMZ No. 3423 (Yannisch-Perron <i>et al.</i> , 1985)
<i>Escherichia coli</i> BL21	Commercial host strain purchased from Stratagene (La Jolla, USA)
<i>Escherichia coli</i> JM105 rec FDH	Rec. <i>Escherichia coli</i> producing FDH from <i>Candida bondinii</i> (Slusarczyk <i>et al.</i> , 2000)
<i>Escherichia coli</i> rec. L-Phe	Cells recieved from IBT 2 of the research center Jülich (Jülich, Germany)

7.1 PROTEIN ANALYSIS

7.1.1 TOTAL PROTEIN DETERMINATION (BRADFORD ASSAY)

For total protein determination the protein assay according to Bradford (Bradford, 1976) was used.

Chemicals:

Ethanol (100 %)	Fluka
H ₃ PO ₄ (85 %)	Merck
Chomassie brilliant blue G250	Fluka

Equipment:

UV-Visible Recording Spectrophotometer UV 160 Shimadzu

Buffer and solutes:

Bradford solution:

100 mg L⁻¹ Comassie brilliant blue G 250
50 ml Ethanol
100 ml H₃PO₄ (85 %)

The solution was adjusted to a final volume of 1 L using ultrapure water.

The solution was stirred over night and filtrated using a fluted filter and stored in a light protected bottle at room temperature.

Standard solutions for calibration:

Bovine Serum Albumin (BSA) solution in the concentrations: 10, 20, 30, 40, 50, 60, 70, 80, 90, 100 µg ml⁻¹ were used for calibration. If the concentration in the sample exceeded 60 µg ml⁻¹ further dilution were required.

Sample Preparation for Protein analysis

900 µl Bradford reagent + 100 µl sample were mixed in a cuvette.

The mixed solution was then incubated for at least 5 min in the dark before photometric determination at 595 nm.

From the extinction value, a blind value (Bradford reagent + water instead of the sample) was subtracted to account for the extinction of the reagent.

The concentration was then determined using an appropriate calibration curve with BSA as standard.

7.1.2 SDS PAGE

For SDS-Page analysis the Pre-Cast-Gel System (NuPAGE[®], Invitrogene GmbH, Karlsruhe, Germany) used according to the suppliers instructions for non reduced samples.

Buffer Gel combination used:

NuPAGE [®] Tris-glycine-Gel 10 %	Tris-Glycine SDS-Running-Buffer
NuPAGE [®] Bis-Tris Gradient Gel 4-12%	MES-Running Buffer

Mark12[™] Unstained Standard (Invitrogene GmbH, Karlsruhe, Germany) was used as molecular weight standard .

Staining: After Electrophoresis the gel was stained using SimplyBlue[™] SafeStain Comassie blue G250 Stain (Invitrogene).

7.1.3 RP-HPLC-ANALYSIS FOR INSULIN PRECURSOR MI3

Equipment:

HPLC Equipment:	AEKTAbasic [™] XT (Amersham, Bioscience, Freiburg, Germany)
Column oven:	Oven T-1 (TECHLAB GmbH, Erkerode, Germany)
Degasing Unit:	X-Act Degasing Unit (Chromatographie Handel Müller GmbH, Fridolfing, Germany)

RP-HPLC-Column: C18 YMC OdDMeSi, (B-564), 120 Å, 5 µm, 125x4mm ID
obtained from Novo Nordisk Protein purification Dpt.
(Gentofte Denmark)

Chemicals:

Na ₂ SO ₄ (anhydrous) p.a.	(Merck, Darmstadt, Germany)
H ₃ PO ₄ 85% p.a.	(Merck, Darmstadt, Germany)
Acetonitril HPLC gradient grade	(Roth, Karlsruhe, Germany)
Ethanolamine p.a.	(Merck, Darmstadt, Germany)
Human Insulin reference solution P45	(Novo Nordisk, Denmark)
Purified MI3 Precursor	(Novo Nordisk, Denmark)

Eluents:

Eluent A 2.8 % (w/w) Na₂SO₄
 0.4 % (w/w) H₃PO₄
 7.7 % (w/w) Acetonitril
 adjusted to pH 2.3 using Ethanolamine

Eluent B 42.8 % (w/w) Acetonitril

Both eluents was filtrated using a 0,45 µm Sartorius cellulose acetate filtration membrane.

Eluent conditions:

Flow: 1 ml min⁻¹
Temperature: 40 °C
Detection: 214 nm
Injection volume: 150 µl (Autosampler)
Initial Eluent conditions: 32 % B

Turbid samples were clarified by centrifugation 5 min (Amicon Micro Centrifuge MC 13).

Table 7-8: Gradient elution-protocol:

	target concentration Eluent B (%)	time to reach target concentration (min)	time to keep on target concentration (min)
Gradient Elution	50	20	0
Cleaning	100	0	2
Regeneration	32	0	20

Calibration:

For calibration a human insulin standard P45 in a concentration range of 0-150 mg L⁻¹ was used.

The retention time was determined using a purified MI3 Standard (Novo Nordisk, Denmark).

Unicorn[™] Regulation Method (Unicorn 3.21 Amersham bioscience)

Method Name: Insulin HPLC**Variables:**

```

Wavelength_1214          (nm)
Wavelength_2off
Wavelength_3off
UV_average_time          2.56  (sec)
Pressure limit            10    (MPa)
Flow_rate 1              (ml/min)
Injection volume          150   (µl)

```

Main method:

```

α Main
  0.00 Base Time (min)
α0.00 Block Start_Conditions
  Start_Conditions
  0.00 Base SameAsMain
  0.00 Wavelength (214)#Wavelength_1 {nm} (OFF)#Wavelength_2 {nm}
  (OFF)#Wavelength_3 {nm} 0.00 AveragingTimeUV (2.56)#UV_Averaging_Time {sec}
  0.00 Alarm_Pressure Enabled (11)#Pressure_Limit {MPa} 0.00 {MPa}
α 0.00 Block Initial_Eluent_Conditions
  Initial_Eluent_Conditions
  0.0 Base SameAsMain
0.00 PumpAInlet A2 0.00 PumpBInlet B2
0.00 ColumnPosition Position2
  0.00 OutletValve F4
  0.00 Flow (1.00)#Flow_rate {ml/min}
  0.00 Gradient (32)#Start_ConcB {%B} 0.00 {base} 0.00
  End_block

  0.00 End_block
α0.00 Block Autosampler_Injection
  Autosampler_Injection
  0.00 Base SameAsMain

```

```

0.00 Message (ID)#Sample_ID Noscreen
0.00 InjectionPartial (1)#Vial_Number (150)#Injection_Volume {ul}
Yes Air 0.00 QuantitationData (Sample)#Quantitation_Type
0.00 End_block
α0.00 Block Wash_Out_Unbound_Sample
Wash_Out_Unbound_Sample
0.00 Base SameAsMain

(0)#Wash_column_with End_block α 0.00 Block Gradient_Elution
Gradient_Elution
0.00 Base Time
α 0.00 Block Gradient_Segment_1
Gradient_Segment_1
0.00 Base SameAsMain
0.00 Gradient (50)#Target_ConcB_1
{%B}(20)#Length_of_gradient_1 {base}
20.00 End_block
0.06 End_block
α0.00 Block Clean_After_Gradient
Clean_After_Gradient
0.00 Base SameAsMain
0.00 Gradient (100)#Conc_of_eluent_B {%B} 0.00 {base}
(2)#Clean_with End_block
α0.00 Block Reequilibration
Reequilibration
0.00 Base SameAsMain
α 0.00 Block Initial_Eluent_Conditions
Initial_Eluent_Conditions
0.00 Base SameAsMain
0.00 PumpAInlet A2 0.00 PumpBINlet B2
0.00 ColumnPosition Position2
0.00 OutletValve F4
0.00 Flow (1.00)#Flow_rate {ml/min}
0.00 Gradient (32)#Start_ConcB {%B} 0.00 {base} 0.00
End_block
(20)#Reequilibrate_with End_block
0.00 End_method

```

7.1.4 FPLC-ANALYSIS FOR hGH

Chemicals and consumables:

Histidine	Merck
Urea	Merck
NaCl	Merck
HCl	Merck
Cellulose acetate filtration membrane (0,45 µm)	Sartorius

Equipment:

HPLC Equipment:	AEKTA ^{basic} ™XT upgraded to an explorer System . (Amersham, Bioscience, Freiburg, Germany)
Desalting column:	HR 10/10 Fast Desalting column (Amersham, Bioscience, Freiburg, Germany)
Ion exchange column:	Mono Q HR 5/5 (Amersham, Bioscience, Freiburg, Germany)

Eluents:

<u>Eluent A</u>	10 mM Histidine in 7 M Urea adjusted to pH 5.9-6.1 using HCl and 0.45µm filtrated (cellulose acetate, Sartorius, Göttingen, Germany)
<u>Eluent B</u>	Eluent A + 30 g L ⁻¹ NaCl adjusted to pH 5.9-6.1 using HCl 0.45µm filtrated (cellulose acetate, Sartorius, Göttingen, Germany)

The hGH-FPLC is a two step procedure including a fast desalting step and an anion exchange step. For that purpose an Äkta™ System was set up using two columns for the respective steps. The switch between these two steps was fully automated and controlled by the Unicorn 3.21 Software (Amersham Bioscience) using the flow path described below.

a STEP I (DESALTING)

Eluent conditions:

Flow:	1 ml min ⁻¹
Temperature:	Room temperature
Detection:	280 nm
Injection volume:	100 µl (Autosampler)
Initial Eluent conditions:	0 % B
Column:	HR 10/10 Fast desalting column

After Sample Injection the sample was eluted with 4 ml Eluent A. The eluted protein fraction were collected in a 2 ml sample loop (at the injection valve) during desalting using the flow path shown in Fig. 7-1.

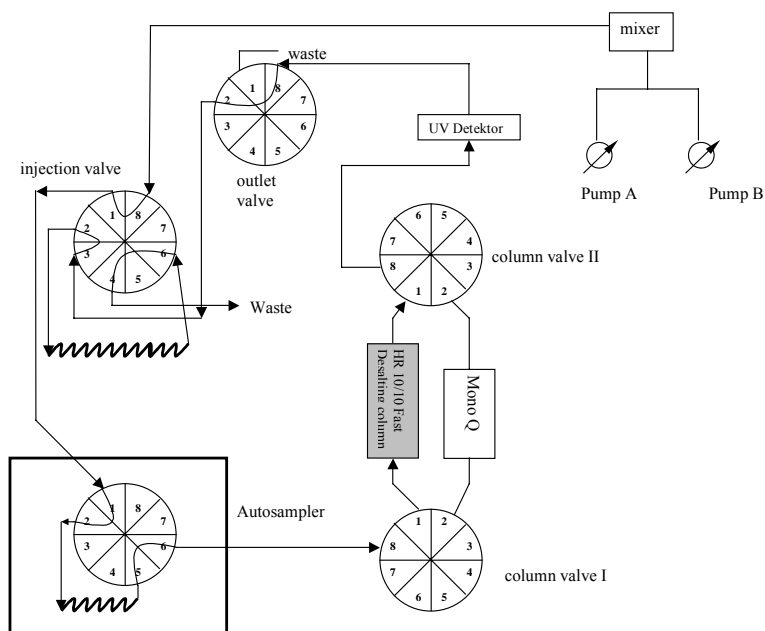


Fig. 7-1: Äkta™ flowpath for fast desalting step.

b STEP II (ANION EXCHANGE CHROMATOGRAPHY)

For the step II the collected sample was injected to the Mono Q column (following the flow path in Fig. 7-2). For elution the elution protocol shown in Table 7-8 was used.

Table 7-9: Gradient Elution- protocol:

	target concentration Eluent B (%)	time to reach target concentration (min)	time to keep on target concentration (min)
wash out unbound sample	0	0	3
Gradient Elution	27.3	22	0
cleaning Mono Q	100	0	5
Reequilibration Mono Q	0	0	8
Switch column position to HR 10/10 Fast desalting and cleaning HR 10/10	0	0	10

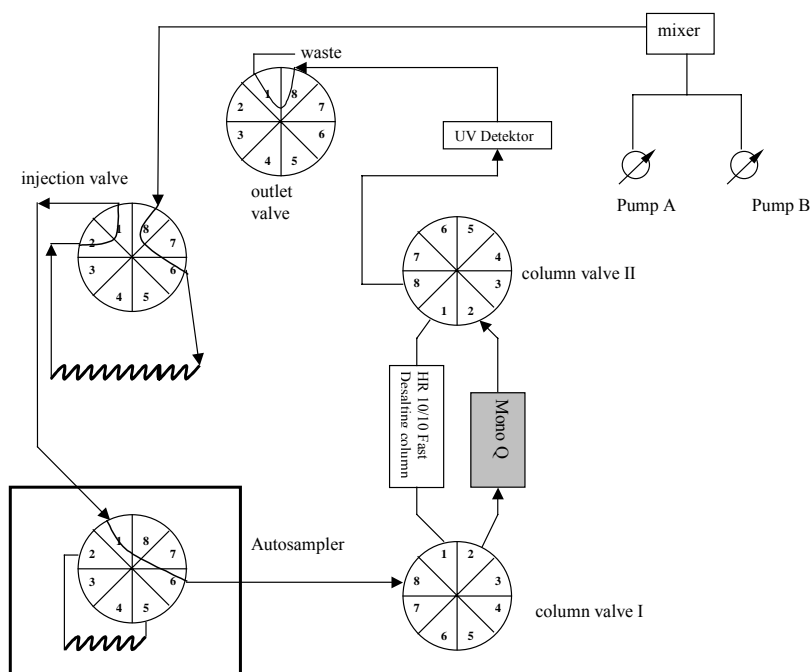


Fig. 7-2: Äkta™ flow path for fast Mono Q anion exchange step

Unicorn regulation method (Unicorn 3.21, Amersham Bioscience)

Method Name: hGH FPLC**Variables:**

```

Wavelength_1      280    (nm)
Wavelength_2      off
Wavelength_3      off
UV_average_time   2.56   (sec)
Pressure limit    10     (MPa)
Flow_rate         1      (ml/min)
Injection volume  100    (µl)

```

Main method:**α Main**

```

0.00 Base Time
α 0.00 Block Start_Conditions
    Start_Conditions
    0.00 Base SameAsMain
0.00 InjectionValve Load 0.00 PumpAInlet A2
    0.00 PumpBInlet B2
    0.00 ColumnPosition Position7
    0.00 OutletValve WasteF1
    0.00 Alarm_Pressure Enabled 1.2 {MPa} 0.00 {MPa}
    0.00 Wavelength (280)#Wavelength_1 {nm} (OFF)#Wavelength_2 {nm}
    (OFF)#Wavelength_3 {nm} 0.00 AveragingTimeUV
    (2.56)#UV_Averaging_Time {sec}
    0.00 Alarm_Pressure Enabled (4.00)#Pressure_Limit {MPa} 0.00
    {MPa}
α 0.00 Block Initial_Eluent_Conditions
    Initial_Eluent_Conditions
    0.00 Base SameAsMain
    0.00 Flow (1.00)#Flow_rate {ml/min}
    0.00 Gradient (0)#Start_ConcB {%B} 0.00 {base}
    0.00 End_block
    0.00 ColumnPosition Position7
    0.00 InjectionValve Load
    0.00 OutletValve FracF2
    0.00 End_block
α 0.00 Block Column_Equilibration
    Column_Equilibration
    0.00 Base SameAsMain (1)#Equilibrate_with AutoZeroUV
    1.00 End_block
α 0.00 Block Autosampler_Injection
    Autosampler_Injection
    0.00 Base SameAsMain
    0.00 Message (ID)#Sample_ID Noscreen
    0.00 InjectionPartial (1)#Vial_Number (100)#Injection_Volume
    {ul} Yes Air 0.00 QuantitationData (Sample)#Quantitation_Type
    0.00 End_block
α 0.00 Block Wash_Out_Unbound_Sample
    Wash_Out_Unbound_Sample
    0.00 Base SameAsMain (4.0)#Wash_column_with End_block α 0.00
Block switsch_to_Mono_Q
    switsch_to_Mono_Q
    0.00 Base SameAsMain
    0.00 Alarm_Pressure Enabled 5.00 {MPa} 0.00 {MPa}

```

```

0.00 InjectionValve Inject
0.00 ColumnPosition Position8
0.00 OutletValve WasteF1
0.00 End_block
α0.00 Block Gradient_Elution
Gradient_Elution
0.00 Base Time
α      0.00 Block Gradient_Segment_0
      Gradient_Segment_0
      0.00 Base SameAsMain
      0.00 Gradient 0 {%B} 0 {base}
      3 End_block
α      0.00 Block Gradient_Segment_1
      Gradient_Segment_1
      0.00 Base SameAsMain
      0.00 Gradient (13.7)#Target_ConcB_1 {%B}
      (11.1)#Length_of_gradient_1 {base} 11.10 End_block
α      0.02 Block Gradient_Segment_2
      Gradient_Segment_2
      0.00 Base SameAsMain
      0.00 Gradient (27.3)#Target_ConcB_2 {%B}
      (11)#Length_of_gradient_2 {base} 11 End_block
α      0.04 Block Gradient_Segment_3
      Gradient_Segment_3
      0.00 Base SameAsMain
      0.00 Gradient (100)#Target_ConcB_3 {%B}
      (0.00)#Length_of_gradient_3 {base} 5 End_block
α      0.06 Block Gradient_Segment_4
      Gradient_Segment_4
      0.00 Base SameAsMain
      0.00 Gradient 0.00 {%B} 0.00 {base}
      8 End_block
0.06 End_block
α0.00 Block Reequilibration
Reequilibration
0.00 Base SameAsMain
0.00 InjectionValve Load
0.00 ColumnPosition Position7
0.00 OutletValve FracF2
0.00 Alarm_Pressure Enabled 1 {MPa} 0.00 {MPa} 0.00 Gradient
0.00 {%B} 0.00 {base}
α      0.00 Block Initial_Eluent_Conditions
      Initial_Eluent_Conditions
      0.00 Base SameAsMain
      0.00 Flow (1.00)#Flow_rate {ml/min}
      0.00 Gradient (0)#Start_ConcB {%B} 0.00 {base}
      0.00 End_block

(10)#Reequilibrate_with End_block
0.06 End_method

```

7.2 PROTEIN ADSORPTION

7.2.1 FINITE BATH UPTAKE EXPERIMENTS

Chemicals and consumables:

Na ₂ HPO ₄	Merck
citric acid	Merck
Tris-(hydroxymethyl)-aminomethan	Roth
NaOH	Merck
NaCL	Merck
HCl	Merck

Adsorbent resins:

Streamline[™] SP
Streamline[™] DEAE
Streamline[™] Q XL
Zirconia S
Zirconia CM
S Sepharose[™] BB
Q Sepharose[™] BB
Streamline[™] Heparin
Streamline[™] Phenyl

Equipment:

Glass filter funnel Por. 3	Robu Glas
Vakuum Pump	ILMAVAC
Orbital shaker Certomat® MO	BBraun
Hanging Bar Spinner Flask	Bellco Glass
Magnetic stirrer MR 3000	Heidolph

Buffer

Buffer 1: pH range 2.6-7.6

30 mM Na₂HPO₄/citric acid conductivity adjusted using solid NaCl.

Buffer 2: pH range 7-9

50 mM Tris/HCl pH conductivity adjusted with solid NaCl

a GENERAL PROCEDURE**Preparation of the adsorbent matrix:**

The required matrix was placed on a filter funnel and washed three times with equilibration buffer (the equilibration buffer was chosen from buffer 1 or 2 and adjusted to the required pH and conductivity). The matrix was filtrated – low pressure conditions – until no further buffer could be removed by filtration.

Preparation of the feedstock:

The feedstock (culture supernatant, clarified homogenate) was adjusted to the required pH by using NaOH 1M or 1M NaOH and conductivity by dilution or adding NaCl. After pH and conductivity adjustment a sample is removed to determine the initial product concentration.

b ADSORPTION KINETICS MI3 PRECURSOR

To determine the adsorption kinetic 50 ml of the feedstock was placed in hanging bar spinner flask (Bellco Glass, Vineland, USA) and was stirred using a magnetic stirrer. 0.1 g (ww) adsorbent was added to the feedstock

To determine the adsorption kinetic at various times (t = 0, 5, 10, 15, 30, 45, 60, 90, 120, 180, 240 min, 15 h) after the adsorbent was added to the solution, a 300 µl sample was taken and the product concentration was determined. The product concentration in the stationary phase was calculated from the decreasing concentration in the liquid phase.

The initial (C_0) and the product concentration at a certain time (C_t) was determined and the capacity (Q) was calculated using Eq. 7-1

$$Q = \frac{V_l(C_0 - C_t)}{V_s}$$

Eq. 7-1

C_0 :	Initial concentration
Q :	Capacity at the time t
V_l :	Volume liquid (feedstock)
V_s :	Volume solid (adsorbent)

For analysis Q_t is plotted versus the time.

c EQUILIBRIUM ISOTHERM

To obtain the Equilibrium Isotherm different adsorbent-feedstock ratios were needed to adjust different equilibrium concentration. This was done by varying the amount of the solid phase (adsorbent) at a constant volume of feedstock.

MI3 Precursor:

500 ml feedstock was placed in a 2 L shake flask and at each preparation a certain amount of adsorbent was added using a 1:5 (weight/volume slurry). The following amounts of adsorbent were investigated: 30, 50, 100, 150, 200, 300, 400, 500, and 1000 μg . Due to the limited product titer and comparably high capacities it was necessary to use rather large amount of feedstock in combination with low amounts of adsorbent.

hGH Precursor:

10 ml feedstock was placed in a 25 ml shake flask and at each preparation a certain amount of adsorbent was added. The following amounts of adsorbent were used: 100, 200, 300, 400, 600, 700, 1000, 1500, 2000 mg.

Each preparation was incubated for 7 h on a orbital shaker (Certomat® MO BBraun, Melsungen, Germany). After incubation the liquid phase was analysed for product concentration (C_{eq}).

To analyse the data equilibrium capacity (Q_{eq}) obtained from Eq. 7-1 was plotted versus the equilibrium concentration in the liquid phase C_{eq} . The respective equilibrium isotherms were fitted using either to the Langmuir model Eq. 6-2 or linear isotherm.

Langmuir Isotherm

$$Q_{eq} = \frac{Q_{max} \cdot k_a \cdot C_{eq}}{1 + k_a \cdot C_{eq}} \quad \text{Eq. 7-2}$$

Linear Isotherm

$$Q = K \cdot C_{eq} \quad \text{Eq. 7-3}$$

Q_{eq} :	Equilibrium capacity
Q_{max} :	Maximum capacity
k_a :	Langmuir constant
C_{eq} :	Equilibrium concentration

d INITIAL ADSORBENT SCREENING

The experimental procedure for initial adsorbent screening is analog to that for the determination of the equilibrium isotherm, with the difference that only one adsorbent/feedstock ratio was used (in this case 1 g adsorbent an 10 ml feedstock). This experiment was also used to define optimized adsorption conditions using various pH, conductivities or adding various salts (HIC).

The respective capacities were calculated using Eq. 7-1.

The adsorbent feedstock ratio used depends on the expected capacity and the product concentration in the feedstock. In case of total protein adsorption, or the absence of detectable differences in the liquid phase concentration a change in the feedstock/adsorbent ratio was carried out.

7.2.2 BREAKTHROUGH ANALYSIS

Equipment:

ÄKTAexplorer™ 100	Amersham Bioscience
Packed bed column C10/20	Amersham Bioscience
Vakuum Pump	ILMAVAC

Chemicals and consumables:

see Finite bath uptake experiments

additionally for larger scale filtration of the feedstock

Peristaltic Pump Verder Peristaltic 2400	Verder, Düsseldorf, Germany
--	-----------------------------

Filter Sartobran P cartridge (0.45 + 0.2 µm pore size)	Sartorius
--	-----------

Adsorbents:

Streamline™ Q XL, SP, DEAE	Amersham Bioscience
Zirconia S	Biosepra

Feedstock preparation:

The feedstock (culture supernatant for the MI3 Precursor and clarified homogenate for the hGH precursor) was adjusted to the required pH using 1 M NaOH or HCl and conductivity by dilution or adding solid NaCl. Before application to the column the feedstock was 0.45 µm filtrated using a dead end cellulose acetate membrane filter (Sartorius) for smaller volumes ($V < 1$ L) and a filter cartridge Sartobran P (Sartorius) for larger volumes .

Column preparation:

The column C 10/20 was packed to a bed height of 5 cm for the MI3 purification protocol and 15 cm for protocols applied for hGH purification. After column packing the column was equilibrated for a minimum of 10 CV using equilibration buffer (buffer 1 or 2 at the same pH and conductivity as the feedstock).

Breakthrough analysis:

All breakthrough experiments were performed in an ÄKTAexplorer 100 System using the method described in Fig. 7-3.

The application volume depended on the capacity. To obtain a complete breakthrough 5 times of the isothermal binding capacity of the adsorbent (obtained from finite bath experiments) in the column were generally applied. Experiments was carried out at various linear velocities ($80 - 300 \text{ cm h}^{-1}$). The flow through was fractionated collecting a fraction volume of 50 ml for MI3 breakthrough analysis and 4 ml for hGH breakthrough. The fractions were analyzed for product concentration as described in chapter 7.1.3 and 7.1.4.

The normalized effluent concentration (X) ($X = C_{\text{eff}}/C_0$, C_{eff} : effluent concentration, C_0 : initial concentration) was plotted versus the normalized throughput (T) ($T = (V_{\text{eff}} C_0)/Q_{\text{eq}} V_s$, V_{eff} : effluent volume, V_s : Volume of the adsorbent) in order to determine the loading capacity. The equilibrium capacity of the stationary phase was determined by integration of the breakthrough curve as described by Yamamoto and Sano (Yamamoto and Sano, 1992).

Fig. 7-3: Unicorn Method breakthrough analysis

Method: DBK

Main method:

```

----- Block : Main -----
0.00      Base CV, (7.85)#Column {ml}, Any
0.00      Block START_CONDITIONS
0.00      Block COLUMN_EQUILIBRATION
0.00      Block FT_Fractionaton
0.1       Block LOAD_SAMPLE_WITH_SYSTEMPUMP

0.10      Block WASH_OUT_UNBOUND_SAMPLE
0.10      Block ELUATE_FRACTIONATION
0.10      Block GRADIENT_ELUTION
0.10      Block cleaning
0.10      Block Reequillibration
0.10      End_method

```

Blocks:

```

----- Block : FT_Fractionaton ----
0.00      Base SameAsMain
0.00      OutletValve F1
0.00      FractionCollector 18 {ml}
0.00      End_block
----- Block : Flow_trough_fractionation -----
0.00      Base SameAsMain
0.00      End_block

```

```
----- Block : START_CONDITIONS -----
0.00      Base SameAsMain
0.00      ColumnPosition (Position2)#Column_position
0.00      Wavelength (280)#Wavelength_1 {nm}, (214)#Wavelength_2 {nm},
(0)#Wavelength_3 {nm}
0.00      AveragingTime (5.12)#UV_Averaging_time {sec}
0.00      Alarm_Pressure Enabled, (1)#Pressure_limit {MPa}, 0.00 {MPa}
0.00      Block INITIAL_ELUENT_CONDITIONS
0.00      AutoZeroUV
0.00      End_block
----- Block : INITIAL_ELUENT_CONDITIONS -----
0.00      Base Time
0.00      MethodBase GradientPump
0.00      BufferValveA1 (A11)#Eluent_A_Inlet
0.00      Gradient (0.00)#Start_ConcB {%B}, 0.00 {base}
0.00      Flow (4)#Flow_Rate {ml/min}
0.10      End_block
----- Block : COLUMN_EQUILIBRATION -----
0.00      Base SameAsMain
0.00      Block SYSTEM_VOLUME_COMPENSATION
#Equilibrate_with AutoZeroUV
5.00      End_block
----- Block : SYSTEM_VOLUME_COMPENSATION -----0.00      Base Volume
8          End_block
----- Block : LOAD_SAMPLE_WITH_SYSTEMPUMP -----0.00      Base Volume
0.00      MethodBase GradientPump
0.00      Gradient 0.00 {%B}, 0.00 {base}
0.00      BufferValveA1 (A18)#Sample_inlet
0.00      InjectionMark
0.00      Flow (1)#Injection_flow_rate {ml/min}
#Volume_of_sample Block COMPLETE_SAMPLE_LOADING 1150.00      End_block
----- Block : COMPLETE_SAMPLE_LOADING -----
0.00      Base Volume
0.00      Block INITIAL_ELUENT_CONDITIONS
0.00      Gradient 0.00 {%B}, 0.00 {base}
12       Block INITIAL_ELUENT_CONDITIONS
12       End_block
----- Block : WASH_OUT_UNBOUND_SAMPLE -----0.00      Base SameAsMain
0.00      FractionationStop
0.00      Flow 4 {ml/min}
0.00      OutletValve F3
#Wash_column_with End_block
----- Block : cleaning -----
0.00      Base SameAsMain
0          Flow 2 {ml/min}
0          Gradient 0.00 {%B}, 0.00 {base}
0          FractionationStop
0          BufferValveA1 A12
0          OutletValve F1
20       End_block
----- Block : Reequillibration -----
0.00      Base SameAsMain
0.00      BufferValveA1 A11
0.00      Flow 4 {ml/min}
20       End_block
```

7.2.3 MODELING OF BREAKTHROUGH CURVES IN PACKED BEDS

Experimental data obtained from breakthrough analysis were fitted using models commonly used for description of packed bed chromatography performance. For data fit the solver software of Microsoft Excel was used. The models are based on different transport limitations. The pore diffusion model (Eq. 7-4) (Hall *et al.*, 1966) describes the diffusion within the particle pores as the dominant transport mechanism.

$$X = 1 - \left(\frac{2.39 - N_p (T - 1)}{3.59} \right)^2$$

$$N_p = \frac{15 (1 - \epsilon) D_e L}{r_p^2 u}$$

Eq. 7-4

with

$$T = \frac{C_0}{Q_{eq}} \cdot \frac{U}{L} \cdot (t - t_0)$$

- C_0 : initial concentration
- L : bed length
- Q_{eq} : equilibrium capacity
- U : velocity
- X : normalized effluent concentration
- t : time
- D_e : effective diffusivity

Solid diffusion Model after Hall et al (Hall *et al.*, 1966) :

The model after hall et al describes the protein transport within the particle based on surface diffusion the loading gradient is the major driving force.

$$X = 1 - 0.078(2.39 - N_p(T - 1))^2$$

$$T = \frac{(Ft - \epsilon V_s)C_0}{Q(C_0)V_s} \quad \text{Eq.}$$

$$7.5 N_p = \frac{15D_p L(1 - \epsilon)}{Ur_p^2}$$

r_p : particle radius (m)

ϵ : void fraction

F : volumetric flow rate (m^3s^{-1})

Pore and film transport after Hall et al (Hall *et al.*, 1966):

The model of Hall et al. consists of two different transport mechanisms:

external transport (Film Diffusion Model)

internal transport (Pore Diffusion Model)

$$T = 1 + \left(\frac{1}{N_p} + \frac{1}{N_f} \right) \left(\frac{\Phi(X) + \frac{N_p}{N_f} (LN(X+1))}{\frac{N_p}{N_f} + 1} \right)$$

$$\Phi(X) \cong 2.39 - 3.59\sqrt{1-X}$$

$$N_p = \frac{15 D_p L (1 - \varepsilon)}{U r_p^2} \quad \text{Eq. 7-6}$$

$$N_f = \frac{3 k_f L (1 - \varepsilon)}{r_p U}$$

$$T = \frac{(Ft - \varepsilon V_s) C_0}{Q(C_0) V_s}$$

This model employs two variables namely the pore diffusion coefficient D_p and the liquid side transport coefficient k_f . are in order to fit the experimental data:

The pore diffusion coefficient was determined from experimental breakthrough data obtained in packed beds . k_f was estimated using correlations, e.g. after Foo and Rice (Skidmore *et al.*, 1990) (Eq. 7) in packed beds or Nelson and Galloway [(Nelson and Galloway, 1975) (Eq. 8) in expanded beds.

Correlation after Foo and Rice

$$k_f = \frac{D}{d_p} \left(2 + 1.45 Re_p^{\frac{1}{2}} Sc^{\frac{1}{3}} \right) \quad \text{Eq. 7-7}$$

Correlation after Nelson and Galloway

$$k_f = \frac{D}{d_p} \left[\frac{2\zeta + \left\{ \frac{2\zeta^2 \cdot (1-\varepsilon)^{\frac{1}{3}}}{[1-(1-\varepsilon)^{\frac{1}{3}}]^2} - 2 \right\} \cdot \tanh(\zeta)}{\frac{\zeta}{1-(1-\varepsilon)^{\frac{1}{3}}} - \tanh(\zeta)} \right]$$

Eq. 7-8

with

$$\zeta = \left[\frac{1}{(1-\varepsilon)^{\frac{1}{3}}} - 1 \right] \frac{\gamma}{2} \text{Re}_p^{\frac{1}{2}} \text{Sc}^{\frac{1}{3}}$$

with $\gamma = 0.6$ for $0.01 < \text{Re}_p < 100$

Solid and pore diffusion after Yoshida et al. (1984)

The Model after Yoshida et al describes breakthrough curves including solid diffusion and pore diffusion.

This Model uses a segment wise description of the breakthrough curve as described in Eq. 8

$$\text{if } \frac{N_f}{N_s} > 1$$

$$\text{for } (T-1) \cdot N_f \leq 1 - \frac{N_f}{N_s} + \frac{N_s}{N_f} - \ln\left(\frac{N_s}{N_f} - 1\right)$$

$$\frac{C}{C_0} = \exp((T-1) \cdot N_f - 1)$$

$$\text{for } (T-1) \cdot N_f \geq 1 - \frac{N_f}{N_s} + \frac{N_s}{N_f} - \ln\left(\frac{N_s}{N_f} - 1\right)$$

$$\frac{C}{C_0} = 1 + \frac{N_f}{N_f + N_s} \cdot \exp\left(\left[-(T-1) \cdot N_s + 1 - \ln\left(1 + \frac{N_f}{N_s}\right)\right] \frac{N_s}{N_f}\right)$$

$$\text{if } \frac{N_f}{N_s} < 1$$

$$\text{for } (T-1) \cdot N_f \leq 1 - \frac{N_f}{N_s} + \frac{N_s}{N_f} - \ln\left(\frac{N_s}{N_f} - 1\right)$$

$$\frac{C}{C_0} = \exp\left[(T-1) \cdot N_f - 1 + \frac{N_f}{N_s} - \frac{N_s}{N_f}\right]$$

$$\text{for } (T-1) \cdot N_f \geq 1 - \frac{N_f}{N_s} + \frac{N_s}{N_f} - \ln\left(\frac{N_s}{N_f} - 1\right)$$

$$\frac{C}{C_0} = 1 + \frac{N_f}{N_f + N_s} \cdot \exp\left(\left[-(T-1) \cdot N_f + 1 - \frac{N_f}{N_s} + \frac{N_s}{N_f} - \ln\left(\frac{N_f + N_s}{N_f}\right)\right] \frac{N_s}{N_f}\right)$$

Eq. 7-9

7.3 BIOMASS-ADSORBENT INTERACTIONS

7.3.1 PULSE-RESPONSE EXPERIMENT

Equipment:

Column:	In house designed EBA column (0.02 i.d.) (Nagel, 2000)	
Pump:	Peristaltic pump Minipulse™ 3,	Gilson
Detector:	Variable wavelength monitor	Knauer

Buffer and biomass suspension:

Biomass suspension

- a) *Saccharomyces cerevisiae* whole cells: Cells suspended in equilibration buffer adjusted to an optical density of $0.5 < OD_{600} > 0.7$
- b) *Escherichia coli* homogenate: Cell debris suspended in equilibration buffer adjusted to an optical density of $0.3 < OD_{600} > 0.5$

Equilibration buffer: Buffer 1 or 2

Column preparation:

The home made EBA column was packed to a sedimented bed height of 10 cm and equilibrated with 10 CV equilibration buffer.

The respective adsorbent was fluidized in a lab scale EBA column until a stable bed expansion was achieved. Following this, a 45 ml pulse of diluted Biomass suspension (*Saccharomyces cerevisiae*, *Escherichia coli* (whole cells or homogenate) suspended in equilibration buffer was injected into the system and analyzed before and after the passage through the column (Fig. 7-4) as described elsewhere (Feuser *et al.*, 1999, Lin *et al.*, 2001).

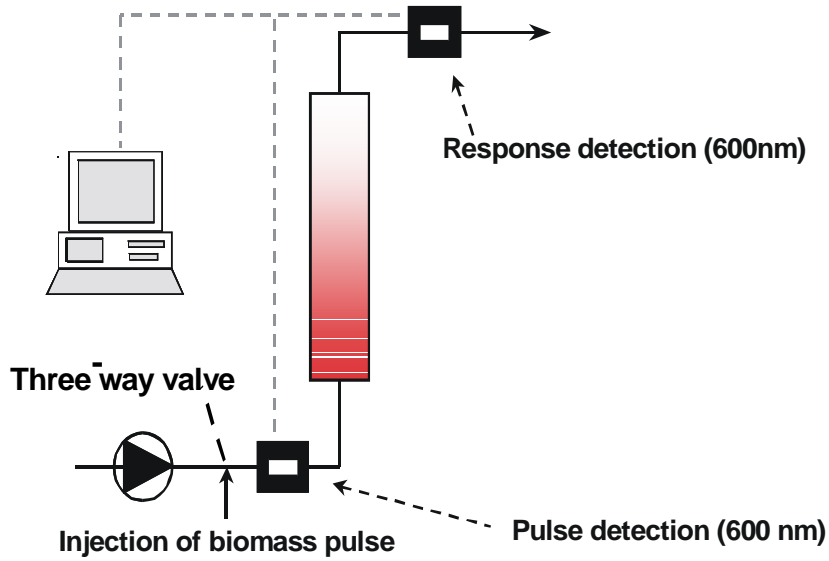


Fig. 7-4: Experimental setup of Pulse-Response experiment

The ratio of the pulse area before entering ($A_{input-pulse}$) and after passage through the column ($A_{pulsresponse}$) results in a cell transmission index (CTI) as described in Eq. 7-10.

$$CTI = \frac{A_{pulsresponse}}{A_{input-pulse}} \quad \text{Eq. 7-10}$$

7.3.2 RESIDENCE TIME DISTRIBUTION (RTD) (Fernández-Lahore *et al.*, 2001)

The fluidisation quality was characterized using an RTD analysis analogous to the RTD analysis in packed bed.

Equipment:

Column:	In house designed EBA column (Nagel, 2000)
Pump:	Peristaltic pump Minipulse™ 3 Gilson
Detector:	Combination Ion-Selective Epoxy Body Electrode (ISE), Cole-Parmer™ Lithium selective (for anion exchange chromatography) Bromide selective (for cation exchange chromatography)
Besta motor valve	Besta-Technik
WTW pH340A Monitor	WTW
Data recording Software Multi/Achat II,	WTW

Column conditions:

Column: home made EBA column 2 cm i.d.

Sedimented bed height: 10 cm

Linear velocity: 300 cm h⁻¹

Buffer and biomass suspension:

Equilibration buffer: Buffer 1 or 2

Tracer: 5 % LiCl (w/V) (for anion exchange chromatography)

5 % Na Br (w/V) (for cation exchange chromatography)

Biomass suspension:

Whole yeast cells or *Escherichia coli* homogenate diluted to a final biomass concentration of 10-15 % ww, pH adjusted using NaOH or HCl, conductivity adjusted by solid NaCl.

The experiments were carried out with 10 cm sedimented bed height and a linear fluid velocity of 300 cm h^{-1} . After equilibration of the bed with the appropriate mobile phase (culture broth or homogenate at the desired biomass concentration, pH and conductivity adjusted by, a $500 \mu\text{l}$ tracer pulse of 5 % (w/V) NaBr for cation exchange chromatography and LiCl (5% w/V) for anion exchange chromatography) was injected at the inlet of the column using a motor valve. The tracer concentration after the passage through the column was detected with a Bromide or Lithium selective electrode installed in a home designed flow cell and connected to a WTW pH340A Monitor (WTW, Weilheim, Germany). The Monitor was connected to a serial port of a PC for data recording using a commercial available software (Multi/Achat II, WTW, Weilheim, Germany). A small amount of tracer was added into the buffer for stable background (10^{-4} M). Due to an exponential correlation between the Electrode signal and the tracer concentration the calibration of the ISE showed to be very important. For calibration the stock solution was diluted as described in Table 7-10 using the desired mobile phase (buffer or biomass suspension).

Table 7-10

No.	Dilution factor	Final concentration	
		Br^- (mM)	Li^+ (mM)
1	20	12.1	59.0
2	50	4.85	23.6
3	100	2.43	11.8
4	200	1.21	5.90
5	500	0.49	2.36
Buffer		0.05	0.2

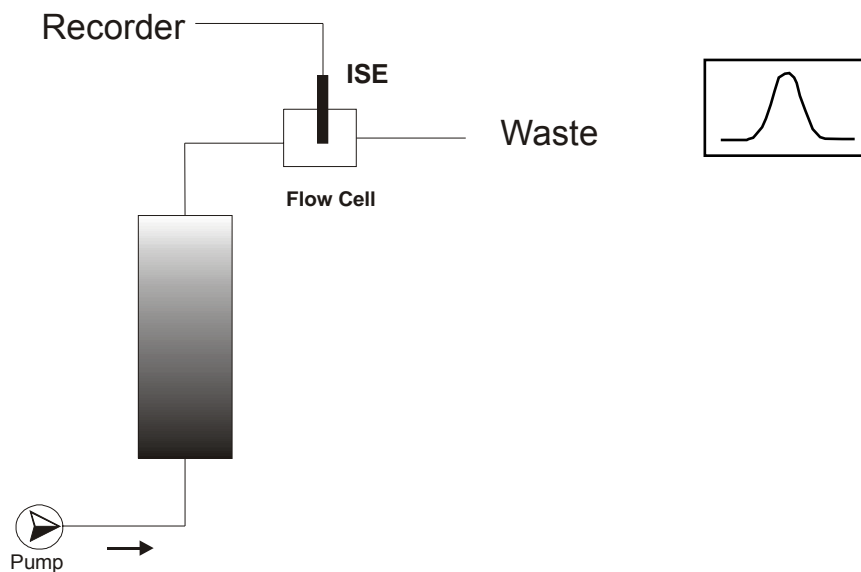


Fig. 7-5: Experimental set-up of RTD measurement.

After calibration of the ISE the respective response signal was translated into a RTD curve and analyzed by the PDE model described in Chapter 1.

7.4 PROTEIN ADSORPTION IN EXPANDED BED MODE

7.4.1 HUMAN INSULIN PRECURSOR MI 3

Equipment:

Column:	In house designed EBA column (Nagel, 2000) Streamline 25 (amersham biosciences, Freiburg, Germany) Streamline 200 (amersham biosciences, Freiburg, Germany)
Pump:	Peristaltic pump Minipulse™ 3, Gilson, Villiers Le Bel, France
Detector:	Knauer variable wavelength Monitor

Lab scale experiments were conducted in a 2 cm id. homemade column or in a Streamline 25 (amersham biosciences, Freiburg, Germany). A Streamline 200 column was used for the pilot scale experiments.

Saccharomyces cerevisiae culture suspension obtained from Novo Nordisk Insulin production Plant (Kalundborg, Denmark) was diluted 1:2 resulting in a biomass concentration of app. 15 % wet weight and adjusted to the required pH and conductivity for sample application. The desired resin is filled into the column to a sedimented bed height of 20 - 22 cm. The bed was equilibrated at 3 m/h with 35 mM Na₂HPO₄/citric acid buffer adjusted to the desired pH and conductivity until a stable fluidized bed was formed. After equilibration the sample was applied with a linear velocity of 200 cm h⁻¹. After application the column was washed in two steps: first equilibration buffer including 3 % glycerol in order to decrease washing volume. After removal of the cells a second washing step was implemented to remove the glycerol. The product was eluted using a pH step elution using Tris/ HCl buffer in ethanol solution. CIP of the stationary phase was performed with an 1 M NaCl solution in 1 M NaOH for 20 sedimented CV with a velocity of 125 cm h⁻¹. All operation were conducted in a upward directed flow keeping the bed expanded throughout the experiment.

7.5 CELL CULTIVATION

All media were sterilized in an autoclave. Temperature sensitive additives supplemented by sterile filtration.

7.5.1 SACCHAROMYCES CEREVISIAE

Shake flask cultures

Medium:

Yeast extract	1 %
Pepton	2 %
Glucose	2 % (a stock solution was autoclaved separately and was supplemented sterile after autoclaved)

Cultivation

100 medium in a 1 L shake flask

Temperature:	30°C
Shaking speed:	120 rpm
Incubation time:	65 h

7.5.2 E. COLI

a SHAKE FLASK CULTURE I (MC1061)

Medium:

The cultivation Media according to Novo Nordisk hGH production was used.

The medium was placed in a shake flask (10 % of max volume) and inoculated with 100 µl/100ml cryo culture.

Incubation conditions

Temperature	37°C
shaking speed:	120 rpm
Incubation time:	16 h

b SHAKE FLASK CULTURE II (ALL OTHER ESCHERICHIA COLI STRAINS)

Medium:

Yeast extract	25 g L ⁻¹
Pepton from Casein	12.5 g L ⁻¹
NaCl	5 g L ⁻¹

adjusted to pH 7.0 using 25 % NaOH

Incubation conditions

Temperature	37°C
Shaking speed:	120 rpm
Incubation time:	16 h

c CELL CULTIVATION PROTOCOL I (ESCHERICHIA COLI MC 1061)

For cell cultivation in a 25 L scale the cultivation protocol of Novo Nordisk hGH production was used.

d CELL CULTIVATION PROTOCOL II (ALL OTHER ESCHERICHIA COLI STRAINS)

preparatory culture: see shake flask culture II

Batch medium

Solution	Substance	final concentration (g L ⁻¹)	V _{stock solution} / ml (10 L) ⁻¹	Dilution	C _{stock solution} (g L ⁻¹)
Basic solution autoclaved in the Fermenter	NH ₄ Cl	0.2	1000	10	2
	(NH ₄) ₂ SO ₄	2	1000	10	20
	KH ₂ PO ₄	13	1000	10	130
	K ₂ HPO ₄	10	1000	10	100
	NaH ₂ PO ₄ -H ₂ O	6	1000	10	60
	yeast extract	3	1000	10	30
Glucose-sol autoclaved separately	Glucose-H ₂ O Batch	2	50	200	400
MgSO ₄ -sol. autoclaved separately	MgSO ₄ -7H ₂ O	1	50	200	200
Na ₂ -EDTA sterile filtrated	Na ₂ -EDTA-2H ₂ O (Titrplex III)	0.0093	2	5000	46.5
1. Vitamine sol. sterile filtrated	Riboflavin /(Vit B2)	0.0005	50	200	0.1
	Thiamin-HCl (B1)	0.05	50	200	10
	Nicotinsäure	0.0025	50	200	0.5
	Pyridoxin-HCl	0.0025	50	200	0.5
	Ca-Phanthotenat	0.0025	50	200	0.5
	Biotin	0.000005	50	200	0.001

	Folsäure	0.00001	50	200	0.002
	cCyanocobalamin (B12)	0.00005	50	200	0.01
2. trace elements	CaCl ₂ ·2H ₂ O	0.04	40	250	10
(in 5M HCl)	ZnSO ₄ ·7H ₂ O	0.002	40	250	0.5
Autosterile	CuCl ₂ ·2H ₂ O	0.001	40	250	0.25
	MnSO ₄ ·H ₂ O	0.01	40	250	2.5
	CoCl ₂ ·6H ₂ O	0.007	40	250	1.75
	H ₃ BO ₃	0.0005	40	250	0.125
	AlCl ₃ ·6H ₂ O	0.01	40	250	2.5
	Na ₂ MoO ₄ ·2H ₂ O	0.002	40	250	0.5
	FeSO ₄ ·7H ₂ O	0.04	40	250	10
Thiamin Sol.	Thiamin HCl	0.1	5	2000	200
sterile filtrated					
Ampicillin-Lsg	Ampicillin	0.1	5	2000	200
sterile filtrated					
IPTG-Lsg	IPTG	0.119145 (5mM)	10	1000	119.145
sterile filtrated					

Feed Medium

Solution	Substance	final concentration (g/L)	V _{stock solution} / ml/10L	Dilution
NH ₄ Cl	0.2	500	10	2
(NH ₄) ₂ SO ₄	2	500	10	20
KH ₂ PO ₄	13	500	10	130
K ₂ HPO ₄	10	500	10	100
NaH ₂ PO ₄ ·H ₂ O	6	500	10	60
Yeast extract sol.	18	240	20.8	375
Glucose-H ₂ O	600	3940	1.27	761.42
MgSO ₄ ·7H ₂ O	10	250	20	200
Riboflavin (Vit B2)	0.0005	25	200	0.1
Thiamin-HCl (B1)	0.05	25	200	10
Nicotinacid	0.0025	25	200	0.5
Pyridoxin-HCl	0.0025	25	200	0.5
Ca-Phanthotenat	0.0025	25	200	0.5
Biotin	0.000005	25	200	0.001
Folsäure	0.00001	25	200	0.002
cCyanocobalamin (B12)	0.00005	25	200	0.01
CaCl ₂ ·2H ₂ O	0.04	20	250	10
ZnSO ₄ ·7H ₂ O	0.002	20	250	0.5

CuCl ₂ ·2H ₂ O	0.001	20	250	0.25
MnSO ₄ ·H ₂ O	0.01	20	250	2.5
CoCl ₂ ·6H ₂ O	0.007	20	250	1.75
H ₃ BO ₃	0.0005	20	250	0.125
AlCl ₃ ·6H ₂ O	0.01	20	250	2.5
Na ₂ MoO ₄ ·2H ₂ O	0.002	20	250	0.5
FeSO ₄ ·7H ₂ O	0.04	20	250	10
Thiamin sol.	1	25	200	200
Thiamin HCl				

Cultivation control:

The feed has been started directly after inoculation. After a phase of maximal growth rate (μ_{\max}) when glucose in the fermenter was metabolised, growth rate was controlled by the glucose feed according to Eq. 7-11.

$$m_s(t) = \left(\frac{\mu}{Y_{X/S}} + m \right) X(t_0) V(t_0) \exp[\mu(t - t_0)] \quad \text{Eq. 7-11}$$

$$\mu < \mu_{\max}$$

The Feed and dissolved oxygen concentration (set point 30 %) was regulated using sequence in Fig. 7-6.

```

IF(pO2.v<pO2.sp){Stirrer.sp=Stirrer.sp (100+pO2.la (pO2.sp-
pO2.v)/10)/100}
IF(pO2.v>pO2.bv){Stirrer.sp=Stirrer.sp (100-pO2.la (pO2.v-
pO2.sp)/10)/100}
IF(Stirrer.sp<100){Stirrer.sp=100}
IF(Stirrer.sp>1250){Stirrer.sp=1250}
Flow.sp=50 Stirrer.sp/1250
Pressure.sp=1.4 Stirrer.sp/1250
IF(Pressure.sp>1.2){Pressure.sp=1.2}
DEF Neustart = 0.0
DEF S0 = 20.0
DEF SF = 600.0
DEF MY = 0.12
DEF Feed = S0/SF MY EXP(MY (SEQ_TIME+Neustart)/3600) 1000/60
Feed_Pump.sp = Feed 100/25
Feed_Pump.bv = Feed_Pump.sp

```

Fig. 7-6: Feed & dissolved oxygen control sequence (Iris)

7.6 CELL DISRUPTION

7.6.1 BEAD MILL

Bench scale

For bench scale experiments a Mixer Mill MM 200 (Retsch, Haan, Germany) was used.

Sample preparation:

1 g Glasbeads ($d=3$ mm) and 1ml Biomass suspension (40 ww in H₂O deionized) were placed in a 2ml Eppendorf cap and milled 10 min at maximum speed and maximum amplitude.

a BEAD MILL

Equipment: Laboratory bead mill Lab Star Netzsch (Selb, Germany) with TriNEX™ mill system

Cryostat Model K140S (Colora Messtechnik GmbH, Lorch, Germany)

The following conditions were used:

Glass beads: $d= 0.5$ mm 560ml in mill chamber

Biomass suspension: 40 % ww in H₂O 800 ml

Agitator speed: 2500 rpm

Flow product pump: 100 ml min⁻¹

Passages through the mill: 6-8

The Biomass suspension was pumped through the mill for different cycles.

7.6.2 FRENCH PRESS

Equipment: French®Press (Thermo Spectronic, Cambridge, UK) equipped with a 40K high pressure cell

Procedure: Confirming the instruction manual using a pre cooled (5°C) high pressure cell

Sample: 40 % ww Biomass suspension in H₂O

Conditions: different pressures and cycle

a HIGH PRESSURE HOMOGENISATION

Pilot scale cell disruption of *Escherichia coli* MC 1061 and JM 105 and rec. FDH

Equipment: APV-Gaulin High pressure homogenizer Type 40MC4-15RBF1

Plate heat exchanger

Cryostat Model K140S (Colora Messtechnik GmbH, Lorch, Germany)

Conditions: continues disruption with different passages through the homogenizer

Pressure and cycle 5 cycles at 500 bar
5 cycle at 1000 bar

Sample 40 % ww Biomass suspension 7 L

Flow Sample Pump 150 L h⁻¹

hGH Production Novo Nordisk

Batch Volume: 800 L

Biomass content: 40 % wet weight

Disruption strategy:

195 L were treated at 50 bar

195 L were treated at 700 bar

The two treated batches were collected with the untreated cell suspension and disrupted an additionally passage through the homogenizer at 700 bar.

7.6.3 ULTRASOUND

Equipment: Bandelin Sonopuls HD 60 (Bandelin GmbH, Berlin, D) equipped with a Mikrotip sonotrode

Conditions:

80 % sonication power

80 cycle duration

10 ml 40 % Biomass suspension in a 50 ml Falcon tube

The Samples are 3 times sonicated for 5 min interrupted by a cooling time of 5 min on ice.

7.7 AQUEOUS TWO PHASE SYSTEM (ATPS)

7.7.1 PREPARATION OF ATPS

The aqueous tow phase systems were produced per weight in a 10 g scale. Certain amounts of Polyethylenglycol (varying molecular weight) and the phosphate salt (K_2HPO_4 and KH_2PO_4 in different ratios) were placed in a graduated glass tube 5g *Escherichia coli* homogenate (bead mill (chapter 7.6.1)) were added and filled to 10g using demineralized water. The tubes were closed and incubated for a min. of two hours in an overhead shaker (Heidolph, Nürnberg, Germany) at room temperature. After mixing the phases were separated by centrifugation (4000 rpm, 15 min).

7.7.2 ULTRAFILTRATION OF ATPS TOP PHASES

a AMICON CELL

In initial ultrafiltraion experiments a stirred ultrafiltration cell (Amicon, Beverla, USA) equipped with membranes of different pore size (YM 10 (10 kD cut off) and YM 30 (30

kD cut off) was used. 10 ml of the ATPS top phase were placed in the stirred UF cell and were diafiltrated through the membrane using a nitrogen pressure of 4 bar. The volume passed through the membrane was supplemented by 25 mM Tris/HCL buffer pH 8,0. The experiment was stopped after 20 ml passed through the membrane. Retentate and filtrate were analyzed for hGH concentration and viscosity.

b CROSS FLOW FILTRATION

For cross flow filtration a Sartocoon[®] II mini module (Sartorius, Göttingen, Germany) 30 kD cut off polysulfon membrane was used. The retentate volume was kept constant at 600 ml by supplementing the filtrated volume by 25 mM Tris/HCL buffer pH 8,0. The trans membrane pressure was adjusted to a constant value of 1,5 bar by varying the cross flow velocity. Retentate and filtrate were analyzed for hGH concentration and viscosity.

7.8 PHYSICAL AND CHEMICAL PROPERTIES OF BIOMASS SUSPENSION

7.8.1 ZETA POTENTIAL

Charged particles were suspended at an appropriate concentration in buffers of various ionic strength. The appropriate concentration of biomass kept at the range of 0.0025 ~ 0.005% dry weight, corresponding to OD₆₀₀ at range of 0.05 ~ 0.1 (0.02% wet weight). The instrument used was a Zetasizer 2000 (Malvern Instruments, UK) with a quartz capillary as electrophoresis cell (50 mm long, cross section 5 mm by 2 mm). Zeta potentials were calculated from the electrophoretic mobility by the equation of Smoluchowski (Shaw, 1980). Measurements were carried out in triplicate and the mean value reported.

7.8.2 SIZE ANALYSIS

Photon Correlation Spectroscopy (PCS) was used for biomass particle size analysis by Malvern Zetasizer 4 (Malvern Instruments, UK).

For measurement the biomass particle are suspended in 100 mM Tris/HCl buffer pH 8 (adjusted to $\kappa = 10 \text{ mS cm}^{-1}$ using NaCl, 0.2 μm filtrated) in a appropriate concentration for the Zetasizer.

Measurements were performed at a detector angle of 90° in a double analysis as a average of 12 sub runs.

7.8.3 VISCOSITY

For dynamic viscosity measurement a Haake rotational viscometer (Rotovisco CV 100 (ME 30 measuring device) Haake, Karlsruhe, Germaany) was used.

Parameters:

t: 1min

T: 20°C

Rotation: 0-300 rpm in 300 steps

Evaluation: Linear Regression

7.9 DNA ANALYSIS

To investigate the DNA size distribution agarose-gel electrophoreses was used.

Gel: 1,5 % w/V agarose including ethidium bromide

Sample Präparation:

1. Precipitation

600 µl Homogenate

+ 100 µl 5M NaCl

+ 80 µl CTAB sol. (10 % Hexadecyltrimethylammoniumbromid (CTAB) in 0,7 % NaCl)

⇒ Incubate 10 min at 65°C

⇒ Centrifugation 5 min 13000 rpm

The supernatant was diluted in TE buffer (10 mM Tris/HCl, 1 mM EDTA, pH 8.0)

2. Gel Samples Preparation

45 µl diluted sample

+ 5 µl Sample buffer (25 % Bromphenol blue, 40 % Sucrose)

⇒ 5 or 10 µl are applied to the gel

⇒ Electrophoresis for 1,5 h at 60 V in Running Buffer (100 mM Tris, 50 mM glacial acetic acid, 1 mM EDTA.

The ethidium bromide stained DNA fragments are separated during electrophoresis and are visualized using UV light.

8 APENDIX

8.1 RTD ANALYSIS

1.1.1 EVALUATION OF RTD CURVE:

For evaluation the response signal has to be translated into a normalized residence time distribution function $E(\theta)$ and plotted versus the dimensionless time ($\theta=t*\tau^{-1}$) as described in textbooks (Levenspiel, 1972). Briefly the following calculations have to be performed:

1. The original data have to be plotted as tracer concentration in the effluent versus time
2. The area under the response pulse has to be determined (0^{th} moment; m_0) by integrating the curve. To avoid integration a simplified solution can be found by approximating the response curve as a series of rectangles, the area is summarized in order to find the total pulse area.

Eq. 8-1:
$$m_0 = \int_0^{\infty} C(t) dt \approx \sum_t C(t) \cdot \Delta t$$

3. $C(t)$ is the average tracer concentration between two measurements and Δt is the time difference between two concentration measurements
4. The mean residence time τ is calculated from the 1^{st} moment (m_1):

$$m_1 = \int_0^{\infty} C(t) \cdot t dt \approx \sum_t C(t) \cdot t \cdot \Delta t$$

Eq. 8-2:

$$\tau = \frac{m_1}{m_0}$$

5. The residence time distribution function $E(\theta)$ is calculated for the whole response curve and plotted versus the normalized time θ :

$$E(\theta) = \frac{C(t) \cdot \tau}{m_0}$$

Eq. 3:

$$\theta = \frac{t}{\tau}$$

8.1.2 TANKS IN SERIES MODEL

The number of theoretical plates can be calculated by a non-linear fit of the analytical solution of the tanks in series model to the experimental RTD curve see Eq. 8-3 or direct from the RTD curve using Eq. 8-4

. This model regards a column as a series of well mixed batch adsorption systems where the number of tanks N (or theoretical plates) Fig. 8-1 characterizes the amount of dispersion

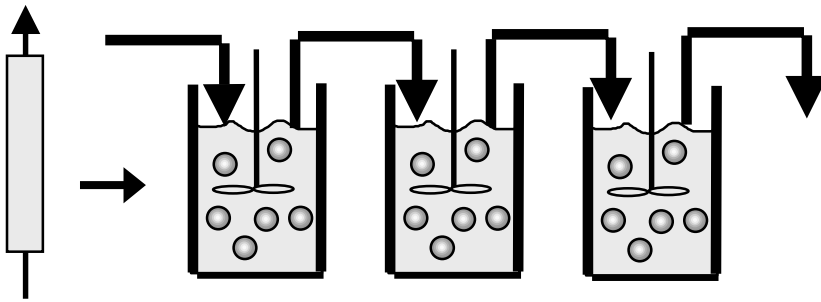


Fig. 8-1: Tanks in series model

$$E(\Theta) = \frac{N_p \cdot (N_p \cdot \Theta)^{N_p-1}}{(N_p - 1)!} \cdot \exp(-N_p \cdot \Theta) \quad \text{Eq. 8-3}$$

$$N_p = \frac{1}{\sigma_\Theta^2} \quad \text{Eq. 8-4}$$

8.1.3 MOMENTS OF RTD

$$m_k = \int_0^{\infty} t^k \cdot C(t) dt \approx \sum_t t^k \cdot C(t) \cdot \Delta t$$

m_k = kth moment of RTD

$$m_0 = A = \sum_t C(t) \cdot \Delta t$$

m_0 = 0th moment of RTD

$$m_1 = \sum_t C(t) \cdot t \cdot \Delta t$$

m_1 = 1st moment of RTD

$$m_2 = \sum_t C(t) \cdot t^2 \cdot \Delta t$$

m_2 = 2nd moment of RTD

$$\mu_k = \frac{m_k}{m_0}$$

μ_k = kth normalised moment

$$\tau = \mu_1$$

τ = mean residence time

$$\sigma^2 = \mu_2 - \mu_1^2 \quad \sigma_{\Theta}^2 = \frac{\sigma^2}{\tau^2}$$

The E-function can be calculated using equation Eq. 8-5

$$E(\Theta) = C(t) \cdot \tau / m_0$$

Eq. 8-5

with $\Theta = t / \tau$

8.2 MODELING OF BREAKTHROUGH CURVES

Expanded Bed Adsorption is performed by frontal application conditions and is primarily a residence time controlled process in the meaning that the residence time in the column ($\tau=L/U$) is usually shorter than the time needed to achieve equilibrium conditions. Similar to packed bed chromatography the process performance is characterized by the adsorption kinetics and thus the dynamic capacity (usually defined at 1-10 % breakthrough) determined by breakthrough analysis. By relating the dynamic capacity to the equilibrium capacity the sorption efficiency (E) can be defined as:

$$E = \frac{Q_{dyn.}}{Q_{eq.}}$$

To obtain an easier comparability between different process conditions, a normalization of the experimental data is necessary. In a normalized chart the dimensionless throughput (T) is plotted versus the dimensionless concentration (X) (see Eq. 8-6).

$$T = \frac{C_0}{Q_{eq.}} \cdot \frac{U}{L} \cdot (t - t_0) \quad \text{Eq. 8-6}$$

$$X = \frac{C}{C_0}$$

$Q_{eq.}$ = equilibrium capacity

C = concentration

C_0 = initial concentration

L = Column length

U = linear velocity

At defined conditions (pH, cond., viscosity, C_0) E is mainly a function of residence time depending on U and L. To obtain the optimized residence time and the optimized U/L ratio (in regard of high throughput and maximized $Q_{eq.}$ usage) breakthrough has to be measured under many different operation conditions. In order to minimize the

experimental effort for process optimization sufficient models, regarding different transport limitation mechanism for packed bed chromatography are available.

8.2.1 TRANSPORT MECHANISM & APPROPRIATED MODELS

a PORE DIFFUSION MODEL (EQ. 4):

The Pore diffusion Model describes the diffusion within the particle following the principle first move than bind.

$$X = 1 - \left(\frac{2.39 - N_p \cdot (T - 1)}{3.59} \right)^2 \quad \text{Eq. 8-7}$$

$$N_p = \frac{15 \cdot (1 - \varepsilon) \cdot D_e \cdot L}{r_p^2 \cdot u}$$

with

$$T = \frac{C_0}{Q_{eq}} \cdot \frac{U}{L} \cdot (t - t_0)$$

C_0 : initial concentration L : bed length

Q_{eq} : equilibrium capacity U : velocity

b SOLID DIFFUSION MODEL AFTER HALL ET AL (Hall *et al.*, 1966) :

The surface diffusion means, once a protein molecule is bound, it experiences the "draft" of the neighbor ligands and it is forced to "jump" to another binding place for that the loading gradient is the major driving force. It follows the rule first bind then move.

$$X = 1 - 0,078 \cdot (2,39 - N_p \cdot (T - 1))^2 \quad \text{Eq. 8-8}$$

$$T = \frac{(F \cdot t - \varepsilon \cdot V_s) \cdot C_0}{Q(C_0) \cdot V_s} \quad N_p = \frac{15 \cdot D_p \cdot L \cdot (1 - \varepsilon)}{U \cdot r_p^2}$$

r_p : particle radius (m)

ε : void fraction

F : volumetric flow rate (m³/s)

8.3 ELECTROSTATIC INTERACTIONS

Eq. 8-9

$$\varphi_{el} = \frac{\varepsilon_0 \varepsilon_r x d (\psi_d^2 + \psi_x^2)}{4(d+x)} \left\{ \frac{2\psi_d \psi_x}{\psi_d^2 + \psi_x^2} \ln \frac{[1 + \exp(-\kappa d)]}{[1 - \exp(-\kappa d)]} + \ln[1 - \exp(-2\kappa d)] \right\}$$

ψ_d	electrostatic surface potential of the adsorbent
ψ_x	electrostatic surface potential of the biomass particle
d	diameter of the adsorbent particle
x	diameter of the biomass particle
κ	reciprocal value of the Debye-Hückel-parameter

→ reciprocal value of the Debye-Hückel-parameter (Lagaly *et al.*, 1997).

$$\kappa^2 = \frac{2F^2}{\varepsilon_0 \varepsilon_r RT} \cdot I \quad \text{Eq. 8-10}$$

F Faraday constant $F = 9,6485 \cdot 10^4$ C/mol

R	gas constant R=8,31451 J/(K*mol)
T	absolute temperature [K] 25°C = 298 K
I	ionic strength

$$I = \frac{1}{2} \sum c_i \cdot z_i^2$$

c	concentration of ion I
z	value of ion I

⇒

$$\kappa^2 = \frac{2F^2}{\varepsilon_0 \varepsilon_r RT} \sum z_i \cdot c_{i,0}$$

for $|z_i^+| = |z_i^-| = z$ and $\sum c_{i,0} = 2 c_0$

$$\kappa^2 = \frac{2F^2}{\varepsilon_0 \varepsilon_r RT} z^2 \cdot c_0$$

for the solvent water (T=298 K and $\varepsilon_r=78,5$) follows (c_0 in mol/L)

$$\kappa = 32.87 \cdot 10^8 z \sqrt{c_0} \quad [\text{m}^{-1}]$$

8.4 PARTICLE SIZE DISTRIBUTION DATA

8.4.1 HOMOGENIZATION TECHNIQUE

Particle size distribution of Escherichia coli JM 101 cells and homogenates obtained by various cell disruption methods, using a 40 % ww suspension in desalted water.

Table 8-1: Peak analysis evaluated by the intensity

Sample	z-average	Mean	Width	Polydispersity
cells	1376,5	1496,4	1356,8	0.158
lab. Bead mill	1173,05	1282,6	1192,2	0.167
French Press	331	269	340,1	0.374
Ultrasound	230	394,4	505,5	0.349

Table 8-2: Raw data of the size distribution (intensity) whole cells and lab bead mill homogenate.

	cells		lab bead mill
Size(nm)	Intensity	Size(nm)	Intensity
227	0	184	0
263	0	215	0
305	0	250	0
354	0	291	0
410	0.1	339	0.1
476	0.4	394	0.4
552	1	459	1
640	2.3	535	2.3
742	4.4	623	4.4
861	7.3	725	7.3
998	10.6	845	10.6
1158	13.5	984	13.5
1342	14.8	1146	14.8
1557	14.2	1334	14.2
1806	11.9	1554	11.9
2094	8.6	1809	8.6
2429	5.5	2107	5.4
2817	3	2453	3
3267	1.4	2857	1.4
3789	0.6	3327	0.6
4394	0.2	3874	0.2
5096	0.1	4512	0.1
5911	0	5254	0
6855	0	6118	0

Table 8-3: : Raw data of the size distribution (intensity) French Press and ultrasound homogenate

French Press		Utrasound	
Size(nm)	Intensity	Size(nm)	Intensity
16	0	23	0
20	0	29	0
25	0	36	0
31	0	44	0
39	0.1	55	0.2
48	0.4	69	0.4
60	1.1	86	1.1
75	2.4	107	2.4
93	4.5	133	4.5
115	7.5	166	7.5
143	10.8	207	10.8
178	13.6	258	13.6
221	14.8	322	14.8
274	14.1	401	14.1
340	11.7	500	11.7
423	8.4	623	8.4
525	5.3	776	5.3
652	2.9	967	2.9
809	1.4	1206	1.4
1005	0.6	1503	0.6
1248	0.2	1873	0.2
1550	0.1	2334	0.1
1924	0	2909	0
2390	0	3626	0

8.4.2 HOMOGENIZATION CONDITIONS IN THE FRENCH PRESS

a OPERATION PRESSURE P = 300 BAR

Table 8-4: Peak analysis evaluated by the intensity

cycle	Mean	Width	z-average	Polydispersity
2	929.5	1408.1	700.7	0.550
4	522.7	785.1	514.7	0.523
6	396.9	546.8	323.4	0.422
8	356.7	490.3	290.6	0.437
10	362.2	498.75	295.5	0.44

Table 8-5: Raw data of the size distribution (intensity)

	2 cycle		4 cycle
Size(nm)	Intensity	Size(nm)	Intensity
24.70	0.00	16.00	0.00
27.00	0.00	18.20	0.00
32.50	0.00	20.90	0.00
35.40	0.00	23.50	0.00
42.90	0.00	27.30	0.00
46.40	0.00	30.40	0.00
56.50	0.00	35.70	0.00
60.90	0.00	39.30	0.00
74.50	0.20	46.60	0.20
79.90	0.20	50.80	0.20
98.20	0.40	60.90	0.40
104.70	0.40	65.70	0.40
129.50	1.10	79.60	1.10
137.30	1.10	84.90	1.10
170.80	2.40	104.00	2.40
180.10	2.40	109.80	2.40
225.10	4.60	135.90	4.60
236.10	4.60	142.00	4.60
296.80	7.60	177.50	7.60
309.60	7.60	183.60	7.60
391.40	10.90	231.90	10.90
406.00	10.90	237.30	10.90
516.00	13.70	303.00	13.60
532.40	13.70	306.80	13.60
680.30	14.90	395.80	14.90
698.10	14.90	396.70	14.90
896.90	14.10	512.90	14.10
915.50	14.10	517.10	14.10
1182.60	11.60	663.10	11.60
1200.50	11.60	675.50	11.60

1559.10	8.30	857.30	8.30
1574.20	8.30	882.50	8.30
2055.60	5.20	1108.40	5.20
2064.30	5.20	1153.00	5.20
2706.90	2.80	1433.00	2.80
2710.20	2.80	1506.30	2.80
3549.60	1.30	1852.70	1.30
3573.20	1.30	1967.90	1.30
4654.60	0.50	2395.30	0.60
4711.10	0.50	2570.90	0.60
6103.60	0.20	3096.80	0.20
6211.30	0.20	3358.70	0.20
8003.60	0.10	4003.70	0.10
8189.20	0.10	4388.00	0.10

Table 8-6: Raw data of the size distribution (intensity)

	6 cycle		8 cycle		10 cycle	
Size(nm)	Intensity	Size(nm)	Intensity	Size(nm)	Intensity	
17.20	0.00	14.70	0.00	14.80	0.00	
17.50	0.00	16.90	0.00	17.00	0.00	
21.90	0.00	18.80	0.00	18.90	0.00	
22.20	0.00	21.30	0.00	21.50	0.00	
27.90	0.00	24.00	0.00	24.20	0.00	
28.30	0.00	26.90	0.00	27.20	0.00	
35.50	0.00	30.70	0.00	31.00	0.00	
35.90	0.00	34.00	0.00	34.40	0.00	
45.20	0.20	39.30	0.20	39.70	0.20	
45.70	0.20	43.00	0.20	43.50	0.20	
57.60	0.40	50.30	0.40	50.80	0.40	
58.00	0.40	54.40	0.40	55.00	0.40	
73.40	1.10	64.40	1.10	65.10	1.10	
73.80	1.10	68.70	1.10	69.50	1.10	
93.60	2.40	82.30	2.40	83.30	2.40	
93.80	2.40	86.90	2.40	87.90	2.40	
119.20	4.60	105.30	4.60	106.70	4.60	
119.20	4.60	109.80	4.60	111.10	4.60	
151.60	7.60	134.70	7.60	136.60	7.60	
151.80	7.60	138.80	7.50	140.50	7.50	
192.60	10.90	172.40	10.90	175.00	10.90	
193.50	10.90	175.50	10.90	177.60	10.90	
244.90	13.60	220.50	13.60	224.00	13.60	
246.50	13.60	221.80	13.60	224.50	13.60	
311.30	14.90	280.40	14.90	283.90	14.90	
314.00	14.90	282.10	14.90	286.90	14.90	
395.70	14.10	354.40	14.10	358.90	14.10	
400.00	14.10	361.00	14.10	367.30	14.10	
503.00	11.60	448.00	11.70	453.70	11.70	

509.70	11.60	461.80	11.60	470.30	11.60
639.40	8.40	566.30	8.40	573.60	8.40
649.30	8.40	590.80	8.40	602.20	8.40
812.80	5.20	715.90	5.20	725.20	5.20
827.30	5.20	755.80	5.20	771.10	5.20
1033.20	2.90	904.90	2.90	916.90	2.90
1053.90	2.80	967.00	2.80	987.40	2.80
1313.40	1.40	1143.80	1.40	1159.10	1.40
1342.80	1.30	1237.10	1.30	1264.30	1.30
1669.60	0.60	1445.80	0.60	1465.50	0.60
1710.70	0.60	1582.70	0.60	1618.80	0.60
2122.30	0.20	1827.50	0.20	1852.70	0.20
2179.50	0.20	2024.80	0.20	2072.80	0.20
2697.80	0.10	2310.00	0.10	2342.30	0.10
2776.70	0.10	2590.40	0.10	2654.10	0.10

b OPERATION PRESSURE P = 482 BAR

Table 8-7: Peak analysis evaluated by the intensity

cycle	Mean	Width	z-average	Polydispersion
1	737.6	1132.1	551.2	0.549
2	468.2	682.6	374.0	0.497
4	308.0	413.2	254.4	0.399
6	268.1	344.2	225.6	0.358
8	259.7	332.4	218.3	0.338
10	247.65	307.8	212.5	0.338

Table 8-8: Raw data of the size distribution operation pressure P = 482 bar (intensity)

Size(nm)	1 cycle		2 cycle		4 cycle	
	Intensity	Size(nm)	Intensity	Size(nm)	Intensity	Size(nm)
18.70	0.00	15.50	0.00	14.60	0.00	
19.50	0.00	16.10	0.00	15.40	0.00	
24.80	0.00	20.20	0.00	18.50	0.00	
25.70	0.00	20.80	0.00	19.30	0.00	
32.90	0.00	26.30	0.00	23.50	0.00	
33.80	0.00	26.90	0.00	24.40	0.00	
43.50	0.00	34.10	0.00	29.70	0.00	
44.60	0.00	34.80	0.00	30.70	0.00	
57.70	0.20	44.40	0.20	37.60	0.20	
58.70	0.20	45.00	0.20	38.70	0.20	
76.40	0.40	57.70	0.40	47.50	0.40	
77.40	0.40	58.10	0.40	48.70	0.40	
101.20	1.10	75.10	1.10	60.10	1.10	
102.10	1.10	75.10	1.10	61.30	1.10	

134.10	2.40	97.10	2.40	76.10	2.40
134.50	2.40	97.60	2.40	77.20	2.40
177.30	4.60	125.50	4.60	96.30	4.60
177.70	4.60	127.00	4.60	97.30	4.60
233.70	7.60	162.20	7.60	121.90	7.50
235.50	7.60	165.10	7.60	122.50	7.50
308.00	10.90	209.60	10.90	154.30	10.90
312.00	10.90	214.70	10.90	154.30	10.90
406.00	13.70	270.90	13.60	194.40	13.60
413.40	13.70	279.20	13.60	195.20	13.60
535.20	14.90	350.10	14.90	244.80	14.90
547.70	14.90	363.10	14.90	247.00	14.90
705.40	14.10	452.50	14.10	308.30	14.10
725.60	14.10	472.20	14.10	312.60	14.10
929.70	11.60	584.80	11.60	388.30	11.70
961.40	11.60	614.10	11.60	395.60	11.60
1225.50	8.30	755.90	8.30	489.10	8.40
1273.90	8.30	798.60	8.30	500.70	8.40
1615.30	5.20	976.90	5.20	616.00	5.20
1687.80	5.20	1038.50	5.20	633.60	5.20
2129.00	2.80	1262.60	2.80	775.90	2.90
2236.20	2.80	1350.50	2.80	801.80	2.90
2806.30	1.30	1631.80	1.30	977.20	1.40
2962.90	1.30	1756.30	1.30	1014.70	1.40
3698.90	0.50	2109.10	0.60	1230.80	0.60
3925.70	0.50	2284.00	0.60	1284.00	0.60
4875.40	0.20	2725.90	0.20	1550.20	0.20
5201.30	0.20	2970.10	0.20	1625.00	0.20
6426.10	0.10	3523.10	0.10	1952.50	0.10
6891.40	0.10	3862.50	0.10	2056.40	0.10
8470.20	0.00	4553.40	0.00	2459.20	0.00
9130.70	0.00	5885.10	0.00	2602.30	0.00

Table 8-9: Raw data of the size distribution (intensity)

	6 cycle		8 cycle		10 cycle	
Size(nm)	Intensity	Size(nm)	Intensity	Size(nm)	Intensity	
15.10	0.00	14.50	0.00	15.40	0.00	
15.90	0.00	15.70	0.00	16.80	0.00	
18.90	0.00	18.20	0.00	19.10	0.00	
19.70	0.00	19.60	0.00	20.60	0.00	
23.60	0.00	22.70	0.00	23.70	0.00	
24.50	0.00	24.30	0.00	25.40	0.00	
29.50	0.00	28.40	0.00	29.40	0.00	
30.50	0.00	30.20	0.00	31.30	0.00	
36.80	0.20	35.50	0.20	36.50	0.10	
38.00	0.20	37.50	0.10	38.50	0.10	
46.00	0.40	44.40	0.40	45.30	0.40	
47.30	0.40	46.50	0.40	47.30	0.40	
57.50	1.10	55.50	1.10	56.30	1.10	
58.80	1.10	57.80	1.10	58.30	1.10	

71.90	2.40	69.40	2.40	69.90	2.40
73.10	2.40	71.70	2.40	71.70	2.40
89.80	4.50	86.70	4.50	86.80	4.50
91.00	4.50	89.10	4.50	88.30	4.50
112.20	7.50	108.40	7.50	107.80	7.50
113.20	7.50	110.60	7.50	108.70	7.50
140.30	10.80	135.50	10.80	133.70	10.80
140.80	10.80	137.40	10.80	133.80	10.80
175.20	13.60	169.30	13.60	164.60	13.60
175.30	13.60	170.70	13.60	166.20	13.60
218.00	14.80	211.70	14.80	202.60	14.80
219.00	14.80	211.90	14.80	206.30	14.80
271.20	14.10	263.20	14.10	249.40	14.10
273.70	14.10	264.60	14.10	256.20	14.10
337.30	11.70	326.90	11.70	307.00	11.70
342.00	11.70	330.70	11.70	318.10	11.70
419.70	8.40	406.00	8.40	377.80	8.40
427.40	8.40	413.40	8.40	395.10	8.40
522.10	5.30	504.20	5.30	465.10	5.30
534.10	5.30	516.70	5.30	490.60	5.30
649.50	2.90	626.10	2.90	572.40	2.90
667.50	2.90	645.90	2.90	609.20	2.90
808.00	1.40	777.60	1.40	704.60	1.40
834.10	1.40	807.40	1.40	756.40	1.40
1005.20	0.60	965.70	0.60	867.20	0.60
1042.30	0.60	1009.20	0.60	939.30	0.60
1250.60	0.20	1199.40	0.20	1067.40	0.20
1302.60	0.20	1261.50	0.20	1166.40	0.20
1555.80	0.10	1489.50	0.10	1313.80	0.10
1627.70	0.10	1576.80	0.10	1448.30	0.10
1935.50	0.00	1971.00	0.00	1617.10	0.00
2034.10	0.00	2463.70	0.00	1798.50	0.00

c OPERATION PRESSURE P = 965 BAR

Table 8-10: Peak analysis evaluated by the intensity 965 bar

cycle	Mean	Width	z-average	Polydispersion
1	361.7	515.2	282.1	0.466
2	299.5	402.8	243.4	0.379
4	266.0	357.2	219.1	0.392
6	273.8	376.0	223.0	0.423
8	293.6	416.7	232.2	0.459
10	297.05	430.6	233.7	0.483

Table 8-11: Raw data of the size distribution 965 bar (intensity)

	1 cycle		2 cycle		4 cycle	
Size(nm)	Intensity	Size(nm)	Intensity	Size(nm)	Intensity	Size(nm)
12.90	0.00	0	0.2	12.90	0.00	11.8
14.40	0.00	0	0.5	12.90	0.00	12.4
16.70	0.00	0	1.1	16.30	0.00	15.1
18.40	0.00	0	1.9	16.30	0.00	15.7
21.50	0.00	0	0	20.50	0.00	19.2
23.70	0.00	0	0	20.60	0.00	20
27.70	0.00	0.1	0.1	25.90	0.00	24.5
30.30	0.00	0.2	3.1	26.00	0.00	25.3
35.80	0.20	0.2	0.2	32.80	0.20	31.2
38.90	0.20	0.4	4.5	32.90	0.20	32.1
46.10	0.40	0.6	0.4	41.40	0.40	39.7
49.90	0.40	1.1	5.6	41.50	0.40	40.7
59.50	1.10	1.4	4.6	52.20	1.10	50.6
64.00	1.10	2.4	6.3	52.50	1.10	51.7
76.70	2.40	2.9	8.9	66.00	2.40	64.5
82.20	2.40	4.6	6.3	66.20	2.40	65.6
99.00	4.60	5.3	10.4	83.30	4.60	82.1
105.40	4.60	7.5	5.7	83.60	4.60	83.2
127.60	7.60	8.4	13.2	105.20	7.50	104.7
135.20	7.60	10.9	4.7	105.60	7.50	105.6
164.60	10.90	11.7	10.4	132.90	10.90	133.4
173.40	10.90	13.6	3.8	133.40	10.90	133.9
212.40	13.60	13.9	0	167.80	13.60	169.9
222.40	13.60	14.1	4.7	168.40	13.60	169.9
273.90	14.90	14.9	3.4	211.90	14.90	215.5
285.30	14.90	17.6	0	212.70	14.90	216.5
353.30	14.10	22.3	0	267.60	14.10	273.4
366.00	14.10	28.3	0	268.60	14.10	275.8
455.70	11.60	35.9	0.2	338.00	11.70	346.9
469.50	11.60	45.6	0.4	339.20	11.70	351.5
587.70	8.30	57.8	1.1	426.80	8.40	440.1
602.30	8.40	73.4	2.4	428.30	8.40	447.8
758.10	5.20	93.1	4.6	539.00	5.20	558.3
772.60	5.20	118.1	7.5	540.90	5.20	570.6
977.80	2.80	149.9	10.9	680.70	2.90	708.3
991.00	2.80	190.1	13.6	683.00	2.90	727
1261.20	1.30	241.2	14.9	859.60	1.40	898.6
1271.20	1.30	306.1	14.1	862.50	1.40	926.3
1626.70	0.60	388.3	11.6	1085.60	0.60	1140
1630.70	0.60	492.7	8.4	1089.10	0.60	1180.2
2091.70	0.20	625.2	5.2	1370.90	0.20	1446.3
2098.20	0.20	793.2	2.9	1375.30	0.20	1503.7
2683.20	0.10	1006.4	1.4	1731.30	0.10	1834.9
2706.30	0.10	1276.9	0.6	1736.80	0.10	1915.9
3441.80	0.00	1620.1	0.2	2186.30	0.00	2327.8
3490.70	0.00	2055.5	0.1	2193.20	0.00	2953.2

Table 8-12: Raw data of the size distribution 965 bar (intensity)

6 cycle		8 cycle		10 cycle
Intensity	Size(nm)	Intensity	Size(nm)	Intensity
0	10.90	0.00	10.10	0.00
0	11.60	0.00	10.50	0.00
0	14.00	0.00	13.10	0.00
0	14.90	0.00	13.50	0.00
0	18.10	0.00	17.00	0.00
0	19.10	0.00	17.50	0.00
0	23.30	0.00	22.10	0.00
0	24.40	0.00	22.60	0.00
0.2	29.90	0.20	28.60	0.20
0.2	31.30	0.20	29.20	0.20
0.4	38.50	0.40	37.00	0.40
0.4	40.20	0.40	37.80	0.40
1.1	49.60	1.10	48.00	1.10
1.1	51.60	1.10	48.80	1.10
2.4	63.80	2.40	62.20	2.40
2.4	66.10	2.40	63.10	2.40
4.6	82.20	4.60	80.60	4.60
4.6	84.80	4.60	81.50	4.60
7.6	105.70	7.60	104.40	7.60
7.5	108.80	7.60	105.30	7.60
10.9	136.10	10.90	135.20	10.90
10.9	139.50	10.90	136.10	10.90
13.6	175.20	13.60	175.20	13.60
13.6	178.90	13.60	175.90	13.60
14.9	225.50	14.90	226.90	14.90
14.9	229.40	14.90	227.30	14.90
14.1	290.20	14.10	293.80	14.10
14.1	294.20	14.10	294.00	14.10
11.6	373.50	11.60	379.60	11.60
11.6	377.30	11.60	380.90	11.60
8.4	480.70	8.30	490.60	8.30
8.4	483.90	8.40	493.50	8.30
5.2	618.70	5.20	634.00	5.20
5.2	620.50	5.20	639.30	5.20
2.9	795.80	2.80	819.30	2.80
2.8	796.30	2.80	828.30	2.80
1.4	1020.60	1.30	1058.80	1.30
1.3	1024.90	1.30	1073.10	1.30
0.6	1308.90	0.60	1368.30	0.60
0.6	1319.20	0.60	1390.20	0.60
0.2	1678.60	0.20	1768.20	0.20
0.2	1697.90	0.20	1801.10	0.20
0.1	2152.80	0.10	2285.10	0.10
0.1	2185.30	0.10	2333.40	0.10

8.4.3 PILOT SCAL CELL DISRUPTION

a *ESCHERICHIA COLI* HOST STRAIN (JM 105)

APV high pressure homogenization

For the cell disruption a 30 % ww *Escherichia coli* cell suspension, obtained from high cell density cultivation, in desalted water was used. The cells has been disrupted by 5 cycle at 500 bar and 5 cycle at 1000 bar in a pilot scale APV Gaulin high pressure homogenizer.

Table 8-13: Peak analysis evaluated by the intensity

cycle	Mean	Width	z-average	Polydispersion
1	990.7	1391.4	789.1	0.497
2	561.6	764.0	457.2	0.438
4	389.5	505.9	324.4	0.361
6	337.8	421.5	287.7	0.359
8	391.9	529.6	319.8	0.416
10	510.95	759.1	399.1	0.532

Table 8-14: Raw data of the size distribution (intensity)

	1 cycle		2 cycle		4 cycle	
Size(nm)	Intensity	Size(nm)	Intensity	Size(nm)	Intensity	
32.80	0.00	23.00	0.00	21.5	0	
42.60	0.00	29.00	0.00	26.9	0	
48.10	0.00	29.50	0.00	33.7	0	
55.40	0.00	36.50	0.00	42.1	0	
60.60	0.00	37.70	0.00	52.7	0.2	
72.10	0.00	45.80	0.00	65.9	0.4	
76.40	0.00	48.20	0.00	82.4	1.1	
93.70	0.20	57.50	0.00	103.1	2.4	
96.40	0.00	61.70	0.20	129	4.5	
121.50	0.20	72.20	0.20	161.3	7.5	
121.90	0.40	79.00	0.40	201.8	10.8	
153.20	0.40	90.70	0.40	252.4	13.6	
158.50	1.10	101.10	1.10	315.8	14.8	
193.20	1.10	113.80	1.10	395	14.1	
206.10	2.40	129.30	2.40	494.1	11.7	
243.60	2.40	143.00	2.40	618	8.4	
268.00	4.60	165.50	4.60	773.1	5.3	

307.10	4.60	179.50	4.50	967.1	2.9
348.50	7.60	211.80	7.60	1209.7	1.4
387.20	7.50	225.50	7.50	1513.2	0.6
453.10	10.90	271.10	10.90	1892.8	0.2
488.20	10.90	283.10	10.90	2367.7	0.1
589.20	13.60	346.90	13.60		
615.60	13.60	355.50	13.60		
766.20	14.90	443.90	14.90		
776.20	14.90	446.50	14.90		
978.70	14.10	560.70	14.10		
996.30	14.10	568.00	14.10		
1234.10	11.70	704.10	11.70		
1295.50	11.60	726.90	11.60		
1556.10	8.40	884.20	8.40		
1684.60	8.30	930.20	8.40		
1962.00	5.20	1110.40	5.30		
2190.50	5.20	1190.40	5.20		
2473.90	2.90	1394.40	2.90		
2848.40	2.80	1523.30	2.80		
3119.30	1.40	1751.10	1.40		
3703.90	1.30	1949.40	1.30		
3933.20	0.60	2199.00	0.60		
4816.30	0.60	2494.60	0.60		
4959.30	0.20	2761.40	0.20		
6253.20	0.10	3192.30	0.20		
6262.80	0.20	3467.70	0.10		
8143.80	0.10	4085.20	0.10		

Table 8-15: Raw data of the size distribution (intensity)

Size(nm)	6 cycle		8 cycle		10 cycle	
	Intensity	Size(nm)	Intensity	Size(nm)	Intensity	Size(nm)
0.00	0.10	17.3	0	14.9	0	
0.00	0.20	19.8	0	16.6	0	
0.00	0.40	22.1	0	19.5	0	
0.00	0.70	24.9	0	21.6	0	
0.00	0.00	28	0	25.6	0	
0.00	0.00	31.4	0	28	0	
0.10	0.20	35.7	0	33.6	0	
0.20	1.10	39.5	0	36.4	0	
0.20	0.60	45.4	0.2	44.1	0.2	
0.40	1.60	49.7	0.2	47.2	0.2	
0.60	1.70	57.7	0.4	57.8	0.4	
1.10	2.10	62.5	0.4	61.3	0.4	
1.40	2.50	73.4	1.1	75.9	1.1	
2.40	2.40	78.7	1.1	79.6	1.1	
2.90	2.40	93.3	2.4	99.6	2.4	

4.50	2.50	99.1	2.4	103.4	2.4
5.30	2.80	118.7	4.6	130.6	4.6
7.50	2.40	124.7	4.6	134.2	4.6
8.40	17.90	150.9	7.6	171.4	7.6
10.80	2.20	157	7.5	174.2	7.6
11.70	33.20	192	10.9	225	10.9
13.60	2.10	197.6	10.9	226.1	10.9
14.10	18.40	244.1	13.6	293.5	13.6
14.80	2.70	248.7	13.6	295.2	13.7
24.30	0.00	310.5	14.9	381.1	14.9
29.70	0.00	313	14.9	387.4	14.9
36.40	0.00	394	14.1	494.7	14.1
44.60	0.00	394.9	14.1	508.4	14.1
54.70	0.10	495.9	11.7	642.2	11.6
67.00	0.40	502.2	11.6	667.2	11.6
82.00	1.10	624.2	8.4	833.6	8.3
100.50	2.40	638.7	8.4	875.5	8.3
123.10	4.50	785.7	5.3	1082.2	5.2
150.80	7.50	812.3	5.2	1148.9	5.2
184.80	10.80	988.9	2.9	1404.9	2.8
226.40	13.60	1033	2.9	1507.7	2.8
277.30	14.80	1244.7	1.4	1823.7	1.3
339.70	14.10	1313.8	1.4	1978.6	1.3
416.20	11.70	1566.8	0.6	2367.5	0.6
509.80	8.40	1670.9	0.6	2596.5	0.5
624.60	5.30	1972.1	0.2	3073.4	0.2
765.10	2.90	2125.1	0.2	3407.3	0.2
937.30	1.40	2482.3	0.1	3989.7	0.1
1148.30	0.60	2702.6	0.1	4471.3	0.1

Pilot scale Bead mill homogenization

For the cell disruption a 30 % ww *Escherichia coli* cell suspension, obtained from high cell density cultivation, in desalted water was used. The cells has been disrupted by 6 cycle at 2500 rpm in a Nertsch Lab Star Bead mill using 0,5 mm beads.

Table 8-16: Peak analysis evaluated by the intensity

Mean	Width	z-average	Polydispersion
802.4	1069.4	669.1	0.361

Table 8-17: Raw data of the size distribution (intensity)

Size(nm)	Intensity
36.40	0.00
44.20	0.00
46.20	0.00
55.30	0.00
58.60	0.00
69.10	0.00
74.40	0.00
86.50	0.00
94.40	0.20
108.20	0.20
119.80	0.40
135.40	0.40
152.10	1.10
169.40	1.10
193.00	2.40
211.90	2.40
245.00	4.60
265.10	4.50
310.90	7.50
331.70	7.50
394.60	10.90
415.00	10.80
500.80	13.60
519.20	13.60
635.70	14.90
649.60	14.80

806.80	14.10
812.80	14.10
1016.90	11.70
1023.90	11.60
1272.30	8.40
1299.60	8.40
1591.80	5.30
1649.40	5.20
1991.50	2.90
2093.40	2.90
2491.60	1.40
2656.80	1.40
3117.30	0.60
3372.00	0.60
3900.20	0.20
4279.70	0.20
4879.60	0.10
5431.80	0.10

b *ESCHERICHIA COLI* FDH PRODUCTION STRAIN (JM 105 REC. FDH)

APV high pressure homogenization

For the cell disruption a 30 % ww *Escherichia coli* cell suspension, obtained from high cell density cultivation, in desalted water was used. The cells has been disrupted by 5 cycle at 500 bar and 5 cycle at 700 bar in a pilot scale APV Gaulin high pressure homogenizer

Table 8-18: Peak analysis evaluated by the intensity

cycle	Mean	Width	z-average	Polydispersion
1	642	914	507	0.470
2	428	587	355	0.452
3	381	518	314	0.407
4	353	471	292	0.385
6	303	381	258	0.342
10	303	389	256	0.362

Table 8-19: Raw data of the size distribution (intensity)

	1 cycle		2 cycle		3 cycle	
Size(nm)	Intensity	Size(nm)	Intensity	Size(nm)	Intensity	
22.90	0.00	17	0.00	18	0	
25.80	0.00	21	0.00	18	0	
29.60	0.00	22	0.00	22	0	
33.00	0.00	27	0.00	23	0	
38.20	0.00	28	0.00	28	0	
42.30	0.00	34	0.00	29	0	
49.40	0.00	36	0.00	36	0	
54.20	0.00	42	0.00	36	0	
63.70	0.20	46	0.20	46	0.2	
69.40	0.20	53	0.20	46	0.2	
82.30	0.40	60	0.40	58	0.4	
88.80	0.40	67	0.40	58	0.4	
106.20	1.10	77	1.10	73	1.1	
113.80	1.10	84	1.10	73	1.1	
137.20	2.40	98	2.40	93	2.4	
145.70	2.40	106	2.40	93	2.4	
177.10	4.60	126	4.60	117	4.6	
186.60	4.60	133	4.50	118	4.6	
228.60	7.60	162	7.60	148	7.5	
239.00	7.60	167	7.50	149	7.5	
295.20	10.90	209	10.90	188	10.9	
306.00	10.90	210	10.90	190	10.9	
381.10	13.60	264	13.60	238	13.6	
391.90	13.60	268	13.60	240	13.6	
492.00	14.90	331	14.90	301	14.9	
501.90	14.90	344	14.90	305	14.9	
635.20	14.10	416	14.10	380	14.1	
642.80	14.10	442	14.10	387	14.1	
820.10	11.60	523	11.70	481	11.6	
823.10	11.60	568	11.60	490	11.6	
1054.10	8.40	658	8.40	609	8.4	
1058.80	8.30	730	8.40	622	8.4	
1350.00	5.20	826	5.30	771	5.2	
1367.00	5.20	938	5.20	789	5.2	
1728.80	2.80	1039	2.90	975	2.9	
1764.80	2.80	1205	2.80	1000	2.9	
2214.00	1.30	1305	1.40	1234	1.4	
2278.50	1.30	1549	1.30	1269	1.4	
2835.30	0.60	1640	0.60	1562	0.6	
2941.70	0.60	1990	0.60	1609	0.6	
3631.00	0.20	2062	0.20	1977	0.2	
3797.80	0.20	2556	0.20	2041	0.2	
4650.00	0.10	2591	0.10	2501	0.1	

Table 8-20: Raw data of the size distribution (intensity)

	4 cycle		6 cycle		10 cycle	
Size(nm)	Intensity	Size(nm)	Intensity	Size(nm)	Intensity	
18	0	18	0	17	0	
18	0	20	0	18	0	
22	0	23	0	21	0	
22	0	24	0	23	0	
28	0	28	0	27	0	
28	0	30	0	28	0	
35	0	35	0	33	0	
36	0	37	0	35	0	
45	0.2	44	0.1	41	0.2	
45	0.2	46	0.1	43	0.1	
56	0.4	54	0.4	52	0.4	
56	0.4	57	0.4	54	0.4	
71	1.1	68	1.1	65	1.1	
71	1.1	70	1.1	67	1.1	
89	2.4	84	2.4	81	2.4	
90	2.4	87	2.4	83	2.4	
113	4.6	105	4.5	102	4.5	
113	4.6	107	4.5	103	4.5	
142	7.5	130	7.5	127	7.5	
142	7.5	132	7.5	128	7.5	
179	10.9	162	10.8	159	10.8	
179	10.9	163	10.8	159	10.8	
225	13.6	201	13.6	198	13.6	
225	13.6	202	13.6	199	13.6	
283	14.9	249	14.8	246	14.8	
284	14.9	250	14.8	249	14.8	
357	14.1	308	14.1	305	14.1	
358	14.1	311	14.1	312	14.1	
449	11.7	380	11.7	379	11.7	
450	11.7	387	11.7	390	11.7	
566	8.4	469	8.4	470	8.4	
568	8.4	482	8.4	488	8.4	
713	5.2	580	5.3	584	5.3	
715	5.2	599	5.3	610	5.3	
898	2.9	716	2.9	725	2.9	
901	2.9	745	2.9	764	2.9	
1130	1.4	884	1.4	901	1.4	
1135	1.4	926	1.4	956	1.4	
1424	0.6	1092	0.6	1119	0.6	
1431	0.6	1152	0.6	1196	0.6	
1793	0.2	1348	0.2	1389	0.2	
1803	0.2	1433	0.2	1497	0.2	
2258	0.1	1665	0.1	1725	0.1	
2271	0.1	1782	0.1	1873	0.1	

Pilot scale Bead mill homogenization

For the cell disruption a 30 % ww *Escherichia coli* cell suspension, obtained from high cell density cultivation, in desalted water was used. The cells has been disrupted by 6 cycle at 2500 rpm in a Nertsch Lab Star Bead mill using 0.5 mm beads.

Table 8-21: Peak analysis evaluated by the intensity

Mean	Width	z-average	Polydispersion
741.95	1043.2	604.9	0.463

Table 8-22: Raw data of the size distribution (intensity)

Size(nm)	Intensity
28	0
31	0
36	0
40	0
47	0
51	0
60	0
65	0
77	0
83	0
100	0
105	0
128	1
134	1
165	2
170	2
213	5
217	5
275	8
276	8
351	11
354	11
446	14
456	14
568	15
587	15
723	14
757	14
921	12

975	12
1172	8
1257	8
1491	5
1619	5
1898	3
2087	3
2416	1
2689	1
3075	1
3465	1

8.4.4 SACCHAROMYCES CEREVISIAE HOMOGENIZATION CONDITIONS IN THE FRENCH PRESS

a OPERATION PRESSURE P = 300 BAR

Table 8-23: Peak analysis evaluated by the intensity *Saccharomyces cerevisiae* 300 bar

cycle	Mean	Width	z-average	Polydispersion
0	9256	13553	7242	0.491
2	3604	5373	2785	0.516
4	1392	1662	1202	0.294
6	2712	4055	2092	0.520
8	2474	3958	1805	0.632
10	3043	5187	2067	0.775

Table 8-24: Raw data of the size distribution (intensity) *Saccharomyces cerevisiae* 300 bar

	Cells		2 cycle		4 cycle
Size(nm)	Intensity	Size(nm)	Intensity	Size(nm)	Intensity
306	0	109	0	103	0
397	0	142	0	126	0
516	0	186	0	154	0
670	0	243	0	189	0
870	0.2	318	0.2	231	0.1
1130	0.4	415	0.4	283	0.4
1467	1.1	543	1.1	347	1.1
1905	2.4	709	2.4	425	2.4
2473	4.6	927	4.6	520	4.5
3212	7.6	1212	7.6	636	7.5
4170	10.9	1583	10.9	779	10.8
5415	13.6	2069	13.6	953	13.6
7031	14.9	2704	14.9	1167	14.8
9130	14.1	3534	14.1	1428	14.1

11854	11.6	4619	11.6	1748	11.7
15393	8.3	6037	8.3	2140	8.4
19987	5.2	7889	5.2	2619	5.3
25952	2.8	10311	2.8	3206	2.9
33698	1.3	13475	1.3	3925	1.4
43756	0.6	17611	0.6	4805	0.6
56816	0.2	23016	0.2	5881	0.2
73774	0.1	30079	0.1	7199	0.1

Table 8-25: Raw data of the size distribution (intensity)

	6 cycle		8 cycle		10 cycle	
Size(nm)	Intensity	Size(nm)	Intensity	Size(nm)	Intensity	
81	0	50	0	39	0	
106	0	67	0	54	0	
138	0	91	0	76	0	
181	0	122	0	105	0	
237	0.2	164	0.2	146	0.2	
310	0.4	220	0.4	202	0.5	
405	1.1	296	1.1	280	1.1	
530	2.4	398	2.4	389	2.5	
693	4.6	536	4.6	540	4.7	
907	7.6	720	7.6	750	7.7	
1187	10.9	969	10.9	1041	11	
1552	13.6	1303	13.7	1445	13.7	
2031	14.9	1752	14.9	2006	14.9	
2657	14.1	2356	14.1	2785	14	
3476	11.6	3168	11.6	3866	11.5	
4547	8.3	4261	8.3	5367	8.3	
5949	5.2	5730	5.2	7451	5.1	
7783	2.8	7705	2.8	10343	2.8	
10183	1.3	10361	1.3	14358	1.3	
13322	0.6	13934	0.5	19932	0.5	
17428	0.2	18738	0.2	27669	0.2	
22801	0.1	25198	0.1	38410	0.1	

b OPERATION PRESSURE P = 482 BARTable 8-26: Peak analysis evaluated by the intensity *Saccharomyces cerevisiae* 482 bar

cycle	Mean	Width	z-average	Polydispersion
2	2185	3208	1707	0.495
4	1543	1945	1305	0.335
6	1594.1	2510.6	1179.4	0.603
8	1433	1920	1179	0.390

Table 8-27: Raw data of the size distribution (intensity) *Saccharomyces cerevisiae* 482 bar

	2 cycle		4 cycle	
Size(nm)	Intensity	Size(nm)	Intensity	
71	0	95	0	
93	0	118	0	
121	0	146	0	
157	0	182	0	
204	0.2	225	0.1	
265	0.4	280	0.4	
344	1.1	347	1.1	
447	2.4	431	2.4	
581	4.6	534	4.5	
755	7.6	663	7.5	
981	10.9	823	10.8	
1275	13.6	1021	13.6	
1657	14.9	1267	14.8	
2154	14.1	1572	14.1	
2799	11.6	1950	11.7	
3638	8.3	2420	8.4	
4728	5.2	3003	5.3	
6145	2.8	3726	2.9	
7986	1.3	4624	1.4	
10379	0.6	5737	0.6	
13489	0.2	7119	0.2	
17532	0.1	8834	0.1	

Table 8-28: Raw data of the size distribution (intensity) *Saccharomyces cerevisiae* 482 bar

	6 cycle		8 cycle	
Size(nm)	Intensity	Size(nm)	Intensity	
36	0	70	0	
48	0	89	0	
63	0	112	0	
85	0	141	0	
113	0.2	178	0.2	
151	0.4	224	0.4	
202	1.1	283	1.1	
269	2.4	358	2.4	
360	4.6	451	4.6	
481	7.6	569	7.5	
642	10.9	719	10.9	
857	13.7	907	13.6	
1145	14.9	1145	14.9	
1529	14.1	1445	14.1	
2043	11.6	1823	11.7	
2728	8.3	2301	8.4	
3644	5.2	2904	5.2	
4867	2.8	3666	2.9	
6501	1.3	4626	1.4	
8683	0.5	5839	0.6	
11597	0.2	7369	0.2	
15489	0.1	9300	0.1	

c OPERATION PRESSURE P = 965 bar

Table 8-29: Peak analysis evaluated by the intensity *Saccharomyces cerevisiae* 965 bar

cycle	Mean	Width	z-average	Polydispersion
0	11855	19727	8296	0.715
2	2078	3709	1313	0.918
4	1566	2702	1045	0.809
6	1495	2597	989	0.828
8	1454	2469	992	0.765
10	1496	2598	990	0.827

Table 8-30: Raw data of the size distribution (intensity) *Saccharomyces cerevisiae* 965 bar

	Cells		2 cycle		4 cycle	
Size(nm)	Intensity	Size(nm)	Intensity	Size(nm)	Intensity	
184	0	18	0	18	0	
252	0	25	0	25	0	
345	0	36	0	36	0	
473	0	51	0	50	0	
648	0.2	73	0.2	70	0.2	
888	0.5	105	0.5	97	0.5	
1217	1.1	150	1.1	136	1.1	
1667	2.5	214	2.5	190	2.5	
2285	4.6	306	4.7	266	4.7	
3130	7.6	437	7.7	371	7.7	
4290	11	624	11	519	11	
5878	13.7	892	13.7	726	13.7	
8055	14.9	1275	14.9	1015	14.9	
11037	14	1822	14	1419	14	
15124	11.6	2605	11.5	1984	11.5	
20725	8.3	3723	8.2	2774	8.3	
28399	5.2	5320	5.1	3879	5.1	
38915	2.8	7604	2.8	5423	2.8	
53326	1.3	10868	1.3	7583	1.3	
73072	0.5	15533	0.5	10602	0.5	
100131	0.2	22199	0.2	14824	0.2	
137209	0.1	31728	0.1	20728	0.1	

Table 8-31: Raw data of the size distribution (intensity) *Saccharomyces cerevisiae* 965 bar

Size(nm)	Intensity	Size(nm)	Intensity	Size(nm)	Intensity
16	0	19	0	17	0
23	0	27	0	23	0
32	0	37	0	32	0
45	0	51	0	46	0
64	0.2	71	0.2	64	0.2
89	0.5	98	0.5	90	0.5
126	1.1	136	1.1	126	1.1
176	2.5	189	2.5	177	2.5
247	4.7	262	4.7	248	4.7
347	7.7	362	7.7	348	7.7
487	11	502	11	488	11
684	13.7	695	13.7	685	13.7
960	14.9	963	14.9	961	14.9
1347	14	1334	14	1349	14
1891	11.5	1849	11.5	1893	11.5
2655	8.2	2561	8.3	2656	8.2
3726	5.1	3547	5.1	3728	5.1

5230	2.8	4914	2.8	5231	2.8
7340	1.3	6807	1.3	7341	1.3
10303	0.5	9429	0.5	10303	0.5
14461	0.2	13062	0.2	14458	0.2
20297	0.1	18095	0.1	20290	0.1

d OPERATION PRESSURE P = 2068 BAR

Table 8-32: Peak analysis evaluated by the intensity *Saccharomyces cerevisiae* 2068 bar

cycle	Mean	Width	z-average	Polydispersion
2	1285	1901	998	0.505

Table 8-33: Raw data of the size distribution (intensity) *Saccharomyces cerevisiae* 2068 bar

	2 cycle
Size(nm)	Intensity
40	0
53	0
69	0
89	0
116	0.2
152	0.4
198	1.1
258	2.4
336	4.6
438	7.6
570	10.9
743	13.6
969	14.9
1263	14.1
1646	11.6
2145	8.3
2796	5.2
3644	2.8
4749	1.3
6189	0.6
8066	0.2
10513	0.1

8.5 ATPS HGH

Table 8-34 ATPS with decreased slat concentration as Salt a mixture of 85,2 % K_2HPO_4 and 14,8 % KH_2PO_4 was used.

	System 1	System 2	System 3	System 4
PEG 400	19.40	19.40	19.40	19.40
Salt	16	14	12	10
comment	cell debris accumulates at the bottom of the Top phase	cell debris accumulates at the bottom of the Top phase	cell debris accumulates at the bottom of the Top phase	no phase system

Table 8-35: ATPS with higher MW PEG and mixtures

ATPS	Chemicals	concentration (%)	Volume of the Top phase (ml)	Yield in the Top phase (%)	comments
1	PEG 600	15	3.2	57	3 phase system
	Salt	16			
2	PEG 600	14.5	6.4	99	just diffuse phase
	Na_2SO_4	10.5			separation
3	PEG 1000	15			just diffuse phase
	Na_2SO_4	10			separation 3 phases
4	PEG 1550	15	4.2	2	3 phase system
	Na_2SO_4	10			
5	PEG 1550	14	3.8	2	3 phase system
	Salt	13			
6	PEG 400	18	7.6	109	stable two phase
	PEG 1550	7			system
	K_2HPO_4	6			
	NaCl	0.5			

9 REFERENCES

- Agosto, M., Wang, N.-H. L. and Wankat, P. C. (1993) Amino acid separation in a multistage fluidized ion exchanger bed. *Ind. Eng. Chem. Res.* , **32**, 2058-2064.
- Albertsson, P.-A. (1960) *Partition of cell particles and macromolecules*, Almqvist & Wiksell, Stockholm.
- Ameskamp, N., Priesner, C., Lehmann, J. and Lutkemeyer, D. (1999) Pilot scale recovery of monoclonal antibodies by expanded bed ion exchange adsorption *Bioseparation*, **8**, 169-188.
- Anspach, F. B., Curbelo, D., Hartmann, R., Garke, G. and Deckwer, W.-D. (1999) Expanded-bed chromatography in primary protein purification *J. Chromatogr. A*, **865**, 129-144.
- Asenjo, J. A. (1990), The rational desing of large scale protein separation In *Separations for Biotechnology*,(Ed, Pyle, D. L.) For SCI by Elsevier applied science, London and New York, pp. 519-528.
- Asplund, M., Barnfield-Freij, A. K., Lundkvist, M. and Rygge, M. (2002), *Development of novel columns for expanded bed adsorption* at the EBA02, St. Petersburg Beach (FL, USA)
- Asplund, M., Ramsberg, M. and Johannson, B. L. (2000) Development of cleaning in place protocol and repetitive application of E. coli homogenate on Streamline Q XL *Process Biochem. Dec. 1989, 212-216*, **35**, 1111-1118.
- Baerns, M., Hofman, H. and Renken, A. (1999) *Chemische Reaktionstechnik*, Thieme Verlag, Stuttgart.

- Barnfield-Frej, A.-K., Hjorth, R. and Hammarstroem, A. (1994) Pilot scale recovery of recombinant annexin V from unclarified *E. coli* homogenate using expanded bed adsorption *Biotechnol. Bioeng.*, **44**, 922-929.
- Bartels, C. R., Kleimann, G., Korzun, J. N. and Irish, D. B. (1958) A novel ion-exchange method for the isolation of streptomycin. *Chem. Eng. Progr.*, **54**, 49-51.
- Bascoul, A., Delmas, H. and Couderc, J. P. (1988a) Caracteristiques hydrodynamiques de la fluidisation liquide-solide: Influence du distributeur *Chem. Eng. Journal*, **37**, 11-24.
- Bascoul, A., Riba, J. P., Alran, C. and Couderc, J. P. (1988b) Influence de la distribution du liquide sur le coefficient de dispersion axiale en fluidisation liquide-solide *Chem. Eng Journal*, **38**, 69-79.
- Biosciences, A. (1999) *Protein Purification Handbook*, Amersham biosciences, Uppsala.
- Biosciences, A. (2002) *Expanded Bed Adsorption Handbook*, Amersham Biosciences.
- Bonnerja, J., Oh, S. and Dunnill, P. (1986) Protein Purification: The right step at the right time *Bio/Technology*, **4**, 945-958.
- Boonaert, C. J. and Rouxhet, P. G. (2000) Surface of lactic acid bacteria: relationships between chemical composition and physicochemical properties *Appl. Environ. Microbiol.*, **66**, 2548-2554.
- Bradford, M. M. (1976) A rapid and sensitive Method for the quantification of microgram quantities of protein utilising the principle of protein-dye binding *J. Anal. Biochem.*, **72**, 248-254.
- Brixius, P. J., Mollerup, I., Jensen, O. E., Halfar, M. and Thömmes, J. (2003) Expanded Bed Adsorption as a Primary Recovery Step for the Isolation of the Insulin Precursor MI3: Process development and scale up *in preparation*.

- Brummelhuis, H. G. J. (1980), Preparation of the Prothrombin complex In *Methods of plasma protein fractionation*,(Ed, Curling, J. M.) Academic Press, New York, pp. 117-128.
- Buchholz, K. and Kasche, V. (1997) *Biokatalysatoren und Enzymtechnologie*, VCH Verl.Ges. , 1997, Weinheim.
- Büchs, J., Mozes, N., Wandrey, C. and Rouxhet, P. G. (1988) Cell adsorption control by culture conditions *Appl. Microbiol. Biotechnol.*, **29**, 119-128.
- Burns, M. A. and Graves, D. J. (1985) Continuous affinity chromatography using a magnetically stabilized fluidized bed *Biotechnol. Progr.*, **1**, 95-103.
- Chang, Y. K. and Chase, H. A. (1996a) Development of operating conditions for protein purification using expanded bed techniques: The effect of the degree of bed expansion on adsorption performance *Biotechnol. Bioeng.*, **49**, 512-526.
- Chang, Y. K. and Chase, H. A. (1996b) Ion exchange purification of G6PDH from unclarified yeast cell homogenates using expanded bed adsorption *Biotechnol. Bioeng.*, **49**, 204-216.
- Chang, Y. K., Chen, Y. H. and Chien, C. H. (1998) Simple two step procedure for purification of cloned small sialidase from unclarified E. coli feedstocks *Enzyme Microb. Technol.*, **23**, 204-210.
- Chase, H. A. (1994) Purification of proteins by adsorption chromatography in expanded beds *TIBTECH*, **12**, 296-303.
- Chase, H. A. and Draeger, N. M. (1992) Expanded bed adsorption of proteins using ion exchangers *Sep. Sci. Technol.*, **27**, 2021-2039.
- Clemmitt, R. H. and Chase, H. A. (2002) Direct recovery of glutathione S-transferase by expanded bed adsorption: anion exchange as an alternative to metal affinity fusions *Biotechnol. Bioeng.*, **77**, 776-785.

- Curvers, S., Brixius, P., Klauser, T., Thommes, J., Weuster-Botz, D., Takors, R. and Wandrey, C. (2001) Human chymotrypsinogen B production with *Pichia pastoris* by integrated development of fermentation and downstream processing. Part 1. Fermentation *Biotechnol. Progr.*, **17**, 495-502.
- Dalboege, H., Dahl, H.-H. M., Pedersen, J., J.W., H. and Christensen, T. (1987) A novel enzymatic method for production of authentic hGH From an *Escherichia coli* Produced hGH-precursor *Biotechnology*, **5**, 10-14.
- Dasari, G., Prince, I. and Hearn, T. W. (1993) High performance liquid chromatography of amino acids, peptides and proteins: CXXIV. Physical characterization of fluidized bed behavior of chromatographic packing materials. *J. Chromatogr.* **566**, 341-350, **631**, 115 - 124.
- Datar, R. V. and Rosen, C.-G. (1996), Cell and cell debris removal: centrifugation and crossflow filtration In *Bioprocessing*, Vol. 3 (Ed, Stephanopoulos, G.) VCH, Weinheim, pp. 472-502.
- Ditz, R. (2002), The value of separation technologies in modern live sciences - Much more than separating the sheep from the goat? at the *SPICA 2002*, Heidelberg
- Draeger, N. M. and Chase, H. A. (1990) Protein adsorption in liquid fluidized beds *I.CHEM.E. Symposium Series*, **118**, 161-172.
- Draeger, N. M. and Chase, H. A. (1991) Liquid fluidized bed adsorption of protein in the presence of cells. *Bioseparation*, **2**, 67-80.
- Engler, C. R. and Robinson, C. W. (1981) Effect of organism type and growth conditions on cell disruption by impingement *Biotechn. Lett.*, **3**, 83-88.
- Felber, S. (2001) *Optimierung der NAD-abhängigen FDH aus Candida boindinii für den Einsatz in der Biokatalyse*, phd-Thesis at the Institute of Enzyme Technology of University of Düsseldorf, Düsseldorf

- Fernández-Lahore, H. M., Geilenkirchen, S., Boldt, K., Nagel, A., Kula, M.-R. and Thömmes, J. (2000) The influence of cell adsorbent interactions on protein adsorption in expanded beds *J. Chromatogr. A*, **873**, 195-208.
- Fernández-Lahore, H. M., Kleef, R., Kula, M.-R. and Thömmes, J. (1999) The influence of complex biological feedstock on the fluidisation and bed stability in Expanded Bed Adsorption *Biotechnol. Bioeng.*, **64**, 484-496.
- Fernández-Lahore, H. M., Lin, D. Q., Hubbuch, J. J., Kula, M. R. and Thömmes, J. (2001) The use of Ionselective Elektrodes for Evaluating Residence Time Distributions in Expanded Bed Adsorption Systems *Biotechn. Prog.*, **17**, 1128-1136.
- Feuser, J., Walter, J., Kula, M.-R. and Thömmes, J. (1999) Cell-adsorbent interactions in expanded bed adsorption of proteins *Bioseparation*, **8**, 99-109.
- Fish, M. F. and Lilly, M. D. (1984) The interactions between fermentation and protein recovery *Bio/Technology*, **2**, 623-627.
- Frank, B. H. and Chance, R. E. (1983) Two Routes for Producing Human Insulin Utilizing Recombinant DNA Technology *Münch. med. Wschr.*, **125 Suppl. 1**, 14-20.
- Garke, G., Deckwer, W. D. and Anspach, F. B. (2000) Preparative two-step purification of recombinant human basic fibroblast growth factor from high-cell-density cultivation of *Escherichia coli* *J. Chromatogr. B*, **737**, 25-38.
- Goeddel, D. V., Heyneker, H. L., Hozumi, T., Arentzen, R., Itakura, K., Yansure, D. G., Ross, M. J., G., M., Crea, R. and Seeburg, P. H. (1979) Direct expression in *Escherichia coli* of a DNA sequence coding for human growth hormone *Nature*, **281**, 544-548.
- Gupta, M. N. and Mattiasson, B. (1994) Novel Technologies in Downstream Processing *Chemistry and Industry*, **17**, 673-675.

- Hall, K. R., Eagelton, L. C., Acrivos, A. and Vermeulen, T. (1966) Pore- and Solid-Diffusion Kinetics in Fixed-Bed Adsorption under Constant-Pattern Conditions *I&EC Fundamentals*, **5**, 212-223.
- Hetherington, P. J., Follws, M., Dunnill, P. and Lilly, M. D. (1971) Release of protein from bakers yeast by disruption *Trans. Instn. Chem. Engrs.* **45**, T353-T359, **49**, 142-148.
- Hjorth, R., Kämpe, S. and Carlsson, M. (1995) Analysis of some operating parameters of novel adsorbents for recovery of proteins in expanded beds *Bioseparation*, **5**, 217-223.
- Hjorth, R., Leijon, P., Barnfield-Frej, A. K. and Jägersten, C. (1998), Expanded bed adsorption In *Bioseparation and Bioprocessing*, Vol. 1 (Ed, Subramanian, G.) Wiley-VCH, Weinheim.
- Hubbuch, J. (2000) *Development of Adsorptive Separation Systems for recovery of Proteins from crude Bioprocess Liquors*, phd-Thesis at the Center of Process Biotechnology
- Department of Biotechnology of Technical University of Denmark, Kopenhagen
- Hubbuch, J. J., Heeboell-Nielsen, A., Hobley, T. J. and Thomas, O. R. T. (2001a),Cacun.
- Hubbuch, J. J., Heeboell-Nielsen, A., Hobley, T. J. and Thomas, O. R. T. (2002) A New Fluid Distribution System For Scale-Flexible Expanded Bed Adsorption *Biotechnol. Bioeng.*, **78**, 35-43.
- Hubbuch, J. J., Mattiesen, D. B., Hobley, T. J. and Thomas, O. R. T. (2001b) High gradient magnetic separation versus expanded bed adsorption: a first principal comparison *Bioseparation*, **10**, 99-112.
- Huddleston, J. G., Wang, R. and Lyddiatt, A. (1994) On the use of mild hydrophobic interaction chromatography for "method scouting" protien purification strategies

- in aqueous two phase systems: A study using model proteins *Biotechnol. Bioeng.*, **44**, 626-635.
- Hunter, R. J. (1981) *Zeta potential in colloid science - principle and applications*, Academic Press Inc., San Diego.
- Hustedt, H., Kroner, K. H., Menge, U. and Kula, M. R. (1985) Protein recovery using two-phase systems *Trends Biotechnol.*, **3**, 139-144.
- Hustedt, H., Kroner, K. H., Menge, U. and Kula, M. R. (1988), *Enzyme purification by liquid-liquid extraction at the Enzyme Engineering*,
- Ives, K. J. (1975) *The scientific basis of filtration*, Noordhoff-Leyden.
- Janson, J. C. and Ryden, L. G. (1998) *Protein Purification second edition*, Willey-VCH, New York.
- Jensen, B. E. and Carlsen, S. (1989) Production of recombinant human growth hormone in *Escherichia coli*: Expression of different Precursors and physical effects of glucose, acetate, and salts *Biotechnology and Bioengineering*, **36**, 1-11.
- Jespersen, A. M., Christensen, T., Klausen, N. K., Nielsen, P. F. and Soerensen, H. H. (1994) Characterisation of trisulphide derivative of biosynthetic human growth hormone produced in *Escherichia coli* *Eur. J. Biochem.*, **219**, 365-373.
- Johansson, H. J., Jagersten, C. and Shiloach, J. (1996) Large scale recovery and purification of periplasmic recombinant protein from *E. coli* using expanded bed adsorption chromatography followed by new ion exchange media *J. Biotechnol.*, **48**, 9-14.
- Kadner, R. J. (1996), Cytoplasmic Membrane In *Escherichia coli and Salmonella CELLULAR AND MOLECULAR BIOLOGY*, Vol. 1 (Ed, Neidhardt, F. C.) ASM Press, Washington, pp. 58-87.
- Kagedal, L. (1998), Immobilized metal affinity chromatography In *Protein Purification second edition*,(Eds, Janson, J. C. and Ryden, L. G.) Wiley-VCH, New York.

- Karau, A., Benken, C., Thömmes, J. and Kula, M.-R. (1997) The influence of particle size distribution and operating conditions on the adsorption performance in fluidized beds *Biotechnol. Bioeng.*, **55**, 54-64.
- Kempken, R., Preissmann, A. and Berthold, W. (1995) Assessment of a disk-stack centrifuge for use in mammalian cell separation *Biotechnol. Bioeng.*, **46**, 132-138.
- Kleinig, A. R. and Middelberg, A. P. J. (1996) The correlation of cell disruption with homogenizer valve pressure gradient determined by computational fluid dynamics *Time Measurements in Pulsed Liquid/Liquid Extractors.*, **51**, 5103-5110.
- Kragl, U., Kruse, W., Hummel, W. and Wandrey, C. (1996) Enzyme engineering aspects of biocatalysis: cofactor regeneration as example *Biotechnol. Bioeng.*, **52**, 309-319.
- Krekeler, C., Ziehr, H. and Klein, J. (1989), Physical methods for characterisation of microbial cell surfaces In *Experienta 45*, Birkhäuser Verlag, Basel, pp. 1047-1055.
- Krekeler, C., Ziehr, H. and Klein, J. (1991) Influence of physicochemical bacterial surface properties on adsorption of inorganic supports *Appl. Environ. Microbiol.*, **35**, 484-490.
- Krützfeldt, R., Roß, A. and Deckwer, W.-D. (1992) Selektive Abtrennung von Adsorberharzen mit dem Klärdekanter *BioEngineering*, **4**, 32-34.
- Kula, M. R. and Schütte, H. (1987) Purification of Proteins and the Disruption of Microbial Cells *Biotechnol. Progr.*, **3**, 31-42.
- Kula, M.-R., Schütte, H., Vogels, G. and Frank, A. (1990) Cell disintegration and purification of intracellular proteins *Food Biotechnol.*, **4**, 169-183.

- Lagaly, G., Schulz, O. and Zimehl, R. (1997) *Dispersionen und Emulsionen: Eine Einführung in die Kolloidik feinverteilter Stoffe einschliesslich der Tonminerale*, Impressum Darmstadt.
- Levenspiel, O. (1972) *Chemical Reaction Engineering*, Wiley, New York.
- Li, J. and MC Landsborough, L. A. (1999) The effect of the surface charge and hydrophobicity of Echerichia coli on its adhesion to beef muscle *Int. J. Food Microbiol.*, **53**, 185-193.
- Lin, D. Q., Brixius, P. J., Hubbuch, J., Thömmes, J. and Kula, M. R. (2002) The Biomass/adsorbent Electrostatic Interactions in Expanded Bed: A Zeta Potential Study *Biotechnol. Bioeng.*, **accepted**.
- Lin, D. Q., Fernández-Lahore, H. M., Kula, M.-R. and Thömmes, J. (2001) Minimising Biomass/Adsorbent Interactions in Expanded Bed Adsorption Processes - A Methological Desing Approach *Bioseparation*, **10**, 7-19.
- Lipke, P. N. and Ovalle, R. (1998) Cell Wall Architecture in Yeast: New Structure and New Challenges *J. Bacteriol.*, **180**, 3735-3740.
- Middelberg, A. P. J. (1995) Process-Scale disruption of Microorganisms *Biotechnol. Adv.*, **13**, 491-555.
- Middelberg, A. P. J., O'Neill, B. K. and Bogle, D. L. (1990) A Novel Technique for the Measurment of Disruption in High-Pressure Homoginization: Studies on E. coli Containing Recombinant Inclusion Bodies *Biotechnol. Bioeng.*, **38**, 363-370.
- Middelberg, A. P. J., O'Neill, B. K. and Bogle, D. L. (1992) A new Model for the Disruption of Escherichia coli by High-Pressure Homoginization Part I. Model Development and Verification *Trans. Instn. Chem. Engrs.* **45**, T353-T359, **70**, 205-212.
- Miyauchi, A., Ebisu, S., Uchida, K., Yoshida, M., Ozawa, M., Tojo, T., Kadowaki, K. and Takagi, H. (1998) Pilot sale production of a recombinant human epidermal

- groth factor, secreted by *Bacillus brevis*, using expanded bed adsorption *J. Ind. Microbiol. Biotechnol.*, **21**, 208-214.
- Mollerup, I., Jensen, S. W., Larsen, P., Schou, O. and Snel, L. (1999), Insulin Purification In *Encyclopedia of Bioprocess Technology: Fermentation, Biotransformation and Bioseparation*, (Eds, Flickinger, M. C. and Drew, S. W.) Wiley & Sons, pp. 1491-1498.
- Möller, H. and Hörnle, R. (1972) *Dechema Monographie*, **69**.
- Mozes, N., Amory, D. E., Leonard, A. J. and Rouxhet, P. G. (1989) Surface properties of microbial cells and their role in adhesion and flocculation *Colloids and Surfaces*, **42**, 313-329.
- Mozes, N., Marchal, F., Hermesse, M. P., Van Hecht, J. L. and Reuliaux, L. (1986) Immobilisation of Microorganisms by Adhesion: Interplay of Electrostatic and Nonelectrostatic Interactions *Biotechnol. Bioeng.*, **30**, 439-450.
- Nagel, A. (2000) *Fließbettadsorption: Stofftransportmechanismen in der Proteinaufarbeitung*, phd-thesis at the of RWTH Aachen, Aachen
- Neihof, R. and Echols, H. (1973) Physicochemical Studies of Microbial Cell Walls I. Comparative Electrophoretic Behavior of intact cells and isolated cell walls *Biochim. Biophys. Acta* **133**, 371-373, **318**, 23-32.
- Nelson, P. A. and Galloway, T. R. (1975) Particle-to-fluid heat and mass transfer in multiparticle systems at low Reynolds numbers *AIChE Journal*, **10**, 605 - 611.
- Nguyen, T. H., Fleet, G. H. and Rogers, P. L. (1998) Composition of the cell walls of several yeast species *Appl. Microbiol. Biotechnol.*, **50**, 206-212.
- Nikaido, H. (1996), Outer Membrane In *Escherichia coli and Salmonella "Cellular and Molecular Biology*, (Eds, Neidhardt, F. C. and al, e.) American Society for Microbiology, Washington DC, pp. 29-43.

- Nitzsche, R. (2002), Möglichkeiten zur Bestimmung der Ladungs-Charakteristik mittels elektrophoretischer Lichtstreuung, Personal communication
- Orlean, P. (1997), Biogenesis of yeast cell wall and surface components In *Molecular and cellular biology of the yeast Saccharomyces*, Vol. 3 (Eds, Pringle, J., Broach, J. and Jones, E.) Cold Spring Harbor Laboratory Press, Cold Spring Harbor New York, pp. 229-362.
- Paustian, T., (2001), *The microbiology textbook*, <http://www.bact.wisc.edu/microtextbook/>
- Popov, V. O. and Lamzin, V. S. (1994) NAD⁺-dependent formate dehydrogenase *Biochemical J.*, **130**, 625-643.
- Pyo, S. H., Lee, J. H., Park, H. B., Hong, S. S. and Kim, J. H. (2001) A large-scale purification of recombinant histone H1.5 from *Escherichia coli* *Protein Expr. Purif.*, **23**, 38-44.
- Rawle, A., *The basic principle of particle size analysis*,
- Reichert, U., Knieps, E., Slusarczyk, H., Kula, M.-R. and Thommes, J. (2001) Isolation of a recombinant formate dehydrogenase by pseudo-affinity expanded bed adsorption *J. Biochem. Biophys. Methods*, **49**, 533-552.
- Roe, S. D. (1987), Whole broth extraction of enzymes from fermentation broths using commercially available adsorbents In *Separations for Biotechnology*, Vol. 1 (Eds, Verall, M. S. and Hudson, M. J.) Ellis Horwood Ltd., Chichester, pp. 210-216.
- Shiloach, J. and Kaufman, J. B. (1999) The combined use of expanded bed adsorption and gradient elution for capture and partial purification of mutant diphtheria toxin (CRM9) from *Corynebacterium diphtheriae* *Sep. Sci. Technol.*, **34**, 29-40.
- Skidmore, G., Horstmann, B. J. and Chase, H. A. (1990) Modelling Single-Component Protein Adsorption to the Cation Exchanger S SEPHAROSE FF *J. Chromatogr.* **566**, 341-350, **498**, 113-128.

- Slusarczyk, H., Felber, S., Kula, M. R. and Pohl, M. (2000) Stabilization of NAD-dependent formate dehydrogenase from *Candida boidinii* by site-directed mutagenesis of cysteine residues *Eur. J. Biochem.*, **267**, 1280-1289.
- Sonntag, H. (1977) *Lehrbuch der Kolloidwissenschaft*, VEB Deutscher Verlag der Wissenschaften, Berlin.
- Stevenson, D. G. (1997) Flow and filtration through granular media--the effect of grain and particle size dispersion *Water Research*, **31**, 310-322.
- Stryer, L. (1994) *Biochemie*, Spektrum akad. Verlag, Heidelberg, Berlin, Oxford.
- Tanford, C. (1961) *Physical Chemistry of Macromolecules*, Wiley, New York.
- Thömmes, J. (1997) Fluidized bed adsorption as a primary recovery step in protein purification *Adv. Biochem. Eng.* **24**, 73-118, **58**, 185-230.
- Thömmes, J. (1999) *Zur Fließbettadsorption als Primärschritt in der Proteinaufarbeitung*, Habilitationsschrift at the Institut für Enzymtechnologie of Heinrich-Heine Universität Düsseldorf, Düsseldorf
- Thömmes, J., Bader, A., Karau, A. and Kula, M.-R. (1997), Integrative antibody purification from whole broth by fluidized bed adsorption In *Animal Cell Technology - From Vaccines to Genetic Medicine*,(Eds, Carrondo, M. J. T., Griffiths, B. and Moreira, J. L. P.) Kluwer Academic Publishers, Dordrecht, pp. 227-234.
- Thömmes, J., Halfar, M., Gieren, H., Curvers, S., Takors, R., Brunschier, R. and Kula, M.-R. (1999) Human Chymotrypsinogen B Production from *Pichia pastoris* by Integrated Development of Fermentation and Downstream Processing. Part 2. Protein recovery *Biotechnol. Prog.*, **17**, 503-512.
- Tiehm, A., Herwig, V. and Neis, U. (1999) Particle size analysis for improved sedimentation and filtration in waste water treatment *Water Sci. Technol.*, **39**, 99-106.

- Trinh, L., Noronha, S. B., Fannon, M. and Shiloach, J. (2000) Recovery of mouse endostatin produced by *Pichia pastoris* using expanded bed adsorption *Bioseparation*, **9**, 223-230.
- van Loosdrecht, M. C., Lyklema, J., Norde, W., Schraa, G. and Zehnder, A. J. (1987a) Electrophoretic mobility and hydrophobicity as a measured to predict the initial steps of bacterial adhesion *Appl. Environ. Microbiol.*, **53**, 1898-1901.
- van Loosdrecht, M. C., Lyklema, J., Norde, W., Schraa, G. and Zehnder, A. J. (1987b) The role of bacterial cell wall hydrophobicity in adhesion *Appl. Environ. Microbiol.*, **53**, 1893-1897.
- van Loosdrecht, M. C., Lyklema, J., Norde, W. and Zehnder, A. J. (1989) Bacterial adhesion: A physicochemical approach *Microb. Ecol.*, **17**, 1-15.
- Vermeulen, T., Le Van, M., Hiester, N. K. and Klein, G. (1973), Adsorption and Ion Exchange In *Chemical Engineer's Handbook*, (Eds, Perry, R. H. and Chilton, C. H.) McGraw-Hill, New York.
- Villiermaux, J. and van Swaaij, W. P. M. (1969) Modele representativ de la distribution des temps de sejour dans un reacteur semi-infini a dispersion axiale avec zones stagnantes. Application a l'ecoulement ruisselant dans des colonnes d'anneaux raschig *Time Measurements in Pulsd Liquid/liquid Extractors.*, **24**, 1097-1111.
- Voute, N., Bataille, D., Girot, P. and Boschetti, E. (1999) Characterisation of very dense mineral oxide-gel composites for fluidized-bed adsorption of biomolecueles *Bioseparation*, **8**, 121-129.
- Weuster-Botz, D., Paschold, H., Striegel, B., Gieren, H., Kula, M.-R. and Wandrey, C. (1994) Continuous computer controlled production of formate dehydrogenase (FDH) and isolation on a pilot scale *Chem. Eng. Technol.*, **17**, 131-137.
- Wheelright, S. M. (1991) *Ion Exchange Chromatography*, Hanser 1991.
- Wheelwright, S. M. (1987) Designing downstream processes for large-scale protein purification *Bio/Technology*, **5**, 789-793.

- Wichmann, R., Wandrey, C., Bückmann, A. F. and Kula, M. R. (1981) Continuous enzymatic transformation in an enzyme membrane reactor with simultaneous NAD(H) regeneration *Biotechnol. Bioeng.*, **23**, 2789-2802.
- Wiese, G. R. and Healy, T. W. (1970) Effect of particle size on colloid stability *Trans. Faraday Soc.*, **66**, 490-499.
- Wong, H. H., O'Neill, B. K. and Middelberg, A. P. J. (1997) A mathematical model for E. coli debris size reduction during high pressure homogenisation based on grinding theory *Time Measurements in Pulsed Liquid/Liquid Extractors.*, **52**, 2883 - 2890.
- Yamamoto, S. and Sano, Y. (1992) Short-cut method for predicting the productivity of affinity chromatography *J. Chromatogr. 566, 341-350*, **597**, 173-179.
- Yannisch-Perron, C., Vieira, J. and Messing, J. (1985) Improved M13 phage cloning vectors and host strains: nucleotide sequences of the M13mp18 and pUC 19 vectors *Gene*, **33**, 103-119.
- Yoshida, H., Kataoka, T. and Ruthven, D. M. (1984) Analytical solution of the breakthrough curve for rectangular isotherm systems *Time Measurements in Pulsed Liquid/Liquid Extractors.*, **39**, 1489-1497.
- Yoshida, H., Yoshikawa, M. and Kataoka, T. (1994) Parallel transport of BSA by surface and pore diffusion in strongly basic chitosan *AIChEJ*, **40**, 2034-2044.
- Young, M. E., Carroed, P. and Ball, R. L. (1980) Estimation of diffusion coefficients of proteins *Biotechnol. Bioeng.*, **22**, 947-955.
- Zanette, D., Dundon, W., Soffientini, A., Sottani, C., Marinelli, F., Akesson, A. and Sarubbi, E. (1998) Human IL-1 receptor antagonist from Escherichia coli: large-scale microbial growth and protein purification *J. Biotechnol.*, **64**, 187-196.
- Zaslavsky, B. Y. (1995) *Aqueous two-phase partitioning: physical chemistry and bioanalytical applications*, Dekker, New York.

-
- Zhou, H., Huxtable, S., Xin, H. and Li, N. (1998) Enhanced high-level expression of soluble 1-aminocyclopropane-1-carboxylase synthase and rapid purification by expanded-bed adsorption *Protein Expr. Purif.*, **14**, 178-184.